New Metallomolecular Wires Based on Carbon-rich Bridging Systems

A systematic study

TESE DE DOUTORAMENTO

João Luís Camacho Baptista Figueira
DOUTORAMENTO EM QUÍMICA

UNIVERSIDADE da MADEIRA
A Nossa Universidade
www.uma.pt

dezembro | 2012

New Metallomolecular Wires Based on Carbon-rich Bridging Systems

A systematic study

TESE DE DOUTORAMENTO

João Luís Camacho Baptista Figueira
DOUTORAMENTO EM QUÍMICA

ORIENTAÇÃO
João Manuel Cunha Rodrigues

CO-ORIENTAÇÃO
Kari Tapani Rissanen

The work presented in this dissertation was performed in the Molecular Materials Research Group of the Madeira Chemistry Research Centre (CQM), University of Madeira, and in the Department of Chemistry, Nanoscience Centre, University of Jyväskylä, Finland. It was financially supported by the Fundação para a Ciência e a Tecnologia through the PhD grant SFRH/BD/29325/2006, and partly by the research projects POCTI/CTM/41495/2001, PTDC/CTM/098451/2008, and CQM Strategic Plan, PEst-OE/QUI/UI0674/2011.

However, a good laugh is a mighty good thing, and rather too scarce a good thing; the more's the pity. So, if any one man, in his own proper person, afford stuff for a good joke to anybody, let him not be backward, but let him cheerfully allow himself to spend and be spent in that way. And the man that has anything bountifully laughable about him, be sure there is more in that man than you perhaps think for.

– *Moby Dick* by Herman Melville

Acknowledgements

You don't have to be a "person of influence" to be influential. In fact, the most influential people in my life are probably not even aware of the things they've taught me.

– Scott Adams

I acknowledge my supervisors and senior collaborators:

To Prof. João Rodrigues, for accepting me in his group since my licentiate degree and continued supervision and guidance throughout my still brief scientific career. Prof. João has molded my professional character.

To Acad. Prof. Kari Rissanen, for receiving me year after year in his group, and treating me as one of his "regular" students. For taking the time to personally teach me XRD.

To Prof. José Carlos Mesquita (University of Madeira, Portugal), for performing the cyclic voltammetry tests on the compounds and the resulting data compilation and reports.

To Mr. Reijo Kaupinen (University of Jyväskylä, Finland), for his continued NMR assistance and teaching and for being one of the best persons I know, always ready with a smile to help anyone.

To Ms. Mirja Lahtiperä (University of Jyväskylä, Finland), for introduction and general operation of the ESI-TOF spectrometer and for the wonderful and priceless insights on the acquisition of organometallic samples.

To Dr. Arto Valkonen (University of Jyväskylä, Finland), for helping me finish some crystal structures preparation for the thesis.

To Prof. Fernando Lahoz (University of La Laguna, Spain), for the solid state fluorescence measurements of the compounds I have prepared.

To Dr. César Fernandes (LREC – Laboratório Regional de Engenharia Civil, Funchal, Portugal), for letting me use LREC's ATR-FTIR to finish some characterization data.

To the CCCEE (Centro de Competência de Ciências Exatas e da Engenharia, University of Madeira) lab technicians, Ms. Ana Paula Tentem and Mrs. Ana Paula Andrade, for their continued lab support throughout all my lab work.

To Dr. Ying Lu (CQM, University of Madeira, Portugal), for running the MS ESI-Ion trap experiments of the ruthenium monohydrido complex.

I acknowledge my laboratory colleagues and friends:

To Manuel Jardim, for the chemistry discussions, for working together in the matters of laboratory management and for being a good friend.

To all my friends, Micaela Fernandes, Rita Andrade, Lilia Camacho, Dr. Carla S. Alves, Dr. Luís Santos, Nilsa Oliveira, Rita Castro, Mara Gonçalves, Cláudia Camacho, Dr. Alireza Nouri, that helped one way or the other with support or simply good mood.

To Dr. Ondřej Jurček, one of my best friends, for helping me time and again to settle and socialize in the busy winter life of Finland and to the rest of all the friends I met on my trips to Jyväskylä and that made my stays several fold better: Asela Manatunga, Chandan Giri, Dr .Nonappa, Dr. Ngong Kodiah Beyeh, Virpi Noponen, Dr. Satu Ikonen, Hana Svobodova, Dr. Jens Bunzen and Jenni Ranta.

To Dr. Visvaldas Kairys, for all the help with GAMESS and its steep learning curve even though I was unable to produce any fitting results for this dissertation. It is still a learning process at this point.

To Ana Cristina Olival, for some melting point measurements and a helpful hand around the lab during her internship.

I acknowledge my family

To my wife-to-be, Sandra Gouveia, for her unyielding support, uplifting and contagious cheerfulness. I have a world of debt to her.

To my parents, Alberto and Fernanda Figueira, for never doubting me and supporting my ambitions and projects no matter what.

I acknowledge the financial support

To FCT (Fundação para a Ciência e a Tecnologia) for the Ph.D. grant SFRH/BD/29325/2006 for this work, research projects POCTI/CTM/41495/2001, PTDC/CTM/098451/2008, and CQM Strategic Plan, PEst-OE/QUI/UI0674/2011.

To the Portuguese National Mass Spectrometry Network (contract RNEMREDE/1508/REM/2005) and to the Portuguese National Nuclear Magnetic Resonance

Network (PTNMR-REDE/1517/RMN/2005-POCI2010/FEDER) for providing equipment essential to this work.

To the Instituto de Emprego da Madeira, for a professional internship that supported the final year of work.

To Centro de Química da Madeira and University of Madeira that provided the workplace and equipment for the majority of the experimental work.

Resumo

Nesta dissertação discute-se os resultados obtidos na preparação de compostos candidatos a serem usados como fios moleculares. Estes compostos utilizam pontes orgânicas derivadas do 1,4-dietinilbenzeno com cadeias laterais alcoxil, assim como terminações compostas por complexos de paládio e ruténio. Os compostos foram caracterizados utilizando as técnicas espectroscópicas habituais tais como RMN ^{1}H, ^{13}C e ^{31}P, MS, FTIR e UV-Vis, bem como voltametria cíclica que permitiu classifica-los de acordo com o sistema Robin–Day e determinar o efeito das pontes e comprimentos das cadeias laterais no transporte de eletrões.

Os ligandos derivados de 1,4-dietinilbenzeno foram preparados através de vias de síntese baseadas, principalmente, em acoplamentos catalisados por paládio (Acoplamento cruzado de Sonogashira). Assim sendo, foi preparada uma família de compostos do tipo 1,4-dietinilbenzeno com um anel e diferentes comprimentos da cadeia lateral alcoxil (OCH_3, OC_2H_5, OC_7H_{15}).

Os complexos binucleares de ruténio revelaram comunicação eletrónica entre os centros metálicos apenas quando os ligandos mais curtos são usados, enquanto os mais longos apresentaram, nos estudos de voltametria cíclica, apenas um par redox característico. Nos resultados de voltametria cíclica observaram-se dois processos irreversíveis de uma onda para os complexos dinucleares de paládio o que faz com que estes complexos possam ser considerados como isoladores moleculares.

O decaimento da fluorescência dos compostos sintetizados (ligandos e complexos) revela um padrão em que os tempos de decaimento decrescem com a coordenação aos complexos metálicos. Tal pode dever-se à redistribuição da carga dos ligandos aquando da coordenação conduzindo a percursos de relaxamento não radiativos. No decorrer do trabalho foram determinadas as estruturas de raios-X, de dois novos ligados e de um composto com paládio.

Verificou-se que as cadeias laterais, quando presentes, melhoram as características de deslocalização de carga dos complexos. Contudo, o efeito introduzido pelas cadeias laterais mais longas é quase negligenciável.

Palavras-chave: Condutores moleculares, difracção de raios X, acoplamento de Sonogashira, paládio, ruténio.

Abstract

This dissertation presents and discusses the preparation of molecular wires (MW) candidates that would then be probed for electron transfer properties. These wires are bridged by 1,4-diethynylbenzene derivatives with alkoxy side chains with palladium and ruthenium metal complex termini. Characterization of these compounds was performed by usual spectroscopic techniques like ^{1}H, $^{13}C\{^{1}H\}$ and $^{31}P\{^{1}H\}$ NMR, MS, FTIR and UV-Vis as well as by cyclic voltammetry which allowed classifying the candidates in the Robin–Day system and determination of bridges side chain and length effects on electronic transport.

Preparation of the 1,4-diethynylbenzene derivatives was done with synthetic pathways that relied heavily in palladium catalyzed cross-couplings (Sonogashira). A family of single ringed 1,4-diethynylbenzene ligands with different length alkoxy side chains (OCH_3, OC_2H_5, OC_7H_{15}) was thus prepared allowing for the influence of these ring decorations to be assessed.

The ruthenium binuclear rods showed communication between metal centres only when the shorter ligands were used whereas the longer Ru complexes showed only one redox pair in CV studies which is in agreement to non-communicating metal centres.

Cyclic voltammetry studies show irreversible one wave processes for palladium dinuclear complexes, making these rods function as molecular insulators.

Fluorescence decay studies performed on the prepared compounds (ligands and complexes) show a pattern of decreasing decay times upon coordination to the metal centres which can due to ligand charge redistribution upon coordination leading to non-radiative relaxation paths.

Regarding the X-ray structures, two new ligand related structures were obtained as well as new structure for a palladium rod.

The effect of the side chains was observed to be important to the wires' electronic properties when comparing with the analogs without a side chain. The effect brought by longer chains is nevertheless almost negligible.

Keywords: molecular wires, X-ray diffraction, Sonogashira cross-coupling, palladium, ruthenium.

List of publications

Articles

Related to this thesis

6-"Synthesis, characterization, X-ray structures, substituent effects and solid-state photoluminescence studies of phenylene ethynylene based dinuclear palladium (II) rods with alkoxy side chains", João Figueira, Wojciech Czardybon, José Carlos Mesquita, João Rodrigues, Fernando Lahoz, Luca Russo, Arto Valkonen and Kari Rissanen. Under preparation.

5-"A convenient route for the preparation of the monohydride catalyst trans-[RuCl(H)(dppe)$_2$] (dppe = $Ph_2PCH_2CH_2PPh_2$): Improved Synthesis and Crystal Structure",
João Figueira, Manuel G. Jardim, João Rodrigues, Arto Valkonen, Kari Rissanen, *Inorg. Chem. Comm.*, **2013**, 29, 123-127.

4-"Three 2,5-dialkoxy-1,4-diethynylbenzene derivatives",
João Figueira, João Rodrigues, Kari Rissanen, *Acta Cryst.*, **2008**, C64, o33-o36.

3-"*trans*-[bis(diphenylphosphino)methane-κ^2P,P']dichlororuthenium(II)dichloromethane disolvate",
João Figueira, João Rodrigues, Kari Rissanen, *Acta Cryst.*, **2006**, E62, m3594-m3596.

2-"*cis*-Aquabis[bis(diphenylphosphino)ethane- κ^2P,P´]-chlororuthenium(II) hexafluorophosphate 1.5-dichloromethane 0.5-water solvate",
Luca Russo, João Figueira, João Rodrigues and Kari Rissanen, *Acta Cryst.*, **2006**, E62, m699-m701.

1-"*cis*-[bis(diphenylphosphino)ethane- κ 2P,P´]dichlororuthenium(II)dichlomethane disolvate",
Luca Russo, João Figueira, João Rodrigues and Kari Rissanen, *Acta Cryst.*, **2006**, E62, m1154-m1155.

Other work

3-"Poly(alkylidenamines) dendrimers as scaffolds for the preparation of low-generation ruthenium based metallodendrimers",
João Rodrigues, Manuel G. Jardim, João Figueira, Marisol Gouveia, Helena Tomás, Kari Rissanen, *New J. Chem.*, **2011**, 35, 1938-1943.

2- "4,4'-[Thiophene-2,5-diylbis(ethyne-2,1-diyl)]dibenzonitrile",
João Figueira, João Rodrigues, Viatslav Vertlib, Kalle Nättinen, Kari Rissanen; *Acta Cryst.*, **2008**, E64, o765-o766.

1-"A Trinuclear Aqua Cyano-bridged Ruthenium Complex $[((\eta^5\text{-}C_5H_5)(PPh_3)_2Ru(\mu\text{-}CN))_2RuCl_2(PPh_3)(H_2O)][PF_6]$: Synthesis, Characterization and Crystal Structure",
Viatcheslav Vertlib, João Figueira, José Mesquita, João Rodrigues, Kalle Nättinen and Kari Rissanen, *Eur. J. Inorg. Chem.*, **2007**, 13, 1920-1924.

Oral presentations

Related to this thesis

2012(2)
"Organic-inorganic hybrid molecular/semiconductor waveguides based on oligo(phenylene ethynylene)s derivatives",
João Figueira, Nilsa Oliveira, Fei Hui, José Carlos Mesquita, João Rodrigues, Kari Rissanen, Workshop nano12 – Shaping the future –, Academia das Ciências de Lisboa, Portugal, 18th October, 2012.

"Oligo(phenyleneethynylene)derivatives for application as organic-inorganic hybrid molecular/semiconductor waveguides",
Nilsa Oliveira, João Figueira, Fei Hui, João Rodrigues, José Carlos Mesquita, Kari Rissanen, F. Lahoz, XXV International Conference on Organometallic Chemistry (XXV ICOMC), September 2-7, Lisbon, Portugal, PSA, F2.8, p.47 2012. (flash presentation)

2011(1)

"Progress on the synthesis and characterization of dinuclear Pd and Ru rods for the preparation of organometallic molecular wires".

João Figueira, José Carlos Mesquita, João Rodrigues, Kari Rissanen, 6th Material Group Meeting/CQM, University of Madeira, Funchal, Portugal, 28th January, 2011.

2010(3)

"Preparation and characterization of Ruthenium and Palladium dinuclear Rods as potential molecular wires",

João Figueira, José Mesquita, João Rodrigues, Kari Rissanen, 7th Supraphone meeting, Maria Laach, Germany, April 29th to May 1st 2010.

"Ruthenium and palladium dinuclear OPE and OTE rods for nanoelectronic applications",

João Figueira, José Carlos Mesquita, João Rodrigues, Kari Rissanen, 2nd Portuguese Young Chemists Meeting, Universidade de Aveiro, Portugal, April 21-23rd, OC-19, 2010.

"Synthesis and characterization of dinuclear Pd and Ru rods for the preparation of organometallic molecular wires",

João Figueira, José Carlos Mesquita, João Rodrigues, Kari Rissanen, 5th Material Group Meeting/CQM, University of Madeira, Funchal, Portugal, 29th January, 2010.

2009(2)

"Preparation of Ruthenium and Palladium Dinuclear OTEs and OPEs Rods for Application as Molecular Wires",

João Figueira, José Carlos Mesquita, João Rodrigues, Kari Rissanen, 4th Material Group Meeting/CQM, Funchal, Portugal, 30th of January, 2009 (Flash presentation).

"Ruthenium and Palladium OPE and OTE bridged rods for Application as Molecular Wires",

João Figueira, José Mesquita, João Rodrigues, Kari Rissanen, XVIII EuCheMS Conference on Organometallic Chemistry, Gutenberg, Sweden, 22-25th June, O-26, 2009.

2008(5)

"Molecular Wires and Metallodendrimers - a "nano" introduction",

João Rodrigues, Helena Tomás, José Carlos Mesquita, João Figueira, Manuel Jardim, Swarup Maiti, Workshop on Coordination and Organometallic Chemistry Towards New Materials, University of Madeira, Funchal, Portugal, 3rd of December 2008.

"Pd and Ru complexes with OPE and OTE bridging ligands for nanoelectronic applications",

João Figueira, José Mesquita, João Rodrigues, Kari Rissanen, Workshop on Coordination and Organometallic Chemistry Towards New Materials, University of Madeira, Funchal, Portugal; 3rd of December, 2008.

"Progress on the preparation of Binuclear Pd and Ru complexes based on OPE and OTE bridging ligands for nanoelectronic applications",
João Figueira, José Mesquita, João Rodrigues, Kari Rissanen, CQM Materials Line Meeting, 29th of October 2008, Funchal/Portugal (Private communication).

"Binuclear Pd and Ru based on OPE and OTE bridging ligands for nanolectronic applications",
João Figueira, João Figueira, Kari Rissanen, Nanoschool 2008, University of Madeira, 13-17th October 2008.

"Novel Dinuclear Oligo(thienyleneethynylene)s Bridged Ruthenium Rods",
João Figueira, João Rodrigues, Kari Rissanen, 3rd Material Group Meeting/CQM, Funchal, Portugal, January, 2008 (Flash presentation).

2007(1)
"Novel Polarised Molecular Wires Based on Transition Metal Complexes of di(4-pyridyl)heterocycles Spacers Bridging Ligands"
João Figueira, Viatcheslav Vertilib, João Rodrigues and Kari Rissanen, 2nd Material Group Meeting/CQM, Funchal, Portugal, January, 2007 (Flash presentation).

2006(1)
"Organometallic Materials for Photonics and Molecular Electronics Nanoscale Devices",
João Rodrigues, Zsolt Csok, Wojciech Czardybon, João Figueira, Manuel Jardim and José Mesquita, Fourteen International Conference on Composites/Nano Engineering (ICCE-14), Boulder, USA, 2-8th July, 2006.

Other work

2012(2)
"Ruthenium poly(alkylidenamine) nitrile dendrimers - a new family of biometallodendrimers",
João Rodrigues, Manuel Jardim, Marisol Gouveia, João Figueira, Helena Tomás, and Kari Rissanen
XXV International Conference on Organometallic Chemistry (XXV ICOMC), September 2-7, Lisbon, OCS3.6, page 42, 2012.

"Low-generation ruthenium based metallodendrimers for biomedical applications",
João Rodrigues, Manuel Jardim, João Figueira, Marisol Gouveia, Helena Tomás, and Kari Rissanen
3rd International Symposium on Biological Applications of Dendrimers, 5th-8th September, Toledo, Spain, OC5, page 39, 2012.

Poster presentations

2012(1)

"Preparation and cyclic voltammetry studies of Ru and Pd phenylene ethynylene and thiophenylene ethynylene rods",

João Figueira, José Carlos Mesquita, Kari. Rissanen, João Rodrigues, XIV Iberic Meeting of Electrochemistry & XVII Meeting of the Portuguese Electrochemical Society, CQM - University of Madeira, Funchal, Portugal, 11-14th of March, PF3 (page 84), 2012.

"Oligo(phenyleneethynylene)derivatives for application as organic-inorganic hybrid molecular/semiconductor waveguides",

Nilsa Oliveira, João Figueira, Fei Hui, João Rodrigues, José Carlos Mesquita, Kari Rissanen, F. Lahoz, XXV International Conference on Organometallic Chemistry (XXV ICOMC), September 2-7, Lisbon, Portugal, PSA, F2.8, page 47 2012.

2011(2)

"Oligo(phenylene ethynylene) bridged $RuCl(dppe)_2$ and $PdCl(PEt_3)_2$ rods: synthesis, electrochemistry, fluorescence and X-ray structures",

João Figueira, José Carlos Mesquita, Arto Valkonen, Natte Nättinen, Kari. Rissanen, Fernando. Lahoz, João Rodrigues, XXII Encontro Nacional SPQ, University of Minho, Braga, Portugal, 3-6th of July, QI-CP 03, 2011.

"Time resolved fluorescence characterization of oligo(p-phenylene ethynylene) based metallic nanorods",

Fernando Lahoz, D. López, João Figueira, José Carlos Mesquita, Nilsa Oliveira, João Rodrigues, Arto Valkonen, Natte Nättinen, Kari Rissanen, TNT – Trends in Nanotechnology, Tenerife, Spain, 21-25th of November, 2011.

2010(2)

"Analysis of Organometallic Compounds by Using Electrospray Quadrupole Ion Trap Mass Spectrometry",

Ying Lu, João Figueira, Manuel Jardim, João Rodrigues, 4th Portuguese Mass Spectroscopy Meeting, FCUL, Lisbon, Portugal, 13-15th of December, P01, page 47, 2010.

"Synthesis and electrochemical studies of molecular wires based on dinuclear Pd and Ru OPE and OTE rods",

João Figueira, João Rodrigues, Luca Russo, Kari Rissanen XII Iberic Meeting of Electrochemistry & XVI Meeting of the Portuguese Electrochemical Society, ISEL, Lisbon, Portugal, 8–11th, September, 2010.

2009(1)

"A new family of Palladium and Ruthenium binuclear rods for electronic applications",
João Figueira, João Rodrigues, Wojciech Czardybon, Luca Russo, Kari Rissanen, 8th Conference on Inorganic Chemistry, Curia, Portugal, 16 – 17th of October, page 101, 2009.

2008(3)

"Novel Binuclear Ruthenium Oligo(thiophenyleneethynylene) rods for Nanoeletronic Applications",
João Figueira, João Rodrigues, Kari Rissanen, 2nd EuCheMS Chemistry Congress, 17-20th of September, Turin, Italy, page 39, VI-2, Nanomaterials, 2008.

"Single Crystal X-Ray Studies of Several Ruthenium Complexes Used as Starting Materials for Organometallic Nanomaterials",
João Rodrigues, João Figueira, Luca Russo, Kalle Nätinnen, Kari Rissanen, ICOMC 2008, 13-18th of July 2008, Rennes, France, page 739, 2008.

"Molecular Materials Based on Organometallic Compounds",
João Rodrigues, João Figueira, Manuel Jardim, Swarup Maiti, José C. Mesquita, NanoSpain 2008, 14-18th of April, Braga, Portugal, page 36, 2008.

2007(2)

"New OPE And OTE Ruthenium Metallomolecular Wires",
João Figueira, José Mesquita, João Rodrigues and Kari Rissanen, 7ª Conferência de Química Inorgânica da Sociedade Portuguesa de Química, Fátima, Portugal, 30th of November to 1st of December 2007.

"New Metallomolecular Wires Based In Oligothiophene Bridging Systems – A Systematic Study",
João Figueira, José Mesquita, João Rodrigues and Kari Rissanen, European School of NanoScience and Nanotechnologies, Grenoble, France, 26th of August to 15th of September, 2007.

Abbreviations and symbols

ν	Infra-red stretching mode
Ac	Acetyl or Acyl group (-C(O)CH_3)
Ar	Aromatic (ring)
ATR	Attenuated Total Reflectance
C60	[C60]Fullerene
CMOS	Complementary Metal Oxide Semiconductor
CNS	Creutz, Newton and Sutin
CNT	Carbon Nanotube
Cp	Cyclopentadienyl (η^5-C_5H_5)
Cp*	Pentamethylcyclopentadienyl (η^5-$C_5(CH_3)_5$)
CP-AFM	Conducting Probe Atomic Force Microscopy
CSD	Cambridge Structural Database
d	doublet (NMR)
dba	Dibenzylideneacetone
DBU	1,8-Diazabicyclo[5.4.0]undec-7-ene
DFT	Density Function Theory
DMBA	*N,N'*-dimethylbenzamidinate
DMSO	Dimethyl sulfoxide
dppe	1,2-Bis(diphenylphosphino)ethane
dppf	1,1'-Bis(diphenylphosphino)ferrocene
dppm	1,2-Bis(diphenylphosphino)methane
EFISH	Electric Field Induced Second Harmonic Generation
eq	Molar equivalent
Eqn.	Equation
ESI-TOF	Electrospray Ionization – Time Of Flight
Et	Ethyl (-CH_2CH_3)
ET	Electron-transfer
Fc	Ferrocene
FTIR	Fourier Transform Infra-Red spectroscopy.
HOMO	Highest Occupied Molecular Orbital
ICT	Intervalence Charge Transfer
ILCT	Inter-Ligand Charge Transfer
IMW	Insulated Molecular Wires
IT	Information Technology
K_c	Comproportionation constant (K_c = exp (ΔE° F/RT)
LEDs	Light-Emitting Diode
LMCT	Ligand To Metal Charge Transfer
LUMO	Lowest Occupied Molecular Orbital
m	medium (IR) or multiplet (NMR)
MeO-DMBA	*N,N'*-dimethyl-3-methoxybenzamidinate
MLCT	Metal to ligand charge transfer
MV	Mixed Valence
NDR	Negative differential resistance
NIR	Near Infra-Red
NMR	Nuclear Magnetic Resonance
NOE	Nuclear Overhauser Effect
OLEDs	Organic Light-Emitting diode
OPEs	Oligo(1,4-phenylene ethynylene)s
OPVs	Oligo(1,4-phenylene vinylene)s
OTEs	Oligo(2,5-thiophene ethynylene)s
OTf	Trifluoromethanesulfonate

OTTLE	Optically Transparent Thin-Layer Electrochemical
Ph	Phenyl
PKS	Piepho, Krauz and Schatz
PPE	poly(phenylene ethynelene)
PPP	poly(*p*-phenylene) polymers
PT	poly(α, α'-thiophene) polymers
q	quartet (NMR)
quint	quintet (NMR)
r.t.	room temperature
Ref.	Reference
s	singlet (NMR) or strong (IR)
SAM	Self-assembled monolayer
Sat.	Saturated
STM	Scanning Tunneling Microscope
STM-BJ	Scanning Tunneling Microscope Break Junctions
STS	Scanning Tunneling Spectroscopy
t	triplet (NMR)
Tacn	*N,N',N''*-trimethyl-1,4,7-triazacyclononane
TBAF	Tetrabuthylamonium Fluoride
t-Bu	*tert*-butyl
TEA	Triethylamine
TMEDA	*N,N,N',N'*-tetramethylethane-1,2-diamine
TMSA	Trimethylsilylacetylene
Tpy	2,2';6',2"-terpyridine
w	weak (IR)
δ	Infra-Red in plane bending or NMR chemical shift

Contents

Acknowledgements vii
Resumo xi
Abstract xiii
List of publications xv
Articles xv
Related to this thesis xv
Other work xvi
Oral presentations xvi
Related to this thesis xvi
Other work xviii
Poster presentations xix
Abbreviations and symbols xxi
Contents xxiii
Figure Index xxix
Scheme Index xxxix
Table index xli
Chapter I – Introduction 1
Introduction 3
I.1. Molecular electronics 3
I.2. Molecular wires 7
I.3. Organic molecular wires 9
I.3.1. Oligo(2,5-thiophene ethynylene)s 9
I.3.2. Oligo(1,4-phenylene ethynylene) 12
I.3.3. Oligo(1,4-phenylene vinylene)s 13
I.3.4. Aromatic ladder oligomers 13
I.3.5. Oligophenylenes 14
I.3.6. Carbon nanotubes 14
I.3.7. Graphene 15
I.4. Metallomolecular wires 16
I.5. Transport and classification of homo binuclear organometallic complexes 19
I.6.1. Binuclear 1,4-diethynylbenzene derivatives and non-innocent ligands in Ru systems 26
I.6. Other metallomolecular wires 31

I.6.1. Metalocumulenic systems 31
I.6.2. Binuclear polyalkynyl bridged systems 34
I.6.3. Mixed systems 40
I.6.4. Other binuclear systems 42
I.6.5. Photonic molecular wires 50
I.7. Side chains and decorations 54
I.8. Alligator clip molecules 59
I.9. Testing of molecular wire candidates 62
I.10. Binuclear palladium and platinum alkynyl rods 66
I.11. Luminescence of binuclear systems 71
I.12. Synthesis of the wires, general review 75
I.12.1. Ligand synthesis 75
I.12.2. Binuclear ruthenium rods synthesis 79
I.12.3. Binuclear palladium rods synthesis 81
Chapter II – Results and Discussion 83
II.1. Synthesis of 1,4-diethynylbenzene and 2,5-thiopene derivatives for use as bridging ligands 85
II.2. Synthesis of the binuclear palladium rods bridged by 1,4-diethynylbenzene derivatives 91
II.3. Synthesis of the binuclear ruthenium rods bridged by 1,4-diethynyl and 2,5-thiophene derivatives 93
II.3.1. 1,4-diethynylbenzene derivatives bridged rods 93
II.3.2. Thiophenylene ethynylene based Rods 98
II.4. Preparation of the “alligator clip” molecules and its coordination to a ruthenium rod 99
II.5. Ruthenium mono hydrido complex 102
II.6. UV-Vis Studies 106
II.6.1. Free ligands 106
II.6.2. Palladium rods 108
II.6.3. Ruthenium rods 112
II.7. Cyclic Voltammetry Studies 115
II.8. NMR Studies 120
II.9. FTIR Studies 123
II.10. MS Studies 126
II.11. Single crystal X-ray diffraction 129
II.11.1. Three (phenylene ethynylene)s (**4c**, **5c**, **5d**) 129
II.11.2. 1,4-bis(4-bromo-1-ethynylbenzene)-2,5-diethoxybenzene (**8b**) 132
II.11.3. 1,4-bis(1,4-diethynylbenzene)-2,5-dimethoxybenzene (**10a**) 134
II.11.4. *trans*-[RuCl(H)(dppe)$_2$] (**34**) 135

II.11.5. *cis*-[Ru(η^2-O_2CCH_3)(dppe)$_2$] (**37**) 136
II.11.6. Palladium phenylene ethynylene rod (**21b**). 137
II.12. Fluorescence decay studies 139
Chapter III – Conclusions and Future Perspectives 143
Chapter IV – Experimental Details and Characterization 149
IV.1. General remarks 151
IV.2. Preparation and characterization of the 1,4-diethynylbenzene and the 2,5-thiophene derivatives 152
IV.2.1. 1,4-diethynylbenzene, **5a** 152
IV.2.2. 1,4-dimethoxy-2,5-diethynylbenzene, **5b** 153
IV.2.3. 1,4-diethoxy-2,5-diethynylbenzene, **5c** 155
IV.2.4. 1,4-diheptoxy-2,5-diethynylbenzene, **5d** 156
IV.2.5. 1,4-dimethoxy-2,5-bis((4-ethynylphenyl)ethynyl)benzene, **10a** 158
IV.2.6. 1,4-diethoxy-2,5-bis((4-ethynylphenyl)ethynyl)benzene, **10b** 160
IV.2.7. 2,5-bis(4-ethynylphenyl)thiophene, **14b** 163
IV.2.8. 2,5-bis((4-ethynylphenyl)ethynyl)thiophene, **18b** 164
IV.3. Preparation and characterization of the palladium rods bridged with 1,4-diethynylbenzene derivatives. 166
IV.3.1. 1,4-bis[*trans*-(ethynyl)Pd(PEt_3)$_2$(Cl)]benzene, **20a** 166
IV.3.2. 1,4-bis[*trans*-(ethynyl)Pd(PEt_3)$_2$(Cl)]-2,5-dimethoxybenzene, **20b** 168
IV.3.3. 1,4-bis[*trans*-(ethynyl)Pd(PEt_3)$_2$(Cl)]-2,5-diethoxybenzene, **20c** 170
IV.3.4. 1,4-bis[*trans*-(ethynyl)Pd(PEt_3)$_2$(Cl)]-2,5-dihethoxybenzene, **20d** 172
IV.3.5. 1,4-bis[*trans*-((4-ethynylphenyl)ethynylethynyl)Pd(PEt_3)$_2$(Cl)]-2,5-dimethoxybenzene, **21a** 176
IV.3.6. 1,4-bis[*trans*-((4-ethynylphenyl)ethynylethynyl)Pd(PEt_3)$_2$(Cl)]-2,5-diethoxybenzene, **21b** 178
IV.4. Preparation and characterization of the ruthenium rods bridged with 1,4-diethynylbenzene and 2,5-thiophene derivatives. 181
IV.4.1. [Cl(dppe)$_2$Ru–C≡C]$_2$–C_6H_4, **23a** 181
IV.4.2. [Cl(dppe)$_2$Ru–C≡C]$_2$–$C_6H_4(OC_2H_5)_2$, **23c** 183
IV.4.3. [Cl(dppe)$_2$Ru–C≡C]$_2$–$C_6H_4(OC_7H_{15})_2$, **23d** 185
IV.4.4. [Cl(dppe)$_2$Ru–C≡C–C_6H_4–C≡C]$_2$–$C_6H_4(OCH_3)_2$, **24a** 188
IV.4.5. [Cl(dppe)$_2$Ru–C≡C–C_6H_4–C≡C]$_2$–$C_6H_4(OC_2H_5)_2$, **24b** 190
IV.4.6. [Cl(dppe)$_2$Ru–C≡C–C_6H_4]$_2$–C_5H_4S, **27** 193
IV.4.7. [Cl(dppe)$_2$Ru–C≡C–C_6H_4–C≡C]$_2$– C_5H_4S, **28** 195
IV.5. Preparation and characterization of other compounds. 198
IV.5.1. *trans*-[RuCl(H)(dppe)$_2$] (**34**) 198
Annexes 203
A.1. Characterization techniques 205

A.1.1. UV-Vis spectroscopy 205
A.1.2. FTIR spectroscopy 205
A.1.3. NMR spectroscopy 205
A.1.4. MS spectroscopy 206
A.1.5. Cyclic voltammetry 206
A.1.6. Single crystal X-ray diffraction 206
A.1.7. Fluorescence decay studies 207
A.1.8. Elemental Analysis 207
A.1.9. Melting point determination 207
A.2. General experimental procedures 208
A.2.1. Williamson substitution 208
A.2.2. Iodination of the 1,4-bis(alkoxy)benzenes 208
A.2.3. Bromination of the 1,4-bis(alkoxy)benzenes 208
A.2.4. Sonogashira coupling reactions 209
A.2.5. Deprotection of "Acetone Protected" ligands 209
A.2.6. Deprotection of trimethylsilyl protected ligands 210
A.2.7. Palladium binuclear complexes. 210
A.2.8. Ruthenium phenylene ethynylene binuclear rods. 210
A.2.9. Ruthenium thiophenylene ethynylene binuclear rods. 211
A.3. Preparation of general starting materials 211
A.3.1. $RuCl_2(DMSO)_4$ (DMSO = dimethylsulfoxide) 211
A.3.2. *cis*-$[RuCl_2(dppe)_2]$ 212
A.3.3. *trans*-$[RuCl_2(dppe)_2]$ 212
A.3.4. $TlPF_6$ 212
A.3.5. *cis*-$[RuCl(dppe)_2][PF_6]$ 213
A.4. NMR Studies 213
A.4.1. Free ligands 213
A.4.2. Palladium rods 217
A.4.3. Ruthenium rods 220
A.5. MS Studies 223
A.5.1. Free ligands 223
A.5.2. Palladium rods 224
A.5.3. Ruthenium rods 227
A.6. CV Studies 230
A.7. XRD Studies 231

1,4-bis(4-bromo-1-ethynylbenzene)-2,5-diethoxybenzene (**8b**).....232
1,4-bis(1,4-diethynylbenzene)-2,5-diethoxybenzene (**10a**).....233
trans-[RuCl(H)(dppe)$_2$] (**34**).....234
cis-[RuCl(η^2-O$_2$CCH$_3$)(dppe)$_2$] (**37**).....235
Palladium phenylene ethynylene rod (**20b**).....237
Nitrile terminated thiophenylene ethynylene (**38**).....238
A.8. Fluorescence decay studies.....240
References.....241

Figure Index

Figure 1. Cartoon depicting Moore's Law across a wide time span.[4] 4
Figure 2. 128Å long organic rod (**1**) prepared by Schumm and co-workers. R = 3-ethylheptyl.[13a] 8
Figure 3. An example (**2**) of a tetrakisporphyrin system (*t*-Bu is *tert*-butyl).[15] 8
Figure 4. The thiophene oligomers (**3**) prepared by the group of Otsubo.[23] 10
Figure 5. The thiophene-containing arylene-ethynylene/arylene-vinylene co-polymer (**4**).[26] 11
Figure 6. The oligo(2,5-thiophene ethynylene) potential wire (**5**) prepared by the group of Tour (Ac = Acetyl $C(O)CH_3$).[27-28] 11
Figure 7. One of Tour's OPE wires (Ac = acetyl group, $C(O)CH_3$).[5] 12
Figure 8. Organic molecular (**7a-b**) wires with switching properties.[5] 12
Figure 9. One of the OPVs studied by Wasielewski and co-workers.[21b] 13
Figure 10. One of the oligo(quinoxaline)s reported by Gourdon.[33] 14
Figure 11. An example of the fluorenone based molecular wires prepared by Bryce's group.[34] 14
Figure 12. OPE rod used by Mayor's group bearing a central 2,6-dibenzylamino core-substituted cromophore. a = phenanthrene π-system; b = OPE rod; c = NDI (N,N-naphtalenediimides) chromophore. Adapted from ref. [36]. ...15
Figure 13. Cartoon of an atom thick graphene sheet.[38] 16
Figure 14. Di-ruthenium systems studied by Mahapatro and co-workers in nanogap molecular junctions. Adapted from ref. [53e]. 20
Figure 15. The ruthenium systems studied by Rigaut and co-workers.[53f, 57] 20
Figure 16. Potential energy curves for electron transfer in ligand-bridged binuclear complexes with (a) negligible, (b) weak ($H_{ab} = \lambda/4$) and (c) strong ($H_{ab} = 3\lambda/4$) electronic coupling. The dotted and solid curves represent the diabatic and adiabatic surfaces, respectively. Adapted from ref. [63].....25
Figure 17. Example of the systems studied by Klein *et al.*; [Ru] = $[RuCl(dppe)_2]^+$). Adapted from ref. [16].....26
Figure 18. Compounds studied by Rigaut and co-workers (**a**). IR changes during the first oxidation of **16a** (right, **16a** → **16a**$^{\bullet+}$, 1,2-$C_2H_4Cl_2$/NBu_4PF_6). Adapted from ref. [66d]. 28
Figure 19. The insulating chain bearing systems prepared by the group of Rigaut (**a**) and the spectroscopic changes upon oxidation in an OTTLE Cell (1,2-$C_2H_4Cl_2$, 0.2 M Bu_4NPF_6) of the system with shorter insulating chain and n = 1 (**b**). Adapted from ref. [53a]. 29
Figure 20. Trimetallic system prepared by the group of Rigaut. Adapted from ref. [46]. 30
Figure 21. (Ethynyl)(vinyl)phenylene bridged triruthenium prepared by the Rigaut group. Adapted from ref. [71]. 30
Figure 22. The tetraferrocenyl-[3]-cumulene reported by Bildstein *et. al.*. Fc = ferrocene. Adapted from ref. [74]..32
Figure 23. Binuclear Ru bis(allenylidene) reported by Guesmi *et al.*. Adapted from ref. [75]. 32
Figure 24. Complex used for the study of the effect of increasing number of double bonds (n = 1-4, P = PPh_3). Adapted from ref. [58, 77].....33
Figure 25. Binuclear Ru cumulene/acetylide reported by Dixneuf's group.Adapted from ref. [78]. 33

Figure 26. Representation of the π-orbital alignment of the allene-bridged bimetallic complexes (**a**) and that of the cumulene-bridged bimetallic complexes (**b**) as well as the respective complexes (**26a-b**). Adapted from ref. [80]. ..34
Figure 27. Series of Cp*Re(NO)(PPh_3) terminated binuclear complexes prepared by Gladisz' group. (n = 2-6, 8, 10). Adapted from ref. [67b, 83]. ..35
Figure 28. The polyalkynyl based binuclear wires (**28**-**32**). Adpted from ref. [85a] (**28**), [87] (**29**), [89] (**30** and **31**), [90] (**32**) and [86] (**33**). ..37
Figure 29. The polyalkynyl based binuclear wires (**34a-i**). Adpted from ref. [52g, 52k] (**34a-e**) and [53g] (**34f-i**)...38
Figure 30. The polyalkynyl based binuclear wires (**35, 36, 37a-c**). Adpted from ref. [52f] (**35**), [52b, 93] (**36**) and [52b] (**37a-c**). ..39
Figure 31. The polyalkynyl based binuclear (**38a-c**). Adapted from ref. [94]. ..39
Figure 32. Example of the type of compounds studied by Chang and co-workers.[95] ..40
Figure 33. $(CH)_{14}$ binuclear cumulenic complex (**41**) with semi-reversible two wave processes (CV plot). Adapted from ref. [96]. ..41
Figure 34. Binuclear systems reported by Gao and co-workers. Adapted from ref. [98]. ..41
Figure 35. Ferrocene systems studied in Li's report. Adapted from ref. [54a]. ..42
Figure 36. $[\{FeCp(CO)_2\}_2\{1,4\text{-}C_6H_4(CN)_2\}][PF_6]_2$ binuclear Fe complex studied by Astruc *et. al*. Adapted from ref. [99]. ..42
Figure 37. One of the wires (**45a**, RuT_5) reported by Barbieri and co-workers. Adapted from ref. [101]. ..43
Figure 38. Trinuclear ethynylthiophene bridged Ru (II) complex. Adapted from ref. [102]. ..44
Figure 39. Cardan type junction reported by Ruben and co-workers. Adapted from ref. [104]. ..45
Figure 40. The ruthenium(II) bis(2,2':6',2''-terpyridine) complexes reported by Harriman and co-workers. Adapted from ref. [105]. ..45
Figure 41. The trimeric complex prepared by Ying and co-workers. Adapted from ref. [106]. ..46
Figure 42. Trinuclear complex prepared by Wong and co-workers. Adapted from ref. [107]. ..46
Figure 43. The Si hybrid wires prepared by the group of Rigaut. Adapted from ref. [66b]. ..47
Figure 44. The norbornyl based systems reported by Eggers and co-workers. R_1= CH_2OCH_3. Adapted from ref. [108]. ..47
Figure 45. Carborane hybrid wires (**53a**) prepared in the group of Low (central moiety is carborane $C_2B_{10}H_{10}$). Adapted from ref. [110]. ..48
Figure 46. "Shish-kebab" type of IMW polymers. Adapted from ref. [112b]. ..48
Figure 47. Molecular wire candidates studied by Jang and co-workers. Adapted from ref. [113]. ..49
Figure 48. Insulated molecular wire prepared by Cacialli *et al.*. Adapted from ref. [114]. ..49
Figure 49. One of the ZnPorphyrin-Paracyclophane-C60 wires studied by Molina-Ontoria *et al.*. Adpted from ref. [122]. ..52
Figure 50. Porphyrin based molecular photonic wire reported by Lindsey and co-workers. Adapted from ref. [123]. ..52
Figure 51. Example of a terpyridyl Ru and Os bi terminated photonic molecular wire. Adapted from ref. [124]. 53

Figure 52. Example of a terpyridyl terminated photonic molecular wire. M = Ru^{2+}, Os^{2+}, n = 1-3. Adapted from ref. [125a].....54
Figure 53. Phenylene vinylene oligomer with methoxy side chains studied by Meyers and colleagues. Adapted from ref. [136].....55
Figure 54. A family of binuclear complexes prepared by Akita and co-workers to test the inclusion of side chains. [Fe] = FeCp*(dppe). Adapted from ref. [82].....55
Figure 55. Study of the effect of the bridging ligand main moiety in FeCp*(dppe) wires. Adapted from ref. [138a].....56
Figure 56. OPV wires studied by Detert and Sugiono. Adapted from ref. [32].....56
Figure 57. Polynuclear complex prepared by Fratoddi *et al.* (**65**) and Khan *et al.* (**66a-h**). Adapted from ref. [140] and [141] respectively.....57
Figure 58. Binuclear ruthenium wires with electron donating and withdrawing side chains. Adapted from ref. [142].....58
Figure 59. Binuclear ruthenium complexes with growing alkoxy side chains. Adapted from ref.[143].....58
Figure 60. Binuclear ruthenium complexes with dendritic side chains. Adapted from ref. [144].....59
Figure 61. The most reported types of "alligator clip" molecules found in the literature. Adapted from ref. [8a], [146], [57, 147] and [57, 147] respectively.....60
Figure 62. Direct C–Au molecular junction reported by Chen and co-workers (n = 1-4). Adapted from ref. [154]. .60
Figure 63. Fullerene C60 terminated wire studied by Bryce and co-workers. Adapted from ref. [155a].....61
Figure 64. Selenium functionalized alligator clips. Adapted from ref. [155b].....61
Figure 65. Pyridine terminated rods. Adapted from ref. [155c].....62
Figure 66. Representative current-distance (I(s)) traces obtained from STM-BJ experiments in UHV (left) and current histograms constructed from plateau values of about 300 I(s) traces (right) for a 4,4'-bis(mercaptoalkyl)-biphenyl derivative. Adapted from ref. [163].....65
Figure 67. Heterometallic rods with $[Pd(PEt_3)_2]$ reported by the group of Gladysz. Adapted from ref. [83b].....67
Figure 68. Molecular Pt^{II} rods studied by Mayor and co-workers (**76c**)[53b] and Shashidhar and co-workers (**77a-e**)[176]. Adapted from refs. [53b] and [176].....68
Figure 69. The RuCp(dppf) terminated wires reported by Ge and co-workers. M = Pd or Pt; P_P = dppf (1,1'-bis(diphenylphosphino)ferrocene).[180].....68
Figure 70. The amine terminated wire reported by Jones *et al.*. Adapted from ref. [181].....69
Figure 71. Palladium diacetylide studied by Koch *et al.*. Adapted from ref. [183].....70
Figure 72. Fluorenone bridged Pt rod. Adapted from ref. [184].....70
Figure 73. Ruthenium polypyridyl dinuclear complex bridged by Pt and Au moieties. Adapted from ref. [185].....71
Figure 74. Photonic molecular wire prepared as an oligomeric platinum acetylide. n = 2, 3, 6 and 10. Adapted from ref. [186b].....71
Figure 75. Bisterpyridyl binuclear ruthenium rod bridged by a 1,1'-diethynylferrocene moiety. Adapted from ref. [187b].....72

Figure 76. Different bridges studied by Dong *et al.* using the terpy-Ru^{2+}-terpy-bridge- terpy-Ru^{2+}-terpy as for **84a-b**; R = alkyl chain. Adapted from ref. [187b]. 73
Figure 77. Terpyridyl Pt rods studied by Sun and co-workers. Adapted from ref. [187h]. 73
Figure 78. Diethynyl carbazole bridged dinuclear Pt and Pd rods. Adapted from ref. [187d]. 74
Figure 79. Diethynylphenylene oxidiazole bridged platinum dinuclear rods. Adapted from ref. [187g]. 75
Figure 80. Example of Ru(II) di-acetylide preparation as reported by Rigaut and co-workers. Adapted from ref. [53a].....81
Figure 81. General synthetic method used for the preparation of palladium acetylides. Adapted from ref. [206]. 81
Figure 82. Bisalkynyl Pd complex preparation by Fischer *et al.*. Adapted from ref. [207]. 82
Figure 83. General synthetic pathway for the preparation of the mono PE bridging ligands. 86
Figure 84. General reaction scheme for the preparation of the single ringed PEs when using the alternative source of alkynyl, 2-methylbut-3-yn-2-ol. 87
Figure 85. General synthetic pathway for the preparation of the tris phenylene ethynylene bridging ligands. 89
Figure 86. General synthetic pathway for the preparation of the thiophene based bridging ligands. 90
Figure 87. General procedure for the preparation of the $[PdCl_2(PEt_3)_2]$ based binuclear rods. 92
Figure 88. General procedure adopted for the preparation of the binuclear PE ruthenium rods. [P] = $P(C_6H_5)_2$; *t*-BuOK = potassium *tert*-butoxide.....93
Figure 89. Preparation of complex **23a** following the Dixneuf method (one pot and two step); where X = Na, Tl or NH_4; [P] = $P(C_6H_5)_2$.....94
Figure 90. $^{31}P\{^1H\}$ NMR (CD_2Cl_2, 161 MHz) spectrum of a one-pot attempt to prepare **23c** with *cis*-$[RuCl_2(dppe)_2]$, **5c**, NEt_3 and $TlPF_6$.....95
Figure 91. General preparation of the thiophene based ruthenium binuclear rods. [P] = $P(C_6H_5)_2$, **i**. -78 ºC, t-BuLi, diethyl ether; **ii**. CH_2Cl_2, r.t. 98
Figure 92. Preparation of the thiol based "alligator clip", as reported by Tour.[238].....99
Figure 93. Modified preparation of the thiol clip. N(*i*-Pr)$_2$Et = diisopropylamine; Ac = acyl ($CH_3C(O)^-$); N,N-DMA = N,N -dimethylacetamide; 1,2-DCE = 1,2-dichloroethane; TMSA = trimethilsilylacetylene. 100
Figure 94. Coordination of the thiol clip (**32**) to the tris PE rod (**24c**).....101
Figure 95. $^{31}P\{^1H\}$ NMR ($CDCl_3$, 161MHz) spectrum of the mixture obtained after several purification attempts of **33**.....101
Figure 96. Reaction conditions used in the preparation of compound **34**.....103
Figure 97. $^{31}P\{^1H\}$ NMR ($CDCl_3$, 161 MHz) spectra of three different attempts (experiments (**3i-3iii**)) to prepare compound **34** (Method 3). 104
Figure 98. Overall mass spectrum of **34** (ESI-TOF, Method 3). 106
Figure 99. Electronic spectra of **5a**, **5b** and **10a** in CH_2Cl_2 at *ca.* $1x10^{-5}$ M. 108
Figure 100. Spectra for the palladium rod **20a** as well as the respective free ligand (**5a**) and starting complex (**19**) in CH_2Cl_2 at *ca.* 1×10^{-5} M for the starting materials and 1×10^{-6} M for the rod. 110

Figure 101. Spectra for the palladium rod (**20b**), as well as the respective free ligand (**5b**) and starting complex (**19**) in CH_2Cl_2 at *ca.* 1×10^{-5} M.....111
Figure 102. Spectra for the palladium rod (**21a**) as well as the respective free ligand (**10a**) and starting complex (**19**) in CH_2Cl_2 at *ca.* 1×10^{-5} M for the starting materials and 1×10^{-6} M for the rod. 112
Figure 103. Spectra for the ruthenium rod (**23c**), as well as the respective free ligand (**5c**) and the corresponding *trans* conformer of the starting complex (**36**) in CH_2Cl_2 at *ca.* 6×10^{-6} M.....113
Figure 104. Spectra for a tris-ringed ruthenium rod (**24b**) as well as the respective free ligand (**10b**) and the corresponding conformer of the starting complex (**36**) in CH_2Cl_2 at *ca.* 6×10^{-6} M. 114
Figure 105. Spectra for the ruthenium rods based on the thiophene ligands (**27** and **28**) as well as the respective free ligands (**14b** and **18b**) and starting complex (**36**) in CH_2Cl_2 at *ca.* 6×10^{-6} M for the complexes and 1×10^{-5} M for the ligands and starting complex. 115
Figure 106. Cyclic voltammograms for the single ringed PE based palladium (**20-d**) rods with alkoxy side chains at 100 mVs^{-1} in CH_2Cl_2 vs. Ag/AgCl (KCl saturated). 116
Figure 107. Cyclic voltammograms for the single ringed PE based ruthenium rods (**23c-d**) with alkoxy side chains at 100 mVs^{-1} in CH_2Cl_2 vs. Ag/AgCl (KCl saturated). 117
Figure 108. Cyclic voltammogram for thiophene based ruthenium Rods (**27** and **28**) at 100 mVs^{-1} in CH_2Cl_2 vs. Ag/AgCl (KCl saturated). 119
Figure 109. ESI-TOF MS spectrum for palladium rod **20c**. 128
Figure 110. ESI-TOF MS spectrum for palladium rod **24a**. 129
Figure 111. ORTEP-3[265] plots of **4c**, **5c** and **5d** (50% probability displacement ellipsoids). 130
Figure 112. Packing plot[266] relative to **4c**. Only C–H···π interactions are shown. 131
Figure 113. Packing plot[266] relative to **5c**. The in-plane interactions are shown. 131
Figure 114. Packing plot[266] relative to **4c**. The C–H···π interactions are shown. 132
Figure 115. Perspective ORTEP-3[265] plot of **8b** (50% probability displacement ellipsoids). 132
Figure 116. Mercury[266] plot of **8b** to show short contacts. 133
Figure 117. Perspective ORTEP-3[265] plot of **9a** (50% probability displacement ellipsoids). 134
Figure 118. Mercury[266] plot of **9c** showing short contacts formed between molecules. 135
Figure 119. ORTEP-3[265] plot of the *trans*-$[RuCl(H)(dppe)_2]\cdot CH_2Cl_2$ in perspective view. The H-atoms, apart from the hydride, as well as, the solvent molecules are excluded for clarity. Thermal displacement ellipsoids were drawn at 30% probability. 135
Figure 120. ORTEP-3[265] plot of *cis*-$[Ru(\eta^2\text{-}O_2CCH_3)(dppe)_2][Cl]$ (**37**) in perspective view. H atoms, the solvent molecules and counter-ion (PF_6^-) are excluded for clarity (30% probability displacement ellipsoids). 136
Figure 121. ORTEP-3[265] plot of *trans*-$[PdCl(PEt_3)_2–C\equiv C–C_6H_4–C\equiv C]_2–C_6H_4(OC_2H_5)_2$ (**21b**). H atoms are excluded for clarity (30% probability displacement ellipsoids). Right side of the molecules was plotted with disordered atoms. 138
Figure 122. Decay of the fluorescence of the free ligands (**5a-d**, **10a-b**) and IRF. 140
Figure 123. Decay of the fluorescence for the Pd rods (**20a-d**, **21a-b**) and IRF. 140

Figure 124. ^{1}H NMR ($CDCl_3$, 400 MHz) spectrum of **5a**.....153
Figure 125. ^{1}H NMR ($CDCl_3$, 400 MHz) spectrum of **5b**. 154
Figure 126. Cyclic voltammograms for the single ringed PE free ligands **5a-b**.....154
Figure 127. ^{1}H NMR ($CDCl_3$, 400 MHz) spectrum of **5c**.....155
Figure 128. ^{1}H NMR ($CDCl_3$, 400 MHz) spectrum of **5d**. 156
Figure 129. Cyclic voltammograms for the single ringed PE free ligands **5c-d**.....157
Figure 130. UV-Vis spectra of the mono ringed PE ligands (**5b-d**) bearing side chains in CH_2Cl_2 at *ca.* $1x10^{-5}$ M. 157
Figure 131. FTIR spectra for the single ringed PE ligands (**5b-d**). 158
Figure 132. ^{1}H NMR ($CDCl_3$, 400 MHz) spectrum of **10a**.....159
Figure 133. ^{1}H NMR ($CDCl_3$, 400MHz) spectrum of **10b**.....161
Figure 134. UV-Vis spectra of the *tris* ringed PE ligands (**10a-b**) bearing side chains in CH_2Cl_2 at *ca.* $1x10^{-5}$ M..161
Figure 135. FTIR spectra for the tris ringed PE ligands (**10a-b**). 162
Figure 136. Cyclic voltammograms for the tris ringed PE free ligands (**10a-b)**.....162
Figure 137. ^{1}H NMR ($CDCl_3$, 400 MHz) spectrum of **14b**.....163
Figure 138. ^{1}H NMR ($CDCl_3$, 400 MHz) spectrum of **18b**.....164
Figure 139. UV-Vis spectra of the thiophene based ligands (**14b**, **18b**) in CH_2Cl_2 at *ca.* $1x10^{-5}$ M. 165
Figure 140. FTIR spectra for the thiophene based ligands (**14b** and **18b**). 165
Figure 141. Cyclic voltammograms for the thiophene based free ligands **(14b** and **18b)**. 166
Figure 142. ^{1}H NMR ($CDCl_3$, 400 MHz) spectrum of **20a**. 167
Figure 143. $^{31}P\{^{1}H\}$ NMR ($CDCl_3$, 161 MHz) spectrum of **20a**. 168
Figure 144. ^{1}H NMR ($CDCl_3$, 400 MHz) spectrum of **20b**.....169
Figure 145. $^{31}P\{^{1}H\}$ NMR ($CDCl_3$, 161 MHz) spectrum of **20b** using H_3PO_4 (85% aq.) as external reference. 170
Figure 146. ^{1}H NMR ($CDCl_3$, 400 MHz) spectrum of **20c**. 171
Figure 147. $^{31}P\{^{1}H\}$ NMR ($CDCl_3$, 161 MHz) spectrum of **20c** using H_3PO_4 (85% aq.) as external reference. 172
Figure 148. ^{1}H NMR ($CDCl_3$, 400 MHz) spectrum of **20d**.....173
Figure 149. $^{31}P\{^{1}H\}$ NMR ($CDCl_3$, 161 MHz) spectrum of **20d**. 174
Figure 150. UV-Vis spectra of the single ringed PE based palladium binuclear rods (**20b-d**) bearing side chains in CH_2Cl_2 at *ca.* $1x10^{-5}$ M. 174
Figure 151. FTIR spectra for the single ringed PE based palladium Rods (**20a-d**). 175
Figure 152. Cyclic voltammograms for Pd rods bridged by the shorter ligands (**20b-d**). 175
Figure 153. ^{1}H NMR ($CDCl_3$, 400 MHz) spectrum of **21a**. 177
Figure 154. $^{31}P\{^{1}H\}$ NMR ($CDCl_3$, 161 MHz) spectrum of **21a**. 177
Figure 155. ^{1}H NMR ($CDCl_3$, 400 MHz) spectrum of **21b**.....179
Figure 156. $^{31}P\{^{1}H\}$ NMR ($CDCl_3$, 161 MHz) spectrum of **21b**. 179
Figure 157. UV-Vis spectra of the tris ringed PE based palladium binuclear rods (**21a-b**) bearing side chains in CH_2Cl_2 at *ca.* $1x10^{-6}$ M. 180

Figure 158. FTIR spectra for the *tris* ringed PE based palladium Rods (**21a-b**). 180
Figure 159. Cyclic voltammograms for Pd rods bridged by the longer ligands (**21a-b**). 181
Figure 160. $^{31}P\{^{1}H\}$ NMR ($CDCl_3$, 161 MHz) spectrum of **23a**. 182
Figure 161. ^{1}H NMR($CDCl_3$, 400 MHz) spectrum of **23c**. 184
Figure 162. $^{31}P\{^{1}H\}$ NMR($CDCl_3$, 161 MHz) spectrum of **23c**.....184
Figure 163. ^{1}H NMR($CDCl_3$, 400 MHz) spectrum of **23d**. 186
Figure 164. $^{31}P\{^{1}H\}$ NMR($CDCl_3$, 161 MHz) spectrum of **23d**. 186
Figure 165. UV-Vis spectra of the single ringed PE based ruthenium rods (**23a**,**c-d**) in CH_2Cl_2 at *ca.* $6x10^{-6}$ M. ..187
Figure 166. FTIR spectra for the single ringed PE based ruthenium rods (**23a**,**c-d**). 187
Figure 167. Cyclic voltammograms for Ru rods bridged by the shorter ligands (**23c-d**). 188
Figure 168. ^{1}H NMR($CDCl_3$, 400 MHz) spectrum of **24a**. 189
Figure 169. $^{31}P\{^{1}H\}$ NMR($CDCl_3$, 161 MHz) spectrum of **24a** using H_3PO_4 (85% aq.) as external reference. 189
Figure 170. ^{1}H NMR($CDCl_3$, 400 MHz) spectrum of **24b**. 191
Figure 171. $^{31}P\{^{1}H\}$ NMR($CDCl_3$, 161 MHz) spectrum of **24b**. 191
Figure 172. UV-Vis Spectra of the tris ringed PE based ruthenium binuclear rods (**24a-b**) in CH_2Cl_2 at *ca.* $6x10^{-6}$ M. 192
Figure 173. FTIR spectra for the tris ringed PE based ruthenium rods (**24a-b**). 192
Figure 174. Cyclic voltammograms for Pd rods bridged by the longer ligands (**24a-b**). 193
Figure 175. ^{1}H NMR($CDCl_3$, 400 MHz) spectrum of **27**. 194
Figure 176. $^{31}P\{^{1}H\}$ NMR($CDCl_3$, 161 MHz) spectrum of **27**. 194
Figure 177. FTIR spectra for the thiophene based ruthenium rod **27** in KBr pellet.....195
Figure 178. ^{1}H NMR($CDCl_3$, 400 MHz) spectrum of **28**. 196
Figure 179. $^{31}P\{^{1}H\}$ NMR($CDCl_3$, 161 MHz) spectrum of **28** using H_3PO_4 (85% aq.) as external reference. 196
Figure 180. UV-Vis Spectra of the thiophene based ruthenium binuclear rods (**27**, **28**) and *trans*-$[RuCl_2(dppe)_2]$ (**36**) in CH_2Cl_2 at *ca.* $1x10^{-6}$M. 197
Figure 181. FTIR spectra for the thiophene based ruthenium rod **28** in KBr pellet.....197
Figure 182. Cyclic voltammograms for Pd rods bridged by the longer ligands (**27** and **28**). 198
Figure 183. ^{1}H NMR (CD_2Cl_2, 400 MHz) of compound **34**. 201
Figure 184. $^{31}P\{^{1}H\}$ NMR (CD_2Cl_2, 161 MHz) of compound **34**.....201

Figure A. 1: $^{13}C\{^{1}H\}$ NMR($CDCl_3$, 100 MHz) spectrum of **5a**. 213
Figure A. 2: $^{13}C\{^{1}H\}$ NMR($CDCl_3$, 100 MHz) spectrum of **5b**. 214
Figure A. 3: $^{13}C\{^{1}H\}$ NMR($CDCl_3$, 100 MHz) spectrum of **5c**.....214
Figure A. 4: $^{13}C\{^{1}H\}$ NMR($CDCl_3$, 100 MHz) spectrum of **5d**. 215
Figure A. 5: $^{13}C\{^{1}H\}$ NMR($CDCl_3$, 100 MHz) spectrum of **10a**. 215
Figure A. 6: $^{13}C\{^{1}H\}$ NMR($CDCl_3$, 100 MHz) spectrum of **10b**. 216
Figure A. 7: $^{13}C\{^{1}H\}$ NMR($CDCl_3$, 100 MHz) spectrum of **14b**. 216

Figure A. 8: $^{13}C\{^{1}H\}$ NMR($CDCl_3$, 100 MHz) spectrum of **18b**. 217
Figure A. 9: $^{13}C\{^{1}H\}$ NMR($CDCl_3$, 100 MHz) spectrum of **20a**. 217
Figure A. 10: $^{13}C\{^{1}H\}$ NMR($CDCl_3$, 100 MHz) spectrum of **20b**. 218
Figure A. 11: $^{13}C\{^{1}H\}$ NMR($CDCl_3$, 100 MHz) spectrum of **20c**. 218
Figure A. 12: $^{13}C\{^{1}H\}$ NMR($CDCl_3$, 100 MHz) spectrum of **20d**. 219
Figure A. 13: $^{13}C\{^{1}H\}$ NMR($CDCl_3$, 100 MHz) spectrum of **21a**. 219
Figure A. 14: $^{13}C\{^{1}H\}$ NMR($CDCl_3$, 100 MHz) spectrum of **21b**. 220
Figure A. 15: $^{13}C\{^{1}H\}$ NMR(CD_2Cl_2, 100 MHz) spectrum of **23c**. 220
Figure A. 16: $^{13}C\{^{1}H\}$ NMR(CD_2Cl_2, 100 MHz) spectrum of **23d**. 221
Figure A. 17: $^{13}C\{^{1}H\}$ NMR(CD_2Cl_2, 100 MHz) spectrum of **24a**. 221
Figure A. 18: $^{13}C\{^{1}H\}$ NMR(CD_2Cl_2, 100 MHz) spectrum of **24b**. 222
Figure A. 19: $^{13}C\{^{1}H\}$ NMR(CD_2Cl_2, 100 MHz) spectrum of **27**. 222
Figure A. 20: $^{13}C\{^{1}H\}$ NMR(CD_2Cl_2, 100 MHz) spectrum of **28**. 223
Figure A. 21: ESI-MS(TOF+) spectrum of **10a**. 223
Figure A. 22: ESI-MS(TOF+) spectrum of **10b**. 224
Figure A. 23: ESI-MS(TOF+) spectrum of **20a**. 224
Figure A. 24: ESI-MS(TOF+) spectrum of **20b**. 225
Figure A. 25: ESI-MS(TOF+) spectrum of **20c**. 225
Figure A. 26: ESI-MS(TOF+) spectrum of **20d**. 226
Figure A. 27: ESI-MS(TOF+) spectrum of **21a**. 226
Figure A. 28: ESI-MS(TOF+) spectrum of **21b**. 227
Figure A. 29: ESI-MS(TOF+) Spectrum of **23a**. 227
Figure A. 30: ESI-MS(TOF+) Spectrum of **23c**. 228
Figure A. 31: ESI-MS(TOF+) Spectrum of **23d**. 228
Figure A. 32: ESI-MS(TOF+) Spectrum of **24a**. 229
Figure A. 33: ESI-MS(TOF+) Spectrum of **24b**. 229
Figure A. 34: ESI-MS(TOF+) Spectrum of **27**. 229
Figure A. 35: ESI-MS(TOF+) Spectrum of **28**. 230
Figure A. 36: Mercury[266] plot of **8c** to show angle formed by the planes of the central and terminal phenyl moieties. Hydrogen atoms omitted for clarity. 232
Figure A. 37: Mercury[266] plot of **8b** to show packing. 232
Figure A. 38: Mercury[266] plot of **8b** to show short contacts in a different perspective. 232
Figure A. 39: Mercury[266] plot of **10a** showing the angle formed between phenyl ring planes. 233
Figure A. 40: Mercury[266] plot of **34** showing packing. 234
Figure A. 41: Mercury[266] plot of **34** showing short contacts. 234
Figure A. 42: Mercury[266] plot of **34** showing CPK model. Chloride perspective (left), hydride perspective (right). 234

Figure A. 43: Mercury[266] plot of **37** showing packing. 235
Figure A. 44: Mercury[266] plot of **37** showing short contacts. 236
Figure A. 45: Mercury[266] plot of angle formed between the phenyl moieties in **20c**. 237
Figure A. 46: Mercury[266] plot of **20b** showing short contacts. 237
Figure A. 47: Mercury[266] plot of **20b** showing packing. 238
Figure A. 48: Perspective ORTEP-3[265] plot of **38**[293] (50% probability displacement ellipsoids). 239
Figure A. 49: Perspective ORTEP-3[265] plot of **38**. 239
Figure A. 50: Mercury[266] plot of **38** to show hydrogen bonding between terminal nitrogen and aromatic hydrogen atoms. 239

Scheme Index

Scheme 1. General representation of electron conduction in a photonic and a redox molecular wire. Adapted from ref. [3b]. 18

Scheme 2. Charge transport though electron or hole transfer. D, B and A are donor fragment, bridging ligand and acceptor fragment, respectivally. Adapted from ref. [2c]. 19

Scheme 3. Charge transport for the systems reported by Rigaut and co-workers at 5K: (a) direct tunnelling for **13a** and **13b** junctions, (b) sequential tunnelling for the **13c** junction. Adapted from refs. [53f, 57]. 21

Scheme 4. Formation of MV compounds (Class I and II) M_1^{n+1}–L–M_2^{n} and M_1^{n}–L–M_2^{n+1} (K_c = comproportionation constant). 21

Scheme 5. Totally delocalized Class III system with a large K_c 22

Scheme 6. Conditions and classification for mixed-valence binuclear systems.Adapted from ref. [58]. 24

Scheme 7. Relation between acetylide, cumulene and carbyne mesomeric forms. Adapted from ref. [72]. 31

Scheme 8. The two types of orientation reported for these dicarboxylate binuclear complexes. Adapted from ref. [103b]. 44

Scheme 9. General cartoon of the FRET process. Adapted from ref. [119]. 51

Scheme 10. Cartoon of a cross-wire junction. Adapted from ref. [158b]. 63

Scheme 11. Cartoon of top-contact junction using metal beads. Adapted from ref. [157]. 64

Scheme 12. Schematic of the experimental setup used by Tao and co-workers. Adapted from ref. [162]. 65

Scheme 13. General mechanism for the Pd catalyzed cross couplings. Adapted from ref. [189, 192]. 77

Scheme 14. Catalytic cycle when Pd^{II} catalyst are used. Adapted from ref. [198]. 78

Scheme 15. General mechanistic pathway for the preparation of Ru acetylides. Adapted from ref. [66c, 203]. 80

Table index

Table 1: Overview of the palladium catalyzed coupling reactions, adapted from ref. [188b, 189]. 76
Table 2: Selected values for maximum absorption peaks and their respective molar extinction coefficients for the free ligands (**5a-d**, **10a-b**, **14b** and **18b**). 106
Table 3: Selected values for maximum absorption peaks and their respective molar extinction coefficients for the palladium rods (**20a-d**, **21a-b**) and the free Pd complex (**19**). 109
Table 4: Selected values for maximum absorption peaks and their respective molar extinction coefficients for the ruthenium rods (**23a,c-d**, **24a-b**, **27** and **28**) and the free Ru complex (**36**). 113
Table 5: Selected electrochemical data for the prepared palladium (**20a-d**, **21a-b**) and ruthenium rods (**23a**,**c-d**, **24a-b**). 120
Table 6: Selected NMR data for the prepared palladium (**20a-d**, **21a-b**) and ruthenium rods (**23a**,**c-d**, **24a-b**, **27** and **28**). Chemical shifts in parenthesis are relative to the free ligands. 122
Table 7: Selected vibrational data for the prepared compounds based on the shorter bridging phenylene ethynylene ligands (**5a-d**), obtained through FTIR-ATR (diamond). 123
Table 8: Selected vibrational data for the prepared compounds based on the longer bridging phenylene ethynylene ligands (**10a-b**), obtained through FTIR-ATR (diamond). 125
Table 9: Selected vibrational data for the prepared compounds based on the bridging thiophenylene ethynylene ligands (**14b** and **18b**), obtained through FTIR-ATR (diamond)[a]. 126
Table 10: Selected ESI-MS(TOF) peaks for the prepared palladium (**20a-d**, **21a-b**) and ruthenium rods (**23a**,**c-d**, **24a-b**). 127
Table 11: Solid state fluorescence time-of-life values for the prepared free ligands (**5a-d**, **10a-b**) and Pd rods (**20a-d**, **21a-b**). 141

Table A. 1: Selected values for the cyclic voltammetry studies of **23c-d**. 230
Table A. 2: Selected crystal data for the structures of **4c**, **5c-d**,[210, 293] **8b**, **10a**, **21b, 34, 37, 38**. 231
Table A. 3: Selected bond (Å) and angle (º) values for **8b**. 233
Table A. 4: Selected bond (Å) and angle (º) values for **10a**. 233
Table A. 5: Selected bond (Å) and angle (º) values for **34**. 235
Table A. 6: Selected bond (Å) and angle (º) values for **37**. 236
Table A. 7: Selected bond (Å) and angle (º) values for **20b**. 238
Table A. 8: Fluorescence decay data for some of the starting materials (**4a-b** and **9b**), some free ligands (**10b**), some Pd rods (**20c** and **21a**) and some Ru rods (**23c-d**, **24a-b** and **39**). 240

Chapter I – Introduction

Introduction

In this chapter, the literature review concerning the general field of Molecular Electronics will be presented. This review is mostly related to the molecular wire materials since it is the main focus of this work. Furthermore, special attention is given to organometallic wires of the M – L – M type (where M is a transition metal centre and L is a bridging ligand). Some of the characterization techniques usually associated with the field of molecular wires will also be discussed as well as fluorescence properties that some of these materials also exhibit.

I.1. Molecular electronics

With the increasing demand for the further miniaturization of the electronic devices that are more and more a part of everyday life, comes the increase of costs and the demand for innovation. Intel®, of which emerged the industry's most known prediction, *Moore's Law*[*] (Figure 1), is already looking beyond CMOS (Complementary Metal Oxide Semiconductor) for alternative computing mechanisms and logic devices, since it expects the physical limits of atomic structures or power density to be reached by 2020.[1-2] Nevertheless, Intel® has announced very recently a breakthrough in the manufacture of chips by finally being able to produce the 3D tri-gate architecture that was reported in 2002. This new architecture is thought to bring better integration, performance, and power efficiency and could, technically, prolong silicon technology's lifespan.[2c, 3]

One of the major limiting aspects of this technology pertains to the doping of silicon with electron donors (n doped) and electron acceptors (p doped) which effectively create the electron and hole-inversion layers. The density of these doping agents is a lot lower than those of the atoms that constitute the bulk of the device. As such, as down scaling is pushed further and further down, the necessity of transistors that would not use doping agents arises.[2a, 2b, 3b]

[*]The law is named after Intel's co-founder Gordon E. Moore, who described the trend in his 1965 paper. It noted that number of components in integrated circuits had doubled every year from the invention of the integrated circuit in 1958 until 1965 and predicted that the trend would continue "for at least ten years".[1]

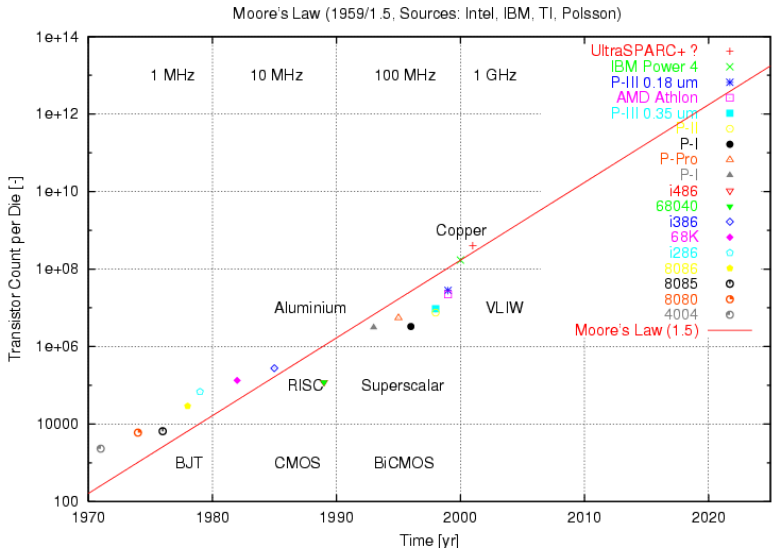

Figure 1. Cartoon depicting Moore's Law across a wide time span.[4]

One other issue related to scaling is a consequence of the current lithography technology used for the preparation of chips. This technique makes use of photo sensitive patterned layers that are engraved by – currently – radiation on the extreme ultraviolet. The obvious roadblock will come when the scale of these patterns is the same or smaller than that of the radiation being used. Immediate analysis of this problem would point to the usage of X-ray radiation or ion/electron beams. The main problem here would of course be the cost and efficiency of the process which is hard to predict but nevertheless carries with it substantial investments.[2a, 2b, 3b]

Furthermore, charge leakage can happen when the silicon oxide layers (isolation) are three atoms thin. Silicon also loses its band structure when used in small sizes. All of these problems and their associated solution will eventually lead to a rise in the cost of building new factories for wafer and chip production.[2a, 2b, 3b, 5]

Moreover, some advances on the application of other types of materials or techniques for the preparation of these devices were reported. For example, usage of GaAs and AlAs, quantum wells, wires and dots, modulation doping (selective doping of layers) and resonant tunnelling. There is however, no contest to silicon oxide as an insulator in the semi-conductor applications.[2a, 2b, 3b, 5]

Other improvements that would lead to smaller and smaller devices still suffer from application constraints, *e.g.*, single electron condensers, which needs either very low temperatures or extremely small size (~ 1 nm) to work at ambient temperature.[2a, 2b]

One of the possible alternatives is to build and tailor these components from the "bottom-up". Effectively preparing these devices from molecular building blocks as it was once envisioned by Richard Phillips Feynman on his famous talk given on December 29th 1959 at the annual meeting of the American Physical Society at California Institute of Technology (Caltech)[6] which can now be found reproduced and referenced in many nanotechnology or nanoscience related articles.[2]

Furthermore, the molecular electronics addressed in this dissertation are those pertaining to the use of molecular scale components instead of the molecular materials for electronics (that encompass films, crystals, LEDs, OLEDs, *etc.*).[2a, 2b, 5]

As such, molecular electronics (sometimes also called plastic electronics) aims to find single molecules or small groups of molecules that can be used as the discrete electronic units, *e.g.* wires, switches, memory as well as gain devices.[7] To achieve this, several steps have to be taken: preparation and characterization of the molecules (with great care given to its properties); oriented arrangement of the single molecules; attachment and effective communication with the outside/macro world and finally electrically addressing single molecule devices.[7]

The importance of this matter was recognized in 2000 with the Nobel prize in chemistry "*for the discovery and development of electrically conductive polymers*" attributed to Professors Alan J. Heeger, Alan G. MacDiarmid and Hideki Shirakawa, as well as in 2001, when Science magazine attributed breakthrough of the year to Heath and co-workers for their cross-bar semi-conductors.[7] Molecular electronics have several intrinsic advantages that arise for their bottom-up origins. One good example of this, is that 500 g of a tris(ethynelene phenylene) organic wire contains around one mole of molecules (*ca.* 6 x 10^{23} molecules) which is in fact more potential molecular wires than the number of transistors (the main component of any modern computer chip) that has ever been made in the history of the world.[5] Notwithstanding, the addressing of large arrays of ordered molecular devices is still impossible, but the potential is high enough to maintain and justify the current and future research efforts.[8] As such, molecular electronics are effectively competitive in terms of substituting the silicon based microelectronics.

There are however several drawbacks to this approach. As much evidenced by the years this subject has already been studied and not yet commercially adopted, it remains a demanding challenge to prepare molecular wires that would be able to grow in length and at the same time, control its shape at each step as well as the purity of the final product. Testing, which means interaction with the macroscopic world is also another hurdle, as the wires would have to be able to communicate with the exterior. Moreover, there is no assurance that these wires will exhibit the same properties as their bulk counterparts or that some other new properties, beneficial or otherwise, will arise from the usage of such small individual devices. Single molecule testing is then very important in this case.[2a, 2b, 8b]

Self-assembly is one of most advantageous characteristics of molecular electronics, since it is known that great ordering and templating are possible using this process. Moreover, as the complexity of scaling-down of silicon devices increases greatly, self-assembly is possible with the smallest of molecular components. Nevertheless, the creation of complex circuitry by this method will be very demanding since, at this point, self-assembly usually yields only mostly regular structures. Also the high number of actual devices produced by this method, and their arrangement, will also prove to be problematic.[2a, 2b, 8b]

Reliability of these molecular devices should be one of the biggest hurdles to surpass, since deformation energies (formation of electronic defects) are smaller than the electron affinities of known organic electronic devices. Other problems like melting points and heat capacity also make the use of such devices less reliable than the established silicon systems.[2a, 2b]

One major concern often brought up when molecular electronics are addressed, is the matter of interconnects. Although monolayer connections present a very successful approach to this problem there is still sizeable lack of understanding of the precise electronic structure of the molecule/metal interface. As such, this creates an essential research topic as any changes to these interconnects will certainly influence the electronic structure of the device.[2a, 2b, 8b]

Power dissipation through the molecular networks, and thus the inherent need for gain, is another current drawback to molecular wires since this would restrict the building of working logic systems.[2a, 2b, 8b]

There are no near-future or cleat-cut solutions to most of these problems and the general idea, albeit a very obvious one is that there will be hybrid silicon/molecular electronic devices.[2a, 2b, 8b]

On a higher engineering level, the next step in molecular electronics would then their implementation in IT (Information Technology) systems. In order to properly prepare systems usable in molecular computing, three accepted approaches have surfaced: Quantum cellular automata which is based on electrostatic field repulsions to transport information throughout the circuitry and has the major benefit of heat generation since only a small portion of the electrons is used (in contrast to classical chips); massively parallelization of components to the point where defects are tolerable like it was demonstrated by Hewlett-Packard™ with their computer TERAMAC (Tera Multiple Architecture Computer).[2c, 9] The third approach uses molecular-scale switches as a part of *nanocell electronic memories* where each molecule performs logic functions, but are not address individually.[2a, 2b, 8b]

I.2. Molecular wires

The focus of this work is indeed molecular wires, a term which has been defined by several authors. Nevertheless it is the description given by Jean-Marie Lehn that is mostly used. As such, a molecular wire is a *one dimensional molecule allowing a through-bridge exchange of an electron/hole between its remote ends/terminal groups, themselves able to exchange electrons with the outside world*.[10] As such, this compound would have to bare two redox-active termini; well-defined structure only achieved by proper synthetic planning as well as to be able to transport charge in an efficient manner over a long distance (nano distances, but longer than typical tunnelling distances < 4 nm). Furthermore transport (or electron transfer, ET) through a discrete molecular wire is only possible when electronic states extend along the molecule to which the carrier must be able to access and travel along them without recombining. Finally these states have to be accessible to the metal electrode or contact with the outside world.[1-2, 11]

Aviram and Ratner[12] proposed in 1974 that some organic molecules could be used as molecular wires or rectifiers and since then the search for this type of compounds has been quite intensive. This effort was accompanied by the preparation of organic molecules that spanned a π-electron network all over its length. These are generally built from very elemental building blocks by iterative steps leading to molecules that can be as long as 128 Å (Figure 2).[13]

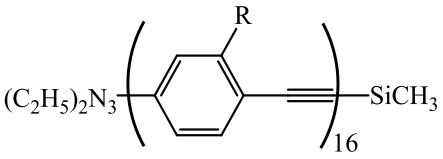

1

Figure 2. 128Å long organic rod (**1**) prepared by Schumm and co-workers. R = 3-ethylheptyl.[13a]

Molecular wires have to be electron or hole conducting in order to effectively transport a current. Furthermore, this electronic pathway is more efficient than electron transport through space. There are several classes of different potential wires. These include, but are not limited to, conjugated hydrocarbons, carbon nanotubes, porphyrin oligomers (*e.g.* Figure 3) or DNA (used as a scaffolding agent which holds fluorescent dyes).[14]

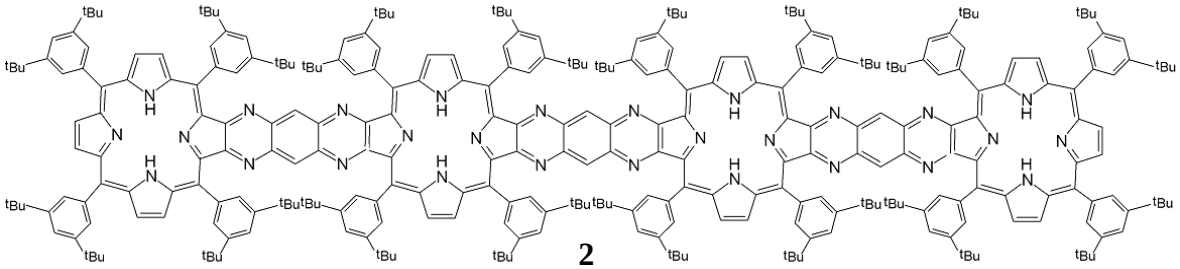

2

Figure 3. An example (**2**) of a tetrakisporphyrin system (*t*-Bu is *tert*-butyl).[15]

Molecules bearing large and robust conjugate backbones are, as expected, an important potential source for molecular electronics. As such, ligand families like aryldiethynyls, alkynyls, arylethynyls and cumulenes have been receiving a lot of attention in the mentioned field [16] as supported by Grozema and co-workers, that found that π-conjugated carbon polymers present comparable (and sometimes) higher hole mobilities as the σ-bonded silicon.[17]

The work presented here, was mainly based on the preparation and characterization of aryldiethynyls as bridging ligands in binuclear $[RuCl(dppe)_2]^+$ and $[PdCl(PEt_3)_2]^+$ molecular wires (where dppe is 1,2-diphenylphosphinoethane and Et is ethyl). As such, the properties relevant to molecular electronics are the most important. Nevertheless, this family is known to have several interesting application in materials that would have reversible redox chemistry, easily accessible mixed-valent states in binuclear complexes, liquid crystalline behaviour, luminescence and third order non-linear optical materials.[16]

I.3. Organic molecular wires

As mentioned previously the first proposed molecular wires were purely organic. As such the research on this type of molecules has been relentless, yielding a variety of candidates that include oligo(2,5-thiophene ethynylene)s (OTEs), oligo(1,4-phenylene ethynylene)s (OPEs), oligo(1,4-phenylene vinylene)s, aromatic ladder oligomers, oligophenylenes and acetylene oligomers. Also included in this classification are carbon nanotubes and graphene.[18]

Conjugation is very important to this type of wires and as such ring co-planarity may influence properties such as delocalization through the wire which will result in increased electronic transport. Rotzler and co-workers reported lower oscillator strength and thus lower quadratic response in EFISH measurements when severe twisting was forced on the rings.[19] Mishchenko and colleagues elaborated on this premise with STM break-junction conductance measurements of a family of biphenyls with constrained torsion angles.[20] The same conclusions were established by experimental as well as theoretical calculations. The importance of the π orbital overlap in these systems was also confirmed as the major factor in electronic transport.[18]

A very popular and efficient way of maintaining rod-like structure as well as maximum orbital overlap (for delocalization) is to use the alkynyl moiety.[5] In spite of its lower transport properties in relation to double bounds, there are some reports related to the transport being limited by structural re-organization in alkenyl (phenylvinylenes) based compounds.[21]

A general overlook of several classes of organic wires follow. It is noteworthy that some are (if not most of them) also used as spacer/bridging ligands for organometallic wires.

I.3.1. Oligo(2,5-thiophene ethynylene)s

The heavily studied poly(α,α'-thiophene) polymers (PT) show some good characteristics, in respect to electronic transport, when compared to the poly(*p*-phenylene) polymers (PPP) and are used in a number of applications usually related to their optoelectronic properties, such as their low bandgap,[22] low temperature phosphorescence and fluorescence (only fluorescent at room temperature)[22g] and as fluorescent biomarkers.[22h] In the case of PT,

reports point out that the charge is not as bound to the ring as in the case of the PPP, thus making it more available for more extensive delocalization. Furthermore, the bonds are shorter for PT (1.48 *vs.* 1.507 Å) making the π contribution larger.[22a, 22b] The increase in chain length can be monitored by the intense red shift observed in the UV-Vis spectrum as the number of thiophene units increases (due the strong π – π* absorption band). Nevertheless, this direct relation is only reproducible for small oligomers, since there is a point when saturation is reached. This deviation from linearity is then the conjugation length. Although most authors have reported conjugation lengths of no more than 20 thiophene units, the group of Otsubo has shown that their 96-mer is in accordance with the linear dependency effectively increasing the conjugation length to at least this 37.2 nm long oligothiophene (Figure 4).[23]

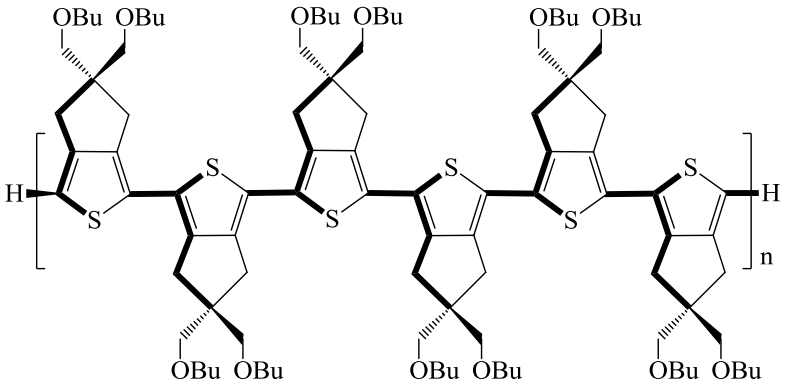

3: n = 1 (**6T**), n = 2 (**12T**), n = 3 (**18T**), n = 4 (**24T**), n = 6 (**36T**), n = 8 (**48T**), n = 12 (**72T**), n = 16 (**96T**)

Figure 4. The thiophene oligomers (**3**) prepared by the group of Otsubo.[23]

As such, the thiophene moiety is an interesting building block for molecular wires. Nevertheless, the steric hindrance brought about in these PT or PPP polymers actually does decrease delocalization. This is due to twisting around the single bond which effectively decreases π overlap, trapping the electrons in a few monomers. In the case of PPP, this conjugation was found to extend only to 3-5 rings.[24] Although adopting a planar configuration on the solid state, the PT has a reported conjugation length of 6 rings.[22b] An acetylene spacer is then a possible way of maintaining the π-orbital overlap as well as linear rigidity, thus and increase the conjugation length.

The 2,5-diethynylthiophene derivatives were deeply studied by Tour and co-workers which produced quite long wires like the one already referenced above with 128 Å.[5, 13a] These

are easily prepared by iterative synthesis that doubles the size of the wire at each step.[5, 13a] The thiophenylene ethynylene class of compounds is also known for its derived polymers which show good photoluminescence and photovoltaic properties. These properties in conjunction with the extended conjugation can also lead to good photonic wires when appropriate acceptors are used.[25]

Moreover, thiophenes and especially polythiophenes have proven to be excellent donor materials for photovoltaic devices. This is generally attributed to a high degree of intermolecular ordering. Studies show that the inclusion of the ethynylthiophene polymer helped improve the photovoltaic properties of the final phenylene-ethynylene-thiophenylene co-polymer (Figure 5).[26]

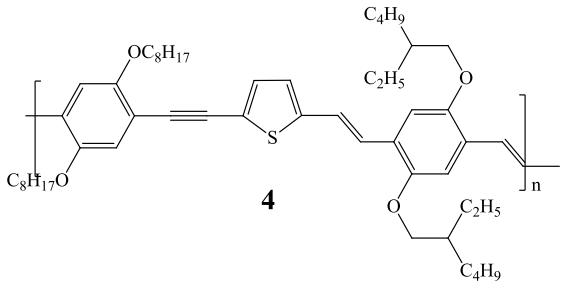

4

Figure 5. The thiophene-containing arylene-ethynylene/arylene-vinylene co-polymer (**4**).[26]

In clear similarity with the report from 1994,[13a] Tour published in 1996[27] and 1997[28] a 2,5-thiophene ethynylene based wire. The wire was predicted to also be 128Å long (Figure 6).[28]

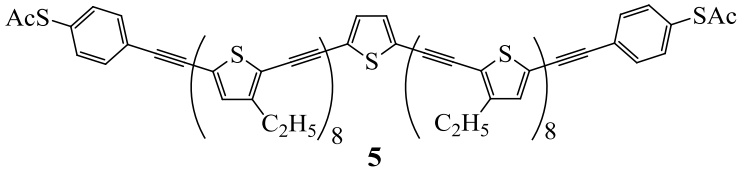

5

Figure 6. The oligo(2,5-thiophene ethynylene) potential wire (**5**) prepared by the group of Tour (Ac = Acetyl $C(O)CH_3$).[27-28]

I.3.2. Oligo(1,4-phenylene ethynylene)

Oligo phenylene ethynylenes have found a very wide range of applications. Some of them involve fluorescence[29] and phosphorescence.[30] This is probably the most studied class of compounds in this research field not only as organic wires *per se* but as bridging ligands for organometallic wires. This is possibly due to its inherent rod-like geometry and the great potential delocalization throughout the π backbone (Figure 7).[5] These compounds are normally prepared by a series of coupling reactions that permit the rapid increase of the wires length, which takes advantage of side chains to maintain the compound soluble (after three phenylene ethynylene moieties, the solubility decreases rapidly in common used solvents).[5]

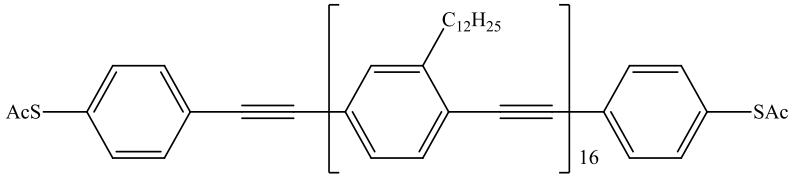

6

Figure 7. One of Tour's OPE wires (Ac = acetyl group, $C(O)CH_3$).[5]

Depending on the attached side chain/group, some interesting properties were found when studying these OPE wires. For example, switching (from conducting to non-conducting) was found in the molecules depicted in Figure 8 as well as negative differential resistance (NDR) behaviour thought to arise from conformational changes.[5]

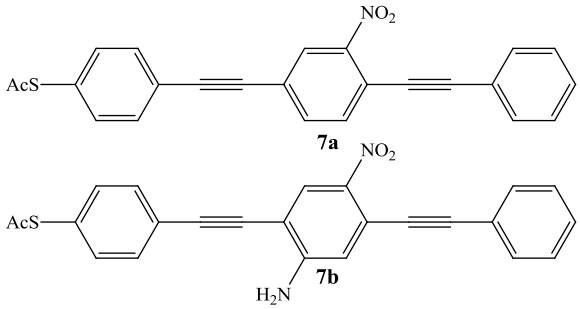

Figure 8. Organic molecular (**7a-b**) wires with switching properties.[5]

I.3.3. Oligo(1,4-phenylene vinylene)s

Oligo(1,4-phenylene vinylene)s (OPVs) have been mostly seen applications in optical and OLED field (used nowadays in their polymer form in OLEDs)[31] but some molecular wires oriented compounds have been reported.[5]

Tour's group also studied this type of compounds while also adding phenylene sidegroups substituents to probe for switching characteristics.[5] Detert and Sugiono studied the effect of electron withdrawing and electron donating groups on the phenylene and vinylene sections of the wire.[32]

Chidsey *et al.* reported an OPV with up to 28Å that acts as good conductors having their electron transfer rates limited by structural reorganization.[21a] Moreover Wasielewski and co-workers[21b] reported that the electron transfer rate in the compound presented, as an example, in Figure 9 is highly depended on the low frequency torsion motion.[21b]

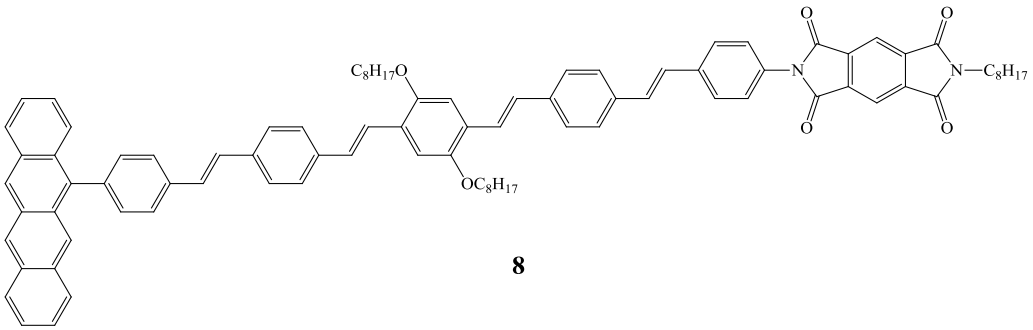

8

Figure 9. One of the OPVs studied by Wasielewski and co-workers.[21b]

I.3.4. Aromatic ladder oligomers

Taking advantage of the inherent rigidity and extended π-conjugation, the preparation of organic ladders has been reported by several authors.[5]

As a good example of these wires, Gourdon and co-workers have reported a series of oligo(quinoxaline)s (Figure 10) and oligobenzoanthracenes prepared by successive condensation reactions, which showed good electron transfer as well as good electron coupling with the used metallic contacts. One of the main advantages of this type of molecules is the absence of internal rotational motion.[33]

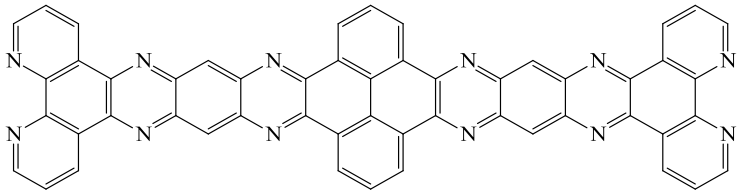

9

Figure 10. One of the oligo(quinoxaline)s reported by Gourdon.[33]

I.3.5. Oligophenylenes

Oligophenylenes have found applications not only in the molecular wires field but also in photoluminescence materials. Nevertheless, oligophenylenes are usually reported either bearing side chains, or incorporating other moieties in the backbone.[5]

Bryce *et al.* prepared a series of fluorenones (example in Figure 11) based molecular wires that show reversible cathodic behaviour in solution which arises from the reduction of the fluorenone moieties, where the oligophenylene is the fluorene portion. Incorporation of oligophenylene moieties is necessary, since as the number of phenyl rings, increases solubility decreases and processability becomes a problem.[34]

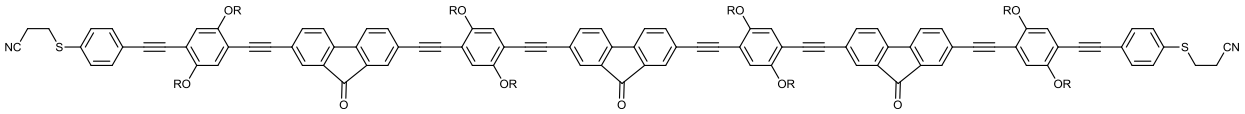

10

Figure 11. An example of the fluorenone based molecular wires prepared by Bryce's group.[34]

Nevertheless, the main disadvantage of oligophenylenes is their torsional twisting caused by steric hindrance between hydrogen atoms of adjacent rings.[5]

I.3.6. Carbon nanotubes

Carbon nanotubes (CNTs), although showing great promise in the field of molecular electronics, suffer from insolubility problems. The most obvious solution would be functionalization of the tubes, but this has proven problematic since the electric properties are

changed and in some cases drastically so.[2a, 5] As an example, orientation of the fluorination along the tubes can lead to insulating or metallic properties as reported by Seifert.[35]

Nevertheless, interesting applications are available in the literature in regard to carbon nanotubes. For example, the group of Mayor, reported the electroluminescence of a OPE (Figure 12) set up in between two metallic carbon nanotube electrodes.[36]

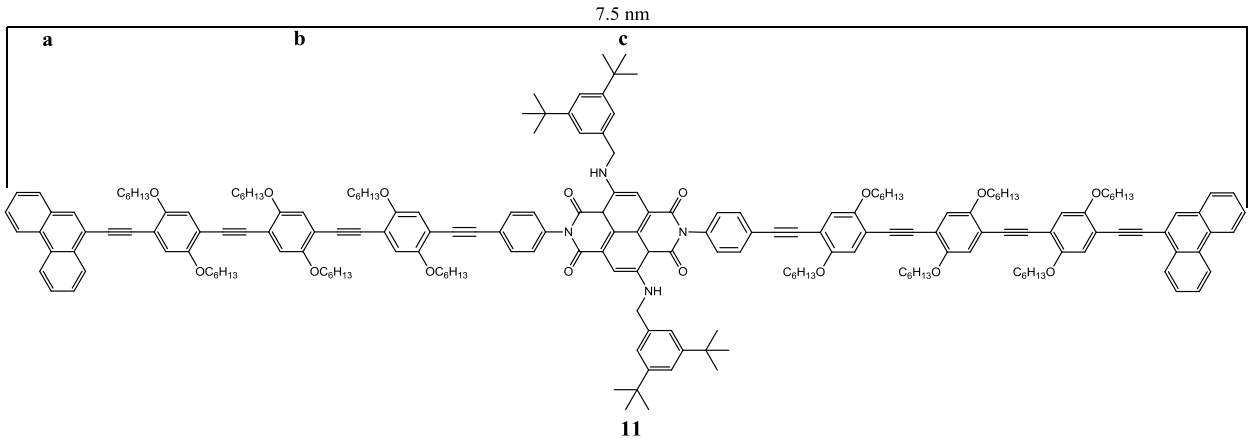

Figure 12. OPE rod used by Mayor's group bearing a central 2,6-dibenzylamino core-substituted cromophore. a = phenanthrene π-system; b = OPE rod; c = NDI (N,N-naphtalenediimides) chromophore. Adapted from ref. [36].

The group thus managed to trap a single molecule in a gap opened in the carbon nanotube by electric breakdown. The OPE was then transplanted to the gap by dielectrophoresis forming molecular junctions with the CNT electrodes. Electroluminescence was observed for potentials over 4V.[36]

I.3.7. Graphene

The 2010 Nobel Prize in physics was awarded to Andre Geim and Konstantin Novoselov "*for groundbreaking experiments regarding the two-dimensional material graphene*". Geim and Novoselov were the first authors to report the preparation (by flaking graphite with adhesive tape) and electric characterization of single layers of graphene (Figure 13).[37]

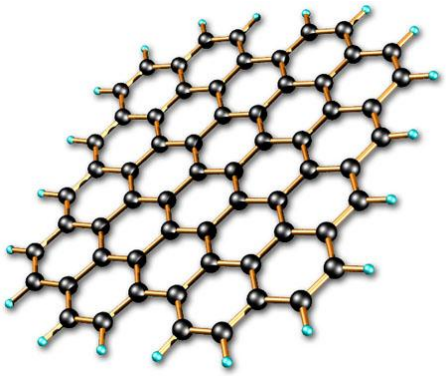

Figure 13. Cartoon of an atom thick graphene sheet.[38]

Since then, the engineering of graphene for electronic applications, especially the preparation of transistor devices boomed in recent years†, mainly due to the recent possibilities to prepare single layer, atom thick slices of this material. Nevertheless, it was the latest developments in growing the material on a wafer that really pushed its properties (better purity, less defects, etc.) and allowed to go from 26 (flaked graphene) to 100 GHz as recently announced by IBM. Even in the case of the flaked graphene, it is a noteworthy advance to the current generation silicon transistors. These grown graphene transistors are expected to be used in a few years for large scale applications and in a decade for computer processors, when the problems associated with integration to the established technology are surpassed‡.[39]

Nevertheless, some recent reports point to a decrease in ballistic conduction in graphene upon very small defects on the sp^2 carbon network, which can indicate some future trouble with modification and functionalization.[41]

I.4. Metallomolecular wires

"Metallomolecular wires" is a fairly general way of describing any complex that is meant to transport electron from on terminal to the other. Nevertheless, the interest of this work

†Searching in Web of Science for graphene, yielded 190 papers in 2004 which grew every year to 4,276 in 2010. Searching for graphene word in the paper title in Science yielded 75 for the same time period.
‡Some of the information was retrieved from an interview done to the authors of ref. [39] available at ref. [40].

lies with the binuclear OPE bridged systems bearing transition metal complexes as terminal redox centres. Although other types of binuclear (or dinuclear) complexes are widely available, the ones referred in this work are those based on the [{ML_n}(μ-bridge){ML_n}] type of complexes (where M is the metal centre, bridge is the bridging ligand and L represents any ancillary ligand) or some kind of derivative. Furthermore, the most important wires for this dissertation are indeed based on a highly conjugated ligand bridging two transition metal complexes like the ones based in 1,4-diethynylbenzene derivatives. For other types of binuclear complexes see, for example, the 2005 review by Ren on di-ruthenium alkynyl complexes[42] or the review on molecular wires bearing clusters termini by Akita and Koike.[43]

As such these metallomolecular wires consist of redox-active metal centres connected by a π-conjugated bridge. These metal fragments add not only sophisticated redox properties but also magnetic ones.[44] Furthermore, metal complexes allow for fine control of electronic and structural properties as a function of the ancillary phosphine ligands (*e.g.* the dppe ligand featured in this work) permitting the easy access to several oxidation states. These can also help stabilize carbon rich species like acetylides and protect not only the coordination site of the ligand, but the bridge itself when, for example bulky phosphines or long alkylphosphines are used.[2c, 3b, 45] Moreover, redox-active metal complexes that include a bridging ligand are of high importance to this matter as stable delocalized mixed-valence (MV) systems are available at low potentials in relatively controlled conditions. The assessment of electronic communication in these systems can also be done using common spectroscopic techniques[46] as described in the next section.

Nevertheless, there are some drawbacks associated with organometallic wires in contrast to their organic counterparts. These are associated to stability of the final systems when labile metals are used which can hinder purification and isolation attempts as well as increase handling difficulty upon preparation and purification.[3b]

Although not a specific property of metallomolecular wires (there are reports of mixed valence organic wires), redox molecular wires are often binuclear transition metal complexes. When the termini are of different redox states a MV system is formed bearing an odd electron. This compound can be generated electrochemically. Further information of the different aspects of this system will be discussed further on. The first report of a MV system was performed by Creutz and Taube[47] in 1969. Redox molecular wires are representative of a simplified

conduction mechanism (Scheme 1) when compared with the photonic wires (briefly described later on).[3b] In respect to binuclear heterometallic systems, Ceccon and co-workers reviewed this matter in 2004[48] and as for trimetallic and polimetallic systems, a very good review was recently published by Low *et al*..[49]

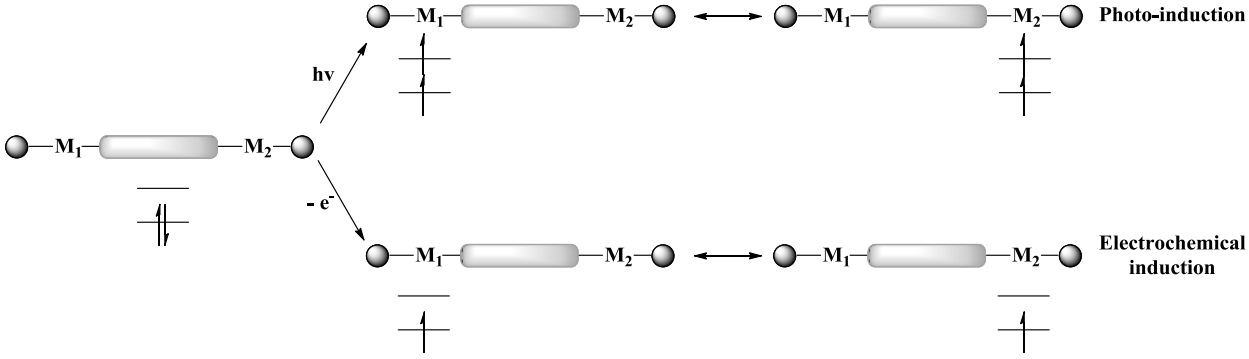

Scheme 1. General representation of electron conduction in a photonic and a redox molecular wire. Adapted from ref. [3b].

As with the organic devices, systems other than wires have already been reported that are based in metal complexes. As an example, there are the single electron transistors based materials with $[Co(tpy\text{-}(CH_2)_5\text{-}SH)_2]^{+}$[50] (where tpy is 2,2';6',2''-terpyridine) and $[\{Me_3tacn)V(CN)_2\}_2(\mu\text{-}C_4N_4)]$[51] (where tacn is (*N,N',N''*-trimethyl-1,4,7-triazacyclononane).[2c]

Regarding the choice of Ru moieties, there have been numerous reports of this metal's ability to work not only as a robust redox centre but also as a connector which allows electron flow between different elements in carbon-rich systems.[52] Furthermore, several reports have pointed out that ruthenium carbon rich complexes display not only interesting properties but also increased conductance when compared to platinum adducts and their organic counterparts.[52g, 52k, 53]

I.5. Transport and classification of homo binuclear organometallic complexes

Electron transport (henceforth transport) across molecules is usually divided into two types: superexchange (coherent superexchange or tunnelling) and hopping (incoherent charge hopping). In the superexchange mechanism, the orbitals of the donor and acceptor fragments are thought to overlap with the HOMO and LUMO of the bridging group, whilst regarding the direct orbital overlaps between donor and acceptor as negligible. This basically amounts to indirect mixing of the donor acceptor wave functions mediated by the bridging component thus leading to an indirect coupling. In the hoping mechanism, the electron (or hole) resides (transiently, Scheme 2) on the bridging group leading to the formation of a chemical intermediate.[54]

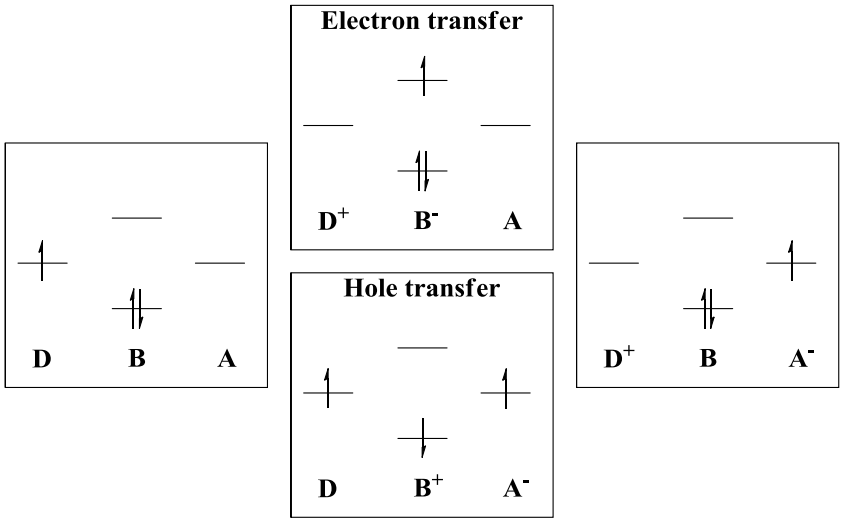

Scheme 2. Charge transport though electron or hole transfer. D, B and A are donor fragment, bridging ligand and acceptor fragment, respectivally. Adapted from ref. [2c].

Although it is thought that superexchange is prevalent in shorter systems, and hoping is then the more viable transport path in longer systems (*e.g.* with more than 4 or 5 phenyl units), recent studies have come to show that the two mechanisms may work together to ensure transport in molecular wires.[2c, 54b, 54c]

For short bridges, the rate of transfer is dependent of the distance between donor and acceptor (type of systems relevant to this work) and decays exponentially with it, but after a

certain length it becomes mostly independent of this distance. This behaviour is usually attributed to coherent tunnelling in the shorter systems and incoherent hoping in the larger systems. Orbitals and energy bands can be regarded, in regular molecules and crystals, as standing waves or interference patterns of the electron wave-function in a static potential.[2c, 55] This makes coherent charge transport a function of quantum interference effects. Nevertheless, real systems are not static and subject to a great number of degrees of freedom. As such in large molecular systems, purely quantum mechanical interference effects are likely to be suppressed.[2c, 55]

Moreover, and in respect to the systems which are interesting for this introduction, Mahapatro and co-workers have reported resonant tunnelling in nanogap self-assembled molecular junctions of *trans*-[$Ru_2(ap)_4((C{\equiv}CC_6H_4)_nS–)_2$] (*n* = 1, 2; ap = anilinopyridinate, Figure 14) along with hysteresis in I-V traces that the group attributes to possible charge storage in the molecules.[53e]

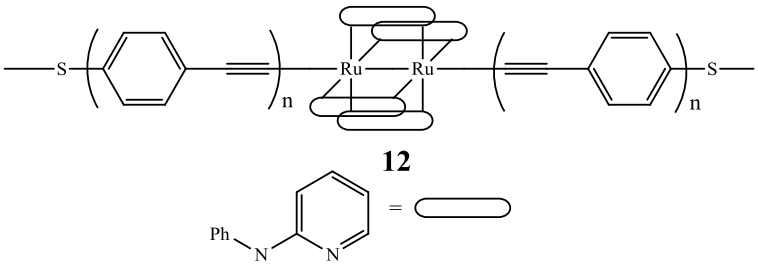

Figure 14. Di-ruthenium systems studied by Mahapatro and co-workers in nanogap molecular junctions. Adapted from ref. [53e].

Rigaut and co-workers[56] also report a series of Ru(dppe)$_2$bis(σ-arylacetylide) systems which, upon study using conducting probe atomic force microscopy (CP-AFM) and crossed-wire junctions, show a very weak dependence of the wire's resistance with the length of the system (β = 0.09Å^{-1}, in Figure 15).

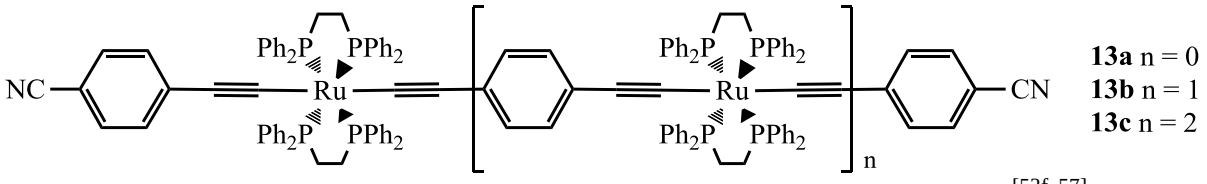

Figure 15. The ruthenium systems studied by Rigaut and co-workers.[53f, 57]

This is indicative of a high degree of electronic coupling throughout the wire coupled with high contact resistance. The group also realised, under low temperature conditions (5K), that the mono and dimetallic systems exhibited direct tunnelling, whereas, the trimetallic complex showed Coulomb blockade-like behaviour (charge injection) as represented by the cartoon in Scheme 3.[53f, 57]

Scheme 3. Charge transport for the systems reported by Rigaut and co-workers at 5K: (a) direct tunnelling for **13a** and **13b** junctions, (b) sequential tunnelling for the **13c** junction. Adapted from refs. [53f, 57].

When studying metal-metal interaction, the most usual systems – also the most important for this work (homo binuclear systems) – are those that have two active redox metal centres in mixed valence with one centre in the oxidation state *n* and the other on the oxidation state *n* + 1 linked by a bridging ligand L. This will make both sites different and create a barrier for their interconversion (characterized by the comproportionation constant $K_c = e^{\Delta EF/RT}$, $n = 1$).[58] This is achieved by submitting the homo bimetallic systems (M^n-L-M^n) to either electrochemical or chemical oxidation/reduction to yield the mixed valence systems (M^n-L-M^{n+1}). A comprehensive review and listing of the one electron oxidation or reduction agents has been reported by Connelly and Geiger.[56]

Although not a direct measure of the delocalization of the mixed-valence complexes, this comproportionation constant K_c (Scheme 4 and 5) is usually large for highly delocalized systems. Robin–Day proposed a classification where the interaction between metal centres could be categorized as Class I for weak or none interacting, Class II for moderate interaction and Class III for very strong interaction.[58-59]

$$M_1^{n}—L—M_2^{n} \;+\; M_1^{n+1}—L—M_2^{n+1} \;\underset{}{\overset{K_c}{\rightleftharpoons}}\; M_1^{n+1}—L—M_2^{n} \;+\; M_1^{n}—L—M_2^{n+1}$$

Scheme 4. Formation of MV compounds (Class I and II) M_1^{n+1}–L–M_2^{n} and M_1^{n}–L–M_2^{n+1} (K_c = comproportionation constant).

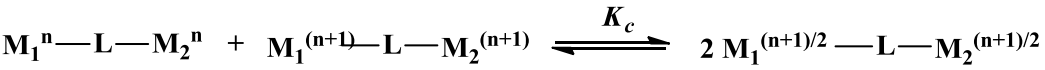

Scheme 5. Totally delocalized Class III system with a large K_c.

Class I compounds bear the properties of the isolated centres, since there is very slow or no electron-transfer. For the Class II complexes, new properties are observed in addition to those of the discrete centres. In this class, communication is weak which means that the systems are valence trapped or charge localized. Finally, for the Class III systems, delocalization is very strong leading to the appearance of unique properties.[58-59]

Hush extended the electronic transfer theory initially introduced by Marcus, to inner sphere transfer transitions, which can be applied to stable mixed-valence complexes.[58, 60] As such these systems usually present an intervalence charge transfer (ICT) in the near infra-red region which can be attributed to optically induced intramolecular electron-transfer. The study of this band along with typical cyclic voltammetry studies allows for the classification of the species.[58, 60]

The observation of the NIR (Near Infra-Red) band is mostly absent in Class I systems, were the charge is completely localized. Class II have experimentally observed ICT band on the NIR region and the actual form of the band will dictate which mathematical approximation to use (Gaussian shape or not). This band is highly solvent dependent since the weaker delocalization can be largely influenced by the solvent contribution. These are also usually broader bands. In the case of Class III systems, the charge is fully delocalized throughout the species and there is barely any influence from the solvent. Bands present higher peak intensity (higher ε) and are normally narrower.[58]

Moreover, species that are closer to the Class II/III border may be characterized by studying the width of the band. Meyer has observed electronic localization, solvent averaging and a residual barrier to electron-transfer arising from intramolecular structural changes.[58, 61]

Nevertheless, Hush's theory is only applicable to weakly interacting systems, since in strongly interacting systems (Class III), the ICT band can no longer be regarded as a transfer from one metal to the other, since the electron is shared equally throughout the system. As such, other methods have been developed to study the Class II and Class III species in more detail. Piepho, Krauz and Schatz (PKS) introduced the vibronic coupling model which enables the

calculation of Class II and III absorption profiles. Creutz, Newton and Sutin (CNS) developed a method which the metal to ligand charge transfer (MLCT) band, in UV-Vis spectroscopy, is used to estimate the type of delocalization of the compound.[58, 62]

Although electrochemical studies, in particular, cyclic voltammetry experiments are not a complete and fail proof indication of a wire's properties, as some compounds with good delocalization through the bridge with low ΔE^{o} (difference in potential between the two reversible waves) can be found, it is, for this specific class of systems, a good and reliable tool to access transport. Moreover, it is also a straightforward way to probe the ability of these systems to be oxidized in molecular junctions.[53a] It is also representative of the stability of the mixed-valence state. Nevertheless, this ΔE is not a direct measure of coupling and thus cannot be used, *per se*, for the classification of the system.[58] The value of ΔE is usually rising with the coupling between metal centres, as well as the K_c constant but there are some systems that present rather small ΔE.[58]

EPR (Electron Paramagnetic Resonance) can also be used to study these species, ideally when the paramagnetic systems have nondegenerate ground-states and hyperfine coupling can be observed. NMR can also be used, but in more specific cases like for example to study V(V) species where the unpaired electrons are in atoms in the close vicinity. This is because most bimetallic organometallic mixed-valence systems are paramagnetic. As stated before, infra-red spectroscopy can also be used to analyse these systems. In Class I and II species, new vibration modes, which are IR silent in totally oxidized or reduced species, turn IR active in the mixed valence state. The same does not happen with Class III complexes.[58] Scheme 6 shows a summary of the conditions normally used to classify these compounds.

In respect to the IVCT (inter-valence charge transition) transition, that can be observed in the binuclear complexes with mixed-valence systems, it can further be considered by examining a system of the type $[\{M_1(L)_n\}(\mu\text{-BL})\{M_2(L)_n\}]$, where M_1 and M_2 are the metal centres, both in the +2 oxidation state, BL is the bridging ligand and L are the metal centre's ancillary ligands. The oxidation of on the metal centres then yields the mixed-valence complex with an overall charge of +5 which equates to a $[M_1^{II}M_2^{III}]$ charge configuration in a fully localised system and a $[M_1^{III/2}\ M_2^{III/2}]$ for the fully delocalised system.[63]

Class I	- Little or no interaction - Small ΔE values (< 120 mV) - Very low K_c (< 10^2) - $H_{ab} = 0$
Borderline Class II/Class III	- Intermediate properties between class II and class III - $\Gamma \approx 0.5$
Class II	- Moderate interaction - Intermediate ΔE values (120 mV < ΔE < 360 mV) - Intermediate K_c ($10^2 < K_c < 10^6$) - $H_{ab} < \lambda/2$ - Broad and weak ICT bands - $\Delta\bar{\upsilon}_{\frac{1}{2}(calc)} < \Delta\bar{\upsilon}_{\frac{1}{2}(obs)}$ - Weakly coupled $0 < \Gamma < 0.1$ - Moderately coupled $0.1 < \Gamma < 0.5$
Class III	- Strong interaction - Large ΔE values (ΔE > 360 mV) - Large K_c values (> 10^6) - $H_{ab} \geq \lambda/2$ - Narrow and intense ICT bands - $\Delta\bar{\upsilon}_{\frac{1}{2}(calc)} >>> \Delta\bar{\upsilon}_{\frac{1}{2}(obs)}$ - $\Gamma >> 0.5$

Scheme 6. Conditions and classification for mixed-valence binuclear systems.Adapted from ref. [58].

As such, the symmetrical binuclear complex is thus described by the parabolic potential energy surfaces represented in Figure 16, where the dimensionless reaction coordinate (X) represents an anti-symmetric combination of the metal-ligand and solvent stretching vibrations. The dotted curves correspond to the wavefunctions $\boldsymbol{\Psi}_a$ and $\boldsymbol{\Psi}_b$ for the valence-localised electronic isomers $[M_1^{II}M_2^{III}]_0$ and $[M_1^{III}M_2^{II}]_0$ respectively, where the odd electron is completely localised in either one of the metal centres. These diabatic states are situated at $X_{min} = 0$ and 1 and it is assumed that they are harmonic with identical force constants. The energy of these states are given by H_a and H_b from Equation (1), where $\hat{H}$ is the effective two-state Hamiltonian operator and λ is the reorganisation energy (from the IVCT band analysis of the NIR spectra).[63]

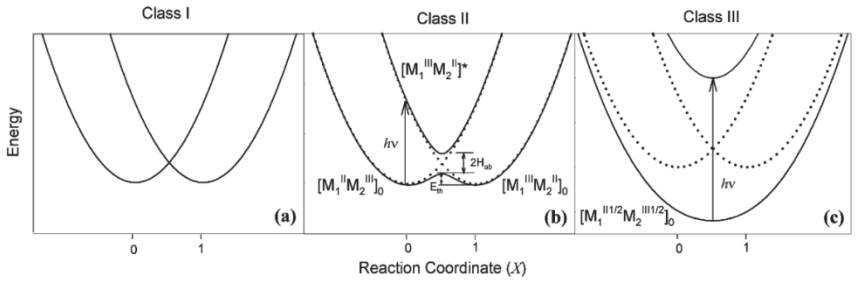

Figure 16. Potential energy curves for electron transfer in ligand-bridged binuclear complexes with (a) negligible, (b) weak (H_{ab} = λ/4) and (c) strong (H_{ab} =3λ/4) electronic coupling. The dotted and solid curves represent the diabatic and adiabatic surfaces, respectively. Adapted from ref. [63].

$$H_a=\langle\Psi_a|\hat{H}|\Psi_a\rangle=\lambda X^2 \text{ and } H_b=\langle\Psi_b|\hat{H}|\Psi_b\rangle=\lambda(X\text{-}1) \quad \textbf{(1)}$$

As observable on the graphic representation, at the intersection of the diabatic surfaces, where X = 0.5, degeneracy is lost by means of wavefunction mixing which results in two new adiabatic surfaces (Figure 16**, b**). The energies relative to the lower and upper adiabatic states, E_- and E_+, respectively, are yielded by Equation (2), and the splitting formed between the surfaces where X = 0.5 is what defines the coupling parameter, $H_{ab}=<\Psi_a|\hat{H}|\Psi_b>$.[63]

$$E_{\pm}=\frac{[\lambda(2X^2\text{-}2X+1)]}{2} - \frac{\left\{[\lambda(2X\text{-}1)]^2+4H_{ab}^2\right\}^{1/2}}{2} \quad \textbf{(2)}$$

The optically-induced vertical transition between the adiabatic states is then the IVCT transition (Equation (3)), which corresponds to the formation of the vibrationally excited state of the ion, $[M_1^{III}M_2^{II}]^*$.[63]

$$\left[M_1^{II}M_2^{III}\right]_0 \xrightarrow{h\upsilon} \left[M_1^{III}M_2^{II}\right]^* \quad \textbf{(3)}$$

The degree of electronic coupling between M_1 and M_2, and the resulting splitting between the adiabatic surfaces are used to classify the mixed-valence system according to the Robin–Day scheme.[58-59] When M_1 and M_2 are sufficiently far apart or their interaction is either spin or symmetry forbidden, the electronic coupling is thus negligible (H_{ab} = 0). This corresponds to a Class I system (Figure 16, **a**). As for the Class II systems, there is weak to moderate electronic coupling between the two metal centres as well as the presence of IVCT bands attributed to vertical transition between the adiabatic states at X_{min} (Figure 16, **b,** $2H_{ab} << \lambda$). Finally, when the centres are strongly electronically coupled ($2H_{ab} >> \lambda$), the thermal barrier

to intermolecular electron transfer is non-existent leading to single minimum of the ground state adiabatic surface (Figure 16, **c**).[63]

It is largely accepted that the effectiveness of molecular wires that are based on the Metal-Bridging Ligand-Metal type of system is determined by the efficiency of the coupling between the *d* orbital of the metal and the frontier *p* orbital of the bridge.[54a]

I.6.1. Binuclear 1,4-diethynylbenzene derivatives and non-innocent ligands in Ru systems

The bonding of acetylide ligands to transition metals is well known. It is described as the overlap of the *sp* hybridized σ orbital of the R–C≡C$^-$ with a metal fragment of similar symmetry which often is composed of a large metal d-orbital component. Although small metal-to-ligand back-bonding may be observed, the most significant π-orbital mixings for these compounds are from filled-filled interactions between metal $d\pi$ and occupied π orbitals from the ligand.[64]

Furthermore the inherent rod like structure of the 1,4-diethynylbenzene derivatives is very interesting in the matter of molecular wires. This is especially true when the preparation of SAMs is considered, since the linear structure would help avoid some structural defects which can arise, for example, with double bond wires[64] even if these are sometimes reported to exhibit better transport properties.[58] Moreover, and although not usually the objective of the usage of these materials, acetylides are also open to further modification, *e.g.*, cummulenes or vinylidenes molecular wires.[65]

As a part of a study to further deepen the properties of aryldiethynyl bridging ligands in binuclear (and also trinuclear) rods, Klein and co-workers reported the effect of the lengthening of this bridge on the communication between the terminal metals (Figure 17).[16]

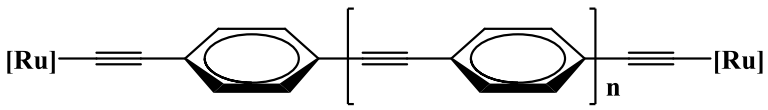

Figure 17. Example of the systems studied by Klein *et al.*; [Ru] = [RuCl(dppe)$_2$]$^+$). Adapted from ref. [16].

It was found, from cyclic voltammetry as well as NIR (near–infra red) spectroscopy studies, that there is indeed delocalization through the ligand to the extent that communication between metals is achieved. However, this property is lost when the system grows to three aryldiethynyl units (n = 2). This conclusion was supported by the single oxidation (or sum of two 1 electron oxidations) found for the longer rods. The NIR spectroelectrochemistry studies also showed that the spectral response of the first (and only) oxidation of the n = 2 rod is basically the same (although blue shifted) as the second oxidation of n = 0, 1 rods. This and the fact that the careful partial oxidation of the **14c** (n = 2) rod which didn't show any proof of a [**14c**]$^{\cdot+}$.[16]

The systems also present decreasing K_c (comproportionation constant) as n increased, reaching $K_c = 0$ for the **14c** (n = 2) rod. The low K_c values obtained point to class II Hush type systems but, the observed narrow bands in the NIR region would be in agreement with a class III mixed valence system. As such, the IR spectroelectrochemistry helped with the classification of these complexes by analysis of the $\upsilon_{(C\equiv C)}$ band upon oxidation of **14a** (n = 0). Thus, it was observed that even after exhaustive oxidation, there was still some residual $\upsilon_{(C\equiv C)}$ band (2071 cm^{-1} – $\upsilon_{(C\equiv C)}$ – in addition to a new at 1966 cm^{-1} – $\upsilon_{(C=C)}$) which means that if this was a fully delocalized system (class III) the original band would completely disappear. This residual band may indicate that the system is not fully delocalized in the IR time scale, thus pointing to a valence-trapped class II system. Further EPR studies show that although the metal contribution is not very high, there is a marked distribution of the spin density of the unpaired electrons throughout the bridge and metal centres.[16] This report is in full agreement with the latest studies performed in the field of Ru molecular wires based of ethynylenephenylene rods which describe these systems as bearing non-innocent ligands, especially by the group of Rigaut.[46, 53a, 57, 66] Nevertheless, the subject was also addressed before by other authors[2c, 67] and will be discussed below. Moreover, the definition of non-innocent ligand was coined by Jørgensen[68] in 1966 and refers to ligands that do not allow for clear assessment of the oxidation of metal centre of the complex.

The oxidation processes are mostly metal based in the bimetallic iron systems whereas the bimetallic Ru systems present ligand dominated oxidations. This is due to the lower energy of the Ru 4*d* orbital in comparison to the Fe 3*d* counterpart as well as the higher ligand contribution of the HOMO (Highest Occupied Molecular Orbital) which ultimately results in the overlap of the *d*π and the appropriate π orbital of the bridging ligand.[53a, 66d]

Rigaut and co-workers[66d] reported the study of a Ru 1,4-diethynylbenzene derived binuclear systems bearing ethynyl and vinyl moieties (**16a-b**, Figure 18, **a**) which were found to exhibit mostly the same behaviour of the symmetric alkynyl (**17**) and vinylidene (**18**) counter-parts in their oxidized cation forms. This was noticeable by the position of the ν(C≡C) bands of $\mathbf{16a}^{\bullet+}$ which coincided with that of $\mathbf{17}^{\bullet+}$. The same was observed for the ν(C≡O) in $\mathbf{16a}^{\bullet+}$ and $\mathbf{17}^{\bullet+}$. The bleaching of the ν(C≡C) corresponding to the neutral compound (leftmost band ~ 2100 cm^{-1} in the IR spectra in Figure 18, **b**) and the rise of the new ν(C=C) band for the monocation (following band at ~ 1900 cm^{-1}) which is in accordance with the ligand centred oxidation processes that were already discussed before.

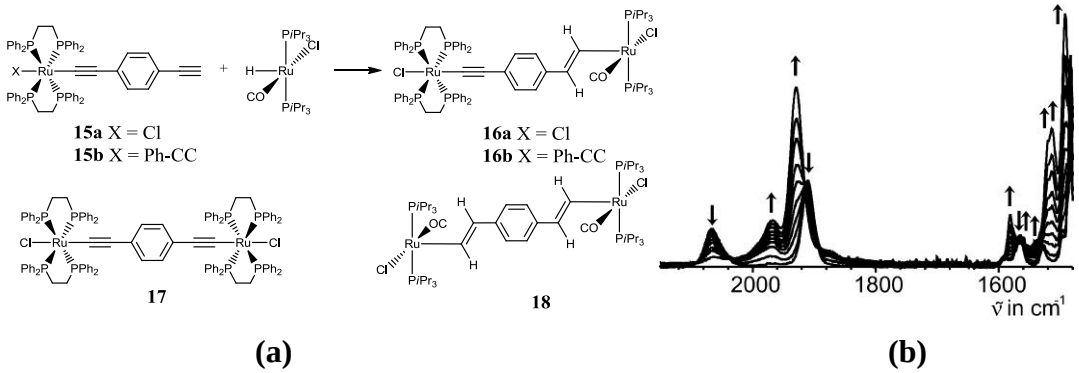

(a) **(b)**

Figure 18. Compounds studied by Rigaut and co-workers (**a**). IR changes during the first oxidation of **16a** (right, **16a** → $\mathbf{16a}^{\bullet+}$, 1,2-$C_2H_4Cl_2$/NBu_4PF_6). Adapted from ref. [66d].

These results provide evidence of delocalization through the Ru moieties and to the phenylacetylide (**15b**). This was noticeable by the red shift on the electronic spectra from **15a** to **15b**. Most of the described behaviour was backed up by EPR experiments.[66d]

Rigaut and co-workers[46, 53a, 57, 66a-e, 69] have been reporting the in-depth study of these types of systems with supporting observation made through spectroelectrochemistry. One of their last reports[53a] presents the preparation and characterization of bi and tri homometallic systems (Figure 19, n = 2 and 3 respectivelly) bearing terminal insulating chains which should provide increased contact resistance and promote coulomb blockade. The group found that, as expected, the redox processes were largely centred on the ligand by studying the bleaching and forming of the acetylide and vinylidene vibration bands, respectively, upon iterative oxidations of the compounds using an OTTLE (Optically Transparent Thin-Layer Electrochemical) cell.

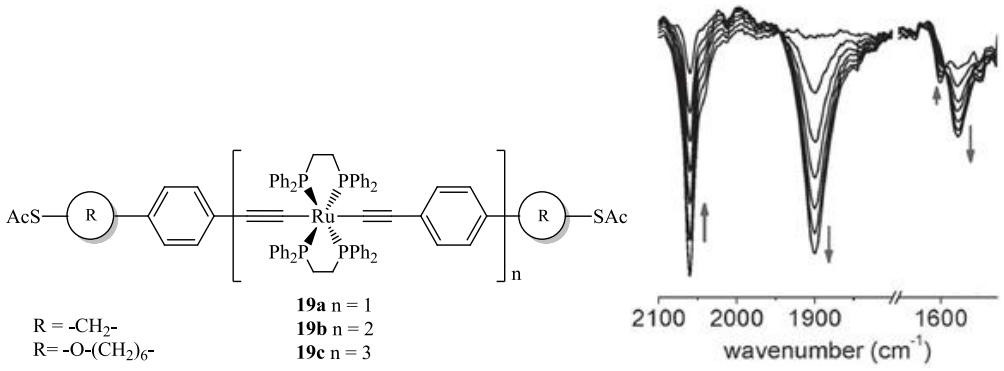

(a) **(b)**

Figure 19. The insulating chain bearing systems prepared by the group of Rigaut (**a**) and the spectroscopic changes upon oxidation in an OTTLE Cell (1,2-$C_2H_4Cl_2$, 0.2 M Bu_4NPF_6) of the system with shorter insulating chain and n = 1 (**b**). Adapted from ref. [53a].

As such it was observed that upon a first oxidation (of the three processes found in the cyclic voltammogram), there was the forming of two new bands at 1962 and 1852 cm^{-1} (vinylidene character). The initial band at 2058 cm^{-1} (acetylide character) was left unchanged by this first reaction. Upon the second oxidation, there is only a shift of the one at 1852 to 1904 cm^{-1}. Thus the remaining acetylide contribution may be attributed to an incomplete delocalisation of the vacancy of one ligand to the other in the IR time-scale which is maintained through the third oxidation. Moreover and although the oxidation are not Ru centred, and an effort is made by the authors to emphasize this aspect of the electrochemistry of these compounds, the number of redox processes is indeed related with the number of metal centres present in the system and ΔE and Kc values of approximately 300 mV and $1.5x10^5$ respectively.[53a] These complexes were later characterized[70] by preparation of SAMs (Self Assembled Monolayers) whereas the group found that the same number of redox processes was found. These processes were also occurring at the approximately the same potentials as for the free wires. Condution tests performed by CP-AFM (conducting probe atomic force microscopy) showed a significant decrease in electronic transport as the length of the wire increased (from **19a** to **19c**) and fitting of the data pointed to a nonresonant tunnelling regime with a β of 1.0 nm^{-1} which is significantly lower than other conjugated molecular wires that undergo tunnelling.[70]

Rigaut and co-workers have also reported the preparation of a trinuclear $Ru(dppe)_2$ wire bearing C_7 bridges which show communication throughout the 28Å span formed by the Ru–C_7–Ru–C_7–Ru system (Figure 20).[46]

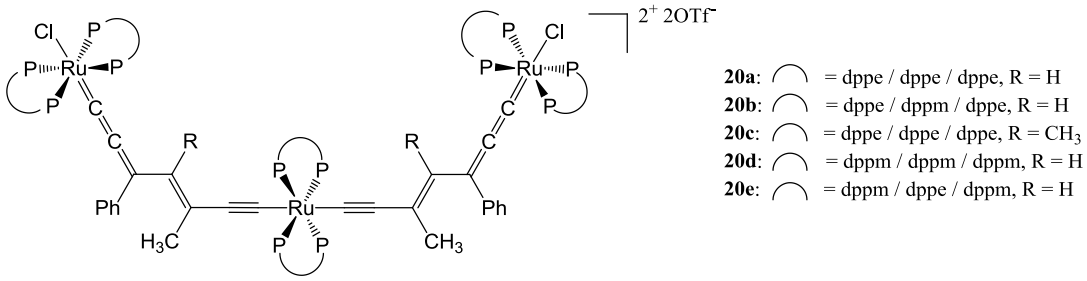

Figure 20. Trimetallic system prepared by the group of Rigaut. Adapted from ref. [46].

In the classical interpretation of the cyclic voltammetry results found by the group of Rigaut, one would be inclined to only attribute full system delocalization if three waves were present in the voltammogram. Nevertheless, the group points out, supporting it with NIR and UV/Vis spectroelectrochemical as well as DFT (Density Functional theory) computational studies, that the two redox processes that were observed are addressable as one process for each half of the system. As such, upon the first oxidation the single electron is delocalized over the two carbon chains through the central Ru moiety.[46]

Rigaut and co-workers have reported[71] the (Ethynyl)(vinyl)phenylene trimetallic wire presented in Figure 21. A non-innocent ligand behaviour was found in compounds **21a-b** which also showed delocalization through the three metal centres and respective organic bridges. Furthermore, these systems show four oxidation states (n = 0 – 4), being that the first three processes are attributed to the redox reactions of each Ru centre (always coupled with the bridge) and the last oxidation is viewed as of the trication.[71]

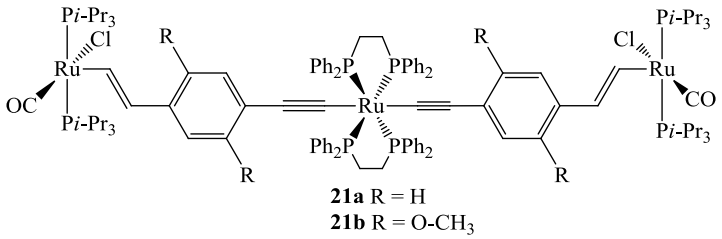

Figure 21. (Ethynyl)(vinyl)phenylene bridged triruthenium prepared by the Rigaut group. Adapted from ref. [71].

I.6. Other metallomolecular wires

Since the OPE Ru and Pd wires were only a part of the large family of molecular wires and as such, have close a relation to other families, some exposition of other bridging systems are discussed (like cumulenic and polyyne systems) to some extent in the following sections.

I.6.1. Metalocumulenic systems

It is noteworthy that although these complexes are usually reported in their discrete forms, the relation between them can be expressed in the following manner (Scheme 7).[72] Nevertheless, this section will address not only cumulenic (cumulenylidene bridging ligands) systems (more than two consecutive double bonds), but also, allenylidene and vinylydene systems. The common point being the carbene like bond to the metal (M=C=C).

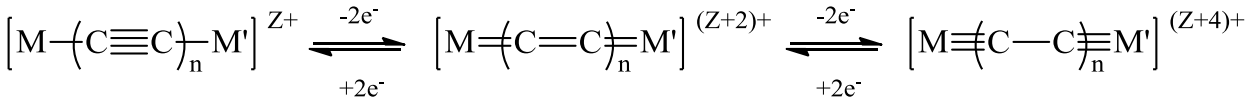

Scheme 7. Relation between acetylide, cumulene and carbyne mesomeric forms. Adapted from ref. [72].

Binuclear cumulenic systems have shown increased promise in this field as they are reported to have good transport properties.[73] Nevertheless, as the size increases and when comparing with polyynes (not isomers, but effectively related by a redox mechanism), the cumulenes exhibit lower stability which should decrease processability as well as working conditions in relation to the application of these materials as usable molecular wires. These chains are also harder to prepare than the polyyne counterparts.[73]

Bildstein and co-workers[74] reported a tetraferrocenyl-[3]-cumulene (Figure 22) that exhibited two reversible redox waves in the CV experiments with the first half-wave shows a cathodic shift (in comparison with free ferrocene) indicative of increased donor capacity brought about by the cumulenic chain.

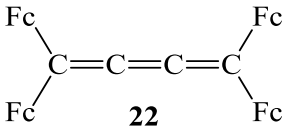

22

Figure 22. The tetraferrocenyl-[3]-cumulene reported by Bildstein *et al.*. Fc = ferrocene. Adapted from ref. [74].

In respect to allenylidene systems, these are usually mononuclear as a function of the short distance that only one of these ligands would be able to cover. Nevertheless, the group of Dixneuf has reported the preparation of a bis(allenylidene-Ru) system (Figure 23) that effectively uses an aromatic moiety to bridge the two terminal moieties. Furthermore, not only communication is promoted between metal centres, but also good ΔE values (between 190 to 270 mV) were observed for the two redox processes.[75]

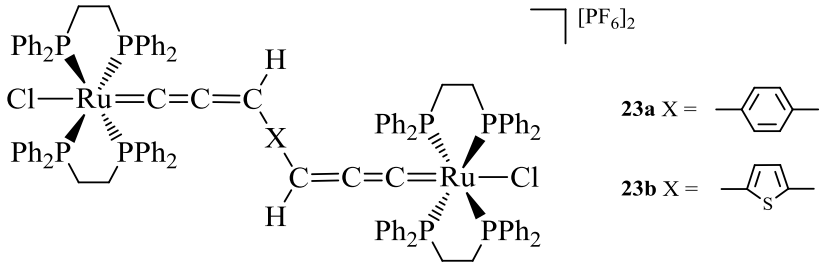

Figure 23. Binuclear Ru bis(allenylidene) reported by Guesmi *et al.*. Adapted from ref. [75].

Furthermore, and in agreement with experimental and computational results, it was also reported that when the bridging chains is comprised of odd numbered CH bridges in cumulenic wires, these are electronically decoupled (unstable open shell triplet) thus making them uninteresting for molecular wire applications (further discussed below).[76]

Apart from pure cumulenic systems, there are, as well, some reports of mixed systems, *e.g.*, the above aromatic bridged bis(allenylidene)[75] and the following bis(acetylide) bridge by a cumulenylydene bridge reported by Gao and co-workers.[58, 77] It was observed, that in the case of the binuclear complexes schematized in Figure 24, the π acceptor ability of the bridging ligand is enhanced as the number of ethenyl segments is increased, which then leads to the decrease of the π electron density of the Ru centres. Furthermore rapid decrease in the intercommunication between Ru centres as the number of ethenyl bonds rises which is immediately verified in the sharp decrease in the ΔE. This also makes the first oxidation event harder to reach (higher

potential is necessary) and there is a characteristic shift to higher energies of the MLCT band ($d\pi$(Ru) → π*(ancillary ligand)). This is attributed to the increase of the π accepting characteristic of the bridging ligand as the number of double bounds increases which makes the electron density on the Ru centres small and making the energy gap between $d\pi$ (Ru) and π* (ancillary) larger and shifting the band to blue.[58, 77]

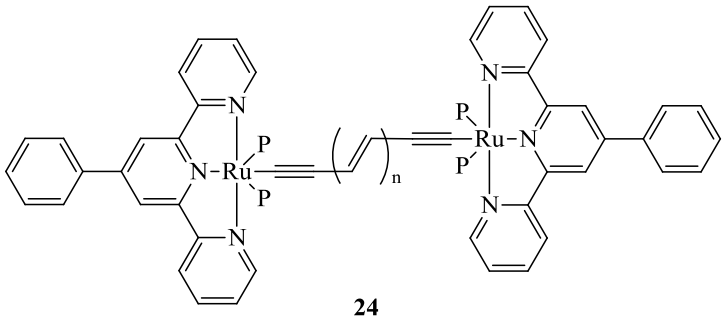

24

Figure 24. Complex used for the study of the effect of increasing number of double bonds (n = 1-4, P = PPh_3). Adapted from ref. [58, 77].

The UV-Vis/NIR high intensity narrow peak ICT as well as it's solvent independency, high K_c and ΔE values of the mono-oxidized complexes point to class III systems. This strong delocalization is lost very rapidly as the length of the system is increased.[58, 77]

The group of Dixneuf also reported the preparation of a mixed cumulene/acetylide binuclear Ru complex (Figure 25). Although two processes were visible in the CV studies, only one is reversible (first one). The group attributed both processes to the oxidation of Ru^{II}/Ru^{III}.[78] A few years later, Bruce and co-workers reported the preparation of analogue compounds using the $Cp^*(dppe)Ru^+$ moiety (instead of $[Cl(dppe)_2Ru]^+$ used by Dixneuf). Nevertheless, no CV data is available for the specific counterpart as the compounds were not prepared with molecular wire application as the main objective.[79]

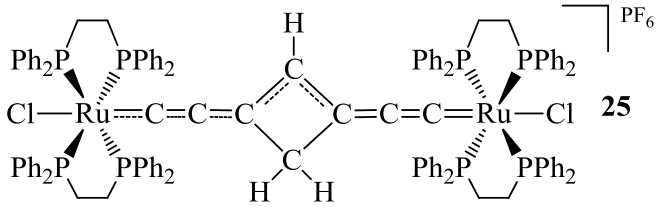

25

Figure 25. Binuclear Ru cumulene/acetylide reported by Dixneuf's group.Adapted from ref. [78].

A very interesting system is reported by Ortega and co-workers.[80] The bridge is formed by rigid *sp* carbons bound to two phosphines which are then coordinated to a $Ru(bpy)_2$ centre (where bpy is 2,2'bipyridine). The importance of a cumulene or allenylidene is directly related to the final orientation of the terminal centres as schematized in Figure 26.[80]

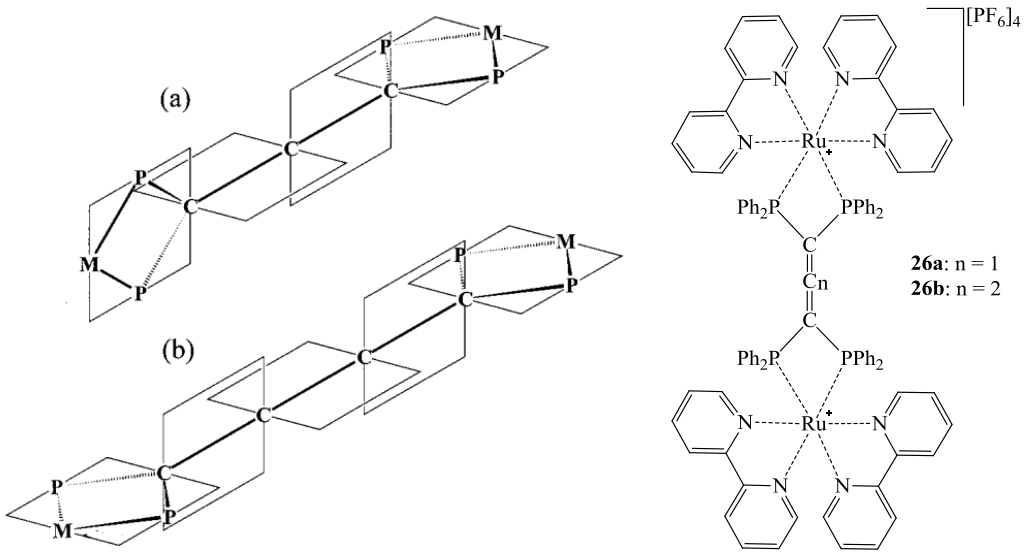

Figure 26. Representation of the π-orbital alignment of the allene-bridged bimetallic complexes (**a**) and that of the cumulene-bridged bimetallic complexes (**b**) as well as the respective complexes (**26a-b**). Adapted from ref. [80].

As such, there is a clear difference between the C_3 bridged (allenylidene, Figure 26, (**a**)) and the C_4 bridged (cumulene, Figure 26, (**b**)) in respect to electron transport. Moreover in the case of the C_3 bridged complex, only one process is visible in the cyclic voltammetry studies (attributed by the authors to two overlapping one-electron processes) which contrasts with the C_4 bridged binuclear complex which exhibits two processes separated by 420 mV pointing to a good inter-metal communication. Furthermore, the authors describe the communication breakage in the C_3 complex as a consequence of the 90º angle formed between the two metal termini in this complex (allenylidene[§], Figure 26, (**a**)). This was also observed for analogue complexes bearing Os centres.[80]

I.6.2. Binuclear polyalkynyl bridged systems

[§]Concerning mononuclear ruthenium allenylidene complexes, Dixneuf[81] has produced a very good review in 2004.

Although the best performing wires candidates, these suffer from the drawback of only being modifiable at the metal centre: Notwithstanding, a large body of work has been performed regarding this specific bridging ligand which will be briefly discussed below.[82]

Closely related to cumulenic systems, polyalkynyl (or polyynediyl) are characterized by the terminal *sp* hybridized carbon, several examples of polyakynyl bridged systems have been reported. One of the first reports of this type of organometallic wires was produced by Gladisz who prepared a series of Cp*Re(NO)(PPh_3) (Cp* = η^5–$C_5(CH_3)_5$, Figure 27, **27**) terminated binuclear complexes, *via* oxidative coupling of the mononuclear compounds bearing half the polyalkynyl chain.[67b, 83]

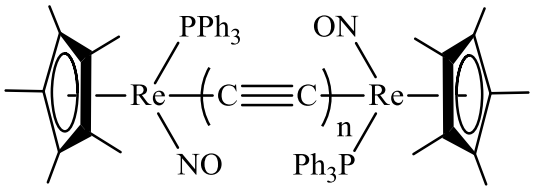

27

Figure 27. Series of Cp*Re(NO)(PPh_3) terminated binuclear complexes prepared by Gladisz' group. (n = 2-6, 8, 10). Adapted from ref. [67b, 83].

This series of Re binuclear complexes was surprisingly air stable (in solid state) at room temperature although not very stable when dissolved. Nevertheless, stability starts to decrease as the bridge grows more than $ReC_{20}Re$ (Re = Cp*Re(NO)(PPh_3), n = 10) resulting in $ReC_{24}Re$ not being possible to prepare. In terms of redox properties the reversibility of the two-wave processes observed for these systems decreases with the increase of the length, already starting to decline from ReC_8Re (with $i_{c/a} > 1$). It was also noted that the first oxidation potentials become higher, signalling a thermodynamically less favourable process. Nevertheless, the second oxidation potentials are barely affected. Furthermore, the communication of Re centres was broken only at the maximum chain length in this report ($ReC_{20}Re$). As such, a single oxidation was observed only in $ReC_{20}Re$ with two wave voltammograms for the remainder of the reported complexes. Moreover, a steep decline in K_c (in CH_2Cl_2) value is observed going from ReC_4Re (~ $1x10^9$) to ReC_6Re (~$1x10^6$) and then stabilizing at the same magnitude order from ReC_8Re to $ReC_{20}Re$ (~ $1x10^3$).[83a]

The group of Gladisz also reported – in the same line of polyalkynyl based complexes – homo and heterometallic M–C_n–M´ rods using Cp*Re(NO)(PPh_3), Cp*Fe(CO)$_2$, Cp*Fe(CO)(PPh_3), Cp*Mo(CO)$_2$, Cp*W(CO)$_2$, Rh(CO)(PPh_3)$_2$ and Pd(PEt_3)$_2$Cl with a C_4 alkynyl bridge, which were studied by UV-Vis, NMR and IR spectroscopy.[67b, 83b] The group also prepared and studied a trinuclear bimetallic rod of the type [{Cp*(NO)(PPh_3)Re–C_4}$_2$–Pd(PEt_3)$_2$]. These complexes will be referred in the Pd rods *section* (I.10).[83b] Notwithstanding, they show one reversible one electron oxidation (36 mV *vs.* Fc, in CH_2Cl_2) followed by a much higher irreversible oxidation (at 129 mV). This observation points to a breakage in communication between Re centres, brought about by the insertion of the Pd moiety. Furthermore, the first oxidation is in line with the analogous mononuclear Re complex (ReC_4, 52 mV) and significantly higher than the ReC_4Re complex where the first and second oxidations (both reversible) are at 15 and 68 mV respectively. Furthermore, the Ph–C≡C–Pd(PEt_3)$_2$–C≡C–Ph had the first (and irreversible) oxidation at 148 mV making it the hardest to oxidize.[83b] Moreover, Gladisz and co-workers also reported a C_8 and C_{12} di [Pt(PhMe)(PPh_3)$_2$] complexes but without any relevant electrochemistry data.[84]

In the same line of work, Lapinte and co-workers[85] reported a bis Cp*Fe(dppe) C_4 bridged wire (Figure 28, **28**) with a K_c of 1.2 x 10^{12}. When the group introduced a phenyl ring, effectively preparing the 1,4-diethynylbenzene derivative, the K_c dropped to 1.2x10^4. Lapinte and Coat[86] then published a Cp*Fe(dppe) C_8 bridged complex analogous to the previous ones (Figure 28, **29**) with a lower *K*c of 2x10^7 (ΔE^0 = 430 mV), which is in good accordance with the effect brought about by the increase of the bridging chain reported by Gladisz (*vide supra*).

Sakurai *et al.*[87] reported a C_{12} bridged bis [Cp*Fe(CO)$_2$] (Figure 28, **30**) but did not present any data pertaining to inter-metal communication. Akita and co-workers[88] prepared a series of C_2, C_4 and C_8 polyynyl bridged bis [Cp*Fe(CO)$_2$] complex but did not perform electrochemical studies.

Bruce, Low and their co-workers[89] have prepared two C_4 binuclear homometallic complexes using [CpRu(PPh_3)$_2$] and [CpRu(PPh_3)(PMe_3)] (Figure 28, **31** and **32**). Four waves were observed for both complexes, consistent with the sequential formal oxidation from [Ru^{II}/Ru^{II}], through [Ru^{II}/Ru^{III}], [Ru^{III}/Ru^{III}], [Ru^{III}/Ru^{IV}] and finally to [Ru^{IV}/Ru^{IV}]. It was also noted that the substitution of the PPh_3 by the more electrondonating PMe_3 phosphine brought about more facile oxidations (respectively E^0= -0.23, 0.41, +1.03, +1.68 V and E^0 = -0.26, +0.33,

+0,97, +1.46 V). Furthermore, IR studies show the decrease in bond order of the diynyl bridge as the complex is oxidised. Kheradmandan *et al.*[90] reported a $Mn(dmpe)_2I$ C_4 bridged complex with a K_c of $5.5x10^{10}$.

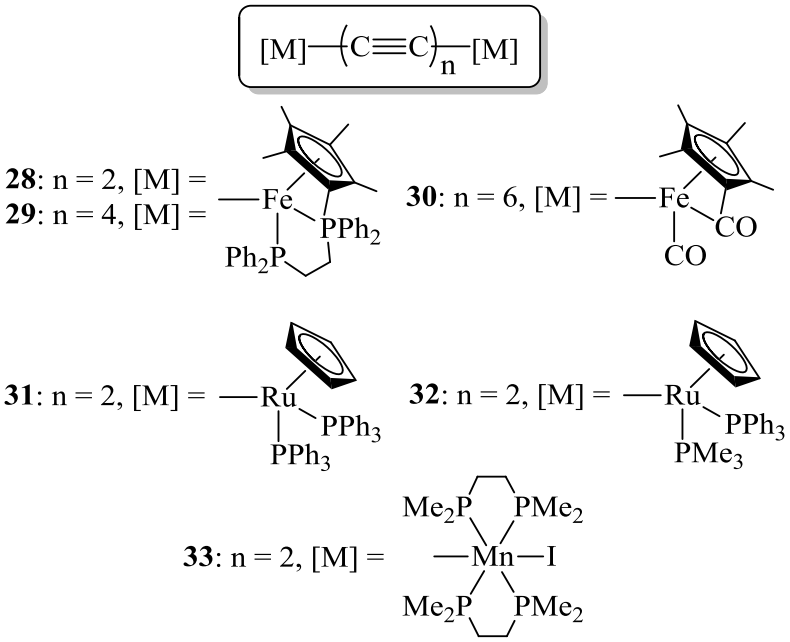

Figure 28. The polyalkynyl based binuclear wires (**28**-**32**). Adpted from ref. [85a] (**28**), [87] (**29**), [89] (**30** and **31**), [90] (**32**) and [86] (**33**).

The group of Ren[52g, 52k, 53g] reported a series of bis ferrocene-ruthenium, in which the two metallic moieties are briged by polyynyl complex with a central di ruthenium DMBA (*N,N'*-dimethylbenzamidinate) moiety (Figure 29, **34,** Fc-C_n-(Ru-$Ru(DMBA)_4$)-C_n-Fc). It was found that for all the reported compounds, there was communication between the Fc moieties, even in the longer bridged cases (**34f-i**).[53g] Furthermore, for compounds **34a-c**, which bears a C_2 bridge from Fc to Ru_2, it is possible to observe 4 redox pairs in the cyclic voltammogram. Two of them are attributed to the two consecutive oxidations of the Ru_2 core and the other two are for the Fc termini (they do not oxidate at the same E^0, thus there is Fc-to-Fc communication).[52g, 52k] Nevertheless, the authors found that when n > 1 (**34d-i**) the second oxidation of the Ru_2 centre is overlapped by first Fc oxidation yielding a 2 electron wave. This assumption was backed-up by spectroelectrochemistry, NIR studies as well as computational modelling.[52k, 53g] The n = 1 (**34a-c**) and n = 2 (**34d-e**) have similar transport properties (described by ΔG_c by the authors) as the analogues that do not have the Ru_2 centre (Fc-C_2-Fc[91] and Fc-C_4-Fc[92] respectively).[52g, 52k] The same trend in decreased communication is also observed for this series of compounds.[52g, 52k, 53g]

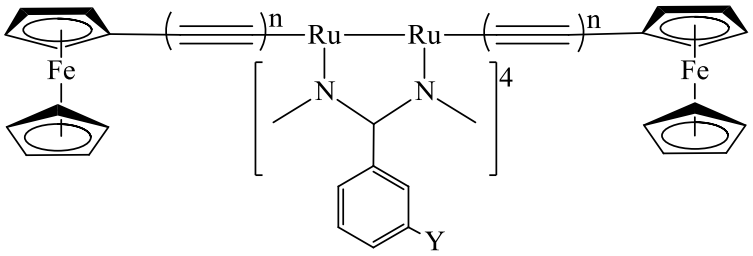

Y \ n	1	2	3	4
H	**34a**	**34d**	**34f**	**34h**
OCH_3	**34b**	**34e**	**34g**	**34i**
OC_4H_9	**34c**	–	–	–

Figure 29. The polyalkynyl based binuclear wires (**34a-i**). Adpted from ref. [52g, 52k] (**34a-e**) and [53g] (**34f-i**).

Yip and co-workers[52f] reported a Pt_2 bridged Fc terminated complex (Figure 30, **35**) which showed communication between the termini although with a low K_c of $3.3x10^4$. This was ascertained from the 2 quasi-reversible process which are attributed to the Fc centres as $[Pt_2(dppm)_2Cl_2]$ does not show any redox processes at the studied potential range.

Wolf[52b, 93] has also reported on a number of Ru based Fc-C_n-Ru-C_n-Fc complexes. It was found that when a $Ru(dppm)_2$ moiety was introduced in the centre of the rod (Figure 30, **36**), the $\Delta E_{½}$ increase in comparison to the Fc–C_4–Fc analogue. This $Ru(dppm)_2$ complex (Figure 30, **36**) presented a 3 reversible wave cyclic voltammogram (one wave for $Ru^{II}/^{III}$ and the other two for the, thus communicating, Fc units). Wolf also observed the effect of the CO ancillary ligand in a series of compounds much like the previous one (Figure 30, **37**). It was found that, although maintaining the communication between Fc units, the oxidation attributed to the Ru centre was not reversible. Furthermore, the delocalization (studied by CV and NIR) was dampened by the presence of the CO ligand and became worse when there were two of these ligands coordinated to the Ru centre. This observation was attributed to the fact that CO is a strong π-acceptor and a poor σ-donor and that the electron which is removed upon oxidation is that of the Ru–CO bonding effectively leading to the decomposition of the compound.[52b]

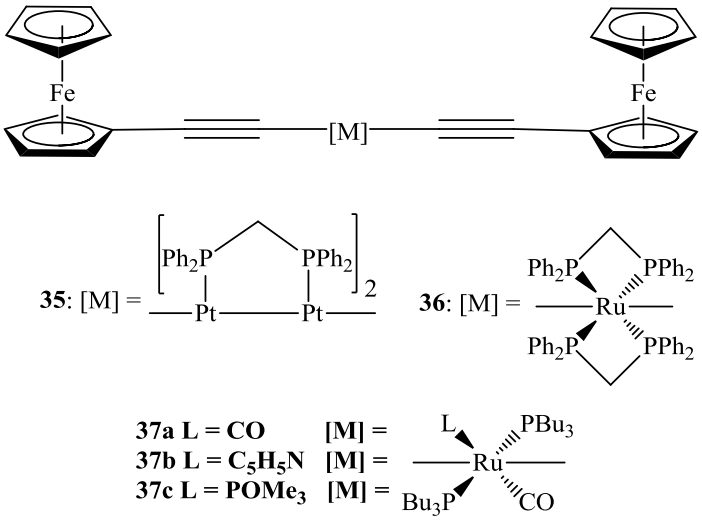

Figure 30. The polyalkynyl based binuclear wires (**35, 36, 37a-c**). Adpted from ref. [52f] (**35**), [52b, 93] (**36**) and [52b] (**37a-c**).

Bruce and Low[94] have published a dialkynyl rod with the Fc unit bridging two terminal CpRu moieties (Figure 30, **38**). It was reported that the compounds exhibited communication between the termini leading to a K_c in the order of $2.9x10^8$ to $4.3x10^{10}$ with wave separations in the 530-620 mV range. The group did not attribute any of the redox processes to the central Fc moiety, but backed up these conclusions with studies of the mono and di nuclear corresponding complexes.

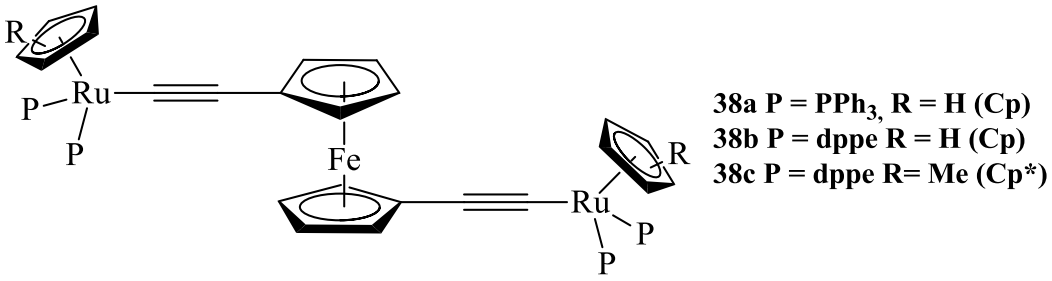

Figure 31. The polyalkynyl ruthenium-iron complexes (**38a-c**). Adapted from ref. [94].

These wires like compounds show the best properties in the matter of transport which can be ascertained by, for example, their high K_c values. Notwithstanding, there is no possible tuning of the bridging polyynyl. On solution would be the inclusion of other centre moieties (like some of the compounds described above), which can be labour intensive in some cases or the

modification of the terminal metal centres two possible solutions which can reduce processability by means of reduced stability or even more reduced solubility. Although 1,4-diethynylbenzene derivatives don't exhibit these high transport properties, the phenyl moieties allow for a great range of modification.[82]

I.6.3. Mixed systems

Some other complexes that include, in their bridging ligand different types of carbon-carbon bonding will be briefly discussed in this section. This is because, it´s not straightforward to classify them by the previous sections. Furthermore, the phenyleneethynylene wire should then be part of this section, but since they are the main subject of this work, special focus was given to that classification.

Chung and co-workers[95] report a comparison of two wires that have either an acetylenic or an olefinic bridge (Figure 32) along with observation made in regard to the influence of the phosphine and the α proton. The group found that the studied compounds presented very high K_c (ranging from 10^7 to 10^{12}). The usage of an acetylenic bridge (Figure 32, **39**) increases the K_c about 70 fold (comparing compound **39** with its olefinic counterpart – not pictured). Furthermore, it was also observed a 3 times increase in the K_c value when using dppe instead of dppm. Finally, and the highest observed difference in K_c value change, was realised when the α proton was substituted with OMe leading to a 800 fold decrease (Figure 32, **40**). This is probably due to expanded π system into the methoxy's oxygen which can lead to a decrease in the Coulombic repulsion between the charges and thus smaller K_c. These conclusions were supported by NIR, UV-Vis and DFT calculation results.[95]

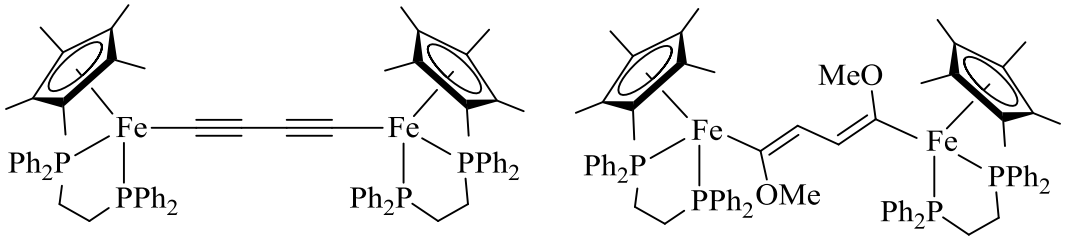

39 **40**

Figure 32. Example of the type of compounds studied by Chang and co-workers.[95]

A $(CH)_{14}$ long bridged binuclear system showing communication between the metal centres (Figure 33) was reported by Yuan and co-workers.[58, 96] A very similar complex, with a $(CH)_{10}$, prepared by Liu and co-workers also exhibits some level of communication between metal centres as realised by the two quasi-reversible redox processes observed in the cyclic voltammetry the group performed. Nevertheless, there is only a 9 mV separation between peak potentials pointing to a weak communication.[97]

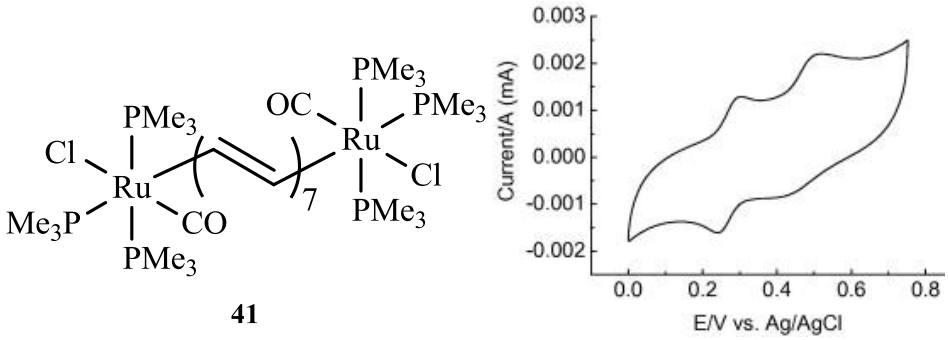

41

Figure 33. $(CH)_{14}$ binuclear cumulenic complex (**41**) with semi-reversible two wave processes (CV plot). Adapted from ref. [96].

Decrease in transport through longer bridges was also reported for aromatic systems such as the ones in Figure 34.[66a, 98]

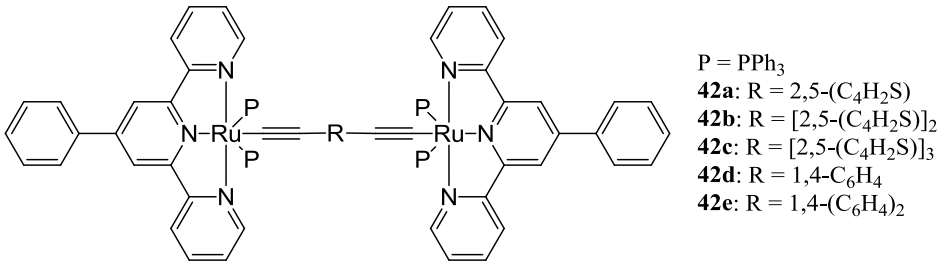

Figure 34. Binuclear systems reported by Gao and co-workers. Adapted from ref. [98].

Li and co-workers[54a] studied transport between two ferrocenyl moieties (Figure 35) and found that sulphur can be used instead of oxygen as an electrically equivalent although oxygen shows superior transmission (attributed to the readily accessible 2*p* electrons). Furthermore, triple bonds were found to attenuate, thus making its use in molecular wire preparation problematic.

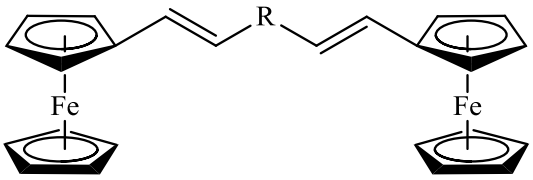

43a: R = S
43b: R = O
43c: R = S
43d: R = CH_2
43e: R = CH_2CH_2
43f: R = C≡C
43g: R = CH=CH
43h: R = PPh
43i: R = P(=O)Ph
43j: R = P(=S)Ph
43k: R = C=O
43l: R = CH^+
43m: R = "-"

Figure 35. Ferrocene systems studied in Li's report. Adapted from ref. [54a].

I.6.4. Other binuclear systems

As would be expectable in this highly explored field, some other types of binuclear or bimetallic systems based in other coordination bridging ligands have been reported. Nevertheless, a recent report by Astruc *et al.*[99] shows that only a slight splitting of $\Delta E_{½}$ = 85 mV (regarded by the authors as indicative of inter-metal communication) on the cyclic voltammogram is visible for [{FeCp(dppe)}$_2${1,4-$C_6H_4(CN)_2$}][$(PF_6)_2$] (Figure 36) which is greatly lower than the reported $\Delta E_{½}$ of 260 mV for the analogue 1,4-diethynylbenzene complex reported by Nervor and co-workers.[100] This was attributed to the fact that the C≡N bond has low energy π-bonding orbitals as a consequence of the 2*p*(N) shell's lower energy which leads to small nitrogen participation in the π-type HOMOs. This leads to a situation where, in the complexes, the mixing of the linker's π-type MOs with the t_2g metallic orbitals is not favoured.[99] In contrast, there is good mixing of the mentioned orbitals in the bis(acetylide) systems as already discussed previously even if in lesser extent than the Ru counterparts.

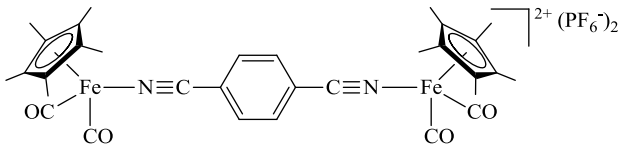

44

Figure 36. [{FeCp$(CO)_2$}$_2${1,4-$C_6H_4(CN)_2$}][PF_6]$_2$ binuclear Fe complex studied by Astruc *et. al*. Adapted from ref. [99].

Barbieri and co-workers reported the preparation of binuclear Ru (II) bypyridine bridged by ethynylene-oligothiophene-ethynylene linker (Figure 37). Polypyridine Ru (II) complexes, either mono or polynuclear are wildly reported in the literature as bearers of

significant properties such that include absorption and emission that make them suitable for several optoelectronic applications. Apart from experimental difficulties, the binuclear Ru (II) oligothiophenes represented in Figure 37 (the other compound, RuT_3, has 3 thiophene moieties instead of 5, RuT_5, as in the figure), the group reported two irreversible oxidations for both the compounds. The increase in ligand length (from 3, T_3, to 5, T_5, thiophene moieties) leads to the decrease of the oxidation potentials and the quasi-reversibility of the processes for the longer ligand, probably due to better stabilization of the oxidized species.[101]

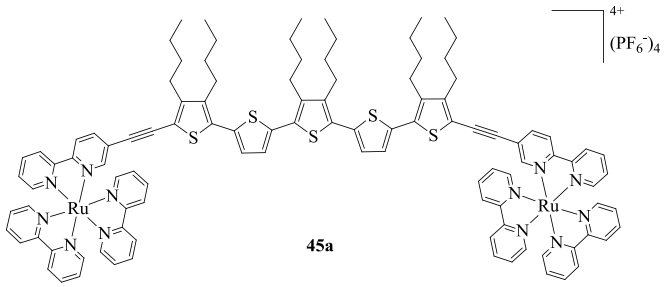

Figure 37. One of the wires (**45a**, RuT_5) reported by Barbieri and co-workers. Adapted from ref. [101].

Both trends are visible in the corresponding complexes that show a thiophene centred oxidation (one electron) at 1.08 and 0.91 V (3 thiophene and 5 thiophene bridged complexes respectively). The second oxidation was considered to be two electrons and attributed to simultaneous oxidation of both Ru (II) centres. The values of 1.33 and 1.32 (respectively for RuT_3 and RuT_5) are very close and denote the low influence of bridge length. The authors expect that the second thiophene oxidation (visible on the free ligands) to be concealed beneath the Ru (II) two electron oxidation. A shift to red and increase on the molar extinction are visible upon increase of the ligand length. This increase is less pronounced in the case if the binuclear complexes.[101] The group had reported earlier the compound depicted in Figure 38 which also only presented one redox process for the three Ru (II) centres.[102]

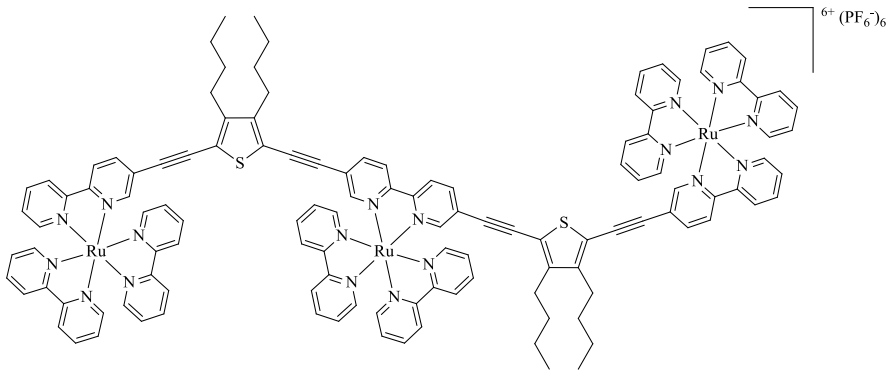

45b

Figure 38. Trinuclear ethynylthiophene bridged Ru (II) complex. Adapted from ref. [102].

The following dicarboxylate binuclear tungsten and molybdenum complexes stand as a great testimonial of the work performed by the Cotton group.[103] These complexes contain metal—metal (MM) quadruple bonds of configuration $\sigma^2\pi^4\delta^2$. Spacer ligands include for the linear complexes (Scheme 8, **A**) oxalate, terephthalate, perfluoroterephthalate, 2,5-dihydroyterephthalate, dithioterephthalate and 2,6-azulenedicarboxylate and for the paddle wheel conformation (Scheme 8, **B**) the ligands can be for example: 3,6-dioxypyridazime, anthracene-1,8-dicarboxylate and 2,7-dioxynaphthyridine. These systems usually show two wave redox processes with better K_c values for tungsten complexes and in their singly oxidized forms (mixed valence system), are seen to traverse from valence trapped, Class II, to fully delocalized, Class III.

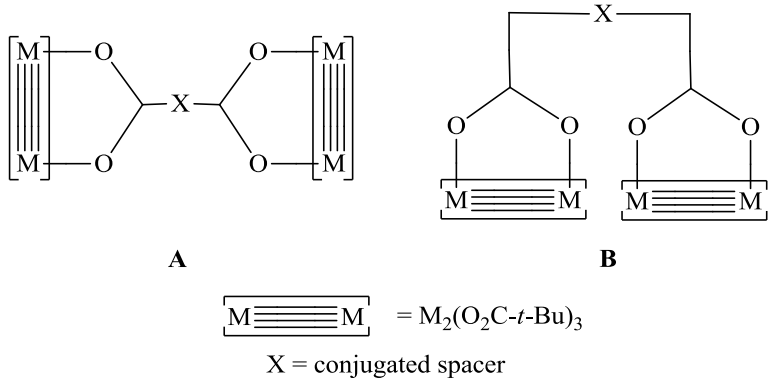

Scheme 8. The two types of orientation reported for these dicarboxylate binuclear complexes. Adapted from ref. [103b].

Another example of similar systems, although not binuclear are the ones reported by Ruben and co-workers[104] showed that the insertion of a ruthenium terpyridine complex permits for continued delocalization throughout the bridge even when submitted to bending in a cardon-joint** type movement (Figure 39).

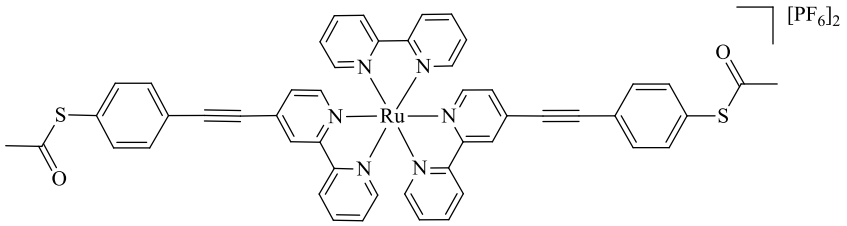

46

Figure 39. Cardan type junction reported by Ruben and co-workers. Adapted from ref. [104].

Harriman an co-workers[105] reported the ruthenium (II) bis(2,2':6',2''-terpyridine) complexes presented in Figure 40. These compounds are comprised of a bridging thiophenyleneethynylene ligand and bis terpyridine Ru termini. In the case of compound **48**, there is a central Zn bis terpyridine motif. Notwithstanding, both the compounds show only one redox process which the group attributes to both Ru centres oxidizing at the same potential and thus implying no communication.

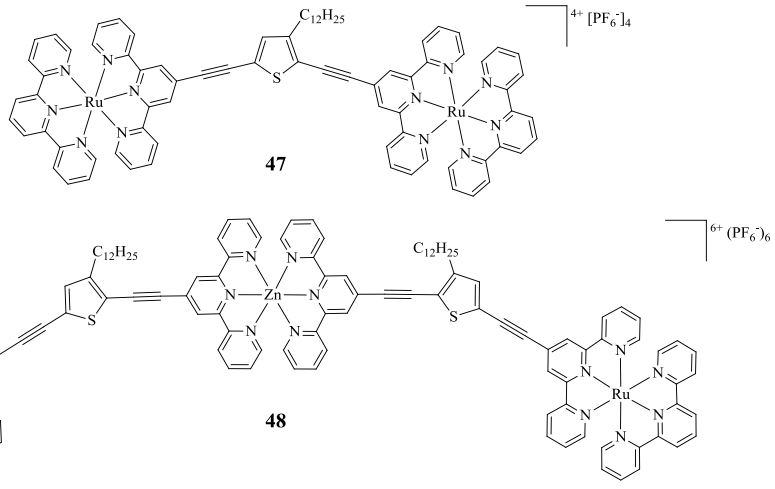

Figure 40. The ruthenium(II) bis(2,2':6',2''-terpyridine) complexes reported by Harriman and co-workers. Adapted from ref. [105].

**Cardan joint or universal joint is a type of mechanical joint or coupling in a rigid rod that allows the rod to 'bend' in any direction.

As an example of a trimeric wire, the interesting report by Ying and co-workers shows that a 20 Å long butadiyn-diyl bridged wire presents delocalization over the extension of the length of the complex (Figure 41).[106] This report is a little shorter than the previous reported trinuclear $Ru(dppe)^{2+}$ complex reported by the group of Rigaut.[46]

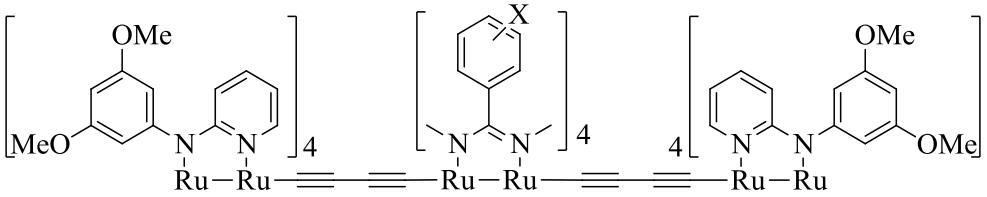

49a: X = MeO
49b: X = 3,5-$(MeO)_2$

Figure 41. The trimeric complex prepared by Ying and co-workers. Adapted from ref. [106].

A very similar complex was reported by Wong but bearing $SiMe_3$ (Figure 42) capping moities. Nevertheless, the group also reports two redox process, although of the quasi-reversible nature.[107]

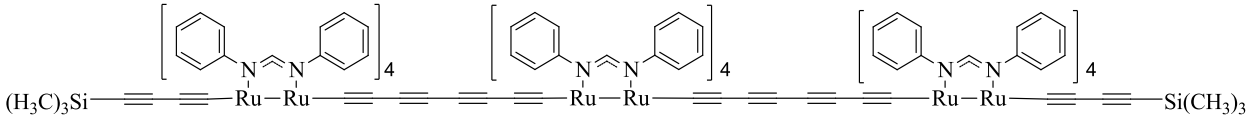

50

Figure 42. Trinuclear complex prepared by Wong and co-workers. Adapted from ref. [107].

Rigaut and co-workers also studied the transport over a Si hybrid bridge (Figure 43). It was found that the system shows two one-electron reversible redox processes for compound **51a**. Nevertheless, the separation between process diminishes as the number of Si units increases and for compound **51c**, only one reversible two-electron process is observed in the cyclic voltammetry studies. Furthermore, the hybrid bridge acts as electron withdrawing since the oxidation potentials are slightly higher than the all-carbon counterparts.[66b]

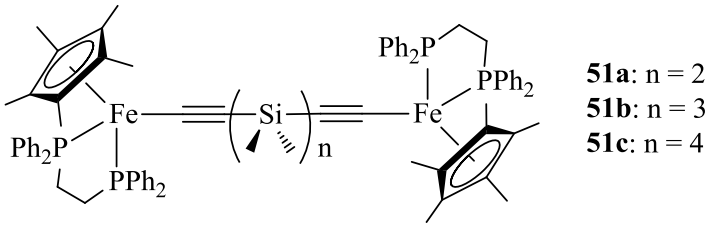

Figure 43. The Si hybrid wires prepared by the group of Rigaut. Adapted from ref. [66b].

Eggers and co-workers described the preparation of ferrocenyl capped norbornyl based wires (Figure 44). These were attached to a gold electrode and their electrochemistry was tested. Furthermore, tests using STM were also performed pointing to good properties. The group compared its rigidity and tilt angle (on the SAMs) to be on par with those of the alkanethiols. Furthermore, it was found that electron transport was produced *via* superexchange.[108] The charge transport mechanism and electron transport properties are supported by groups that produced similar results.[2c, 109]

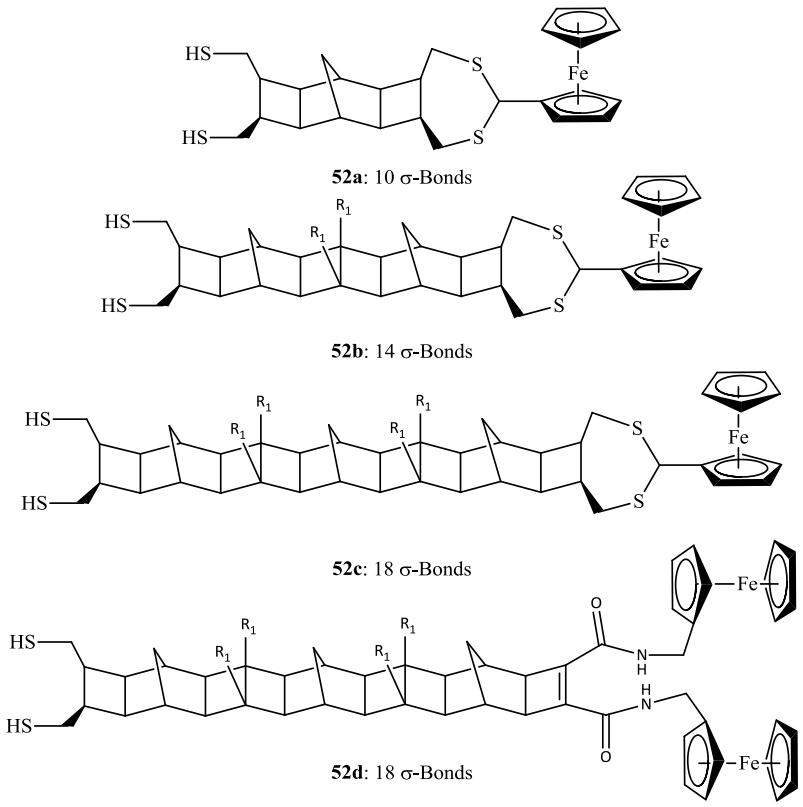

Figure 44. The norbornyl based systems reported by Eggers and co-workers. R_1= CH_2OCH_3. Adapted from ref. [108].

The group of Low[110] prepared carborane hybrid wires [{Ru(dppe)Cp*}$_2${μ-1,12-(C≡C)$_2$-1,12-$C_2B_{10}H_{10}$}] (Figure 45, **53a**) and [{Ru(dppe)Cp*}$_2${μ-1,10-(C≡C)$_2$-1,10-$C_2B_8H_8$}] (**53b**) also bearing inter-metal communication by evidence of two reversible one-electron processes in the cyclic voltammetry. Notwithstanding, the separation of the two processes were rather small with K_c of 35 and 116 (for **53a** and **53b**, respectively).

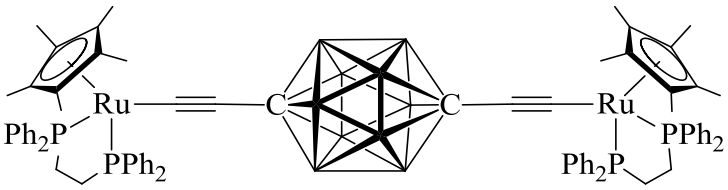

53a

Figure 45. Carborane hybrid wires (**53a**) prepared in the group of Low (central moiety is carborane $C_2B_{10}H_{10}$). Adapted from ref. [110].

Insulated molecular wires (IMW) have been getting some attention lately because of the fine tuning and better controlling of the conducting properties of already known conducting polymers or oligomers like for example some polyaniline materials.[111] These wires may be rotaxanes or pseudorotaxanes with conducting inner rods or polymer wrapped wires, where the conducting wire resides on the cavity formed by the insulating polymer or in the case of the dendronized IMWs, the actual wire has a repeating dendron moiety that isolates the inner backbone (Figure 46).[112]

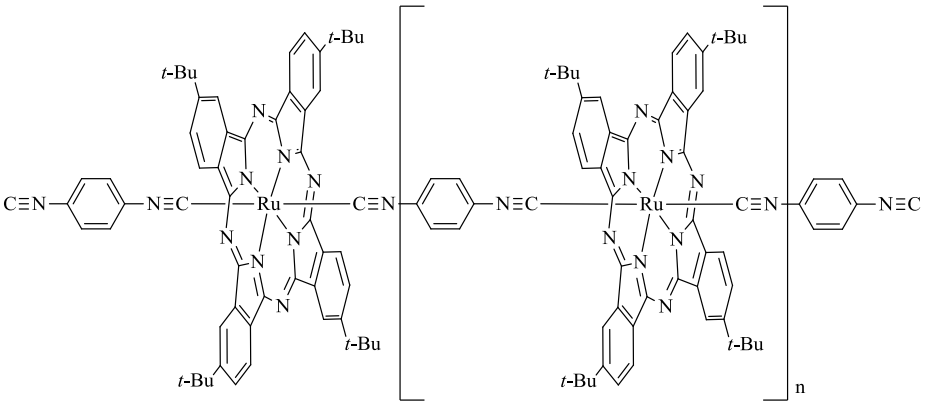

54

Figure 46. "Shish-kebab" type of IMW polymers. Adapted from ref. [112b].

Jang and co-workers[113] reported the preparation of Rh–Rh wires (Figure 47) based on the $Rh(CO)_2Cl(amine)$ moiety. Nevertheless, the report does not include any relevant transport studies but does mention a shift to blue on the absorption spectrum of the solid samples when longer amines are used. This is attributed to van der Waals forces rising from packing that increase metal–metal distance.

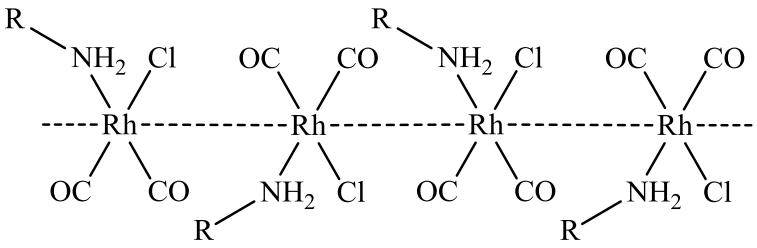

55a: R = C_4H_9
55b: R = *t*-Bu
55c: R = Ph
55d: R = *N*-C_5H_5N
55e: R = CH_3
55f: R = C_8H_{17}
55g: R = $C_{18}H_{37}$

Figure 47. Molecular wire candidates studied by Jang and co-workers. Adapted from ref. [113].

Cacialli *et al.*[114] reported the preparation of a polyrotaxan molecular wire (Figure 48) constituted by an organic conjugated polymer threaded through cyclodextrin insulating rings. The group used these compounds to produce LEDs since these wires behave as semiconductors.

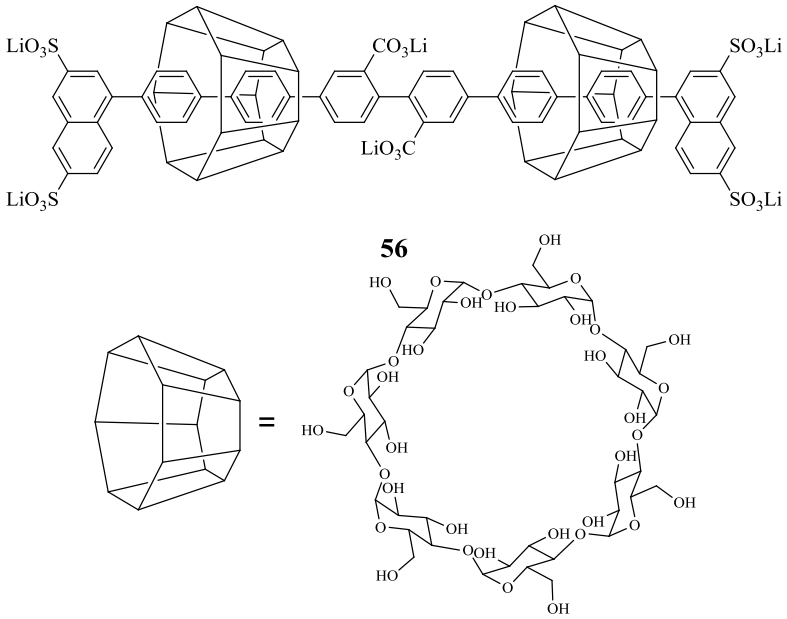

Figure 48. Insulated molecular wire prepared by Cacialli *et al.*. Adapted from ref. [114].

The group managed, by using this strategy to minimized inter-strand interactions and packing effects that lead to luminescence quenching and shift emission to a broader and longer wavelength (red shift). As such blue LEDs were produced, which attending to the fact that these are organic LEDs, is an important breakthrough.[114] Similar compounds have since been reported by Chang and co-workers in regard to thin film preparation[115] and by the group of Seki.[116] For a review about this subject see the report of Frampton and Anderson.[112a]

I.6.5. Photonic molecular wires

One of the major trends in molecular electronics believes that these new molecular devices will be driven by light. As such, light sensitive or light powered, so called photonic molecular wires are a very important field of research. Main advantages of photonic wires relate to their facile addressability (*e.g.* by wavelength or polarization), picosecond reaction rates and tailoring output performance. Moreover, light related quantum phenomena (like single to triple state quantum jumps, on-off fluorescence blinking, *etc*) is observable at ambient temperature whereas low-temperature is required for molecular electronics.[14a] However promising, the photonic molecular devices face the same roadblocks associated to molecular wires. These problems were already discussed and are related to implementation and connectivity to extra-nano world.

These wires work by absorption of light by one of the chromophores that compose the wire generating an excited state which is transmitted through the wire to the collecting chromophore where the photon is emitted.[14a, 117]

Visible light excitation can induce charge transfer from the excited donor to the acceptor or from the donor to the excited acceptor (by producing a spatially separated radical ion pair). These processes can be characterized by electron transfer rate constants (k_{ET}, Equation (4)).[117]

$$k_{ET}=k_0 e^{-\beta R_{DA}} \quad \textbf{(4)}$$

Where k_0 is a kinectic preexponential factor, R_{DA} accounts for the donor-acceptor distance, and β is the so called attenuation factor which is often used a measure for the wire-like behaviour of the compound in study. This is due to its dependence on coupling between the donor and acceptor terminals and energy of electron/hole transfer states localized there in. This

constant can vary from 1.0 to 1.4 $Å^{-1}$ for protein structures and from 0.01 to 0.04 $Å^{-1}$ for highly π-conjugated bridging structures.[117]

The Förster Resonance Energy transfer (FRET, also sometimes called Fluorescence resonance energy transfer) is the inherent mechanism to this transfer. It is non-radiative and based on the interaction between the electric field of the transition dipole moments of donor (emission) and acceptor chromophores. (Scheme 9) This leads to an interesting situation where most of the fluorescence does not originate from the molecules directly excited by the incident light but from molecules that receive the energy *via* FRET process. Furthermore, it is necessary that the acceptor is able to absorb at the donor emission wavelength. Donor should have high absorption and thus high extinction coefficient and should also be a fluorophore. The acceptor does not need to be a strong absorber.[118]

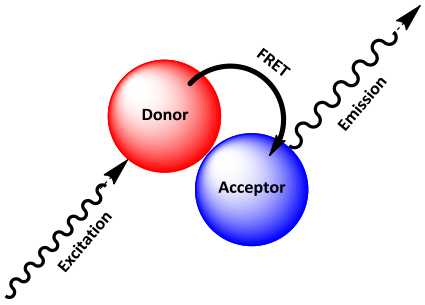

Scheme 9. General cartoon of the FRET process. Adapted from ref. [119].

There are several other details pertaining to the FRET process (*e.g.* the Förster radius which is the distance at which the energy transfer is 50% efficient) that will not be discussed here as there are not relevant to the remainder of the work. Comprehensive coverage of this matter is made on the book by Lakowicz[118] and in the mini-review by García-Parajó.[14a] One of the most well-known applications for FRET is related to protein binding: two residues are labelled with a donor and acceptor and if FRET emission (from the acceptor) is observed, then there was binding between those residues. Even if direct binding is not achieved, absorption/emission ratios for known FRET pairs permits the estimation of distance between the donor and acceptor and thus the residues.[118]

Porphyrins and phtalocyanines have been heavily studied in respect to their applications in the field of photonic molecular wires. This class of dyes shows not only good electrochemical but also good photophysical properties. They possess 11 and 19 π bonds respectively and can

bind almost every metal in the periodic table. There is a great range of literature regarding all the properties, application and chemistry of the referred class of compounds.[120] Porphyrin base systems can range from the more often found porphyrin – spacer – porphyrin[120-121] to the Porphyrin – spacer – fullerene reported below.[122]

Molina-Ontoria *et al.* reported an [2,2']Paracyclophane-based wire a favoured electron direction which is from the C_{60} donor to the zinc porphyrin (Figure 49). The authors admit that the dominant charge transfer process is by hole transfer with β values in the 0.039 $Å^{-1}$ range from excitation of the porphyrin fragment. Nevertheless the inclusion of the paracyclophane moiety disrupts the delocalization.[122]

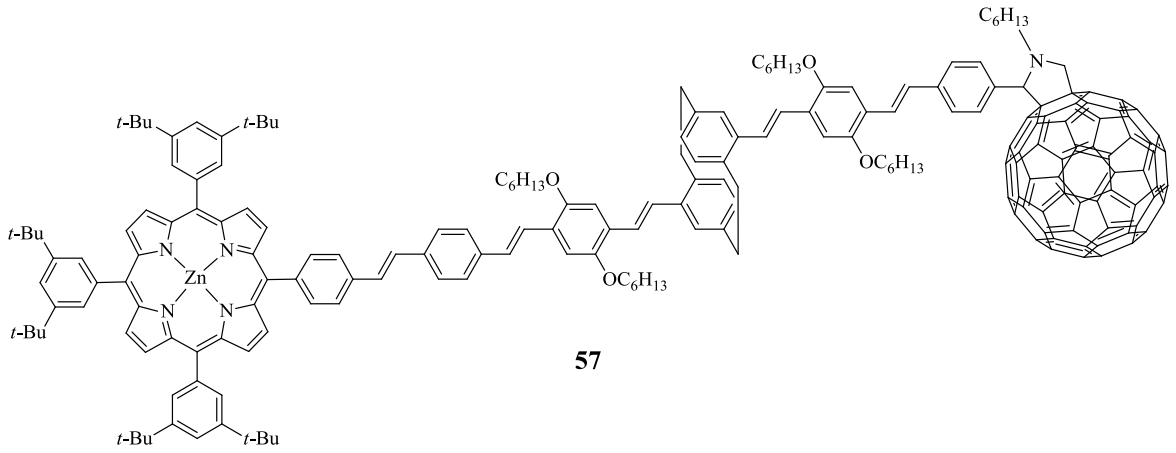

57

Figure 49. One of the ZnPorphyrin-Paracyclophane-C60 wires studied by Molina-Ontoria *et al.*. Adpted from ref. [122].

The group of Lindsey[123] has also reported an array of porphyrin base molecular photonic wires that uses a dye to harvest the light (Figure 50).

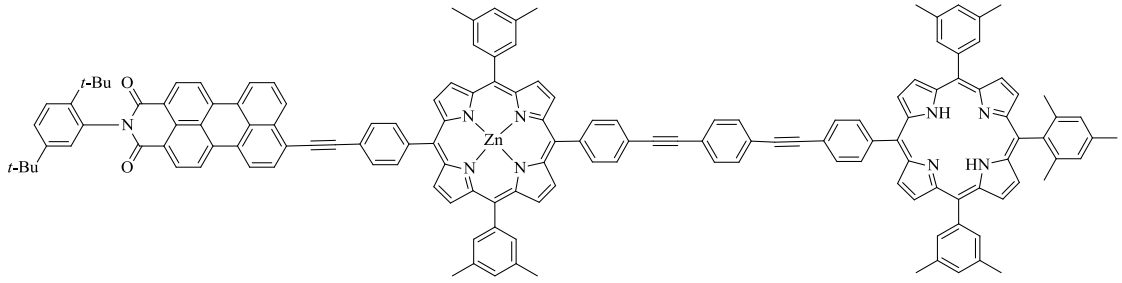

58

Figure 50. Porphyrin based molecular photonic wire reported by Lindsey and co-workers. Adapted from ref. [123].

Furthermore, there are, as expectable for this type of complexes (known for their light harvesting properties), reports of photonic molecular wires bearing terpyridyl Ru and Os terminals (Figure 51).[124] In this study, there is a quenching of the fluorescence of the spacer by charge transfer to the complex terminals as the resulting absorption spectra exhibit behaviour of the exited Ru and Os moieties. This is true for both homonuclear and heteronuclear wires. Nevertheless in the case of the latter, quenching of the Ru moiety was also observed by charge transfer to the Os terpyridyl complex. Moreover, this transfer is dependent on the length of the spacer.[124]

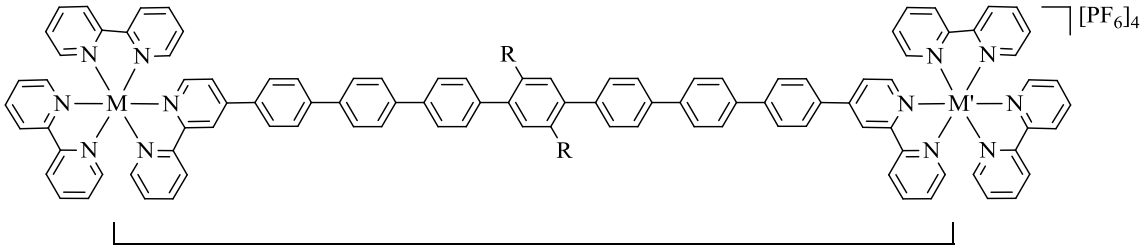

59

M = M' = Ru : $[Ru(bpy)_3\text{-}(Ph)n\text{-}Ru(bpy)_3]_4^{+}$
M = M' = OS : $[Os(bpy)_3\text{-}(Ph)n\text{-}Os(bpy)_3]_4^{+}$
M = Ru; M' = Os : $[Ru(bpy)_3\text{-}(Ph)n\text{-}Ru(bpy)_3]_4^{+}$

n = 3, 5, 7
R = n-hexyl

Figure 51. Example of a terpyridyl Ru and Os bi terminated photonic molecular wire. Adapted from ref. [124].

As with the porphyrin based wires, the terpyridyl terminated analogues have also privileged from close attention. Testing of conditions like spacer twisting – in the case of biphenylene type bridges – controlled by a crown ether and its interaction with cations (Figure 52). Nevertheless, the most interesting finding in this report is the dihedral angle dependence for light-induced electron transfer is in fact 45º.[125] Electron exchange is attributed to nuclear tunnelling through the σ-bond when the angle is 90º and to super-exchange between the phenyl rings when they are co-planar (dihedral is 0º).[125a]

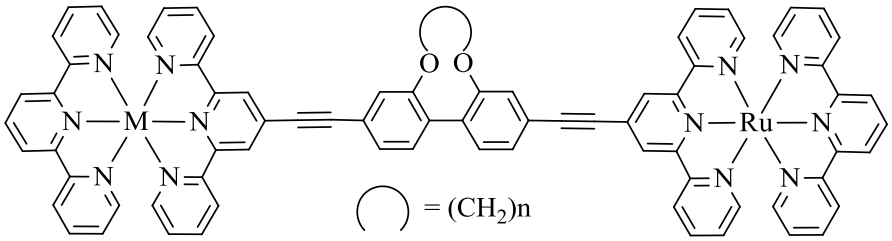

60

Figure 52. Example of a terpyridyl terminated photonic molecular wire. M = Ru^{2+}, Os^{2+}, n = 1-3. Adapted from ref. [125a].

I.7. Side chains and decorations

Side chains have the major advantage of increasing solubility.[126] This is a legitimate concern once the number of phenylene ethynylene units increases. These decorations also facilitate the preparation of thin films,[5, 127] increase solubility in light emitting polymers,[128] improving optimal interface with other co-polymers in bulk hetero-junction solar cell devices,[129] improve electroluminescence in PPE (poly(phenylene ethynylene)) materials by forming lamellar structures that maintain long-range order,[130] inhibit chain to chain interactions and more regular polymerizations,[24] emission colour shifting in electroluminescent materials,[131] improving and tuning formation of thin films for photovoltaic cells,[132] enable the preparation of larger thiophene oligomers[23] (non-substituted limit is the 8-mer[133]), such as the 48-mer oligothiophene,[134] and the 96-mer (by β blocking to improve α selectivity).[23] In this work, the importance of side chains is studied in regard to their effect on the electronic properties of binuclear Ru and Pd complexes. The side chains that were used are based on alkoxy 2,5 derivations on the central phenyl ring and as such their electron donating properties will be a good addition to the improvement in processability brought by the improved solubility of the longer rods.

Reports of the decrease of the oxidation potential as a result of methyl (donor) β-substitution in tiophene[135] as well as the decrease in the E_g (energy gap, $E_{HOMO} - E_{LUMO}$) yielded by methoxy (also donor) substitution in phenylene vinylene oligomers[136] (Figure 53) further emphasizes the importance of side chain usage and manipulation.

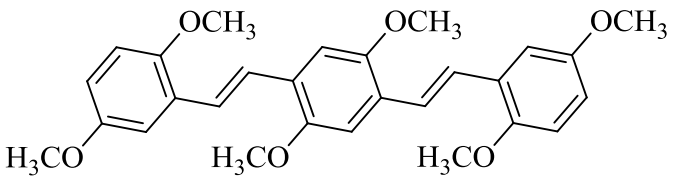

61

Figure 53. Phenylene vinylene oligomer with methoxy side chains studied by Meyers and colleagues. Adapted from ref. [136].

Akita and co-workers[82] reported the increase in delocalization and consequently the inter-metal communication when electron donor decorations are used on the bridging ligands (Figure 54) . What this means is that the electron communication increases from **62g** to **62a**.

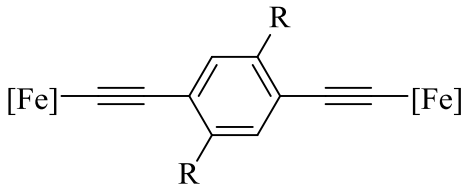

62a: R = $N(CH_3)_2$
62b: R = OCH_3
62c: R = CH_3
62d: R = CH_3
62e: R = H
62f: R = F
62g: R = CF_3

Figure 54. A family of binuclear complexes prepared by Akita and co-workers to test the inclusion of side chains. [Fe] = FeCp*(dppe). Adapted from ref. [82].

Several other authors have reported the same behaviour.[66b, 137] The added electron donation from the side chains increases the electron density at the metal centres, which in turn makes the oxidation of the neutral species easier. Moreover, the extra electron donation should stabilize further the monocation leading to an anodic shift of the second oxidation and thus larger ΔE. UV-vis/NIR studies also backup these observations with $\Delta\bar{\upsilon}_{1/2}$ (obs) significantly lower than the $\Delta\bar{\upsilon}_{1/2}$ (calc) (narrower ICT bands) which is congruent with Class III systems.

Several authors have reported the preparation of binuclear Cp*Fe(dppe) systems.[138] One interesting observation was done when using the biphenyl ligand (Figure 55 **63c**) which severely hindered the communication between metals which is in agreement with what was reported by Mayor and co-workers[18-19] and referenced previously. Complexes **63a**, **63d** and **63e** are attributed to Class III by means of CV, UV-vis/NIR analyses and **63b** by only CV which is inconclusive. There was also an observable increase in metal to metal communication when Cp*

was used instead of Cp on the complex terminals, due to the former's better electron donating power. Moreover, Δ*E* increased from 280 to 360 mV from **63d** to **63e** further reinforcing the observation that increased electron density is beneficial to inter metal communication.[138]

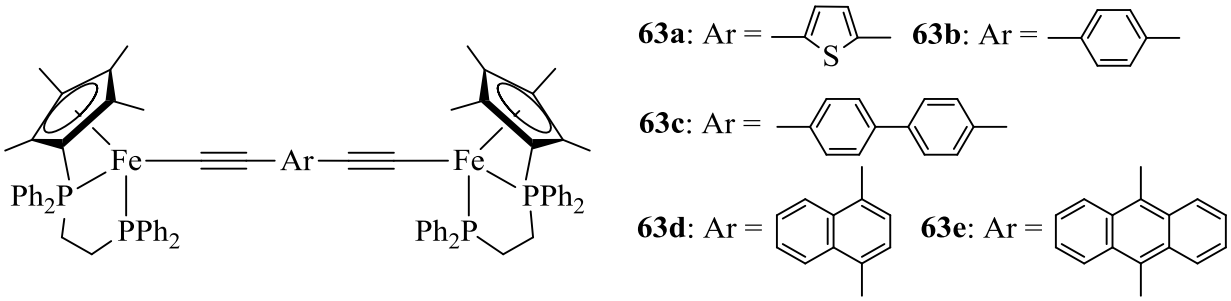

Figure 55. Study of the effect of the bridging ligand main moiety in FeCp*(dppe) wires. Adapted from ref. [138a].

Recursive usage of the nitro group was made by the group lead by Tour[5, 139] when testing potential organic molecular wires for switching behaviour as already mentioned.

Detert and co-workers[32] also studied the effect of electron withdrawing or donating substituents on OPV wires (Figure 56). It was observed that while the substituents allowed for further electronic tuning if attached to the phenylene moieties leading only small changes were visible on the resulting spectra. However, when the vinylidene fragments where modified (R_3 = H to CN), heavy bathochromic shifts were observed.

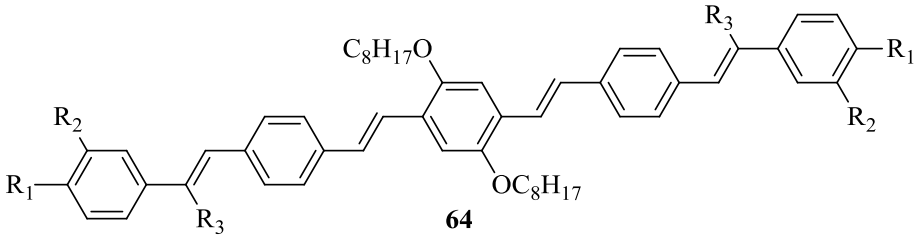

64

R_1 = CH_3, OC_6H_{13}, Br, CN, NO_2, H, OC_3H_7 or Cl
R_2 = H, CF_3, CN, R_4, $SO_2C_{10}H_{12}$, H or CF_3
R_2 = H or CN

R_4 = 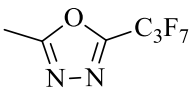

Figure 56. OPV wires studied by Detert and Sugiono. Adapted from ref. [32].

Fratoddi *et al.*[140] showed that there was a visible increase in emission intensity and relative quantum yield (about 3.16% increase) between polynuclear Pt complexes with longer alkoxy side chains ($OC_{16}H_{33,}$ **65**, Figure 57) in relation with the complexes with the shorter counterparts (OC_4H_9). On the other hand Khan *et al.*[141] reports that incorporation of side chains on the aromatic moiety has only a slight effect on the electronic properties of the Pt polynuclear complexes represented in Figure 57. This is somewhat unexpected since the series of compounds runs through electron withdrawing (**66c-f**) and donating (**66a-b**, **g-h**).

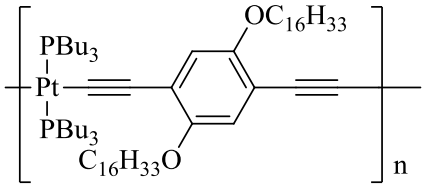

65

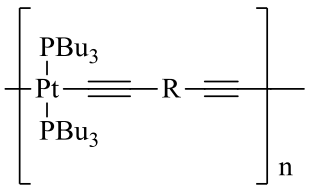

66a: R = C_6H_4
66b: R = $C_6H_3(NH_2)$
66c: R = C_6H_3F
66d: R = $C_6H_2F_2$
66f: R = C_6F_4
66g: R = $C_6H_2(OCH_3)_2$
66h: R = $C_6H_2(OC_8H_{17})_2$

Figure 57. Polynuclear complex prepared by Fratoddi *et al*. (**65**) and Khan *et al.* (**66a-h**). Adapted from ref. [140] and [141] respectively.

Liu and co-workers[142] studied the effect of increasing and decreasing the electron donating effect of decorations attached to a central phenyl ring on a series of binuclear ruthenium complexes (Figure 58). In general the group found that the electron withdrawing aspect of decorations like fluoride (e.g. **67d**, **67k**) decreases the electronic communication between centres. This was accessed by comparing the values for $\Delta E_{½}$ (since two redox processes are observed for these complexes) that range from 350 mV for compound **67j** (where $R_1 = R_2 = OCH_3$, donating group) to 180 mV for **67l** (where $R_1 = R_2 = CF_3$, withdrawing group). K_c values also support this assessment since, the respective values for **67j** and **67l** are 8.2×10^5 and 1.1×10^3.[142] The group continued to study the influence of side chains by preparing another series of binuclear ruthenium complexes[143] but at this point, different alkoxy chains with growing lengths were used (Figure 59, **68a-g**), as well as with a longer organic bridge (Figure 59, **69a-c**).

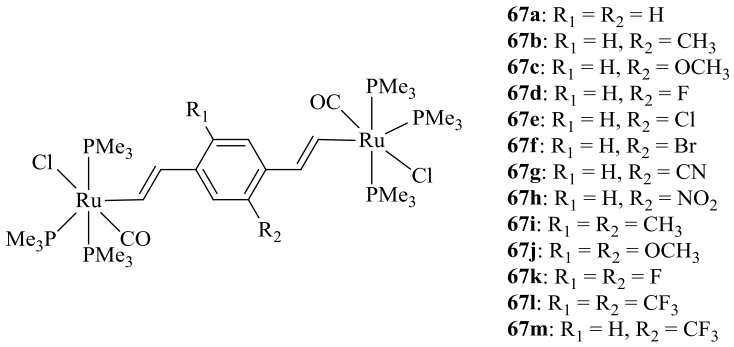

Figure 58. Binuclear ruthenium wires with electron donating and withdrawing side chains. Adapted from ref. [142].

The group observed that $\Delta E_{½}$ and K_c only changed from **68a** to **68b** and then maintained their values through the series (**68b-g**). Furthermore, the difference was small with 350 to 370 mV for $\Delta E_{½}$ and 8.2×10^5 to 1.8×10^5 for K_c. In respect to the systems with longer bridge (**69a-c**), the separation, $\Delta E_{½}$, between the redox processes was even smaller, with the highest value being for **69b** with 120 mV and with a K_c of only 1.1×10^2.[143]

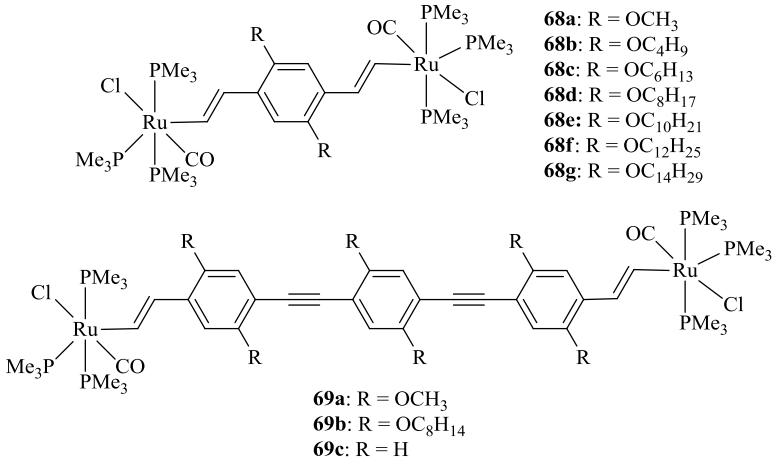

Figure 59. Binuclear ruthenium complexes with growing alkoxy side chains. Adapted from ref.[143].

Still using the same ruthenium moiety Liu and co-workers[144] prepared binuclear ruthenium complexes with dendritic side chains (Figure 60). Nevertheless, CV studies show that as the dendritic attachments grow (**70a** to **70c**), there is no significant change in the electrochemical properties since $\Delta E_{½}$ and K_c are *ca.* 0.34 mV and 5×10^5 respectively for the three complexes.

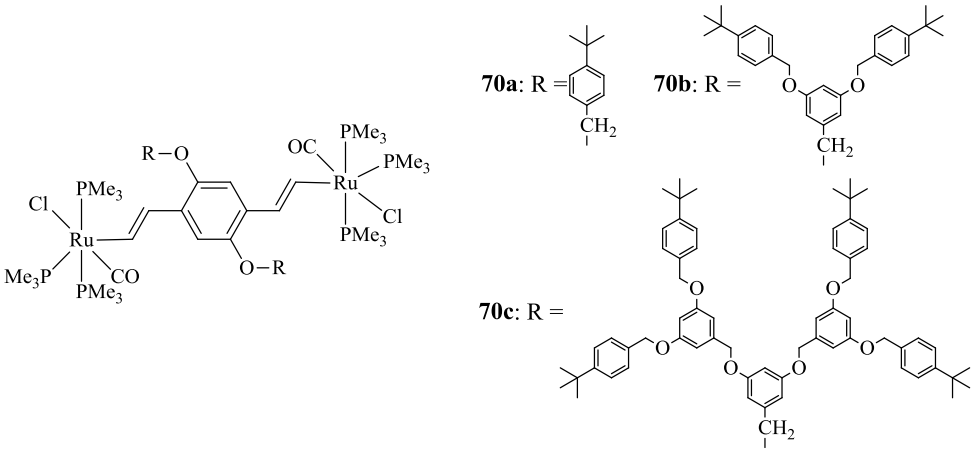

Figure 60. Binuclear ruthenium complexes with dendritic side chains. Adapted from ref. [144].

I.8. Alligator clip molecules

Albeit the various approaches used to characterize a molecular device in terms of its application to molecular applications, one important facet of this characterization is the junction between the metal lead (from the testing device) to the molecule. This connection, a part of the wire molecule is normally described as an "alligator clip". This is the section of the molecular wire which is responsible for the attachment and communication with the outside world. It is the most used form of facilitating single molecule transport measurements as it enables the formation of SAMs (self-assembled monolayers) on an electrode. Theses SAMS can then be scanned by several techniques.[18] Tour reported in 1998[8a] the mechanically controllable break junction testing of a series of phenylene-ethynylene oligomers that were bound between two gold electrodes. The testing molecule for this technique was benzene-1,4-dithiol.[8a] Since then the thiol anchoring (Figure 61, **71a**, protected) is the most used "alligator clip" which can be attributed to the strong chemical bond to the metal leads that ensures that the current flow is only affected by the wires HOMO level.[18]

Notwithstanding of the great breakthrough, the lack of reproducibility that can derive from the molecule not being properly bonded to both electrodes, effective binding site of the thiol on the gold surface as well as molecule orientation have sparked some studies in this matter.[18, 145] Other popular types of alligator clip molecules reported in the literature include the

4-ethynylpyridine,[146] isocyanobenzene,[57] benzonitrile,[147] and 3-alkyl-1,2-dithiolane[57, 147] (Figure 61, respectively, **71b-c**). Nevertheless, there is a myriad of potential alligator clip motifs. These are usually chosen in regard to the type of substract (*e.g.* gold or silica) that is going to used or in regard to chemical stability to other functional groups (*e.g.* when the chemiadsorption is performed).[18] As such the electrode biding site can be acetylenes,[148] amines,[149] nitriles,[20] carboxylic acids,[149b] phosphines,[149c] sulfides,[149c] fullerenes,[150] thiocarbamates,[151] phenylenes[152] and π–π system in benzene stacks.[153]

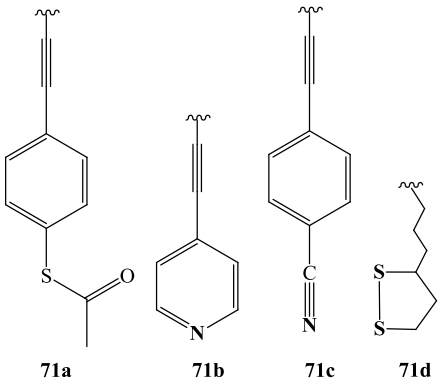

Figure 61. The most reported types of "alligator clip" molecules found in the literature. Adapted from ref. [8a], [146], [57, 147] and [57, 147] respectively.

Recently, Chen and co-workers[154] reported the preparation of direct covalent C–Au molecular junctions (Figure 62) starting from $SnMe_3$ terminated precursors. The group reported good coupling between the π-conjugated wire and the gold leads.

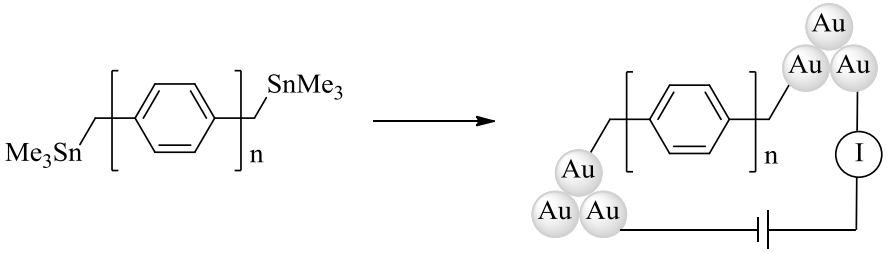

Figure 62. Direct C–Au molecular junction reported by Chen and co-workers (n = 1-4). Adapted from ref. [154].

The last advances on this subject point to the preparation of tripodal clips that increase not only stability and biding ratio, but also improve electronic transport.[155] Bryce and co-

workers[155a] have recently reported the usage of fullerene C_{60} as the alligator clip to connect an organic bridge (Figure 63) to two gold leads. The group observes that the C_{60} motifs not only work as an alligator clip, but also as something of a molecular beacon that is easy to spot for imaging purposes. This clip also allowed for room temperature measurements in STM-BJ experiments. Notwithstanding, there was a large range of conductance plateaus which made attribution conductance values to single molecules not possible.

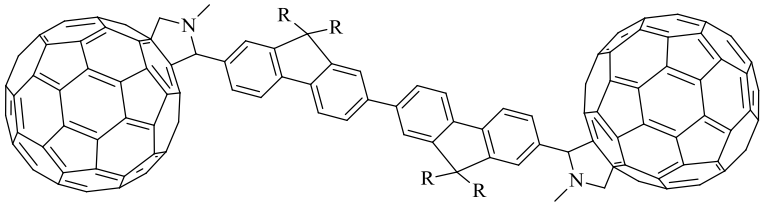

72

Figure 63. Fullerene C60 terminated wire studied by Bryce and co-workers. Adapted from ref. [155a].

Ie *et al.*[155b] have developed tripodal motifs with selenium functional groups (Figure 64). These clips suffer deprotection by H_2SO_4 to form Se-Au bonds (on Au electrodes). The group compared the Se compounds with thiol counterparts since the later are the most used when chemiabsording to gold. They found that the selenol compounds (Figure 64) show an electronic state more suitable to reduce the barrier for molecular conductance. This observation was performed in accordance to XPS (X-ray photoelectron spectroscopy) measurements.

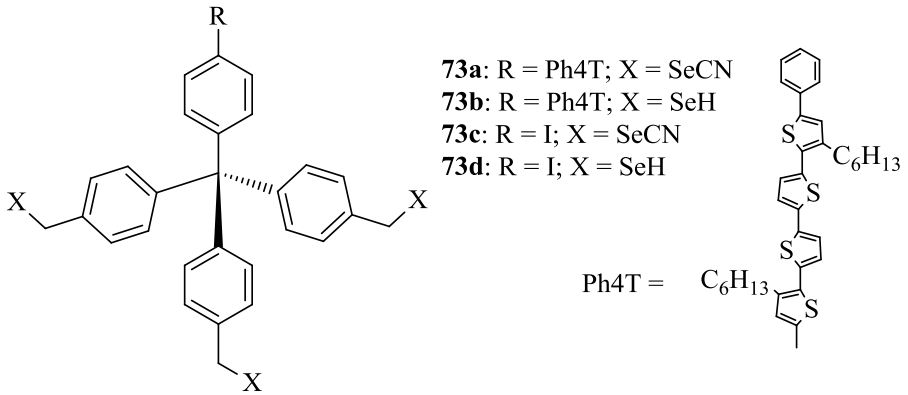

Figure 64. Selenium functionalized alligator clips. Adapted from ref. [155b].

The same group also prepared[155c] pyridine terminated dimers (Figure 65) to probe for π hybridization from the pyridine ring to the metal lead. It was observed that not only the hybridization occurred, but also that the tripodal arrangement brought not only greater adsorption (in comparison with single pyridine terminated rod) to a gold substract but also adds increased robustness under bias (whilst testing the monolayers). The group also found that the conduction values for this compound were higher than any other rods with single pyridine clips.[155c]

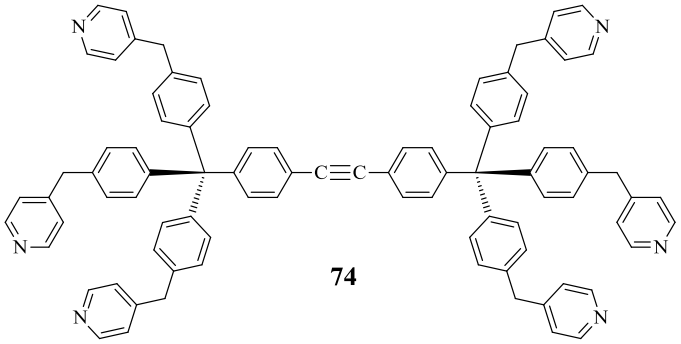

74

Figure 65. Pyridine terminated rods. Adapted from ref. [155c].

I.9. Testing of molecular wire candidates

Several methods have been used to measure transport in molecules or small groups of molecules. These include mechanical or electromigration break junctions, nanopores, crossed-wire junctions, mercury drop electrodes and several scanning probe methods like scanning tunnelling spectroscopy (STS), STM (Scanning Tunnelling Microscope) or conducting probe atomic force microscopy.[14b] These experiments suggest that transport is controlled by the molecules' properties, the contacts ("alligator clips") and the metal leads. Also of importance are: the molecular length (as discussed before), conformation, HOMO/LUMO gap and its alignment with the metal's Fermi level[††] as well as the molecule-metal (lead) coordination geometry.[18, 157]

Another method for metal-molecule-metal linkage testing is the crossed-wire juctions[157-158] (Scheme 10). These junctions are composed of the molecule being studied

[††]It pertains to the top energy level of the electrons of the metal and is situated in the conduction band for conductor materials [156]

modified as a SAM on an electrode forming one wire. The other wire is then brought in tunnelling distance and a Lorentz force acts on further bringing the orthogonal wires together. The Lorentz force is controlled by the current and an external magnetic field and can thus be used to change the pressure exerted on the molecule. These experiments are generally used in the study of subtle effects like the pressure exerted by the top contact on the conductance of molecular devices.[157-158]

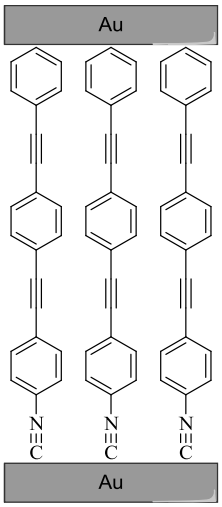

Scheme 10. Cartoon of a cross-wire junction. Adapted from ref. [158b].

Metal beads are also used as electrical leads that have the advantage of covering relatively few molecules which is advantageous when trying to study single molecule conductance.[157-158] This method (Scheme 11) has the main advantage of the conductance values not being as dependent on the pressure of the probe tip like in other direct measure (where the tip contacts directly with the molecules).[157]

First reported by Whitesides,[159] mercury drops have been used as a simple and low-cost way to study metal-molecule-metal junctions. This method, allows not only for a mercury-molecule-metal (where the metal can be the typical gold electrodes) where the scanning tip contacts with the mercury drop it can also be used in mercury-molecule-mercury systems. Notwithstanding some of good results[160] in molecular and solid state electronics, the lack of robustness and low integrability make mercury drops unsuitable for general application.[157]

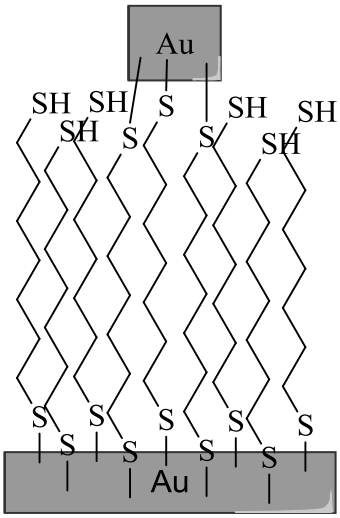

Scheme 11. Cartoon of top-contact junction using metal beads. Adapted from ref. [157].

More challenging than the previous methods, the preparation of vacant nanogaps requires a mechanism to manipulate metal-metal distances with subnanometer precision which is beyond the current lithography limits. To surmount this challenge, two solutions were found. The first one is based on controlled deposition or erosion of metal which is on a feedback loop that allows for constant monitoring of the resistance. As soon as a tunnelling distance between the leads (that form by deposition or erosion) is attained, the process is stopped. The second method employs a sacrificial layer that is removed after the metal leads are formed. For nano sized gaps, molecular monolayers are employed.[157] Although the preparation of these types of gaps is difficult, the advantage of comparing a junction without and then with the wire being tested is very interesting. Furthermore, horizontal electrode geometries are also available by these methods and the underlying substrate can serve as a third electrode allowing for further characterization.[157]

One of the used methods of vacant nanogap preparation is the mechanical break junction. In this method a metal wire is strained to the point of breakage by a piezoelectric fulcrum. When the wire breaks, the molecular wire candidates bridge the gap and establish communication between the two tips.[157, 161] Using this technique, the conductance of 1,4-benzenedithiol was studied by Tao and co-workers[162] by using the experimental setup which is depicted in Scheme 12. The molecular junction was formed by pulling a gold STM tip out of contact with the gold substrate in the presence of the sample molecules. At this point the

potentials (electrochemical gate voltages) of the gold substrate and gold STM tip were controlled in accordance to a reference electrode (Ag wire) using a gold counter electrode and a bipotentiostat. The group reported that the probability of benzene-1,4-dithiol junctions is only about 30-40%. This was inferred by the small amount of conduction curves on which steps were (when the junction is broken). Furthermore, broad conduction histograms point to variation of molecule-electrode geometry.[162]

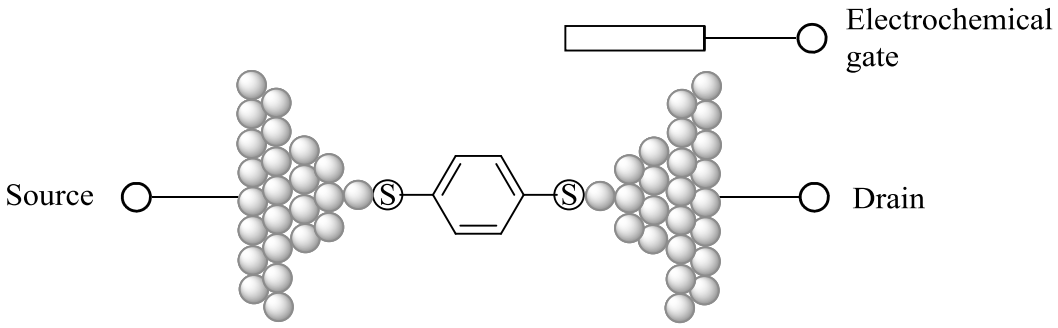

Scheme 12. Schematic of the experimental setup used by Tao and co-workers. Adapted from ref. [162].

Nevertheless, the usage of STM-BJ (Scanning Tunnelling Microscope Break Junctions) allows for the addressing of single molecules. This is done by observing the steps that can be related to the breaking of junctions between the STM tip and the molecules (Figure 66). As such, the conductance of a single molecule can be estimated.[163]

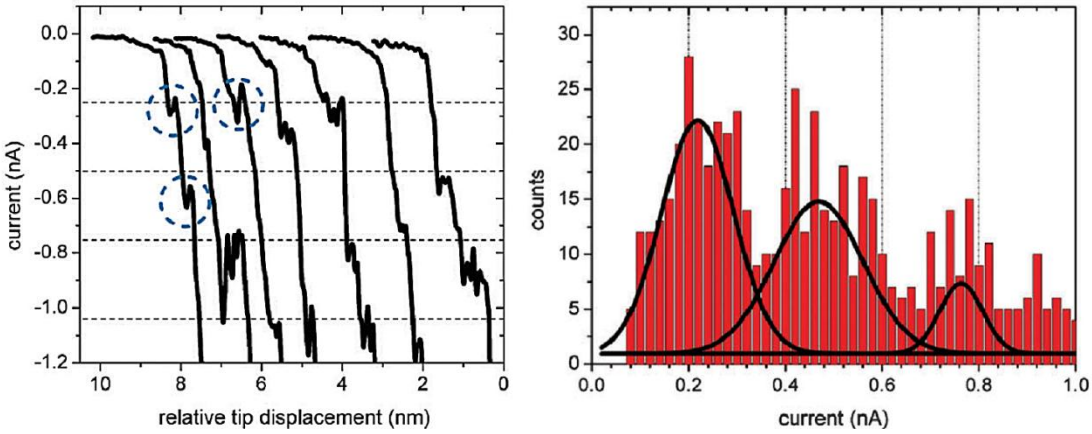

Figure 66. Representative current-distance (I(s)) traces obtained from STM-BJ experiments in UHV (left) and current histograms constructed from plateau values of about 300 I(s) traces (right) for a 4,4'-bis(mercaptoalkyl)-biphenyl derivative. Adapted from ref. [163].

This technique is used for a range of different molecules, some without an anchoring group and also for some hybrid materials like carbon nanotube bridged by single molecules.[20, 53b, 104, 164] Other methods in this class include electromigration[157, 165] – electro momentum from current ramping force the formation of gaps; lithography[157, 166] – electron beams are used in conjunction with silicon nitride membranes in order to decrease electron backscattering thus improving the resolution; oblique angle evaporation of metal vapour[157, 167] – the photoresist layer is suspended above the substrate layer thus increasing the deposition angle and decreasing the deposition thickness; Focused ion beams of Ga^{+}[157, 168] can be condensed down to ~ 10 nm but when used in conjunction with silicon slit to deposit $W(CO)_6$ gas, distances of < 3nm are achieved. Among the most recent advances in this area, are the atomic rulers,[157, 169] where molecular or atomic films are used to generate nanosized electrodes. These rulers act then as temporary scaffolds for the metal electrodes and are removed to leave a vacant gap between the electrodes.

I.10. Binuclear palladium and platinum alkynyl rods

Pd-σ-alkynyls are usually reported for the preparation of homometallic organometallic polymers[170] or some heterometallic rods (with the incorporation of Ru, Fe or Ni metal centres).[83b, 107, 171] In contrast, the preparation of discreet binuclear Pd rods is scarcely reported and only a few studies are known.[172] Some binuclear dialkynyl bridged complexes have been reported by the group of Gladysz (Figure 67).[83b] They present (the three examples of Figure 67) one electron reversible wave which the group attributes to the Re centre and one irreversible process that should be attributed to the Pd centre. The group also observes that, through comparison with similar complexes, the central Pd (Figure 67, **75b**) moiety is responsible for Re to Re communication interruption.

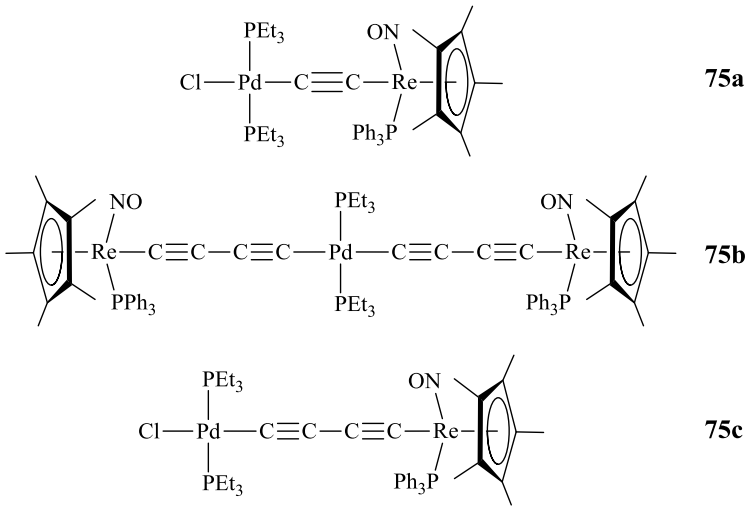

Figure 67. Heterometallic rods with $[Pd(PEt_3)_2]$ reported by the group of Gladysz. Adapted from ref. [83b].

Although chemically very similar, Pt and Pd complexes exhibit distinct electronic properties to the level of polarization of the π* features of the C≡C bond as noted by Battocchio and co-workers.[173]

Studies by Battocchio[173] showed that these compounds (Pd^{II} and Pt^{II} rods) form square planar systems with the bridging oligophenylyne ligands which in principle, would contribute to increase the π delocalization from the ring to the metal centre thus improving the conducting properties of the rod. This co-planarity between metal centre and the π system of the ligand is dictated by the ligand as Onitsuka and colleagues reported for 1,4-diethynylbenzene palladium complexes. These complexes present the metal centres slightly twisted out of the plane because of steric hindrance caused by the phosphane groups of the metal centre.[174] As such, choosing a bridging ligand that, in addition to a solid conjugate backbone, also promotes co-planarity and process ability is of great importance. As recent developments came to show, the structure and geometry of the target systems greatly influence its properties thus making a molecule as for example the insulator reported by Mayor and co-workers (Figure 68, **76c**)[53b] or as reported by other authors[175] still maintain conduction through the wire. Shashidhar and co-workers[176] prepared the series of compounds in Figure 68 (**76a-e**) in order to study the effect of the metal centre's ancillary ligands on the rods electronic properties. They found a correlation between σ-donation of these ligands ($PCy_3 > PBu_3 > PPh_3 > P(OEt)_3 > P(OPh)_3$, **76a-e**, respectively), and the HOMO-LUMO gap (from UV spectroscopy analysis). As such, weak σ-donor/strong π-acceptor ligands lower the gap and the strong σ-donor/weak π-acceptor phosphines bring the

energy gap to higher levels. Notwithstanding the effect is rather small and the HOMO-LUMO gap values (3.4-3.5 eV) are indicative of a semi-conductor.

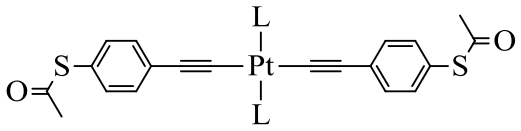

76a: L = PCy_3
76b: L = PBu_3
76c: L = PPh_3
76d: L = $P(OEt)_3$
76e: L = $P(OPh)_3$

Figure 68. Molecular Pt^{II} rods studied by Mayor and co-workers (**76c**)[53b] and Shashidhar and co-workers (**77a-e**)[176]. Adapted from refs. [53b] and [176].

In tetraethynylethene based diacetylide Pt^{II} rods, a significant influence of the insertion of the metal centre was observed by Siemsen and co-workers.[177] There is, nevertheless a noticeable decrease in conjugation through the π backbone as a consequence of the Pt which was later supported by the report of Mayor[53b] that observed a characteristic insulator behaviour for a diacetylide Pt rod. Despite the general weak π backbonding character of these square-planar Pt (and Pd) complexes, Osella and co-workers reported an increase in conjugation in a heterometallic rod brought about by the insertion of a $Pt(PBu_3)_2$ centre was also reported by Osella *et al.*[178] with the separation of the reversible redox waves of the terminal ferrocenyl centres which otherwise show only one wave.[92, 179]

Ge and co-workers[180] report the preparation of two trinuclear wires bearing [RuCp(dppf)] (where dppf is (1,1'-bis(diphenylphosphino)ferrocene, Figure 69) termini and a bridging Pd or Pt centre. The group observed two sets of redox process. One is attributed to the Ru^{II}/Ru^{III} centre and the other to the ferrocenium/ferrocene (Fc^{+}/Fc) of the dppf ligand and as such no communication between the two Ru centres is observed.

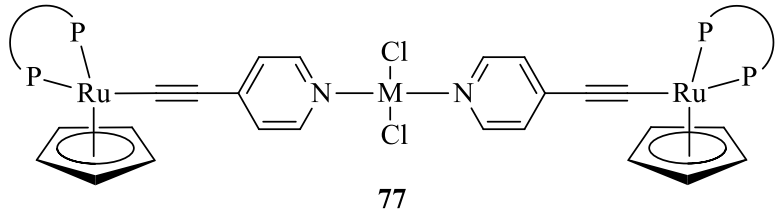

77

Figure 69. The RuCp(dppf) terminated wires reported by Ge and co-workers. M = Pd or Pt; P_P = dppf (1,1'-bis(diphenylphosphino)ferrocene).[180]

Lavastre describes[171b] a $Pd(PBu_3)_2$ moiety, inserted in the middle point of the binuclear $RuCl(dppe)_2^+$ 1,4-diethynylbenzene rod, acting as an insulating building block and breaking the conjugation which results in only one reversible CV wave for the Ru^{II}/Ru^{III} system (from distinct two waves for the same system). Weng also reports[83b] lessened delocalization on $\{[Cp^*Re(NO)(PPh_3)–(C\equiv C)_2]_2Pd(PEt_3)_2\}$ but is unable to ascertain if this is provoked by the Pd moiety or by quite long carbon chain bridging the two Re metal centres.

Low observes[2c] that in the matter of ground-state electron transfer, metals like Pd^{II}, Pt^{II}, Au^{II} and Hg^{I} are not efficient components of bridge that aims to transport electron from one terminal to the other.

Nevertheless, Jones and co-workers[181] observed two sets of distinct redox process (attributed to the triarylamine redox centres) in the Pt bridged wire presented in Figure 70. The group observed that in comparison an all organic analogue previously reported by Lambert[182] (with a phenylene unit instead of the Pt metal ion), the wave separation is almost the same (60mV for the all organic and 65 mV for this system). It is noteworthy that the group had to use differential pulse voltammetry to separate the two waves and that a K_c of only 13 was calculated.[181]

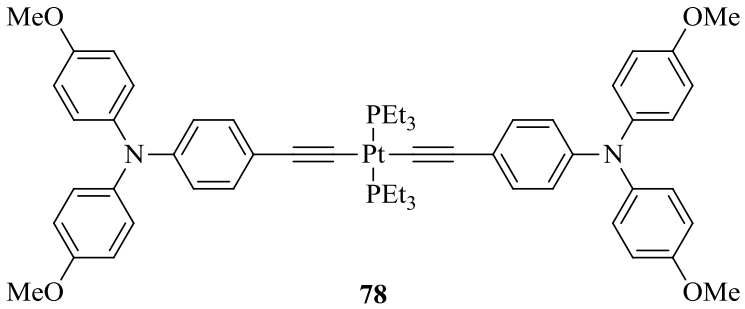

78

Figure 70. The amine terminated wire reported by Jones *et al.*. Adapted from ref. [181].

Koch *et al.*[183] have reported the preparation of a mononuclear Pd complex bearing bisacetylide ligands (Figure 71, **79a-h**). The group observed similar redox profile for all the compounds with an irreversible oxidation wave between 950 and 820 mV (DMF/0.1 M $[nBu_4][PF_6]$). Furthermore, as the electron density of the alkyne ligands increased, the oxidation potential of the complex decreased.

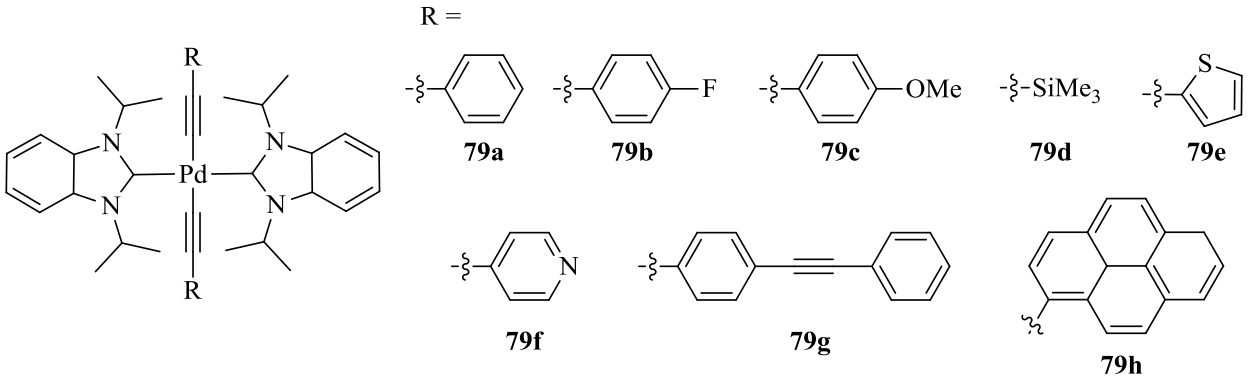

Figure 71. Palladium diacetylide studied by Koch *et al.*. Adapted from ref. [183].

Lin and co-workers[184] have reported a bisethynylphenylferrocene wire bridged by a bis fluorenone platinum centre (Figure 72). The group observed that apart from the reversible redox pair attributed to the Fc^{+}/Fc process, another irreversible oxidation of Pt^{II} to Pt^{III} was observed at higher potentials. Once more, no communication between the rods termini was attained. Similar results were presented by the same group before[52d], but the compounds featured thiophene moieties instead of the fluorenone units.

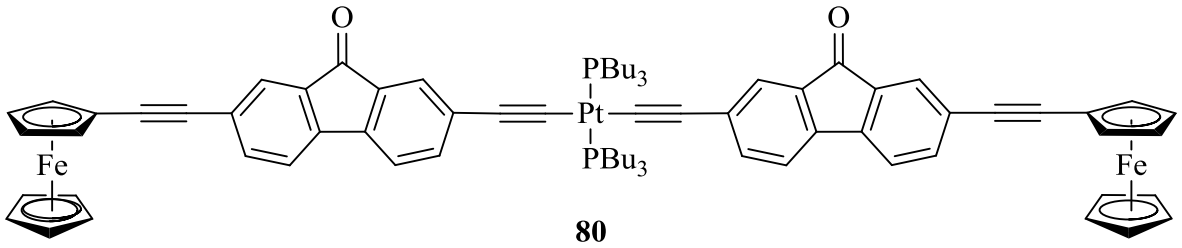

Figure 72. Fluorenone bridged Pt rod. Adapted from ref. [184].

Nozaki and co-workers[185] bridged two ruthenium polypyridyl moieties using a $Pt(Bu_3)_2$ as well as Au diacetylide bridge (Figure 73, **81** and **82** respectively). Although two redox reversible redox processes were found for these compounds, they were attributed to the Ru^{II}/Ru^{III} pair and to phenantroline ligand and as such are not to be confused with intercommunication between metal centres.

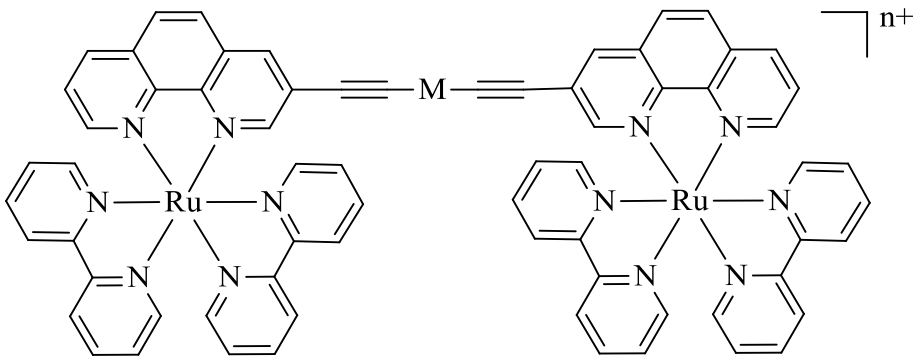

81: M = $PtP(Bu_3)_2$; n = 4
82: M = Au; n = 3

Figure 73. Ruthenium polypyridyl dinuclear complex bridged by Pt and Au moieties. Adapted from ref. [185].

Schanze and co-workers have reported[186] an oligomeric platinum acetylide (Figure 74) that works as photonic molecular wires by electron hole transference. The group suggests diffusive transport by a site-to-site hopping mechanism with hopping times of ~ 27 ps for triplets and < 10 ps for electrons.

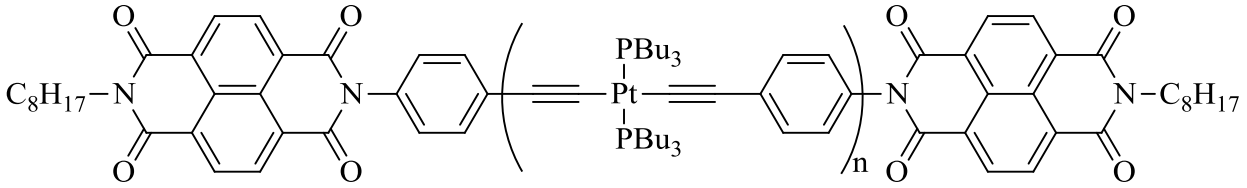

83

Figure 74. Photonic molecular wire prepared as an oligomeric platinum acetylide. n = 2, 3, 6 and 10. Adapted from ref. [186b].

I.11. Luminescence of binuclear systems

The luminescence properties of organometallic compounds are well documented. [187] The inclusion of transition metal moieties gives access to efficient spin-orbit coupling which in turns enables the population of excited states of triplet character and phosphorescence

characteristic of organometallic compounds. As such the coordination of the organic compounds to metal centres can enrich the emission properties by enabling access to new excited-state characters.[187i] As this theme is extensive, only examples of alkynyl complexes of Pd, Pt and Ru will be discussed below.

Dong *et al.* [187a-c] reported a bisterpyridyl binuclear ruthenium rod bridged by a 1,1'-diethynylferrocene moiety (Figure 74, **84a-b**). The group reports two reversible waves attributed to Ru^{II}/Ru^{III} and Fc/Fc^{+} as described for other systems above.

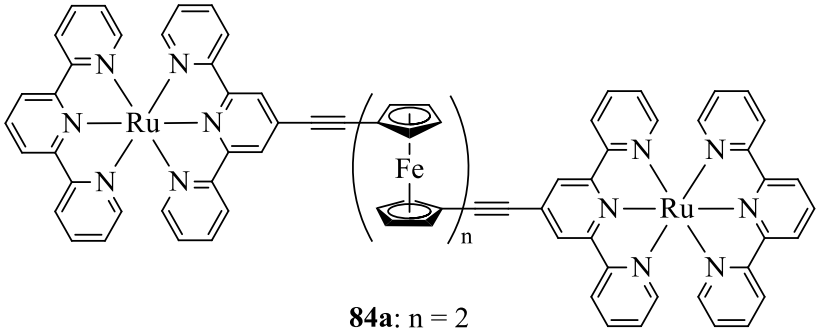

84a: n = 2
84b: n = 3

Figure 75. Bisterpyridyl binuclear ruthenium rod bridged by a 1,1'-diethynylferrocene moiety. Adapted from ref. [187b].

Since the ferrocene moiety is known to quench triplet MLCT states, the group found that there is a marked decrease in fluorescence decay times for the **84b** (3 ferrocenyl moieties, 24 ns) in relation to **84a** (2 ferrocenyl moieties, 67 ns). The quantum yield is nevertheless very low in both cases with values of *ca.* 1×10^{-4}. Wu *et al.*[187j] worked on very similar complexes (to **84a-b**) bearing polyethynyl ferrocene bridged complexes with also agreeing results. The group also studied other spacers (instead of the 1,1'-diethynylferrocene) as represented in Figure 76. Among these bridges, the quantum yield was around $14\text{-}40\times10^{-4}$ for the shorter bridges like **84d-g** and *ca.* 1×10^{-4} for the longer bridges like **84c**,**h**. Nevertheless, the **84j** (n = 1-5) series showed very lower quantum yields even with small n values and decreased when the number of ethynylthiophene units increased. Triplet decay times also followed these trends with an above average value for **84d** with 720 ns (among the 110 ns average).[187b]

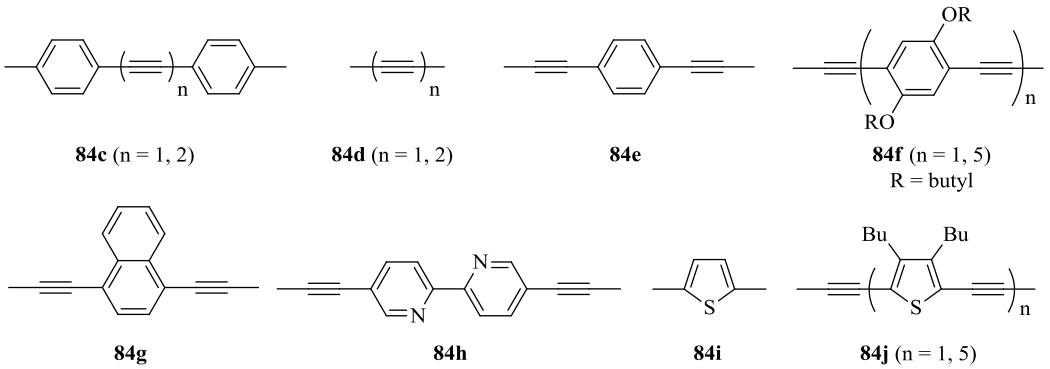

Figure 76. Different bridges studied by Dong *et al.* using the terpy-Ru^{2+}-terpy-bridge- terpy-Ru^{2+}-terpy as for **84a-b**; R = alkyl chain. Adapted from ref. [187b].

Ji *et al.*[187h] studied the photophysical properties of a family of Pt terpyridyl rods bridged by fluorenyl motif (Figure 77). The group found fluorescence decay times in the order of microseconds (from picoseconds for the free ligands) which were attributed to triplet excited state. Furthermore, as the emission is affected by solvent nature, with coordinative solvents (*e.g.* CH_3CN) inducing a negative solvathochromic effect on the fluorescence of these complexes, a Pt process is expected.

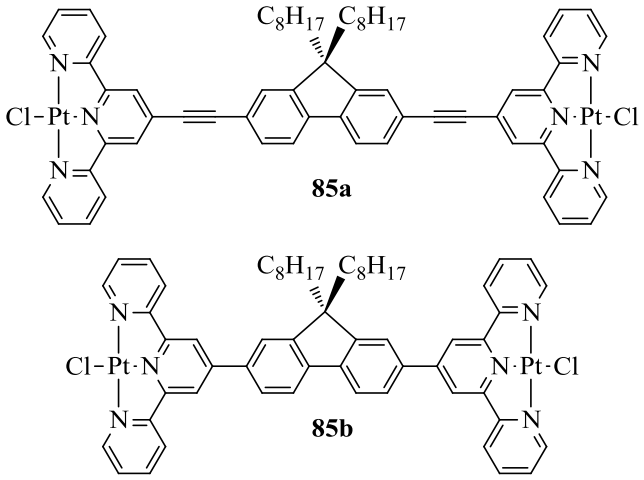

Figure 77. Terpyridyl Pt rods studied by Sun and co-workers. Adapted from ref. [187h].

Furthermore, non-coordinative less polar solvents like CH_2Cl_2 increase the luminescence characteristic of the compounds further supporting the Pt influence in the corresponding electronic transition is attributed to a mixture of MLCT/ILCT (Inter-Ligand Charge Transfer). The drop in quantum yield is more marked with values in the order of 98% for

the free ligands, whereas the complexes only attain 7 and 12% (**85a** and **85b** respectively). This also can be attributed to the triplet excited state origin of the emission in contrast to the mostly singlet ILCT emissions of the free ligand.[187h]

Yam and co-workers[187d] reported the carbazole bridged dinuclear Pd and Pt rods in Figure 78. The palladium rod (**8a**) was non-emissive in solution (CH_2Cl_2) whereas 2.9 μs decay times were found for this compound in the solid state (77 K). The platinum analogues (**85b-e**), although showing emission in CH_2Cl_2 solutions, presented very low decay times (< 0.1 μs) and the solid state decay (77 K) times were similar to **86a**. When testing glass samples of this series (**86a-e**, 77 K, EtOH/MeOH 4:1, v/v), luminescence increased drastically, with decay times going up to 50 μs.

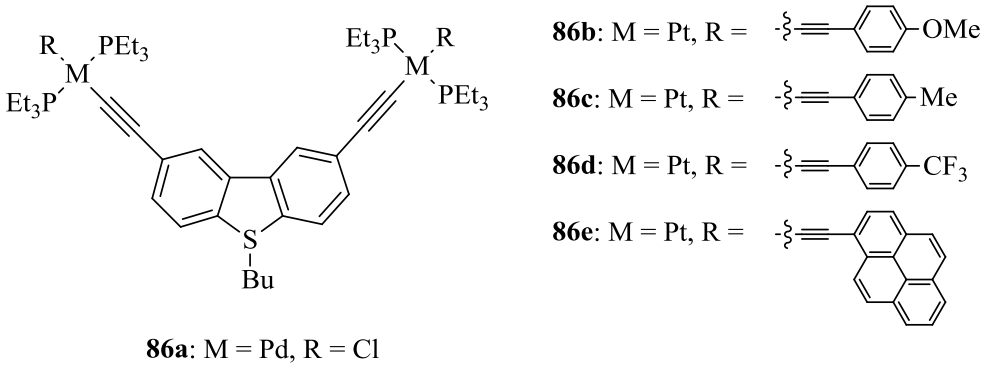

Figure 78. Diethynyl carbazole bridged dinuclear Pt and Pd rods. Adapted from ref. [187d].

Chan *et at.*[187g] reported the dinuclear platinum rods (**87a-c**) presented in Figure 79. These complexes are bridged by a diethynylphenylene oxidiazole moiety. Compound **87a** is non-emissive in solution or solid state at room temperature, but the modified **87b-c** have quantum yields of 0.17 and 0.20 respectively (CH_2Cl_2 solution). Decay times are higher in solution for both **87b-c** in relation to solid state values at room temperature but increase at low temperature (77 K). Both solid state and glass form (EtOH-MeOH 4:1, v/v) at low temperature for **87b-c** are one order higher than the ambient temperature counterparts.

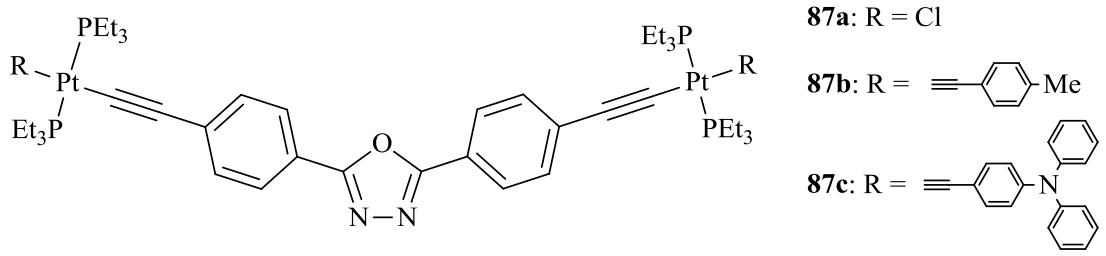

Figure 79. Diethynylphenylene oxidiazole bridged platinum dinuclear rods. Adapted from ref. [187g].

I.12. Synthesis of the wires, general review

In the following section, a general review will be performed regarding the most important synthetical pathways used for the preparation of the compounds described in the next chapter.

I.12.1. Ligand synthesis

Although not overly complex, the syntheses of the ligands described in this work were heavily based in quite modern C–C coupling reactions. The importance of these techniques was recently noted by the Noble Prize in chemistry (2010) attributed to Richard Heck, Ei-ichi Negishi, and Akira Suzuki "*for palladium-catalyzed cross-couplings in organic synthesis*". It is noteworthy that these methods are not restricted to the usage that was given in this dissertation. As such, several methods (Table 1) have been reported and developed in the years following the famous report by Heck, of the vinylic substitution reactions with aryl halides. The R group is usually a sp^2 hybridised carbon, whereas the X group is generally an halogen (I, Br or Cl) or trifluoromethanesulfonate (OTf). Furthermore the nature of R' and M are chosen in accordance to the specific coupling being performed.[188]

Moreover, the palladium cross-coupling of an organometal (R^1M, R^1 can be aryl, alkenyl, alkynyl, allyl, benzyl, propargyl, alkyl, cyano, or enoxy) with an organic electrophile (R^2X, R^2 can be aryl, alkenyl, alkynyl, allyl, benzyl, propargyl, alkyl, or acyl) has been adopted as the most general and selective method for C–C formation. During the thirty years since its appearance, it has been considered superior to the similar procedures that rely on Ni, Cu or Fe as the catalysts. The organometallic compounds can contain a range of several metals. These can be

Zn, Al or Zr in the case of the Neghishi coupling; B for the Suzuki coupling, Sn in the Stille coupling as well as several others like Li, Mg, In, Si, Cu and Mn.[189]

Table 1: Overview of the palladium catalyzed coupling reactions, adapted from ref. [188b, 190].

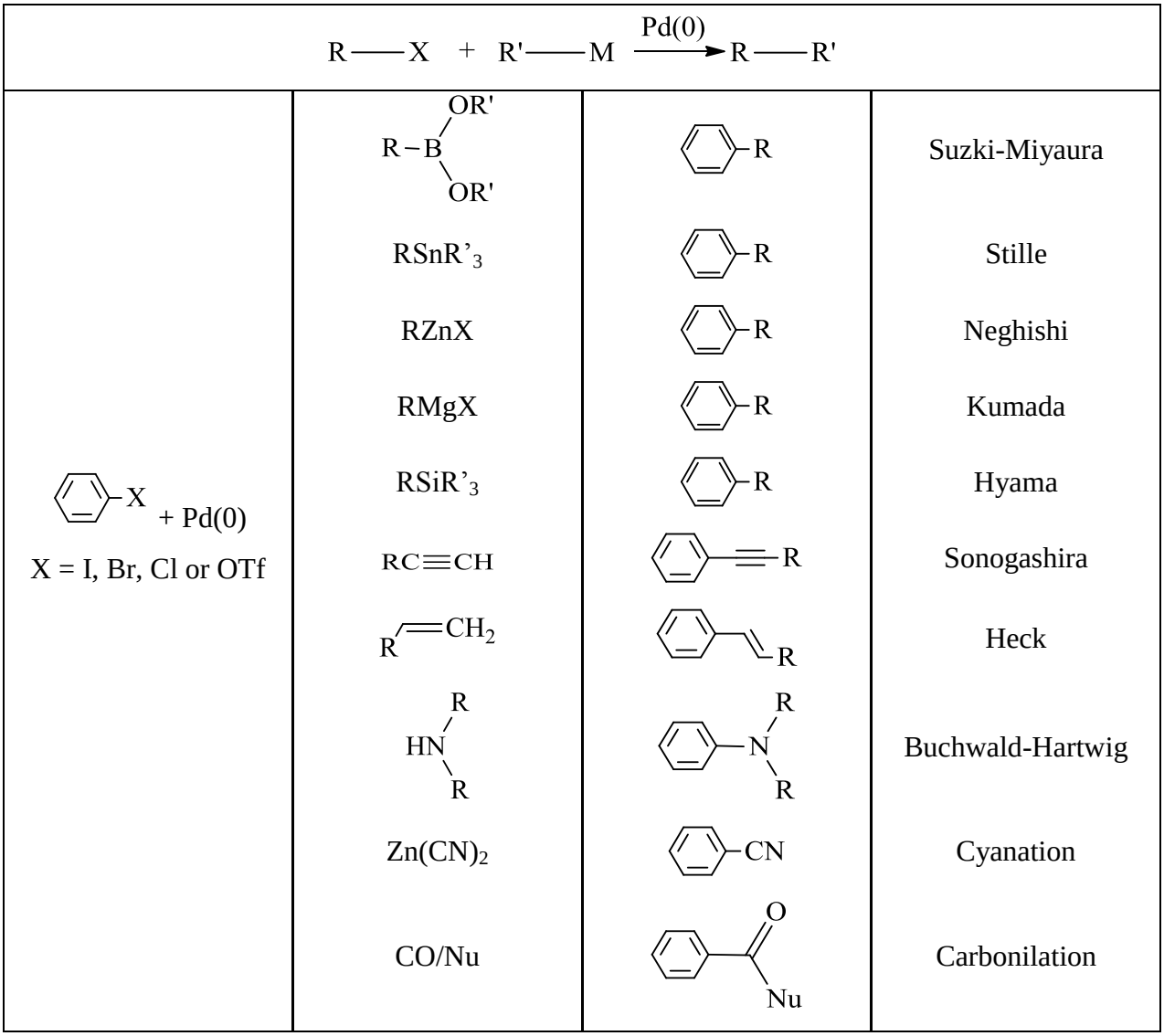

Nu = nucleophile

These reactions are believed to follow a very similar catalytic cycle (Scheme 13). The Pd(0) can be formed *in situ* when using species like $Pd_2(dba)_3$, $Pd(OAc)_2$ or $PdCl_2(PPh_3)_2$ (where dba is dibenzylideneacetone, OAc is acetate and Ph is phenyl) and the necessary ligand. Already prepared Pd(0) like $[Pd(PPh_3)_4]$ or $[Pd(P\mathit{t}Bu_3)_2]$ are also used but are more sensitive and may expire during storage. The choice of the ancillary ligand will affect the coupling. A strong σ

donating ligand, like the trialkylphosphines will increase electronic density accelerating the oxidative addition of the catalyst to the substrate which is the generally accepted rate determining step. The ligand will also affect the mechanism of this addition. Bulky ligands, in particular phosphine ligands, accelerate the elimination step. The rate of this step is determined by the cone angle (also known as Tolman angle)[191] produced by the ligands.[190, 192] The general mechanism for the Pd catalyzed couplings follows in Scheme 13.

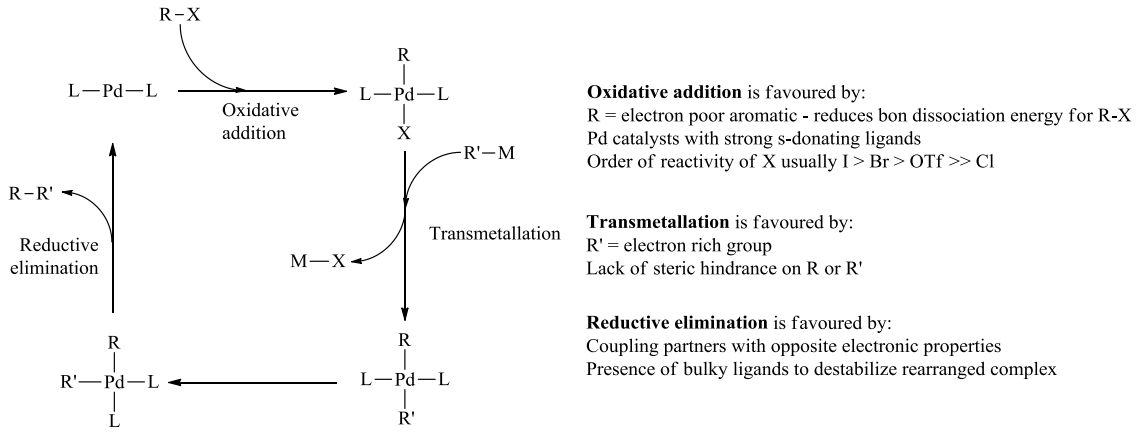

Scheme 13. General mechanism for the Pd catalyzed cross couplings. Adapted from refs. [190, 192].

Depending on the synthetic problem, several reactions were tested. The Pd catalyzed couplings like Sonogashira[193] and Negishi[194] couplings for the insertion of triple bonds. For Ar–Ar coupling (where Ar is aromatic ring), the tested coupling reactions were the Suzuki[195] and the Stille[196] couplings.

An overview of the methods that were used in this work is presented below.

The Castro-Stephens method of coupling copper-acetylide and an aryl halide[197] was modified by Sonogashira and Hagihara by adding the palladium catalyst and preparing the organocopper precursor in *situ*.[193] It can also be named by the Heck-Cassar-Sonogashira-Hagihara reaction.[198] This is the *de facto* method for the insertion of a triple bond and largely a consequence of the simplicity of the starting materials, mild coupling conditions and tolerance to a great range of functional groups.[192] It is also a very hot topic in current chemistry as the new Pd sources (like Silica supported Pd[199]), copper free methods (preventing the oxidative homo-coupling of the acetylenes) [200] are being heavily researched as well as development of milder reaction conditions for inactivated organic electrophiles.[189d, 192-193]

Concerning the Pd catalyst, the usage of Pd^0 reduces the amount of side products as none of the alkyne reagent is consumed for the formation of active Pd species. Nevertheless, $Pd(PPh_3)_4$ (Pd^0) is somewhat sensitive and the quality of the commercial available sources can vary wildly (both in quality and in activity). Moreover, $Pd(PPh_3)_4$ is less active when compared to the also often used $PdCl_2(PPh_3)_2$ as a result of the two extra PPh_3 ligands. Furthermore the Pd(II), in its $PdCl_2(PPh_3)_3$ form, is not active, and this is why it consumes some alkyne as schematized in Scheme 14. Iodoarenes favour the coupling reaction to the point where in some cases the change from bromide to iodide starting materials allows for room temperature reaction instead of 80ºC. Furthermore as a smaller catalyst load is usually enough when reacting iodoarenes (from 5% to 0.1% in some cases). Furthermore, reaction rate increases as the electron-withdrawing characteristic of the haloarene substituent increases. Meta substituents decrease the efficiency of the coupling in contrast to the *ortho* and *meta* ones. Finally, the choice of the base, although sometimes not given a lot of concern, has a marked influence on the reaction's yield. Triethylamine (TEA) is the general and universal base used for Sonogashira couplings, but it was found that piperidine yields better results when iodoarens are used and for the case of bromoarenes, Hünig's base is the best choice.[198]

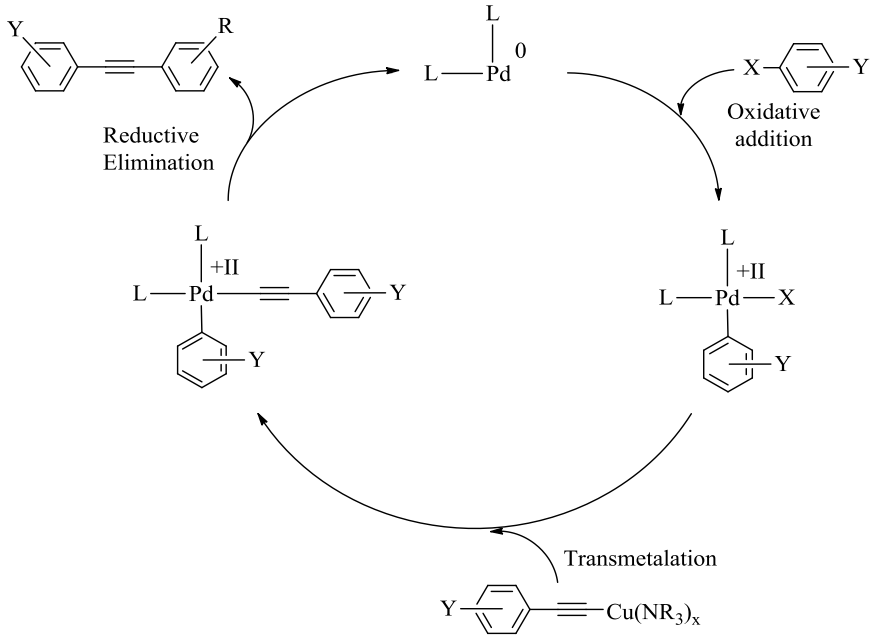

Scheme 14. Catalytic cycle when Pd^{II} catalyst are used. Adapted from ref. [198].

The Negishi coupling, reported with organometallics derived from Al, Mg, Zn and Zr, is usually associated to the organozinc precursors and it is also widely used with aryl chlorides and with alkynes which contain electron-withdrawing groups. Pd/dppf based catalysts have shown good results in this coupling reaction.[189b, 189e, 194] Alkynylzinc precursors generally present higher reactivity in comparison to their stannane counterparts. Nevertheless the usage of the former is still not as represented as the Sonogashira or Stille couplings. This could be attributed to their high water and air sensitivity. Moreover, organozinc reagents show good chemoselectivity despite their higher nucleophilicity. The alkynylzinc reagents are usually prepared *in situ* before the addition of the catalyst and the organic electrophile starting from the lithium or Grignard precursors. Anhydrous $ZnBr_2$ and $ZnCl_2$ are used as the Zn source and low temperature is required.[192]

Stille coupling was reported by Stille and Milstein in 1978[196] coinciding with a report from Kosugi and co-workers[201] for basically the same method. Nevertheless, the procedure reported by Stille showed better results. This nomenclature is generally applied to the coupling of an organic electrophile with an organotin reagent. The tin derived organometallics have their strongest advantages on the tolerance to several functional groups, which eliminates the need for protective groups. Usually water and air-stable, these compounds allow for easy isolation and storage. Nevertheless, the largest disadvantage is the high toxicity of the stannyl reagents. This toxicity increases with the number of alkyl groups and with the decrease of the length of these chains.[192]

Suzuki-Miyaura (usually only called Suzuki) coupling[189a, 195] is the cross-coupling of organoboron reagents with organic electrophiles. Boron organometallics have lower toxicity, like the organozinc reagents from Negishi coupling, but are not water and air stable like the organostannyls. Alkynylboranes are known to be easily hydrolyzed.[189a, 192]

I.12.2. Binuclear ruthenium rods synthesis

As already exposed above, one of the most promising metallic fragments to use in the preparation of organometallic molecular wires is *trans*-$[RuCl(dppe)_2]$ as it is found to be suitable for ground-state electron-transfer or transport. Furthermore the ancillary phosphines not only, contribute to the stability of the final system but also to the solubility of the molecular system

which is an important parameter having in view the technological applications. The *trans*-[RuCl(dppe)$_2$] fragment (as well as similar complexes) provides filled orbitals of proper symmetry to interact with relatively low-energy, unoccupied π* orbitals of the bridges. Finally, this fragment, bears one further labile position (chloride) which permits for further attachment of the molecular "alligator clips" as well as increasing the wires length.[2c]

Moreover, the usage of the Ru(dppe)$_2$ moiety improves and affords stable oxidized complexes. [202]

Typical synthesis of these rods – specifically the coordination of bridging ligand to the ruthenium moiety – is performed by following the method wildly reported and originally described by Dixneuf [66c, 203] and further refined by Rigaut and co-workers[53a, 66d]. This consists on the activation of the initial ruthenium complex *via* chloride abstraction to the 16 electrons precursor and then reaction with the terminal alkyne. The pathway leading to the acetylide is mostly regarded as Ru(η^2-alkyne) to Ru(η^1-vinyledene) as several reports manage to trap this intermediary complex by reacting it with, *e.g.*, alcohol yielding (alkoxy)alkylideneruthenium complexes (Scheme 15).[66c, 203]

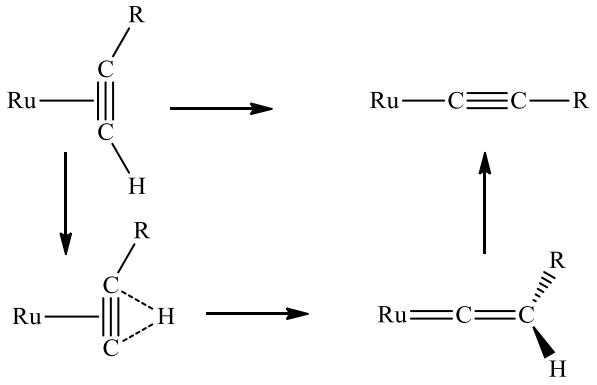

Scheme 15. General mechanistic pathway for the preparation of Ru acetylides. Adapted from ref. [66c, 203].

When preparing diacetylides (as would be necessary for the preparation of the thiol terminated wires), the usage of the vinylidene intermediary (as represented in Figure 83) gives better reaction yields as reported by Rigaut and co-workers.[53a] This method has also been thoroughly used for the preparation of Fe acetylides.[82, 100, 204]

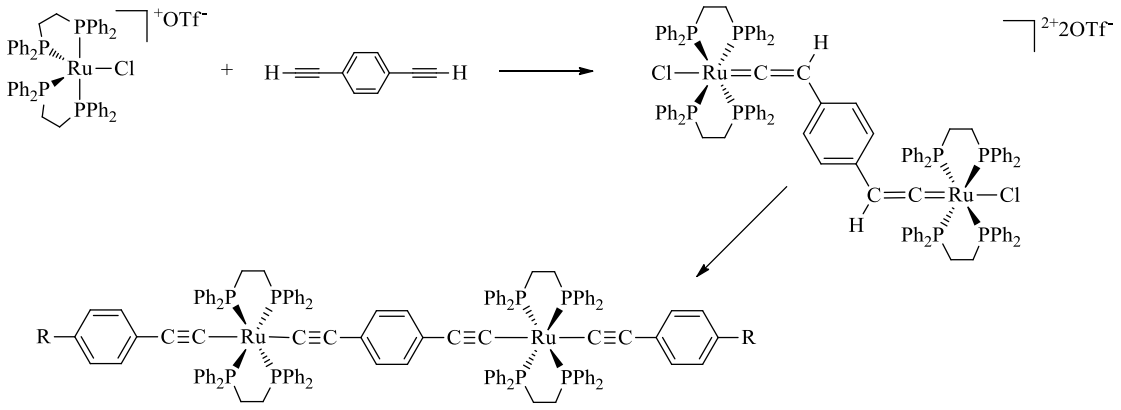

Figure 80. Example of Ru(II) di-acetylide preparation as reported by Rigaut and co-workers. Adapted from ref. [53a].

I.12.3. Binuclear palladium rods synthesis

Synthesis of alkynyl palladium(II) are usually based on the condensation of the alkyne with the chloro-palladium (II) starting complex (Figure 81). A polar solvent is normally used or if the solubility of the reagents permits it, the base – normally a secondary amine – is used as solvent as well. A copper catalyst, often CuCl, is also used.[205] Controlling the stoichiometry of the reagents is enough, in most cases, to determine the product. As such, mononuclear, diacetylide complexes and even organometallic copolymers are formed when changing just the relative quantities of the starting materials (excluding then catalyst load, temperature or solvents). [205a]

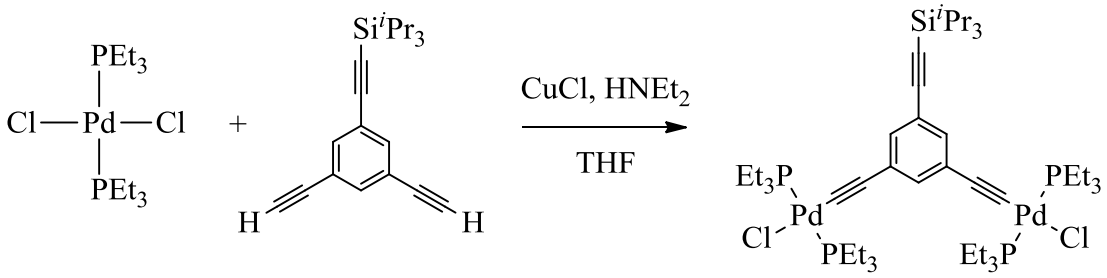

Figure 81. General synthetic method used for the preparation of palladium acetylides. Adapted from ref. [206].

Fischer and co-workers[207] report the preparation of a diacetylide palladium complex (Figure 82, **88**). It is noteworthy that the same procedure used for the preparation of binuclear monoacetylide complexes (reported above) is the same for diacetylide with just the change in stoichiometry. Furthermore, the group also prepared the Ag-C≡C-R intermediate in order to increase the yield (to almost quantitative, from *ca.* 48%).

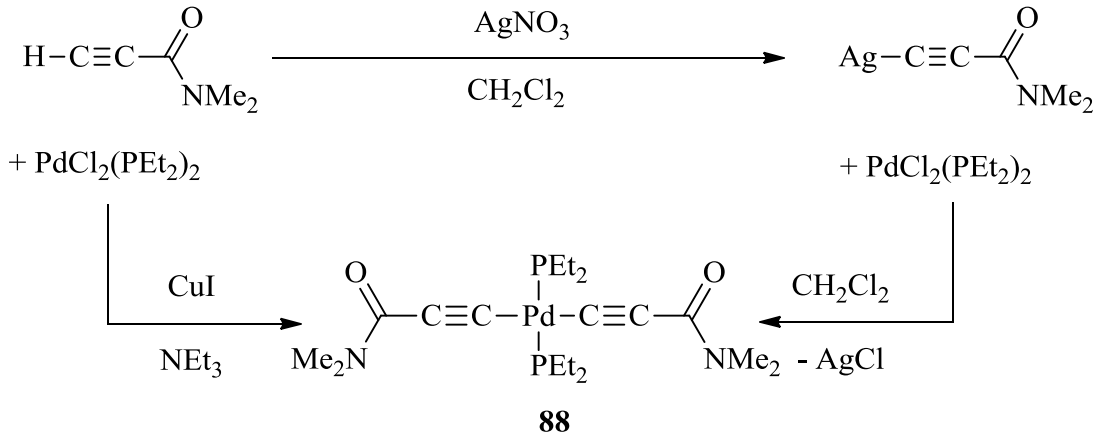

88

Figure 82. Bisalkynyl Pd complex preparation by Fischer *et al.*. Adapted from ref. [207].

Chapter II – Results and Discussion

In this chapter an exposition of the preparation of the rods will be performed. As such, the synthetic pathways used to obtain the oligo phenylene ethynylene ligands (or oligo thiophenylene ethynylene), with different length alkoxy side chains is discussed. The synthetic pathway leaned heavily on the use of Sonogashira couplings (already discussed above) for both the insertion of the coordinating moiety (the terminal alkynyl) as well as growing the ligand in length. These compounds would then be used as bridges by coordinating them to the $[RuCl(dppe)_2]^+$ or $[PdCl(PEt_3)_2]^+$ to form binuclear homometallic rods.

Although the palladium rods preparation was straightforward and coordination of all the 1,4-diethynyl derivatives to the Pd centre was achieved, the synthesis of the ruthenium counterparts was not as immediate. The literature procedures are mostly one-pot methods where the ligand would coordinate to ruthenium moiety after chloride abstraction would be performed *in situ*. It was found that this method would lead to the formation of several side products and make the purification efforts long which in turn would enable more side product formation.

These rods were then put through a range of spectroscopic analysis such as FTIR, UV-vis absorption, NMR and MS spectroscopy as well as cyclic voltammetry. The resulting data is discussed and co-related in order to characterize the organometallic rods as potential candidates for molecular wire device production. Single crystal X-ray diffraction was also performed for some of the obtained compounds and is also discussed. Moreover, some other work that is indirectly related to the general theme will also be presented, *e.g.*, the ruthenium mono hydrido (**34**) that was obtained as a side product. This compound was later prepared, on purpose, giving yield to a new, faster way to reach this species.

II.1. Synthesis of 1,4-diethynylbenzene and 2,5-thiophene derivatives for use as bridging ligands

In this section, the preparation of the bridging ligands is presented as well as discussed. Reaction conditions were adapted from the literature but optimization was done by testing and repeated preparation of the several compounds throughout the work progress. Detailed reaction procedures are available in Chapter IV. The compounds 1,4-diethynylbenzene (**5a**),[208] 1,4-diethynyl-2,5-dimethoxybenzene (**5b**),[209] 1,4-diethynyl-2,5-diethoxybenzene (**5c**)[210] and 1,4-

diethynyl-2,5-bis(heptyloxy)benzene (**5d**)[210] were prepared following the general synthesis presented in Figure 83. The halogenated starting materials were available commercially for **5a** and **5b**, but the respective precursors for **5c** and **5d**, compounds **2a** and **2b,** were first prepared by Williamson substitution (Figure 83, step **i**), to insert the side chains, following a modified procedure reported by Weder and co-workers.[130]

Bromination[211] was also attempted instead of iodination (Figure 83, step **ii**). Nevertheless, the reaction cost, was basically the same as in the iodination,[130] making the later better suited for the next steps (cross-coupling, step **iii**). Notwithstanding, the yield) was significantly lower for the iodination (~30% *vs.* ~ 60% for bromination) but it is preferable to repeat this reaction than the following Sonogashira couplings. This is because palladium catalysts and TMSA are very expensive‡‡. Depending on the yield of step **ii**, the compounds could be purified by crystallization or by column chromatography, but usually the later was required.

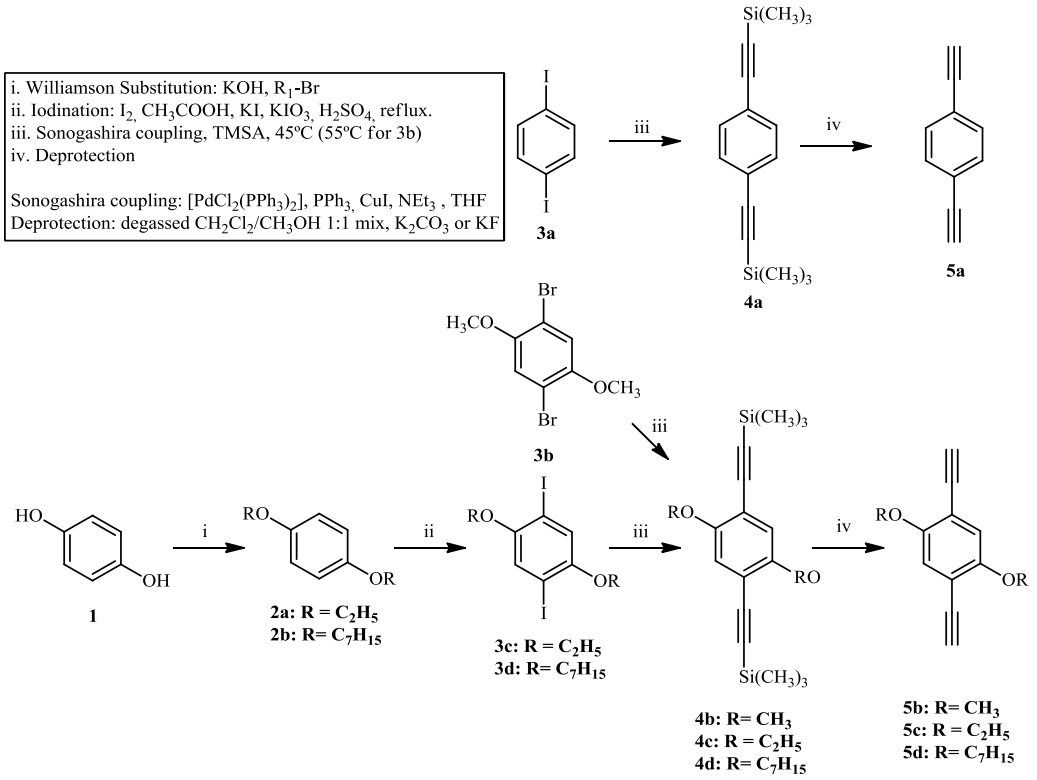

Figure 83. General synthetic pathway for the preparation of the mono PE bridging ligands.

‡‡TMSA is 586.50€ for 100g. $[PdCl_2(PPh_3)_2]$ and $[Pd(PPh_3)_4]$ are 136.10€ and 229.30€ for 5g (Acros, 14/07/2011, Portuguese ratings). Extra work hours not accounted for.

The Sonogashira couplings were performed following the multiple reports by Tour in his 2003 book[212] and modified in accordance to other reports.[130, 198, 210, 212-213] It is important to highlight that even with the ring deactivation brought about by the side chains, there was no significant loss in reactivity that was not inherent to the available halide (brominated *vs.* iodinated precursors). This coupling follows as reported when using the more stable *trans*-$[PdCl_2(PPh_3)_2]$ with reactions taking from 1 h for the smaller iodinated starting materials (Figure 83, **3a**, **3c**, **3d**, at room temperature – r.t.), to *ca.* 24h for the coupling of the bromide terminated longer ligands (Figure 85, **8a**, **8b**, at 55ºC).

Compounds **3a**, **3c** and **3d** were also used in their brominated version leading to lower yields, longer reaction times and harder purification. Moreover, preparation of these ligands (only **3c** and **3d** were tested) was also attempted using 2-methyl-3-butyn-2-ol[142, 214] instead of trimethylsilylacetylene as the alkynyl source (Figure 84). Although the coupling reaction yields (Figure 84, step **i**) obtained were higher (from *ca.* 50 to 70% yield, and the starting material is significantly cheaper), the deprotection step (Figure 84, step **ii**) was too harsh (ground NaOH or KOH in refluxing toluene) and the increased yield that was gained from the coupling step, was lost in the deprotection step. Further discussion of this method is done for the thiophene based ligands (**14b** and **16b**).

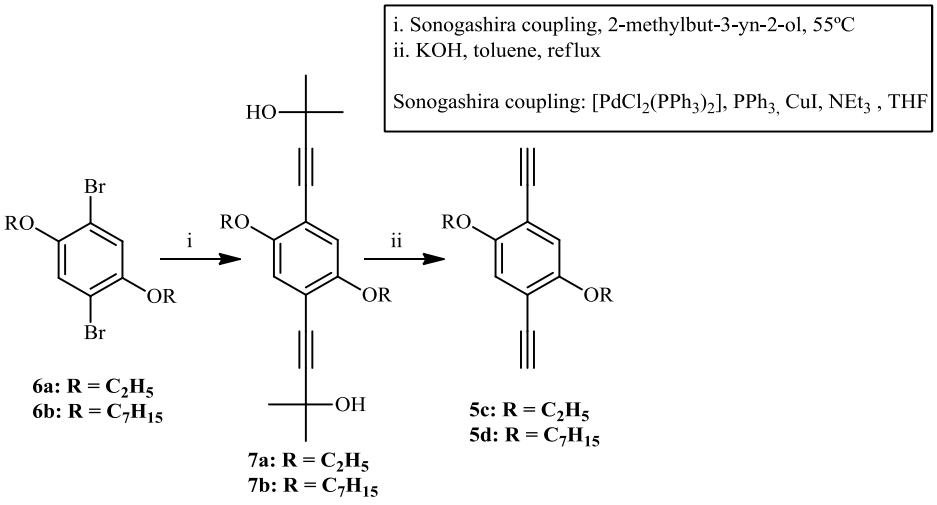

Figure 84. General reaction scheme for the preparation of the single ringed PEs when using the alternative source of alkynyl, 2-methylbut-3-yn-2-ol.

The use of the Pd catalyzed couplings entails most of time, since it is necessary to isolate and purify the products by column chromatography. As such, and regardless of the chosen conditions, purification of products had to go through at least one column. This makes the preparation of the tris PEs bridging ligands extremely time consuming, especially since the side products include mono coupling generated bis PEs (with the central dialkoxy moiety) which have very similar separation properties to the desired product. This would lead to a long and laborious chromatography using pure *n*-hexane (or petroleum ether 40-60 ºC fraction). Several eluent mixes were tested but to no avail.

For the protodesilylation (henceforth deprotection, Figure 85, step **iv**) of the longer bridging ligands (**10a** and **10b**), KF[215] was found to be more effective. Nevertheless, K_2CO_3 (Figure 85, step **iv**)[130, 198, 210, 212-213] was enough to deprotect the shorter ligands in 2 h. This reaction is usually fast and filtration through a celite/silica plug yields almost pure compound. The proton source is attributed[216] to the methanol which also works as a co-solvent for the inorganic base. Tetrabuthylamonium fluoride (TBAF) was also used for this deprotection reaction and was especially useful while preparing the thiol alligator clip (section II.4). In this case and since the reaction is performed usually in THF (or in some reported cases in CH_2Cl_2) the proton was found to originate from an elimination (similar to the Hoffman elimination) of the proton from the tetrabuthylamonium cation.[217] TBAF was significantly harder to work with, as well as more expensive and less stable than K_2CO_3 (or KF) and was thus remitted to specific usage such as the already referred thiol molecule (discussed further down).

As already reported above, the preparation of the tris ringed PEs (Figure 85) suffered from low yields and laborious separation and purification through column chromatography. Special care had to be taken when preparing the reaction, since lower quality palladium catalyst or bad nitrogen purging would mean incomplete coupling of both sides of the starting dialkynyls (**5b-c**). This would result in almost inseparable mixes of **9a** (or **9b**) and the related bis ringed PE. In these cases, it was found that it was better to repeat the reaction than to process the reaction mixture.

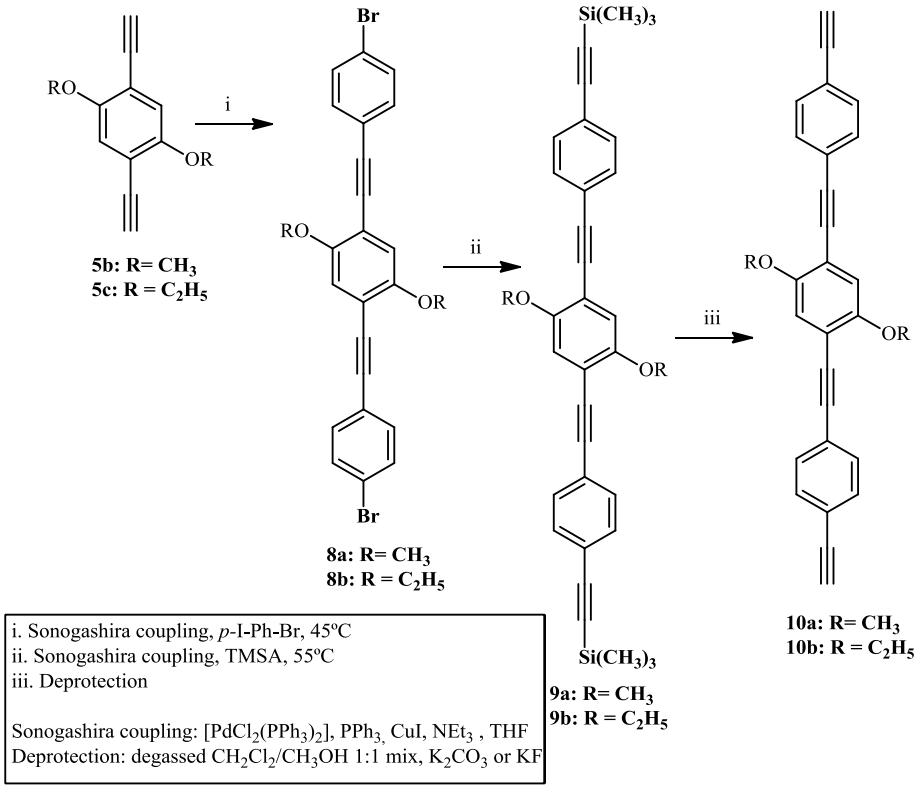

Figure 85. General synthetic pathway for the preparation of the tris phenylene ethynylene bridging ligands.

In an effort to prepare thiophene organometallic wires, thiophene based bridging ligands were also prepared using the already described Sonogashira coupling procedure as well as the Stille coupling (Ar–Ar). Reaction schemes are presented in Figure 86.

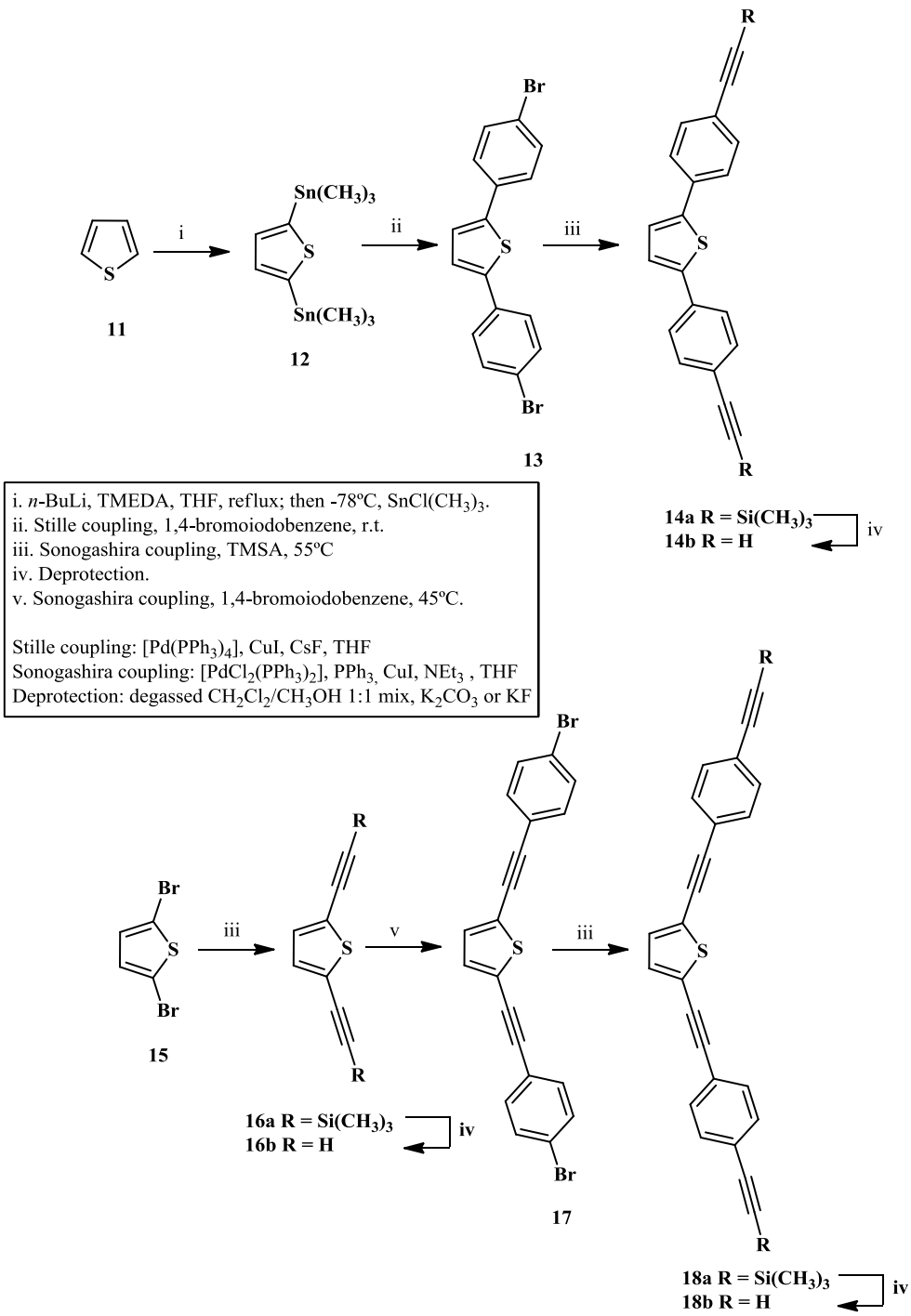

Figure 86. General synthetic pathway for the preparation of the thiophene based bridging ligands.

For the preparation of ligand **14b** (Figure 86), it was necessary to perform a Stille coupling. As such the organotin precursor (**12**) was prepared *via* lithiation of thiophene (**11**) and consecutive transmetalation with $SnCl(CH_3)_3$ to yield compound **12**. This reaction is aided by the

complexation of Li^+ with TMEDA (*N,N,N',N'*-tetramethylethane-1,2-diamine) which effectively polarizes even more the Li-C (Li-Thiophene) bond.[218] The precursor (**12**) was then coupled to 1-bromo-4-iodobenzene *via* the Stille coupling. Following a report by Mee and co-workers,[219] CsF was used as the base for this reaction yielding very good results. Although organostannyl compounds have the somewhat large disadvantage of being toxic,[220] all the reaction yields, as well as workup and purification steps involved in the preparation of the precursor and the actual coupling were far cleaner (far less side products) than any other Suzuki attempt made previously for the same compounds. The usage of CsF also has the advantage of being easily filtered away when used in excess.

Preparation of the very similar **18b** was performed following the same procedure that was employed for the tris ringed PEs (**10a**-**b**) ligands, starting from the commercially available 2,5-dibromothiophene. The preparation of compound **16a** (and therefore **16b**) was also attempted using 2-methyl-3-butyn-2-ol[142, 214, 221] to introduce the acetylene moiety (referred above for the protected precursors **7a**-**b**). The main appeal of this method is based upon the commercial costs[§§] of 2-methyl-3-butyn-2-ol *vs.* tetramethylacetylene (TMSA) as well as the good yield generally obtained. Nevertheless, the deprotection method is very harsh and prone to side products. The success of this "acetone protected" method was not repeated for the thiophene based compounds, since even after a successful coupling, the NaOH promoted deprotection (in refluxing toluene) never yielded the desired 2,5-diethynylthiophene (**16b**). Nevertheless, the method remains an important way of generating the PE precursors.

II.2. Synthesis of the binuclear palladium rods bridged by 1,4-diethynylbenzene derivatives

Despite most of the recent publications regarding the usage of palladium in the preparation of molecular wires pointed to disruption of the delocalization through the wire, it was chosen to test the prepared ligands with the *trans*-$[PdCl_2(PEt_3)_2]$ (where Et is C_2H_5, ethyl) moiety. This was because preliminary attempts were successful and reports of discrete (not

[§§]2-methyl-3-butyn-2-ol is 24.60€ for 250mL and TMSA is 586.50€ for 100g from (Acros, 13/07/2011, Portuguese ratings).

polymer based) binuclear palladium rods were not as popular as, *e.g.*, ruthenium rods which can be, to some degree, attributed to the easy polymerization of these materials. Furthermore, some other properties, like fluorescence could also be studied additionally to transport capabilities. The general procedure is reported in Figure 87 and detailed in Chapter IV.

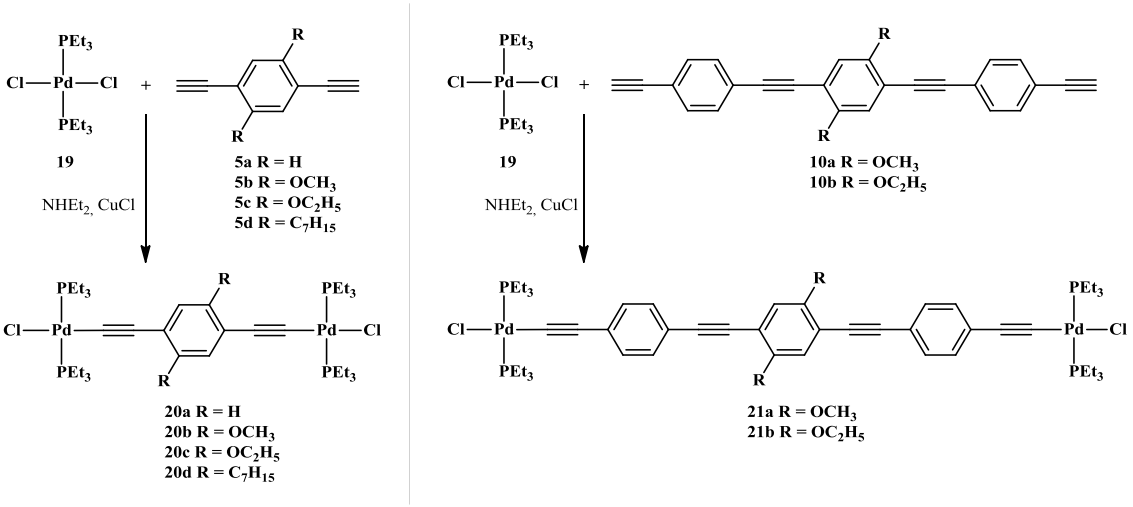

Figure 87. General procedure for the preparation of the $[PdCl_2(PEt_3)_2]$ based binuclear rods.

These complexes were prepared following a method reported by Takahashi's group[170a, 170c, 170d, 172d, 174, 222] in the field of rod like platinum and palladium polymer chemistry. The reaction occurred on the presence of catalytic amounts of CuCl*** which was previously dried at 120 ºC for at least 2 h (but usually overnight). It was observed that the reaction was over very fast, usually in the few first minutes with the rapid formation of a suspension right after the addition of the CuCl (similarly to the Sonogashira reaction). Furthermore, the work-up and purification were generally simple enough, since the complexes were only readily soluble in halogenated solvents. Moreover, solids were stable at room temperature and under normal atmosphere whereas solutions of these complexes were stable enough to be washed with water also under normal atmosphere. Reaction yields were good (63-83 %).

Compound **20a** (R = H) was previously reported by Nast and Beyer in 1980[223] but with bare minimum characterization. Compound **21b** yielded crystals with enough quality for single crystal X-ray diffraction. The crystal of **21b** is discussed in section II.11.

***CuI can also be used, similarly to the palladium catalyzed cross-couplings (*e.g.* the referred Sonogashira coupling).

II.3. Synthesis of the binuclear ruthenium rods bridged by 1,4-diethynyl and 2,5-thiophene derivatives

II.3.1. 1,4-diethynylbenzene derivatives bridged rods

Although initially thought to be straightforward since the described procedures pointed to simple one-pot methods, the preparation of binuclear complexes *via* coordination of the terminal bis-alkynyl ligands to the ruthenium moiety proved troublesome and a great deal of experimentation was necessary to finally be able to produce the desired compounds.

The binuclear PE bridged complexes were prepared following a modified Dixneuf[66a, 81, 171, 208, 224] method as presented in Figure 88 and Figure 89 (further details are available in Chapter IV) which is based[66a, 81, 171, 208, 224] on *in situ* abstraction of the chloride from *cis*-$[RuCl_2(dppe)_2]$ to form the activated penta-coordinated $[RuCl(dppe)_2][PF_6]$ (**22**). Compound **23b** was not prepared.

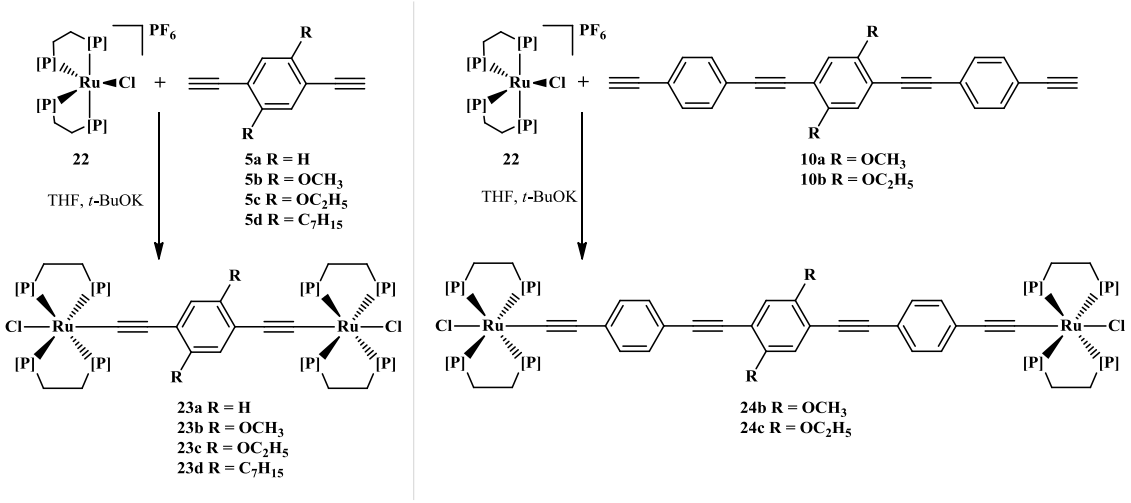

Figure 88. General procedure adopted for the preparation of the binuclear PE ruthenium rods. [P] = $P(C_6H_5)_2$; *t*-BuOK = potassium *tert*-butoxide.

Compound **22**, a 16 electron complex, is then reactive towards the ligand's terminal acetylene leading to the formation of the vinylidene complex (Figure 89, **26**) which is then

deprotonated by an organic base like triethylamine or diethylamine to form the desired bis-(ruthenium acetylide) complex (Figure 89, **23a**).

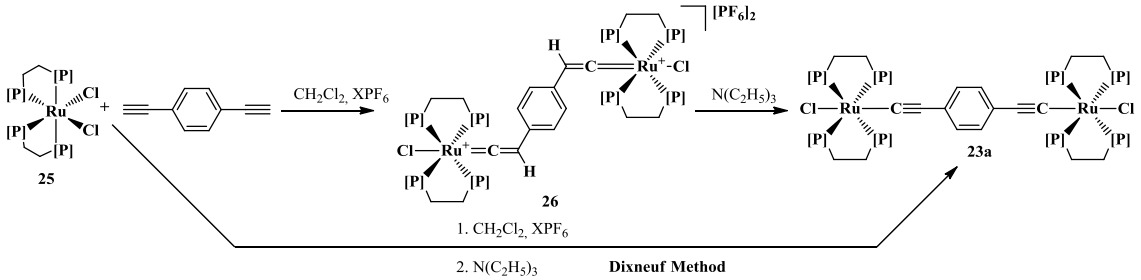

Figure 89. Preparation of complex **23a** following the Dixneuf method (one pot and two step); where X = Na, Tl or NH_4; [P] = $P(C_6H_5)_2$.

As such, the first attempts to prepare the ruthenium rods with 1,4-diethynylbenzene derivatives with side chains were thus performed in accordance with this method using the C_2 ligand (**5c**) to prepare compound **23c**, but very little success was attained since very complex mixtures were always obtained as observable by the ^{31}P NMR spectrum in Figure 90.

Throughout this work, repeated allusion to ^{31}P NMR signal will be made since this is a very fast and efficient way to follow the progress of these reactions. This is because the desired compounds are expected to be in the *trans* conformation (in accordance with the structure in Figure 88, **23a,c–d**) and as such, the respective ^{31}P NMR signal would then be a singlet at around 48-50 ppm (CD_2Cl_2, 161MHz),[224c] Moreover, if the reaction progressed as intended, any extra signals would correspond to excess $[RuCl(dppe)_2][PF_6]$ (triplets at 83 and 57 and heptet at -147 ppm[224c, 225]) since the vinylidene intermediary was expected to react completely with the excess base in accordance to its reported (and also observed) high reactivity.

Despite several attempts, the desired binuclear complexes where never the major product when the one-pot method was employed. Curiously, since no report of this was found, the complex *trans*-$[RuCl_2(dppe)_2]$ was sometimes registered as the major product even when initial checking by ^{31}P NMR would point to total consumption of the starting *cis*-$[RuCl_2(dppe)_2]$ (total remission of triplets at 59 and 47 ppm, ^{31}P NMR 161 MHz). Since the signal at 44 ppm (^{31}P NMR, ^{31}P NMR 161 MHz)[225] was found in all the attempts, the immediate conclusion would be that it belonged to the severally less reactive *trans*-$[RuCl_2(dppe)_2]$[224c, 225] (in comparison to its *cis* isomer). As such, preparation of the activated starting material,

$[RuCl(dppe)_2][PF_6]$,[225] was performed separately in order to minimize either isomerization[226] of the starting *cis*-$[RuCl_2(dppe)_2]$ or the amount of the chloride salt that would be present (in different soluble forms). The latter is a result of the chloride abstraction (usually precipitates and at room temperature it only forms from the *cis* starting material or very slowly from the *trans* isomer) and can be TlCl, NaCl, NH_4Cl or AgCl, when using, respectively $TlPF_6$, $NaPF_6$, NH_4PF_6 or AgOTf (OTf is trifluoromethanesulfonate, $SO_3CF_3^-$). It was later observed that the 44 ppm signal would continue to be registered after some time even when preparing $[RuCl(dppe)_2][PF_6]$ separately. Nevertheless, this extra step resulted in better control over the reaction's side products yielding cleaner reaction mixtures.

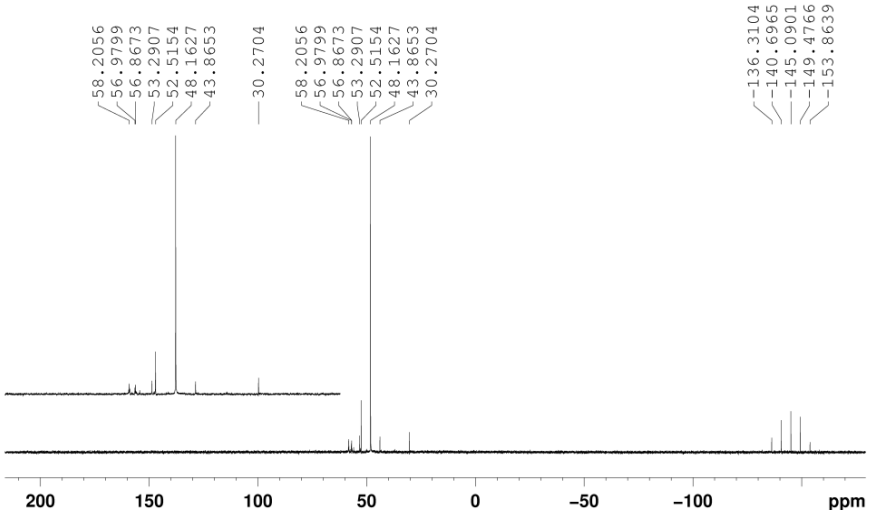

Figure 90. $^{31}P\{^1H\}$ NMR (CD_2Cl_2, 161 MHz) spectrum of a one-pot attempt to prepare **23c** with *cis*-$[RuCl_2(dppe)_2]$, **5c**, NEt_3 and $TlPF_6$.

It is uncertain how the *trans* isomer of the starting material is formed (or in this case, re-formed), since it was also observed in later attempts that started from pure $[RuCl(dppe)_2][PF_6]$. Decomposition of the sample in the NMR tube upon dissolution with $CDCl_3$, may constitute circumstantial evidence of re-insertion of the chloride from the NMR solvent but no conclusive results were obtained on this matter.

Furthermore, hydrolysis of PF_6^-, reported to occur with as much as 0.5% of H_2O[227] in a solution of $LiPF_6$, always leads to the formation of HF[227-228] (regardless of starting salt) which is able to re-protonate[229] the ruthenium acetylide (PF_6^- would then be present as an impurity in the

form of the respective salt) forming the vinylidene which is more reactive and prone to other reactions (*e.g.* methoxide insertion from methanol[230]).

Despite the possible decomposition of the PF_6^- anion, it was observed that this counter-ion, in conjunction with Tl^+, formed the best abstracting salt for this work. The preparation and handling of $TlPF_6$ should always be performed very carefully as it is very poisonous, and since its commercial alternative is expensive[†††], other alternatives were tested. In the case of $NaPF_6$, its high hygroscopicity was very hard to control and after one month the crystalline substance had a wet looking aspect (even when kept in the desiccator). Moreover, $NaPF_6$ was also inefficient in the preparation of $[RuCl(dppe)_2][PF_6]$ from *cis*/*trans* mixtures of $[RuCl_2(dppe)_2]$ (low reactivity towards the *trans* isomer reported[225]). NH_4PF_6 was also tested but its reaction with *cis*-$[RuCl_2(dppe)_2]$ was found to be comparatively too slow. Finally, AgOTf was also used with some success, especially in the preparation and isolation of $[RuCl(dppe)_2]^+$ precursor. This is due to its good solubility in CH_2Cl_2. Nevertheless, control of the reaction progress is usually performed (explained above) by ^{31}P NMR and OTf does not have any phosphorus atoms, making a problematic synthesis (at the time) harder to follow resulting in trace amounts of the corresponding salt.

Moreover, the sensitivity to light of AgOTf as well as its high hygroscopicity was an added concern. For all these reasons, it was finally decided to use $TlPF_6$ in spite of its risks.

As with chloride abstractors, also two organic bases were tested as deprotonating agents of the vinylidene intermediary. These seemingly unnecessary trials were based on the initial bad results and since some authors report the usage of such strong bases like NaOMe or KOH (methanol solution),[231] another organic base, DBU (1,8-Diazabicyclo[5.4.0]undec-7-ene)[232] was tested instead of the classic triethylamine. Notwithstanding the better results provided by DBU (faster deprotonation), any excess of this base was increasingly hard to remove after the reaction was over. Nevertheless, the best results were obtained when using potassium *tert*-butoxide (*t*-BuOK),[66f] resulting in faster and cleaner reactions since any excess base was easily removed by filtration. As starting materials are concerned, special care was taken in the purity and storage of the deprotected di-alkynyls, as their decomposition, especially the smaller ones (**5a-d**), under room temperature and atmosphere was visible very fast. Furthermore, as already noticeable by the above description, increasing quantities of $[RuCl(dppe)_2][PF_6]$ became

[†††] $TlPF_6$ is 205€ for 5g from Alfa-Aesar (Portuguese ratings, 25-07-2011).

necessary for the several attempts that were made, as such, the preparation of *cis*-[$RuCl_2(dppe)_2$] was found to be too long (as repeated crystallization is necessary to separate it from the *trans* isomer) and was later done starting the *cis/trans*-[$RuCl_2(dppe)_2$] (see Annex A.3.5) obtained when preparing *cis*-[$RuCl_2(dppe)_2$].

As already referred, an effort to separate as much of the reactional steps was done to reduce side products and decrease necessary purification. After the addition of the free ligand to the [$RuCl(dppe)_2$][PF_6] solution and the reaction was confirmed by ^{31}P NMR to have stopped, it was once again filtrated and evaporated before the next step. The resulting solid is then re-dissolved in CH_2Cl_2 and *t*-BuOK (or NEt_3) is added prompting the immediate colour change from dark red/brown to dark orange. Nevertheless, it was later realized that it was not necessary to perform the filtration and evaporation before the addition of the base as long as the reaction was not left for too long before the final addition (2 h was found to be enough). It is noteworthy that both reactions (formation of **26** and **23a**, Figure 89) are fast in respect to the studied compounds and that initially, when the first problems were encountered, extended periods of time were being allotted for the one-pot reaction and at least one night periods were used for the separated reactions. It is not only unnecessary, but severally increases the side product formation.

Finally, purification of the rods was one of the most troublesome steps to overcome. There is probably no better indication of this, that the several side products that were found while trying to purify the reaction mixtures during crystallization. Column chromatography was attempted, as well as filtration through alumina or pre-treated silica (with triethylamine) but the results were never satisfying since the rods are only soluble in either halogenated or very polar solvents that, when used in the column, would also elute the undesired components of the mixture. As successful as it can be for a number of other organometallic applications – a good example would be the preparation of *cis*-[$RuCl_2(dppe)_2$] (see annex A.3.2) –, purification by crystallization did not work for these rods. Severe proof of this was the several single crystals that were obtained with enough quality to resolve a structure, but from side-products. As such, a complex of aqua ruthenium,[233] a ruthenium monohydrido, a ruthenium carboxylate as well as two different crystals of the starting material[234] were all obtained while trying to purify the rods by crystallization (usually from CH_2Cl_2 and diethyl ether biphasic diffusion). These structures were or will be published as soon as possible by us.

Moreover, the only method that was successful in the purification of the ruthenium rods was by washing the resulting solid with a mix of degassed MeOH and CH_2Cl_2 (30:1). Nevertheless, it was only useful when the components of the product mix were the desired rod and the starting $[RuCl(dppe)_2][PF_6]$. Repeated washing (normally at least four times, 15 mL for 500 mg of mixture) was necessary to get the pure rod.

Notwithstanding the previous report of **23a**,[171b] it was chosen to prepare it, in order to better compare the electrochemistry results of the new rods with those in the literature. Furthermore and despite our several attempts to prepare **23b**, it was not possible to isolate the desired compound. Despite our difficulties in the preparation of compound **23b** Rigaut and co-workers[71] reported very recently its synthesis.

II.3.2. Thiophenylene ethynylene based Rods

Using the thiophene based ligands, described in section II.1, two new binuclear rods were also prepared as described in Figure 91.

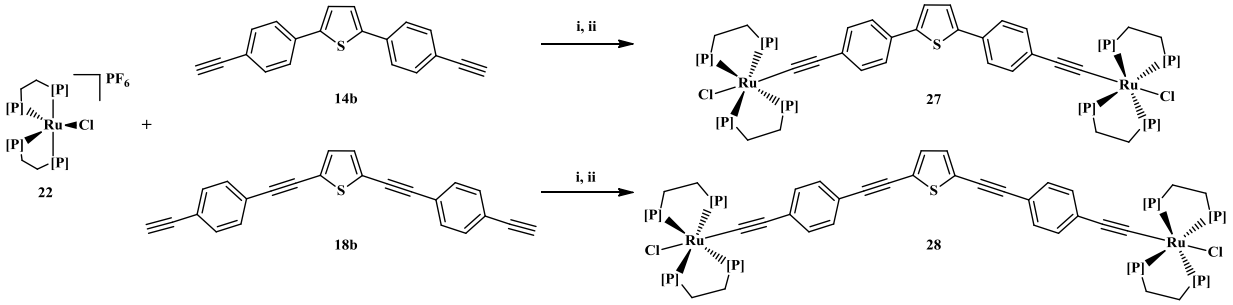

Figure 91. General preparation of the thiophene based ruthenium binuclear rods. [P] = $P(C_6H_5)_2$, **i**. -78 ºC, t-BuLi, diethyl ether; **ii**. CH_2Cl_2, r.t.

The classic method of first preparing alkali metal acetylides for ligand displacement with the desired transition metal complex halide was initially also attempted but without success for the PE rods described above, but was employed successfully for the preparation of the two thiophenylene ethynylene rods (**27**, **28**) described in Figure 91. This method is indeed similar to the coordination of the PE ligands to the palladium moieties reported above, where Cu(I) is used (catalytically) instead of Li (I). Moreover and although not part of the presented results, a test

using Cu(I) for the ruthenium PE ligands was attempted, but once more a very complex reaction mixture was obtained. The Li-acetylide method was adapted from reports of Rigaut[235] as well as from Long and Williams[236] and Albertin *et al.*.[237]

II.4. Preparation of the "alligator clip" molecules and its coordination to a ruthenium rod

The thiol based 4-ethynyl-1-thioacetylbenzene[238] was vastly used by Tour (as well as other groups) and is the most reported option (due to the exceptional binding to gold electrodes), leading to reduce experimental variables and comparable results. As such, it was chosen as the molecule to cap the rods described above.

To prepare this compound, several synthetic pathways were tested for the preparation of this compound and special attention was of course given to the procedure[238] reported by Tour for the preparation of the intermediary (Figure 92, **29**).

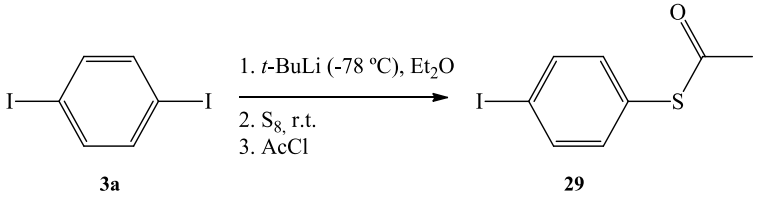

3a **29**

Figure 92. Preparation of the thiol based "alligator clip", as reported by Tour.[238]

This procedure was in fact tried several times but with very little success, since the yields from this first step (attachment of alkynyl moiety follows, Figure 93) were very small (*ca.* 10-15 %). Furthermore, some authors[239] also report that they were also unable to repeat this procedure. As such another alternative would be to start from the commercial 4-bromothiophenol, protect it (acylation) and then proceed to do the Sonogashira coupling. This did not work, since the acyl protection does not withstand the harsher conditions necessary to perform the coupling on the phenyl bromide. This was later found to be already reported by Collman and colleagues,[239b] which managed to protect the thiol group using pyridylethyl. Although the

starting material is indeed commercial, the method requires eight distinct steps to finally yield the acyl protected 4-ethynylthiophenol.

The compound was finally prepared *via* a modified method reported by Percec *et al.*[239a] schematized in Figure 93. Some of the modifications were personally suggested by Marcel Mayor (University of Basel). This method is similar to an earlier report by Sita and co-workers.[240]

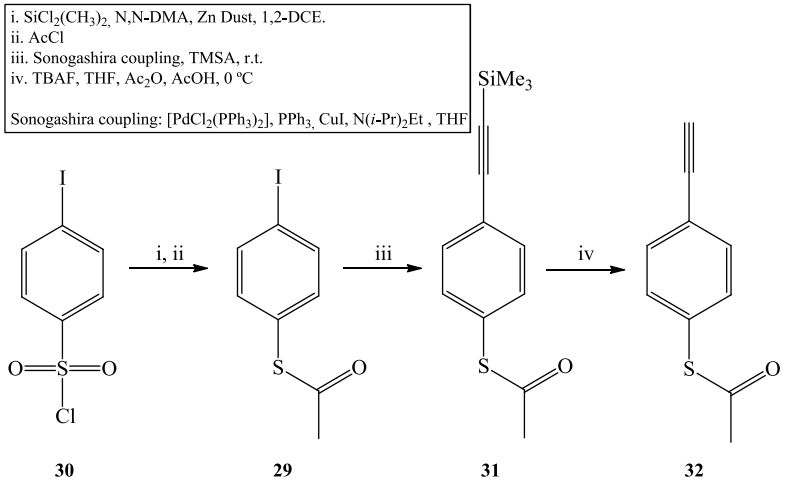

Figure 93. Modified preparation of the thiol clip. N(*i*-Pr)$_2$Et = diisopropylamine; Ac = acyl ($CH_3C(O)^-$); N,N-DMA = N,N -dimethylacetamide; 1,2-DCE = 1,2-dichloroethane; TMSA = trimethilsilylacetylene.

This method proved to be straightforward as long as the purification of the final product (**32**) was performed quickly. This was verified after an initial unsuccessful attempt where extraction of **32** was performed before the column chromatography. When the chromatography was done directly with the reaction mixture (THF was evaporated, but the remainder of the solvents were present) it was possible to separate the product in good yield (60 %). Furthermore, and despite being slightly more expensive than the initial method, the difference is easily justified by ease of preparation and yields (from 15% to 60%). The clip (**32**) was then coordinated to the ruthenium binuclear rod **24b** as described in Figure 94.

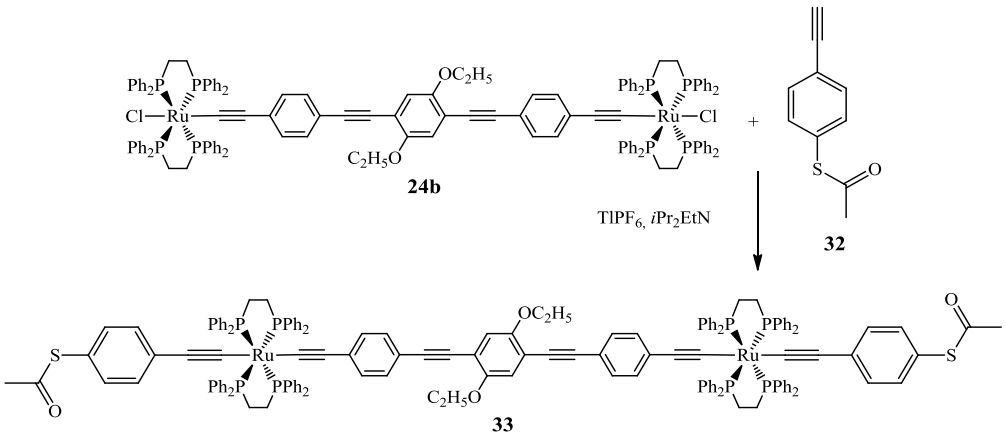

Figure 94. Coordination of the thiol clip (**32**) to the tris PE rod (**24c**).

As a consequence of the problems encountered in the preparation of compound **29** as well as the troublesome synthesis of the binuclear ruthenium rods (**23a-d**), this final step of the synthetic plan was attempted only once and at the end of the available time. As such, only one attempt to prepare a full molecular wire candidate (with terminating thioacetyl moieties) was performed. The resulting yellow solid presented the following ^{31}P NMR ($CDCl_3$, 161MHz) spectrum (Figure 95).

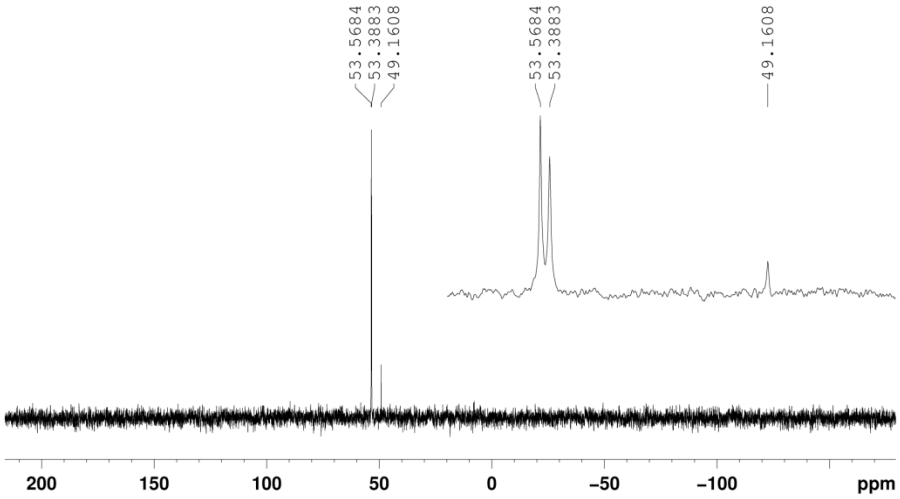

Figure 95. $^{31}P\{^{1}H\}$ NMR ($CDCl_3$, 161MHz) spectrum of the mixture obtained after several purification attempts of **33**.

The spectrum was initially composed of three signals (and the heptet at *ca.* -147 ppm attributed to excess $TlPF_6$). The major peaks, at *ca.* 53 ppm, are indeed indicative of a successful

reaction, since diacetylides of $[Ru(dppe)_2]^{2+}$ moiety are reported[53a, 57] to present a singlet at around this chemical shift. Even after consecutive attempts to purify and separate the components of the mixture, it was not possible and the final product exhibited the two singlets (53.4 and 53.6 ppm) that are visible in Figure 95. It is not obvious what these two singlets can be attributed to, as both are at the expected chemical shift for a $Ru(dppe)_2^{2+}$ diacetylide. Furthermore, changes in conformation at the metal centre (*i.e.* from *trans* to *cis*) would no doubt cause coupling and some form of triplet would be visible. The most probable explanation would then be a very similar side product. The peak at *ca.* 49 ppm has the same chemical shift as the starting rod **24b** and was not present before the purification steps and can probably be attributed to some degree of decomposition during this phase. It is noteworthy, that since this was the first attempt performed for this reaction some considerations were made: the chosen rod was a tris PE (**24b**) that (as discussed further on) does not have the best attributes in regard to electron transport but has outstanding stability even in solution when compared to the single PE rods (**23a**,**c-d**); furthermore, diisopropylamine was used instead of *t*-BuOK since it is milder. As it was not possible to isolate the compound, no further characterization was performed.

II.5. Ruthenium mono hydrido complex

The ruthenium dppe moiety, $[Ru(dppe)_2]^{2+}$, has been thoroughly used as a starting material in a multitude of applications which range from molecular wires,[53a, 66e, 70-71, 241] catalysis,[242] materials with NLO properties,[243] agents against tuberculosis[244] and metallodendrimers.[243b, 245] During the preparation of the ruthenium rods described above one of the several side products[233] was the monohydrido ruthenium complex *trans*-$[RuCl(H)(dppe)_2]$ (**34**). Compound **34** was first reported by Chatt and Hayter[246] and later on by Chin *et al.*[225] as result of the treatment of $[RuCl(H_2)(H)(dppe)_2][BPh_4]$ with LiCl and acetone overnight.[225] Since Wilkinson reported[247] in 1967 the usage of $[RuCl(H)(PPh_3)_3]$ for the hydrogenation of olefins, ruthenium hydrido complexes have seen their main application as catalysts.[248] Although monohydrido catalysts are more uncommon, they still remain an important subject in the field and a relevant application for the mentioned complexes.[249] Therefore, hydrido and

dihydrido ruthenium complexes are important precursors for the preparation of related compounds[225, 250] and, as intermediates, play a crucial role in several catalytic processes.[251]

The preparation of ruthenium monohydrido complexes can be achieved by the reaction of the dichloride (*e.g.* $[RuCl_2(PPh_3)_3]$) with molecular hydrogen in ambient pressure as initially reported by Wilkinson and co-workers.[247, 252] However, other reports point to the preparation of these complexes by using reducing agents like $LiAlH_4$, $LiHBEt_3$ and $NaBH_4$.[253] Another hydrogen source, often used in catalysis, relies on alcohols, especially secondary ones for the hydrogen transfer which is usually described as a *β*-hydride shift. The successful preparation of a monohydrido Ru(II) complex was reported by Shen and co-workers[254] using *sec*-butanol as the hydrogen source which is a modification of the initial report from Grubbs and co-workers.[255]

Compound **34** was thus prepared *via* the treatment of *cis*-$[RuCl(dppe)_2][PF_6]$ in methanol with potassium *tert*-butoxide (*t*-BuOK), as the base at room temperature. The reaction proceeds cleanly in *ca.* three minutes with an excellent yield of 95% (Figure 96). The reaction proceeds through the same mechanism as the monohydrido analogue of Shvo-type catalysts reported by Casey *et al.*.[249c, 249d]

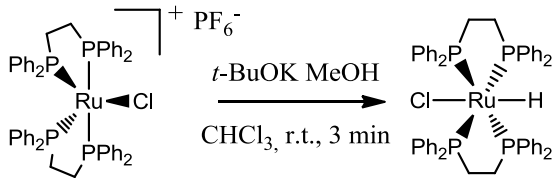

21 **34**

Figure 96. Reaction conditions used in the preparation of compound **34**.

Three methods were thus employed to prepare compound **34**. Method 1 is related to obtaining the compound as a side product and yielded the crystal later discussed in the single crystal X-ray diffraction section of this work. Method 2 was the NMR testing performed to check if the compound was forming and finally Method 3 is the Schlenk tube preparation of the compound.

The NMR tube experiment (Method 2) and the subsequent ^{31}P NMR ($CDCl_3$, 161 MHz) study confirmed that the formation of the Ru monohydrido complex is almost instantaneous upon addition of the base by immediate observation of colour change from red to pale yellow.

The immediate rising of a singlet at 63.8 ppm is observed and comes at the almost complete expense of the triplets attributed to *cis*-[RuCl(dppe)$_2$][PF$_6$] (**35**) at 82.4 and 54.5 ppm.[225]

A larger scale synthesis (Method 3) was designed to isolate the product in order to complete the characterization. Three different experiments (Figure 97, **3i**-**3iii**) were made to isolate **34**. In the first two, *t*-BuOK was added in solid form and different stirring/reaction times. The resulting ^{31}P NMR spectra are presented in Figure 97 and clearly shows that a complex mixture was obtained when solid *t*-BuOK is added directly into a solution ($CHCl_3$ and MeOH) of *cis*-[RuCl(dppe)$_2$][PF$_6$] (**21**) (Figure 97, **i**) and **ii**)).

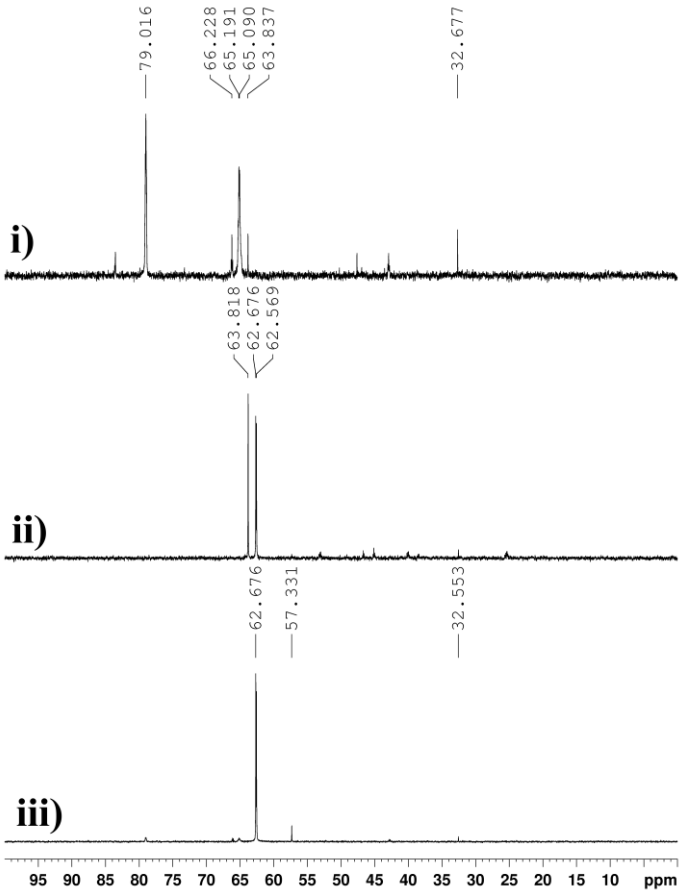

Figure 97. ^{31}P{^{1}H} NMR ($CDCl_3$, 161 MHz) spectra of three different attempts (experiments (**3i**-**3iii**)) to prepare compound **34** (Method 3).

The stirring time in the experiment **3i** was 4 h and in **3ii** only 15 min. This lead to further production of side products as it is clearly observed in Figure 97, **i**). The ^{31}P NMR

spectrum of the **3i** presented in Figure 97 shows a multitude of NMR resonances indicating decomposition or formation of several unidentifiable products.

Due to the sensitivity of **34** the best yield of it was reached in *ca.* three minutes in experiment **3iii**, by addition (under stirring and argon atmosphere) of a solution of *t*-BuOK (in MeOH) to **21** in $CHCl_3$ in a 4:1 molar ratio, followed by quick filtration and recrystallization from CH_2Cl_2/Et_2O. The reaction is fast and clean as long as removal of excess *t*-BuOK and the KPF_6 side product is done as soon as it is over.

In respect to the NMR characterization, the original synthesis[225] reported a singlet (toluene-d_8) for compound **34** in the ^{31}P NMR spectrum which was also observed for this compound in the several solvents that were tested ($CDCl_3$, CD_2Cl_2 and toluene-d_8, Method 3) A quintet at -18.5 ppm (^1H NMR) is also observed due to the coupling between the P (dppe) and the hydride atoms also forming the). Since the P atoms of the dppe ligands are equivalent, the splitting is due to the $J_{(H,P)}$ and two signals (broad) are observed in the case of the CH_2–CH_2 bridge of the dppe in the ^1H NMR spectrum (*ca.* 2.1 and 2.6 ppm).

Mass spectroscopy studies (ESI-MS/MS ion trap) of the crystals (**34**, Method 1) showed a peak at 899.1 *m/z* which corresponds to $[Ru(H)(dppe)_2]^+$. Furthermore, tentative evidence of the complex $[RuCl(OMe)(dppe)_2]$ (intermediary) was found in the form of a peak at 949.0 *m/z* which would correspond to $[RuCl(O)(dppe)_2]^+$ (loss of CH_3) and to $[Ru(OMe)(dppe) + PF_6]^+$ at 1074.1 *m/z* which is the base peak. Regarding the purposeful preparation of this complex (Method 3), the MS characterization (by ESI-TOF) is in accordance showing the $[Ru(H)(dppe)_2]^+$ peak at 899.2, and the $[Ru(H)(dppe)_2 + MeOH]^+$ at 931.2 *m/z*. An overall spectrum is shown in Figure 98.

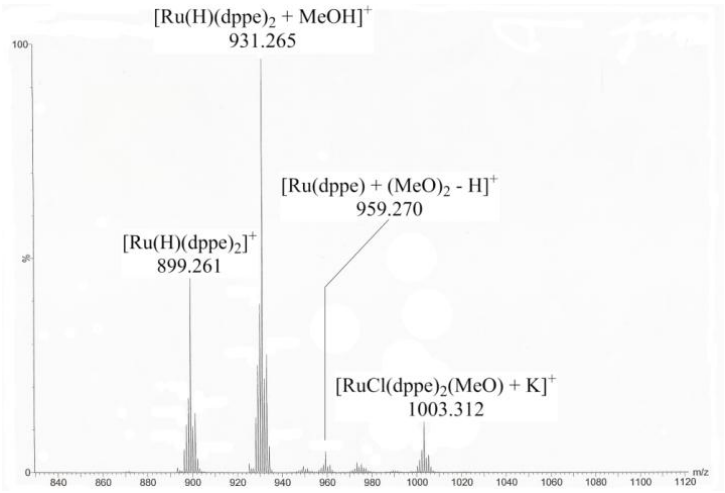

Figure 98. Overall mass spectrum of **34** (ESI-TOF, Method 3).

II.6. UV-Vis Studies

In this section the absorption spectra will be presented and discussed for both families of rods in relation to their free ligands. This will permit to probe metal-ligand interaction as charge transfer bands may present information in regard to delocalization of the electronic density of the ligand to the metal centre.

The UV-Vis studies (absorption spectra) were performed in CH_2Cl_2 unless otherwise noted. As such no specific studies regarding solvent influence were performed since the rods only showed suitable solubility in halogenated solvents.

II.6.1. Free ligands

Table 2 holds the maximum absorption peaks and their respective molar extinction coefficients for the free ligands prepared in this work. The spectra relative to selected free ligands is presented in Figure 99.

Table 2: Selected values for maximum absorption peaks and their respective molar extinction coefficients for the free ligands (**5a-d**, **10a-b**, **14b** and **18b**).

Shorter phenylene ethynylenes			**Longer phenylene ethynylenes**			**Thiophenylene ethynylenes**		
	λ_{max}	**ε**		**λ_{max}**	**ε**		**λ_{max}**	**ε**
5a	235	3	**10a**	248	18	**14b**	234	15
	290	16		316	28		265	4

5b	231	26	**10b**	375	27	**18b**	356	29
	262	21		249	25		257	15
	271	33		318	41		365	43
	346	10		377	41			
5c	231	18						
	261	13						
	271	21						
	336	5						
5d	232	14						
	262	10						
	271	16						
	338	5						

λ is the wavelength (nm) and **ε** is the molar extinction ($\times 10^3$ $M^{-1}cm^{-1}$);

The chosen spectra (Figure 99) depicts the variation in the absorption spectrum when the side chains are inserted (from **5a** to **5b**) and when the ligand is further elongated with the insertion of two extra 4-ethynylphenyl moieties (from **5b** to **10a**).

The immediate observation from Figure 99 is the shift to red of the $\pi \rightarrow \pi^*$[256] transition as the electronic density and conjugation increases. This transition shifts from 289 to 346 nm (**5a** and **5b** respectively, 57 nm) when the methoxy side chains are inserted on the 2,5 positions of the phenyl ring (**5b**). This band further shifts to red (to 374nm, **10b**) when the ligand is elongated as a consequence of the increased conjugation. A new $\pi \rightarrow \pi^*$ band is present on the spectrum of **10a** which can be attributed to the 4-ethynylphenyl moieties at 316 nm. Moreover, there is an accentuated increase in the **ε** of these bands that go from 10 to 27 $\times 10^3$ $M^{-1}cm^{-1}$ (~ 1:3)from the shorter to longer ligand (**5b** to **10a**). The decrease in ***ε*** which is visible from **5a** to **5b** (16 to 10 $\times 10^3$ $M^{-1}cm^{-1}$) could be attributed to the delocalization of the ligands electron density over the side chains which would be in accordance to a higher electron density noticeable by the shift to red.

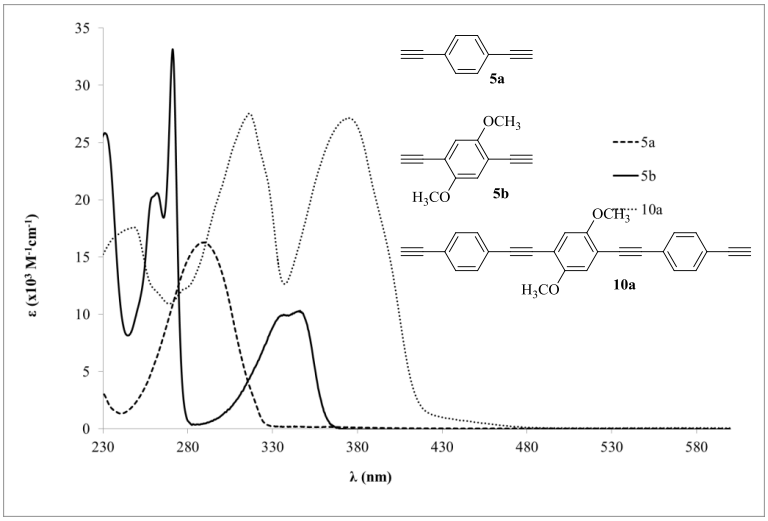

Figure 99. Electronic spectra of **5a**, **5b** and **10a** in CH_2Cl_2 at *ca.* $1x10^{-5}$ M.

The band at *ca.* 235 nm (although very close to the solvent absorbtion) for **5a** is relative to forbidden $\pi \rightarrow \pi^*$ transitions. Bands with high ***ε*** located on the 220-250 nm zone can be attributed to $\pi \rightarrow \pi^*$ transition from the side chains.[256]

This behaviour is observed throughout the other free ligands. On the matter of increasing side chain length, the visible effect is related to decrease in **ε** as the side chain lengthens (see Chapter IV.2). As the side chain increases in size from **5b** to **5c** and finally to **5d**, the value of **ε** decreases from 10, 6 and 5×10^3 $M^{-1}cm^{-1}$ respectively.

In the case of the tris ringed PE (**10a** and **10b**), there is a notable increase in ε as well as a marked red shift in relation to the single ringed counter parts (*e.g.* 374 nm: 27×10^3 $M^{-1}cm^{-1}$ for **10a** in comparison to 10×10^3 $M^{-1}cm^{-1}$ from **5b**). Furthermore, there is also a red shift when compared with the similar 1,4-diphenylethynylbenzene reported by Nakatsuji[257] in 1992 with this peak at 322 nm. Nevertheless this report was from a $CHCl_3$ solution which might account for the high ε of 62×10^3 $M^{-1}cm^{-1}$.

In the case of the thiophene based ligands, **18b** shows a higher **ε** for the $\pi \rightarrow \pi^*$ band in relation to the analogue **14b**. There is also a slight red shift (~ 8 nm) observed for **18b** in relation to the shorter and steric hindered **14b** (364 nm: 43×10^3 $M^{-1}cm^{-1}$ and 356 nm: 29×10^3 $M^{-1}cm^{-1}$ respectively).

II.6.2. Palladium rods

Table 3 holds the maximum absorption peaks and their respective molar extinction coefficients for the palladium dinuclear rods prepared in this work. Selected UV-Vis spectra for the prepared palladium rods are presented and discussed below.

Table 3: Selected values for maximum absorption peaks and their respective molar extinction coefficients for the palladium rods (**20a-d**, **21a-b**) and the free Pd complex (**19**).

Free Pd complex			Shorter Pd rod			Longer Pd rod		
	λ_{max} (nm)	**$\varepsilon \times 10^3$ $M^{-1}cm^{-1}$**		**λ_{max} (nm)**	**$\varepsilon \times 10^3$ $M^{-1}cm^{-1}$**		**λ_{max} (nm)**	**$\varepsilon \times 10^3$ $M^{-1}cm^{-1}$**
19	229	5	**20a**	232	16	**21a**	237	22
	323	7		277	19		275	22
				314	27		333	25
			20b	238	25		385	42
				283	27	**21b**	236	18
				302	33		275	17
				362	32		336	20
			20c	238	26		385	35
				273	29			
				302	35			
				353	31			
			20d	237	25			
				274	26			
				283	26			
				302	32			
				351	25			

In Figure 100 the spectra relative to the palladium rod (**20a**) based on the single ringed free ligand without any side chains (**5a**) is presented and compared to the starting materials. The absorption spectrum of **20a** appears to be a sum of the spectra of the starting materials with a peculiarity: the peaks have blue shifted.

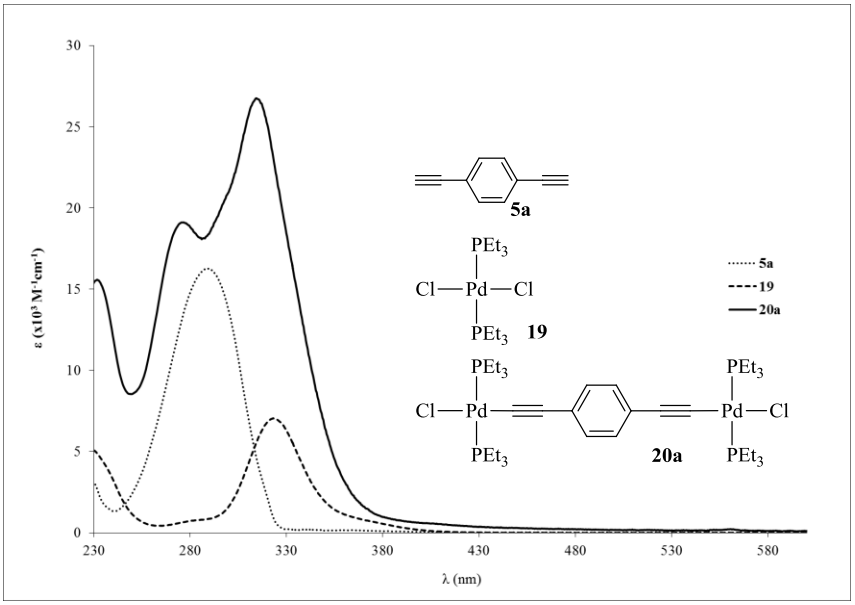

Figure 100. Spectra for the palladium rod **20a** as well as the respective free ligand (**5a**) and starting complex (**19**) in CH_2Cl_2 at *ca.* 1×10^{-5} M for the starting materials and 1×10^{-6} M for the rod.

In the case of the other palladium rods, the shift is in the expected low energy direction (red shift) as further conjugation is brought about by the coordination. Moreover, the high similarity between the absorption of the starting ligand and the resulting complex (as exemplified in Figure 101) is an indication of the predominantly ligand character of the transitions ($\pi \rightarrow \pi^*$) responsible for the absorption spectrum of the complex. This was reported by several other authors[206, 258] who also admitted some degree of MLCT (metal-to-ligand charge transfer) for the low energy bands ($d_\pi \rightarrow \pi^*$(C≡C-R)) in similar compounds. Furthermore, some red shift is also visible upon coordination to the Pd moiety as seen in Figure 101 (**5b** to **19b**) with a value of 30 nm.

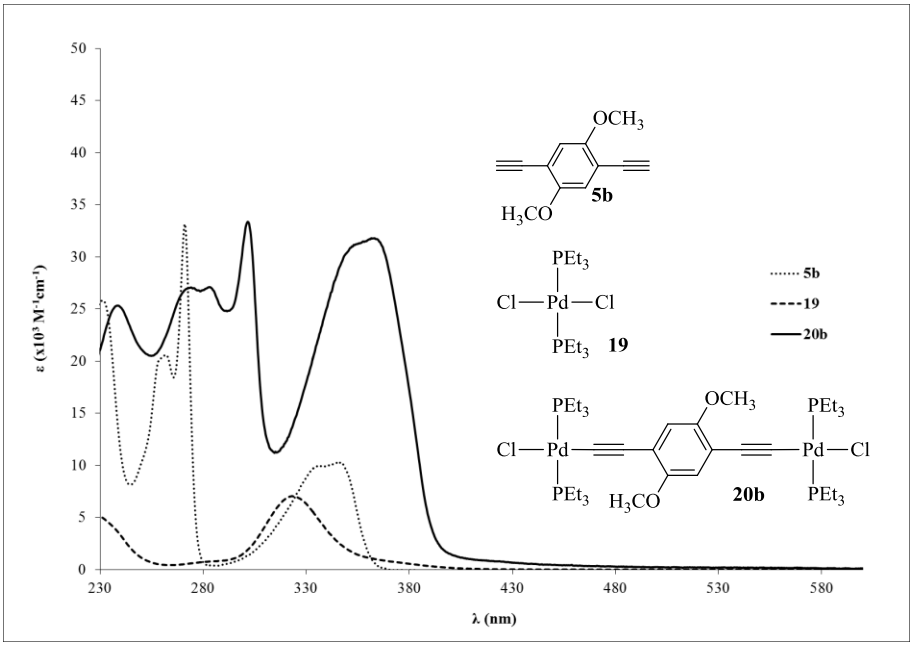

Figure 101. Spectra for the palladium rod (**20b**), as well as the respective free ligand (**5b**) and starting complex (**19**) in CH_2Cl_2 at *ca.* 1×10^{-5} M.

Nevertheless, the red shift is not that significant for either the single or tris ringed rods (with side chains). In the case of **5b** to **10a**, the variation is from 346 to 361 nm (14 nm) and for **20b** to **21a** (Figure 102), it is from 374 to 385 nm (11 nm) which is even lower that the single ringed case. The increase of ε is also lower in the case of the tris ring palladium rods (**20b** and **20c**, about two fold relative to free ligands) when compared to the single ringed counterparts (**20b-d**, about three fold in relation to the free ligands). This can point to lesser conjugation which might be due to trapped electronic density on the ligand. Furthermore, the increase in side chain length is mostly inconsequential after a length of two carbons (**5c**, in the specific case of the studied alkoxy chains) with small variations on absorption maxima (1-5 nm) when changing only the alkyl length. The same behaviour is also observed in respect to **ε**, since from **20c** to **20d** (30 to 25 × 10^3 $M^{-1}cm^{-1}$).

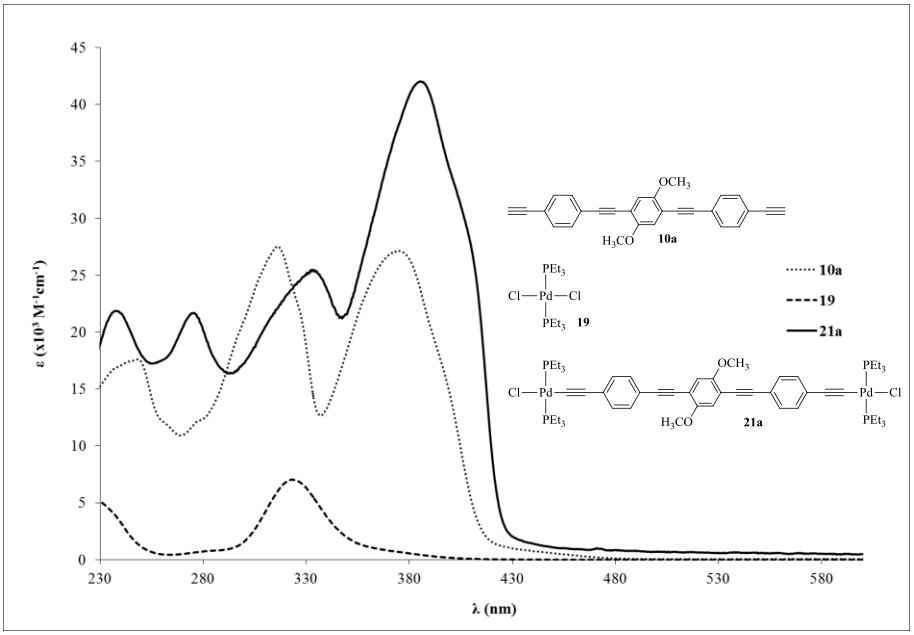

Figure 102. Spectra for the palladium rod (**21a**) as well as the respective free ligand (**10a**) and starting complex (**19**) in CH_2Cl_2 at *ca.* 1×10^{-5} M for the starting materials and 1×10^{-6} M for the rod.

II.6.3. Ruthenium rods

Table 4 holds the maximum absorption peaks and their respective molar extinction coefficients for the palladium dinuclear rods prepared in this work.

The UV-Vis spectra concerning ruthenium binuclear rods present high energy bands (*ca.* 230 nm) which are attributed to the intraligand $\pi \rightarrow \pi^*$ and $n \rightarrow \pi^*$ transitions of the dppe phenyl groups[83b] as well as the ligands. Nevertheless, the low energy peak that is present at approximately 386 nm for the single ringed rods (Figure 103, **23c**) is attributed to $d_\pi(Ru) \rightarrow \pi^*$ (C≡C-R) MLCT transition.[66c, 180] This absorption band does not depend on the length of the side chain since there is basically no shift from **23c** to **23d** (387 and 386nm respectively). Notwithstanding, the actual inclusion of a side chain has a marked shift on this band, since the value for the MLCT of **23a** is of 369 nm ($\Delta\lambda$ = 17 nm to the side chain bearing rods). Although not as significant as the red shift observed upon insertion of the side chain on the free ligands (**5a** to **5b**, $\Delta\lambda$ = 57 nm) this shift is still marked.

Table 4: Selected values for maximum absorption peaks and their respective molar extinction coefficients for the ruthenium rods (**23a,c-d**, **24a-b**, **27** and **28**) and the free Ru complex (**36**).

Free Ru complex			Longer PE Ru rods			TE Ru rods		
	λ_{max} (nm)	$\varepsilon \times 10^3$ $M^{-1}cm^{-1}$		λ_{max} (nm)	$\varepsilon \times 10^3$ $M^{-1}cm^{-1}$		λ_{max} (nm)	$\varepsilon \times 10^3$ $M^{-1}cm^{-1}$
	231	6		249	91		225	34
36	252	6	**24a**	311	34	**27**	253	55
	310	1		434	69		437	33
				248	88		225	68
			24b	313	33	**28**	254	50
				438	72		456	34

Shorter PE Ru rods		
	λ_{max} (nm)	$\varepsilon \times 10^3$ $M^{-1}cm^{-1}$
23a	245	103
	370	38
23c	255	102
	317	20
	387	52
23d	258	101
	314	19
	386	50

Molar extinction is also barely affected by the lengthening of the alkyl chain (52 to 50 × 10^3 $M^{-1}cm^{-1}$ from **23c** to **23d**). The shoulder at *ca.* 310-316 nm presents only in the alkoxy decorated rods (**23c-d**, **24a-b**) can also be attributed to red shifted n → π* transitions from the side chains.

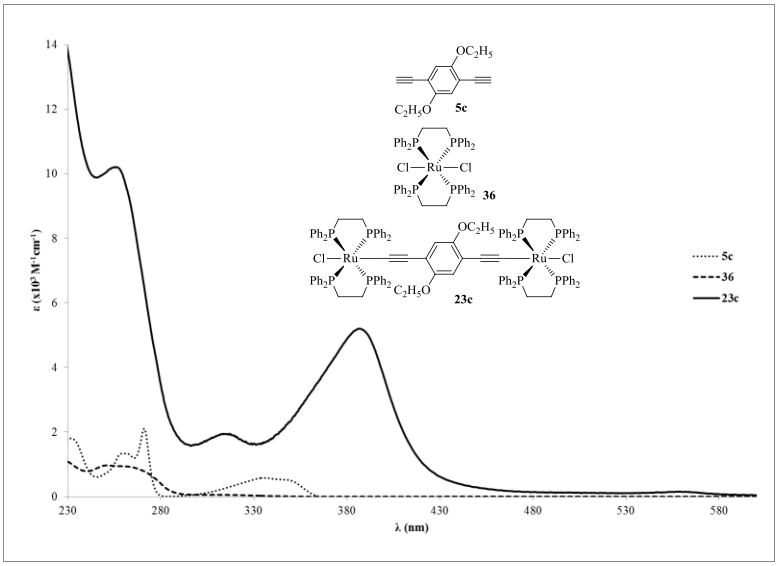

Figure 103. Spectra for the ruthenium rod (**23c**), as well as the respective free ligand (**5c**) and the corresponding *trans* conformer of the starting complex (**36**) in CH_2Cl_2 at *ca.* 6×10^{-6} M.

In the case of the tris-ringed ruthenium rods, there is a slight shift on the $d_\pi(Ru) \rightarrow \pi^*$ (C≡C-R) MLCT transition from 434 to 438 nm (**24a** to **24b**, respectively, Figure 104). The difference in ε is also in the 3×10^3 $M^{-1}cm^{-1}$ range. Moreover, the referred MLCT band is predominant for all the entire ruthenium rods and is severely red shifted in comparison to the low energy bands of the starting free ligands in clear contrast to the palladium rods.

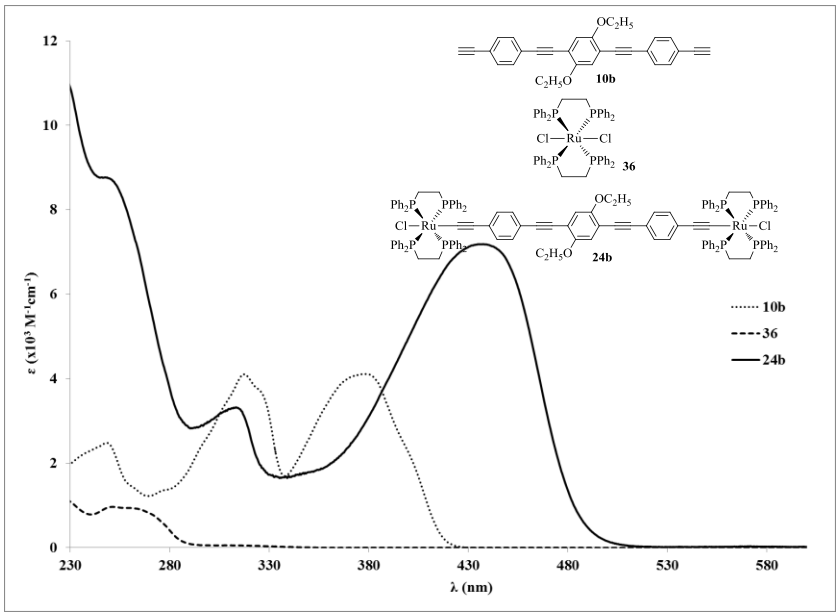

Figure 104. Spectra for a tris-ringed ruthenium rod (**24b**) as well as the respective free ligand (**10b**) and the corresponding conformer of the starting complex (**36**) in CH_2Cl_2 at *ca.* 6×10^{-6} M.

As for the spectra of thiophene based rods, these present a new wide band at 456 and 437 nm for **28** and **27** respectively (both very broad, Figure 105). Curiously, compound **27** shows the most red-shifted MLCT band in relation to the **28** which still presents a band at 456 nm that is very similar to the starting free ligand. This observation points to a marked ligand character of this absorption. It was expected that the steric hindrance between the thiophene and phenyl rings would break the conjugation and thus yield higher energy MLCT band or just a larger ligand character for **27**. A possible explanation for this difference might indeed reside on this hindrance which divides the complex in two halves that absorb as two *trans*-[$Cl(dppe)_2Ru$-C≡C-Ph-C_4H_2S)] moieties, whereas **28** has a marked ligand character due to trapping of the electron density on the ligand backbone which in turn leads to the higher energy MLCT band (with lower ε). Finally, the low ε d-d transition observed at high concentrations for the starting *trans*-[$RuCl_2(dppe)_2$], if present are expected to be covered by the MLCT bands.

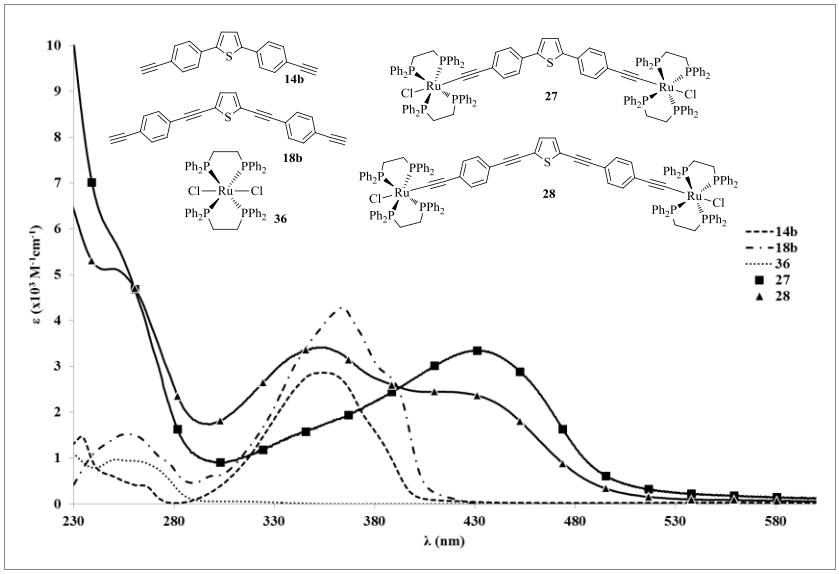

Figure 105. Spectra for the ruthenium rods based on the thiophene ligands (**27** and **28**) as well as the respective free ligands (**14b** and **18b**) and starting complex (**36**) in CH_2Cl_2 at *ca.* 6×10^{-6} M for the complexes and 1×10^{-5} M for the ligands and starting complex.

II.7. Cyclic Voltammetry Studies

Cyclic voltammetry (CV) studies were performed in order to probe the effect of highly conjugated bridge upon the redox processes of the metal centres connected by that ligand. As described along the introduction chapter, CV allows for immediate probing of inter-metal communication on these binuclear bridged systems, since this type of behaviour is normally characterized by two CV waves as the termini of the rod go through the redox reactions at different potentials. The presented cyclic voltammograms are at 100 mVs^{-1}. These voltammograms were collected starting at 0.0 V unless otherwise noted. Half-wave potentials were calculated based on Equation (5).[259]

$$E_{1/2} = \frac{E_{pc} + E_{pa}}{2} \quad \textbf{(5)}$$

For the working electrode, platinum was used. The reference electrode was Ag/AgCl saturated in KCl. Finally, the secondary electrode was also platinum and all tests were carried out at room temperature (*ca.* 20 ºC) in CH_2Cl_2 using NBu_4PF_6 as the supporting electrolyte.

The free ligands (voltammograms presented in Chapter IV) only present an irreversible oxidation wave when the side chain is introduced: the **5a** ligand does not show any oxidation wave, but a peak at *ca.* 1.5 V for single ringed – **5b-d**, – and 1.4 V for the tris ringed – **10a-b** ligands which is difficult to characterize as it develops in the electrochemical limits of the solvent. This wave is most likely the one-electron oxidation of the phenyl ring which shifts to lower energies by the electron donating effect of the alkoxy side chains. Whilst working with similar compounds, other authors[260], have performed the same attribution. It is noteworthy that the reduction of the tris ringed free ligands, **10a-b**, is electrochemically observed.

The palladium rods show the existence of two electrode processes, one first irreversible process and a second one probably irreversible (Figure 106, single ringed rods, **20b-d**). Reduction is observable in the compound with the longer side chain (**20d**) but not significantly, indicating a chemical reaction step. The first oxidation wave width of the compounds with alkoxi side chains (**20b-d**) suggest that this conversion is $1e^-$, which can be indicative the formation of the Pd^{II}/Pd^{III} pair. A following conversion to Pd^{III}/Pd^{III} could characterize the process at higher potentials, but once again, the similarity to the free ligands as well as the region where it is observed is close to the electrochemical process of the solvent making it difficult to characterize. The first process observed for the rods with smaller side chains (**20a-b**) tend to the irreversible.

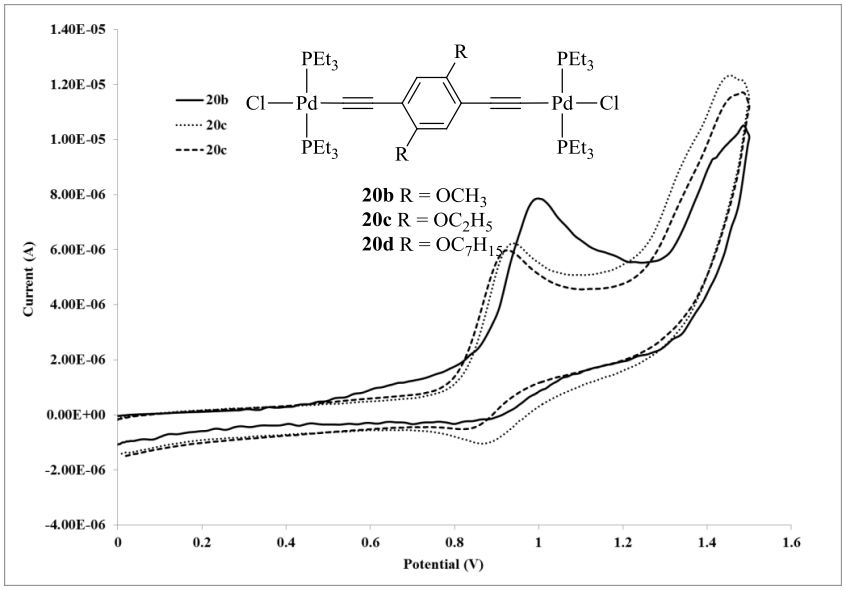

Figure 106. Cyclic voltammograms for the single ringed PE based palladium (**20-d**) rods with alkoxy side chains at 100 mVs^{-1} in CH_2Cl_2 vs. Ag/AgCl (KCl saturated).

The most striking aspect of the aggregated voltammograms in Figure 106, is that there is a shift of the first process to higher anodic potentials when the side chain is introduced (**20a** 890 mV to *ca.* 996 mV for **20b**). This value then shifts back down with the increase of the side chain's length (**20c** and **20d**). The first oxidation then appears to stabilize after a side chain of C_2 (**20c**) since for **20d** (side chain of OC_7), the values are very close (945 and 927 mV respectively).

Nevertheless, this decrease from OC_1 to OC_2 side chain is not very pronounced when observing the prepared tris ringed palladium rods (values for the first oxidation are presented in Table 5), since the anodic potentials for these oxidation processes are already very close (1.31 V for both compounds **21a** and **21b**) and actually higher than that of the **20a** (with no side chain) and very close to the ones observed for the free ligands (**10a** and **10b**). This observation further cements the expected low delocalization not only through the palladium centre but also through these longer ligands.

In contrast, the single ringed ruthenium rods (**23c-d**), present the two quasi-reversible processes (Figure 107).

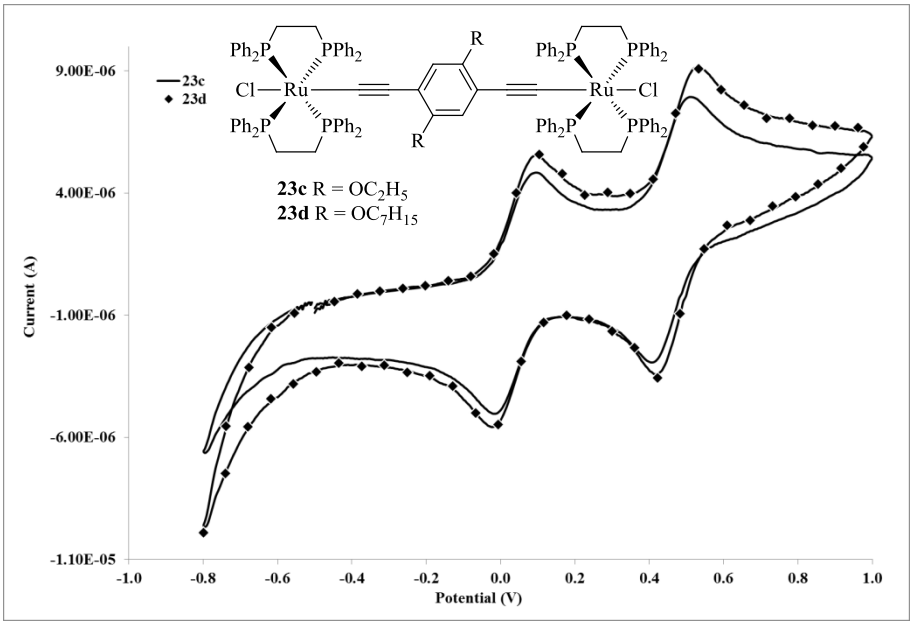

Figure 107. Cyclic voltammograms for the single ringed PE based ruthenium rods (**23c-d**) with alkoxy side chains at 100 mVs^{-1} in CH_2Cl_2 vs. Ag/AgCl (KCl saturated).

These processes are in agreement with the reports found in the literature for similar compounds and are usually attributed to the discrete Ru^{II}/Ru^{III} oxidation of both centres (termini), but are actually not isolated to the metal and are thus related to the bridging ligand as already explained in the introduction chapter.[46, 53a, 53f, 57, 66a-e, 69, 78, 81, 203b, 203c, 235] These two wave processes are in fact normally used as an indicator of inter-metal communication based on electronic delocalization through the bridging ligand.

The first oxidation is observed around 42 mV for both compounds but the second oxidation is slightly higher for the second oxidation (460 and 480 mV for **23c** and **23d**, respectively). Furthermore, high $\Delta E_{½}$ (418 and 436 mV respectively) and high K_c values (1.1×10^7 and 2.4×10^7 respectively) point to borderline Class III mixed valence systems in the Robin–Day[11, 48, 53c, 58-59] classification which would mean that there is a largely delocalized system.

Regarding the *tris* ringed ruthenium systems (**24a-b**, Table 5), only one redox process is observed at *ca.* 550 mV (effectively isolating systems). This process is at a slightly higher potential than that of *trans*-$[RuCl_2(dppe)_2]$ (**36**, 580 mV) and, in comparison with the single ringed systems it would correspond to the first oxidation but at a potential close to the second oxidation. Moreover, both ruthenium centres suffer the Ru^{II} to Ru^{III} oxidation simultaneously and thus pointing to broken delocalization along this longer bridging ligand. There is also a slight increase in anodic potential as the side chain increases from 548 to 563 mV, for **24a-b** respectively.

Finally, the thiophene based ruthenium rods (Figure 108, **27** and **28**) also present a quasi-reversible redox process at 529 mV for **27** and at 547 mV for **28**. The higher anodic potential relative to **28** can be attributed to the inverse of what would be expected from this compound. *i.e.*, increased delocalization through the backbone as derived from better coupling through the triple bonds that are not present in **27**. Nevertheless, this could indeed be attributed to further decoupling brought about isolation of both metal centres (and respective bridging ligand halves) effectively creating two systems constituted by the rods halves that effectively go through the electrochemical reaction at the same potential.

Furthermore, these values are only slightly lower than *trans*-$[RuCl_2(dppe)_2]$ (**36**, 580 mV).

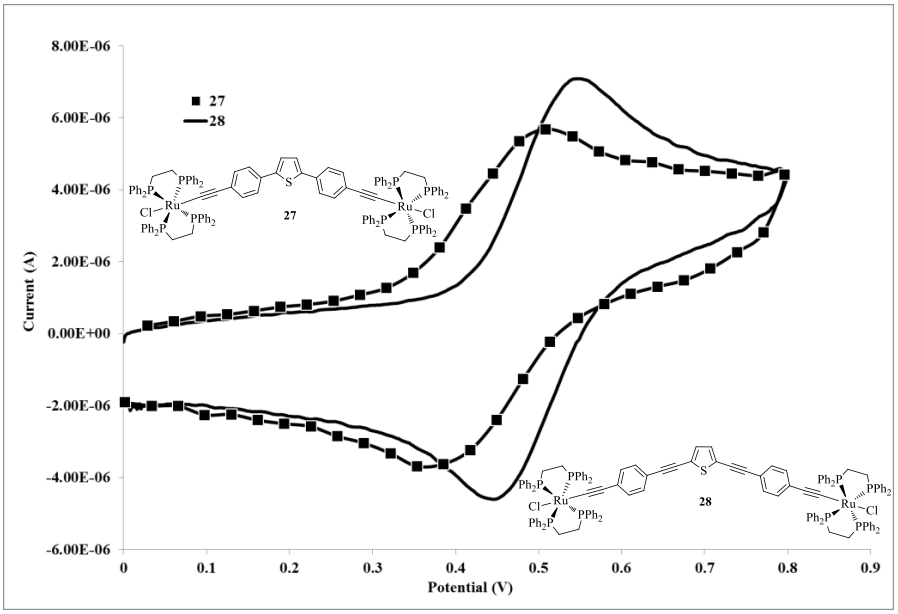

Figure 108. Cyclic voltammogram for thiophene based ruthenium Rods (**27** and **28**) at 100 mVs^{-1} in CH_2Cl_2 vs. Ag/AgCl (KCl saturated).

The calculated data for reversibility determination and wave details of compounds **23c-d** is available in Table A. 1. (Annex A.6) Table 5 contains selected data for the studied compounds. The comproportionation constant ($K_c = e^{\Delta EF/RT}$) is only calculated for compounds **23c-d** as these are the only ones that present quasi-reversible two wave redox processes (the two anodic potential values presented in Table 5). This constant is thus calculated from the $\Delta E_{½}$ and is regarded, as exposed in Chapter I, as an indirect measure of the electronic delocalization in this type of systems.

Table 5: Selected electrochemical data for the prepared palladium (**20a-d**, **21a-b**) and ruthenium rods (**23a**,**c-d**, **24a-b**).

Pd rods	E_{pa} / mV	Ru rods	E_{pa1} / mV	E_{pa2} / mV	$\Delta E_{½}$ / mV (K_c)
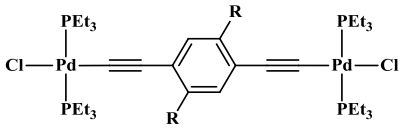		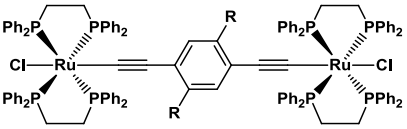			
20a R = H	890.4	**23a**[a] R = H	-328[a]	13	314 (6.0×10^6)
20b R = OCH_3	996.0				
20c R = OC_2H_5	945.0	**23c** R = OC_2H_5	41.0	459.9	418.0 (1.1×10^7)
20d R = OC_7H_{15}	927.0	**23d** R = OC_7H_{15}	43.9	479.7	436.7 (2.4×10^7)
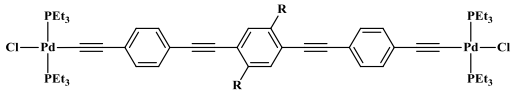		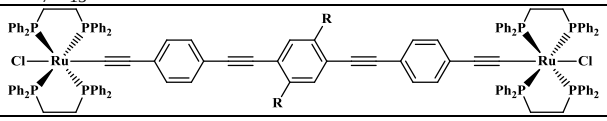			
21a R = OCH_3	1314	**24a** R = OCH_3	515.9		
21b R = OCH_3	1314	**24b** R = OC_2H_5	563.1		
		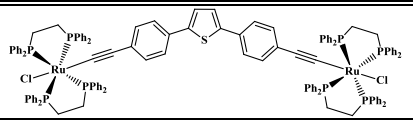			
		27	529		
		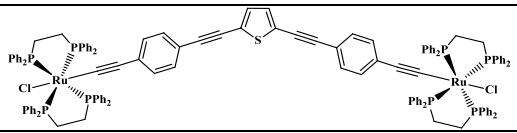			
		28	547		

[a] From ref. [16].

II.8. NMR Studies

Comparison of NMR chemical shifts can provide some insight into the degree of delocalization of the electronic density over the wire. As such, some selected data regarding the studied Pd and Ru rods are presented in Table 6. When comparing the Pd rods complexes with the free ligands, the ^1H shows mostly shielding of the aromatic (no more than ½ ppm) and side chain protons (no more than 0.1 ppm). The aromatic protons show very similar chemical shifts in comparison with the free ligands (*e.g.* **20b**, OCH_3 6.69 from 6.98 free) and the same observation

can be made for the first protons of the side chains (*e.g.* **20b**, OCH_3 3.74 from 3.87 free). Furthermore, the values for the equivalent protons across Pd rods are relatively closer. This can be observed for the side chains as well as for the aromatic protons. The Ru rods show an aromatic region rich in NMR signals which are difficult to assign to specific protons of the complexes due to the dppe ligands. Nevertheless, in the case of the thiophene based complexes (**24** and **28**) some significant deshielding is observed for the terminal phenyl rings which shift from *ca.* 7.47 to 6.60 ppm upon coordination to the $RuCl(dppe)_2$ moiety. This can safely be attributed to delocalization of electron density throughout the Ph–C≡C–Ru backbone. In the case of the side chains, the observations are similar to what was found for the Pd rods with slight chemical shift variations with no more than 0.2 ppm. Attribution of this slight increase (comparing with Pd rods) may be attributed to a higher delocalization but these differences are too small.

The palladium rods (**20a-d**, **21a-b**) all show ^{31}P NMR singlets at around 18 ppm which only about 1 ppm more than the free palladium starting material *trans*-$[Pd(PEt_3)_2Cl_2]$ (**19**). There is no significant change in this value throughout the series with the small variations being mostly incomparable. Perhaps the main difference in the NMR data of the palladium rods is the virtual coupling observed in the ^{13}C NMR. This C–P coupling[261] which was found at around 15 ppm in the ^{13}C spectra for all the rods.

In relation to the Ru rods, the difference between samples for the ^{31}P NMR was basically inexistent, with all complexes showing a singlet at *ca.* 48ppm (CD_2Cl_2). This value was then maintained through shorter to longer bridging ligands (**23a**,**c-d** to **24a-b**) and even when changing the bridging ligand's main moiety to thiophene (**27** and **27**). When comparing the average 48 ppm signal for the Ru rods with the appropriate free complex (*trans*-$[RuCl_2(dppe)_2]$), a deshielding of *ca.* 3 ppm is found which is in line with coordination of this type of ligands.

On a final note, significant attribution and discussion of the ^{13}P NMR spectra is difficulted by the shifting of the C–M carbon in relation to the free ligand as well as that the C≡C carbons show values that may be close to the aromatic ones or have very low intensity since they are quaternary (slow relaxation and no NOE – Nuclear Overhauser Effect – enhancement). Also, the Ru rods had to be characterized using CD_2Cl_2 since the stability in $CDCl_3$ was observed to be smaller this can explain the 0.2 ppm difference observed for the OCH_n protons discussed above.

Table 6: Selected NMR data for the prepared palladium (**20a-d**, **21a-b**) and ruthenium rods (**23a**,**c-d**, **24a-b**, **27** and **28**). Chemical shifts in parenthesis are relative to the free ligands.

	Palladium Rods **δ /ppm [a] (*J* / Hz)**		**Ruthenium Rods** **δ / ppm [b] (*J* / Hz)**
20a	**^{1}H**: 7.07 (7.56 Ar-H) **^{13}C**: 15.51 (t, J_{C-P} = 16) **^{31}P**: 18.1	**23a**	**^{31}P**: 48.8
20b	**^{1}H**: 3.75 (3.87 OCH_3), 6.69 (6.98 Ar-H) **^{13}C**: 15.32 (t, J_{C-P} = 14), **^{31}P**: 18.1		–
20c	**^{1}H**: 3.97 (4.07 OCH_3), 6.69 (6.89 Ar-H) **^{13}C**: 15.74 (t, J_{C-P} = 14) **^{31}P**: 18.3	**23c**	**^{1}H**: 3.68 (4.07 OCH_3) **^{31}P**: 48.2
20d	**^{1}H:** 3.89 (3.97 OCH_3), 6.69 (6.95 Ar-H) **^{13}C**: 15.32 (t, J_{C-P} = 14), **^{31}P**: 18.3	**23d**	**^{1}H**: 3.73 (3.97 OCH_3) **^{31}P**: 48.3
21a	**^{1}H**: 3.90 (3.91 OCH_3), 7.01 (7.03), 7.21 (d, 7.47 Ar-H), 7.42 (d, 7.52) **^{13}C:** 15.83 (t, J_{C-P} = 14), **^{31}P**: 18.4	**24a**	**^{1}H**: 3.68 (3.91 OCH_3) **^{31}P**: 48.5
21b	**^{1}H**: 4.10 (4.11 OCH_3), 6.95 (7.01), 7.21 (d, 7.47 Ar-H), 7.40 (d, 7.49) **^{13}C**: 15.82 (t, J_{C-P} = 14), **^{31}P**: 18.3	**24b**	**^{1}H**: 4.11 (4.11 OCH_3) **^{31}P**: 48.6
	–	**27**	**^{1}H**:6.64 (7.47 Ar-H) **^{31}P**: 48.8
	–	**28**	**^{1}H**: 6.54 (7.47 Ar-H) **^{31}P**: 48.6

[a] In $CDCl_3$; **[b]** in CD_2Cl_2 (see text); ^{1}H NMR at 400 MHz, ^{13}C at 100 MHz, ^{31}P at 161 MHz; d = doublet; t = triplet;

II.9. FTIR Studies

Some important information can be obtained from the analysis of vibrational peaks from FTIR spectra. This data can be related to electronic delocalization from the ligand bridge to the metal centre (or *vice versa*). The Infra-red spectra were collected using a Bruker Tensor 27 FTIR spectrophotometer equipped with an ATR (Attenuated Total Reflectance, diamond) add-on which permitted the use of powder samples of the tested compounds without any requirement for a matrix. Samples were collected at a resolution of 2 cm^{-1} using a spectral range of 4000 to 400 cm^{-1}. The FTIR data for compound **28** was obtained in the same conditions described above but instead of an ATR add-on, a KBr pellet was prepared to collect the spectrum in transmittance mode. Selected peak information for the shorter phenylene ethynylene ligands and the respective palladium and ruthenium rods is presented in Table 7.

Table 7: Selected vibrational data for the prepared compounds based on the shorter bridging phenylene ethynylene ligands (**5a-d**), obtained through FTIR-ATR (diamond).

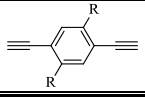	**Free Ligands**		**Palladium Rods**		**Ruthenium Rods**	
		$\tilde{\nu}$ **(int., mode) / cm^{-1}**		$\tilde{\nu}$ **(int., mode, $\Delta\tilde{\nu}$) / cm^{-1}**		$\tilde{\nu}$ **(int., mode, $\Delta\tilde{\nu}$) / cm^{-1}**
R = H	**5a**[a]	3292 (s, $\nu_{C\equiv C\text{-}H}$) 2104 (vw, $\nu_{C\equiv C}$) 642 (s, $\delta_{C\equiv C\text{-}H}$)	**20a**	2118 (w, $\nu_{C\equiv C}$, 14); 1498 (m), 1452 (m), 1409 (m), 1378 (m) (ar. $\nu_{C=C}$)	**23a**	2049 (w, $\nu_{C\equiv C}$, 55) 14856 (w), 1433 (m) (ar. $\nu_{C=C}$)
R = OCH_3	**5b**	3257 (s, $\nu_{C\equiv C\text{-}H}$) 2106 (vw, $\nu_{C\equiv C}$) 655 (s, $\delta_{C\equiv C\text{-}H}$) 1495 (m), 1464 (m), 1455 (m), 1445 (m), (ar. $\nu_{C=C}$)	**20b**	2115 (s, $\nu_{C\equiv C}$, 9) 1493 (m), 1454 (m), 1410 (m), 1385 (m) (ar. $\nu_{C=C}$)		–
R = OC_2H_5	**5c**	3266 (s, $\nu_{C\equiv C\text{-}H}$) 2109 (vw, $\nu_{C\equiv C}$) 651 (s, $\delta_{C\equiv C\text{-}H}$) 1497 (m), 1475 (m), 1401 (m), 1391 (s), 1367 (w) (ar. $\nu_{C=C}$)	**20c**	2113 (w, $\nu_{C\equiv C}$, 4) 1498 (m), 1478 (m), 1410 (m), 1390 (m) (ar. $\nu_{C=C}$)	**23c**	2057 $\nu_{C\equiv C}$, 52) 1485 (w), 1432 (m), 1433 (m) 1392 (w) (ar. $\nu_{C=C}$)
R = OC_7H_{17}	**5d**	3262 (s, $\nu_{C\equiv C\text{-}H}$) N/V ($\nu_{C\equiv C}$) 661 (s, $\delta_{C\equiv C\text{-}H}$) 1500 (m), 1469 (m), 1387 (m) (ar. $\nu_{C=C}$)	**20d**	2118 (w, $\nu_{C\equiv C}$) 1498 (m), 1473 (m), 1455 (m), 1412 (m) (ar. $\nu_{C=C}$)	**23d**	2065 (w, $\nu_{C\equiv C}$) 1486 (m), 1432 (w), 1383 (w) (ar. $\nu_{C=C}$)

[a] From ref. [262]. ar. = aromatic; int. = intensity; N/V = not visible; s = strong; vw = very weak; m = medium; w = weak.

The free ligands display typical stretching bands for the aromatic rings. Nevertheless, the PE based ligands (**5a-c** and **10a-b**) display very weak bands relative to $\nu_{C\equiv C}$ (C≡C stretching). This is the reported behaviour[256] for highly symmetric internal alkynes (R-C≡C-R'), but can also be observed for the terminal alkynes like the ones that are presented in this work, since they too, are highly symmetric. Moreover, the visible peaks have a value of approximately 2105 cm^{-1} for all the PE ligands (single and tris ringed, **5a-c** and **10a-b,** Table 7 and 8 respectively). As for the absence of a visible peak for **5d** this is due to the absorption of the diamond crystal used for ATR having a high absorption zone in the 2100 cm^{-1} region

Notwithstanding, the sharp strong peaks for $\nu_{C\equiv C\text{-}H}$ are always visible at around 3250 cm^{-1} for all the free ligands, including single and tris ringed PE (**5a-d** and **10a-b**) as well as the thiophene based ones (**14b** and **18b,** Table 9). Some degree of decreasing intensity was observed for the tris ringed PE (**10a-b**) ligands in comparison to the single ringed (**5a-d**) for the $\nu_{C\equiv C\text{-}H}$ which may be attributed to decreasing polarization on this bond for the larger systems.

Nevertheless, the bending mode peaks ($\delta_{C\equiv C\text{-}H}$, *ca.* 650 cm^{-1}) display mostly the same intensity. As for the relative energies of these peaks, the wavenumber values do not vary significatively or in a recognizable pattern staying around 3260 cm^{-1} for the PE based ligands. The same behaviour was observed for the energies of the bending modes of these ligands. The thiophene based ligands (**14b** and **18b**) present a higher energy $\nu_{C\equiv C\text{-}H}$ at *ca.* 3280 cm^{-1} but similar $\delta_{C\equiv C\text{-}H}$ energies. Moreover, these ligands also display, in contrast with the PE ligands, the $\nu_{C\equiv C}$ peaks at 2200 and 2106 cm^{-1} for terminal and internal $\nu_{C\equiv C}$ respectively.

In regard to the palladium rods (**20a-d** and **21a-b**, Table 7 and 8 respectively), the $\nu_{C\equiv C\text{-}H}$ is obviously not present in the respective spectra. Furthermore the $\nu_{C\equiv C}$ is now very visible (in the range of 2110 to 2117 cm^{-1}) and with medium to strong intensity as it would be expectable from the largely polar system Pd-C≡C-Ph.

Curiously, the other $\nu_{C\equiv C}$ is still not visible for the tris ringed rods (**20a-b**) even after coordination. This can point to maintenance of the ligands symmetry even after coordination. Regarding the $\nu_{C\equiv C}$ peaks, there is a slight shift to higher energies upon coordination (*ca.* 8 cm^{-1} in all cases), which points to an increasing bond strength, which is not the case in the ruthenium rods discussed further on. Moreover, the values are similar to those reported in the literature.[170b, 258e]

Table 8: Selected vibrational data for the prepared compounds based on the longer bridging phenylene ethynylene ligands (**10a-b**), obtained through FTIR-ATR (diamond).

		Free Ligands $\tilde{\nu}$ **(int., mode) / cm^{-1}**		**Palladium Rods** $\tilde{\nu}$ **(int., mode, $\Delta\tilde{\nu}$) / cm^{-1}**		**Ruthenium Rods** $\tilde{\nu}$ **(int., mode, $\Delta\tilde{\nu}$) / cm^{-1}**
		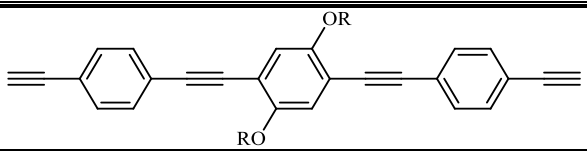				
R = CH_3	**10a**	3271 (m, $\nu_{C\equiv C-H}$) 2102 (vw, $\nu_{C\equiv C}$) 655 (s, $\delta_{C\equiv C-H}$) 1510 (w), 1500 (w), 1492 (w), 1461 (w), 1936 (m) (ar. $\nu_{C=C}$)	**21a**	2110 (w, $\nu_{C\equiv C}$, 8) 1508 (m), 1488 (m), 1457 (m), 1397 (m) (ar. $\nu_{C=C}$)	**24a**	2061 (w, $\nu_{C\equiv C}$, 41) 1509 (w), 1485 (m), 1433 (w) 1432 (m) 1396 (w) (ar. $\nu_{C=C}$)
R = C_2H_5	**10b**	3275 (m, $\nu_{C\equiv C-H}$) 2105 (vw, $\nu_{C\equiv C}$) 661 (s, $\delta_{C\equiv C-H}$) 1516 (m), 1499 (w), 1490 (w), 1474 (w), 1417 (m), 1403 1392 (m) (ar. $\nu_{C=C}$)	**21b**	2112 (w, $\nu_{C\equiv C}$, 7) 1510 (m), 1487 (m), 1454 (m), 1413 (m) 1377 (m) (ar. $\nu_{C=C}$)	**24b**	2067 (w, $\nu_{C\equiv C}$, 38) 1508 (w), 1485 (m), 1413 (w) 1432 (m), 1412 (w) (ar. $\nu_{C=C}$)

[a] ar. = aromatic; int. = intensity; N/V = not visible; s = strong; vw = very weak; m = medium; w = weak.

Regarding the $\nu_{C=C}$ relative to aromatic rings, the main observation would be the decrease in peaks at the respective region. This could be related to a smaller number of IR active vibration modes brought about by the steric hindrance of the terminal metalation.

Pertaining the FTIR spectra of the ruthenium rods (**23a**,**c-d** and **24a-b**, Table 7 and 8 respectively), the immediate observation is the decreased frequency values relative to the $\nu_{C\equiv C}$ bands which exhibit a variation of *ca.* 50 cm^{-1} in relation to the starting material (free ligands). This is indicative of delocalization of the electronic density. Furthermore, the $\nu_{C\equiv C}$ is of 2048 cm^{-1} for **23a** and jumps to *ca.* 2060 cm^{-1} for all the rods with side chains (**23c-d** and **24a-b**). This bond strengthening could be attributed to the electronic donation of the alkoxy side chains that help fill the gap that was created upon delocalization to the terminal ruthenium centres. This was also observed in the electronic spectra. Furthermore, there is still no evidence of the internal $\nu_{C\equiv C}$ peaks on the tris ringed systems (**24a-b**). As for the region correspondent to aromatic $\nu_{C=C}$, some extra peaks are visible in relation to the palladium rods (**20a-d** and **21a-b**), but these could very well be attributed to the phenyl rings from the ancillary ligand's (dppe), supporting the hypothesis of decreased vibration modes.

In the case of the thiophene based ruthenium rods (**27** and **28**, Table 9), both the vibration modes relative to metal bound triple bonds, $\nu_{C\equiv C\text{-}Ru}$, have a value close to 2058 cm^{-1} pointing to a very similar electronic density, at least in the Ru–C≡C–Ph system. Furthermore, not only this mode gains quite a high intensity but also shifts to lower energies (from 2108 to 2059 cm^{-1} in the case of **28**; not visible for the starting material of **27**, respectively **14b**). The internal $\nu_{C\equiv C}$ for **28** was almost unaffected by the coordination, only losing about 11 cm^{-1} (from 2201 to 2190 cm^{-1}) in the process. Finally, the $\nu_{C\equiv C}$ is visible in **27** due to the coordination. As mentioned before, this could be another case of loss of symmetry brought about by the bulky Ru moieties.

Table 9: Selected vibrational data for the prepared compounds based on the bridging thiophenylene ethynylene ligands (**14b** and **18b**), obtained through FTIR-ATR (diamond)[a].

		Free Ligands $\tilde{\nu}$ **(int., mode) / cm^{-1}**		**Ruthenium Rods** $\tilde{\nu}$ **(int., mode, $\Delta\tilde{\nu}$) / cm^{-1}**
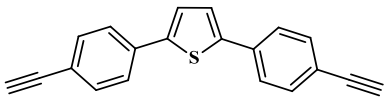	**14b**	3292 (m, $\nu_{C\equiv C\text{-}H}$) 666 (m, $\delta_{C\equiv C\text{-}H}$) N/V ($\nu_{C\equiv C}$) 1488 (w), 1449 (w), 1406 (w), (ar. $\nu_{C=C}$)	**27**	2058 (m, $\nu_{C\equiv C}$) 1489 (m), 1435 (m) (ar. $\nu_{C=C}$)
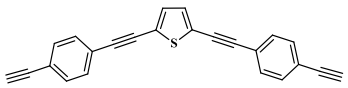	**18b**	3284 (s, $\nu_{C\equiv C\text{-}H}$) 644 (s, $\delta_{C\equiv C\text{-}H}$) 2202 (w,br), 2106 (w) ($\nu_{C\equiv C}$) 1525 (w), 1484 (w), (ar. $\nu_{C=C}$)	**28**	2191 (w, $\nu_{C\equiv C}$, 11), 2069 (s, $\nu_{C\equiv C}$, 37)

[a] except compound **28**, which was analysed in KBr pellet; ar. = aromatic; int. = intensity; N/V = not visible; s = strong; vw = very weak; m = medium; w = weak.

II.10. MS Studies

Discussion of the main MS data is performed bellow in order to show that coordination of the ligands effectively occurred to form the binuclear rods that were intended. The peaks which were found through ESI-TOF mass spectroscopy for the palladium and ruthenium rods are presented in Table 10. ESI-TOF spectra were collected with a Micro-mass LCT spectrometer by direct infusion of a methanol/CH_2Cl_2 solution prepared in the following manner: very low

concentration 1 mL solution of the sample (0.5 mg mL^{-1}) was prepared in CH_2Cl_2 as the stock solution; dilution of 50 µL of this sample in 1 mL of methanol was then prepared and injected. The methanol contained 0.1% of formic acid.

Table 10: Selected ESI-MS(TOF) peaks for the prepared palladium (**20a-d**, **21a-b**) and ruthenium rods (**23a**,**c-d**, **24a-b**).

	Palladium rods		**Ruthenium rods**
	Ion (*m/z*)		**Ion (*m/z*)**
20a	727.0 $[M\text{-}Cl\text{-}PEt_3+H]^+$, 845.1 $[M\text{-}Cl]^+$, 903.1 $[M+Na]^+$.	**23a**	960.3 $[M\text{-}Cl_2]^{2+}$, 1025.4 $[(dppe)_2Ru\text{-}C\equiv C+P]^+$
20b	907.7 $[M\text{-}Cl]^+$, 963.1 $[M+Na]^+$		–
20c	933.1 $[M\text{-}Cl]^+$, 991.1 $[M+Na]^+$	**23c**	2078.7 $[M]^+$, 1021.8 $[M\text{-}Cl]^{2+}$
20d	1131.3 $[M+Na]^+$	**23d**	2218.9 $[M]^+$
21a	1105.3 $[M\text{-}Cl_2]^+$, 987.1 $[M\text{-}Cl\text{-}PEt_3]^+$, 881.3 $[M\text{-}(Pd(PEt_3)_2Cl)+PEt_3]^+$, 763.2 $[M\text{-}(Pd(PEt_3)_2Cl)]^+$,	**24a**	1283.5 $[M\text{-}RuCl(dppe)_2\text{-}Cl]^+$, 1090.4 $[M\text{-}Cl_2]^{2+}$
21b	1133.3 $[M\text{-}Cl]^+$	**24b**	1311.3 $[M\text{-}RuCl(dppe)_2\text{-}Cl]^+$, 1105.8 $[M\text{-}Cl_2]^{2+}$
	–	**27**	2148.6 $[M]^+$, 2113.6 $[M\text{-}Cl]^+$
	–	**28**	1081.4 $[M\text{-}Cl]^{2+}$, 1063.4, $[M\text{-}(RuCl(dppe)_2)+P+C]^+$

Regarding the ESI–TOF analysis of the palladium Rods, $[M\text{-}Cl]^+$ peaks were found for most of the compounds (except **20d**). Furthermore, $[M+Na]^+$ ion peaks were also observed for all the studied compounds. For **20a**, an ion peak of 727.0 *m/z* was observed which corresponds to $[M\text{-}Cl\text{-}PEt_3+H]^+$. In comparison to the ruthenium rods, the palladium analogues are more stable and molecular ions are easier to isolate without much tuning of the ESI parameters. For the tris ringed palladium rods (**20a-d**, **21a-b**), $[M\text{-}Cl_2]^+$ and $[M\text{-}Cl]^+$ (as observed in Figure 109 for **20c**) were found for both the compounds and by using harsher ionization condition, several other ions were visible for **21a**, like for example 881.3 *m/z* which presents a $[M\text{-}(Pd(PEt_3)_2Cl)+PEt_3]^+$ formal composition. Similar fragmentation and cleavage is found in the literature.[83b]

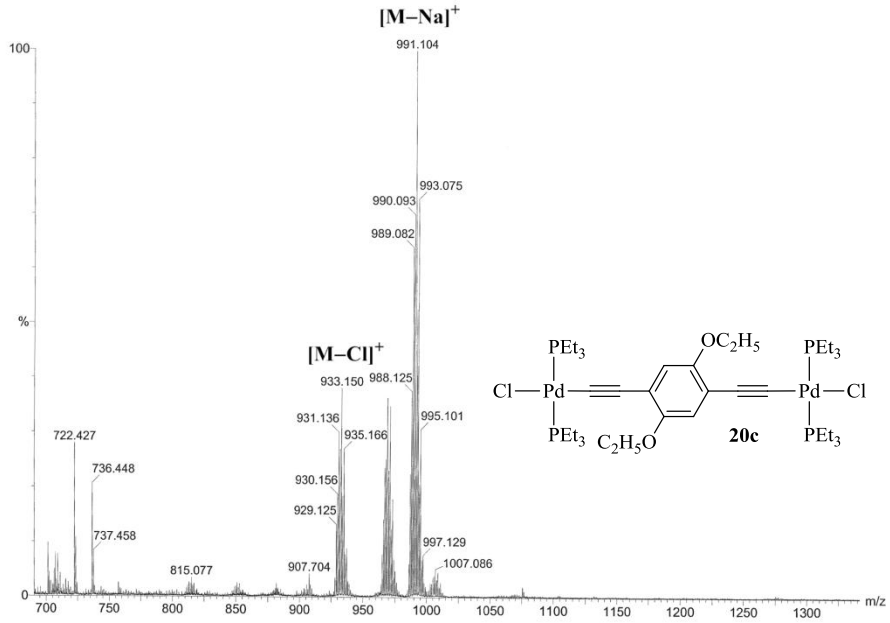

Figure 109. ESI-TOF MS spectrum for palladium rod **20c**.

In the case of the ruthenium analogues, these generally display the double charged peak with a loss of two chlorides (**23a** and **24a-b**). Furthermore, these rods are stable enough to also display molecular ions in some cases (**23c-d**). Extra ion peaks include a formal composition of $[(dppe)_2Ru–C{\equiv}C+P]^+$ visible in the MS spectrum of **23a** at 989.3 *m/z*. Strange formal compositions like these are not without other counterparts in the literature.[83b] Moreover, this is the base peak for **23a** and its isotope pattern was verified. Another common ion peak is the one for $[Ru(dppe)_2]^+$. It is usually found at 897.3 *m/z* as the base peak and was also reported with a single charge by Humphrey and co-workers.[263] The fragmentation at the triple bond originates ions of the type $[M\text{-}RuCl(dppe)_2\text{-}Cl]^+$ where the second Ru centre is lost, as well as the chloride for the remaining centre. This ion was found for **24a** (Figure 110).

Finally and in respect to the thiophene based ruthenium rods, either a double charge ion (**28**, 1081.4 $[M\text{-}Cl]^{2+}$) or a single charged ion were found (**27**, 2148.6 $[M]^+$) pointing to good stability. Nevertheless, a 15% intensity peak of formal composition $[M\text{-}(RuCl(dppe)_2)+PC]^+$ was also found for **27** at 1270.5 *m/z*.

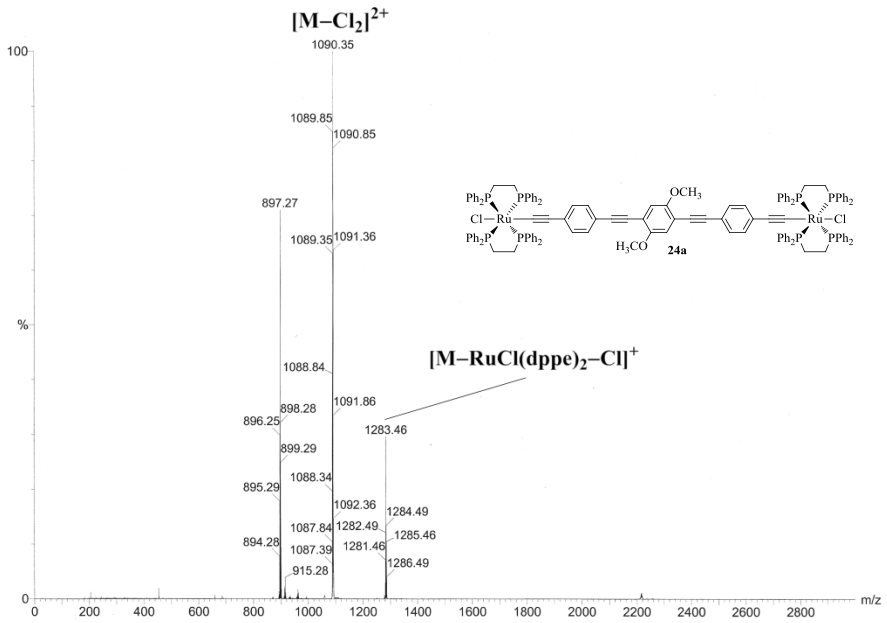

Figure 110. ESI-TOF MS spectrum for palladium rod **24a**.

II.11. Single crystal X-ray diffraction

In this section the discussion and presentation of the crystal structures that were obtained on the course of the PhD work. These structures can give precious clues regarding the orientation of the phenyl rings in relation to the metal centres (in the case of the Pd and Ru rods) as well as orientation and possible influence of the side chains in rod conformation and dihedral angles. Furthermore, the packing and orientation of the molecules in the crystal can provide some insight on future solid state applications of these materials.

Structures of the bridging ligands (**4c**, **5c**, **5d**, **8b** and **10a**) are presented as well as one palladium rod (**21b**). Crystals of starting materials based on the $[RuCl_2(dppe)_2]$ moiety were also obtained (**34**, **37**). The structures were compared with the literature using the Cambridge Structural Database (CSD, version 5.33, August 2012 update).

II.11.1. Three (phenylene ethynylene)s (4c, 5c, 5d)

Along the preparation of the free ligands and their respective precursors, crystals were obtained with enough quality for structure resolution. The crystal structures of **4c** (protected **5c**

with $Si(CH_3)_3$), **5c** and **5d** and shown in the Figure 111).[210] In regard to the similar structures found in the CSD, only five diethynylbenzene derivatives with alkoxy side chains were found.

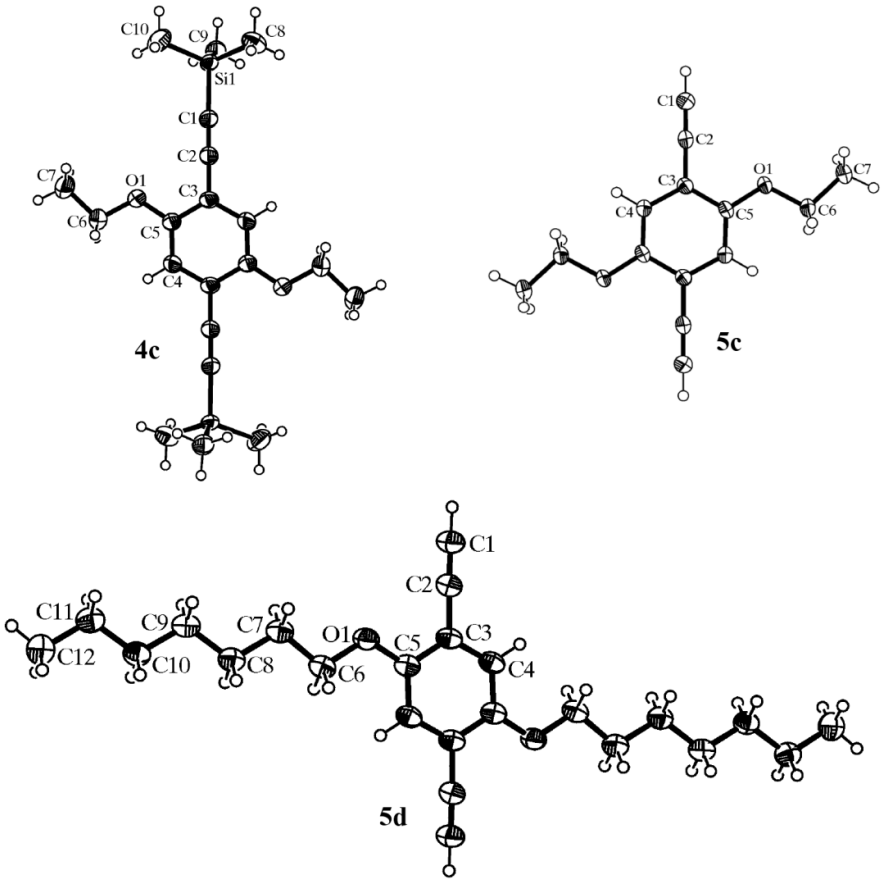

Figure 111. ORTEP-3[264] plots of **4c**, **5c** and **5d** (50% probability displacement ellipsoids).

All three compounds (**4c**, **5c-d**) display C–H···π interactions from the terminal methyl moiety of the side chains and the π system of the triple bond of the adjacent molecule.

Compound **4c** do not show any unusual values in regard to the bond distances and angles. The intermolecular interaction found for **4c** is the C–H···π interaction between the methylene H atoms of the ethoxy group and the terminal acetylenic C atom (2.86 Å with an angle of 153º). Another intermolecular interaction, albeit weaker, is also observed between adjacent trimethylsilyl groups (2.39 Å). Figure 112 shows the interactions (stronger ones only).

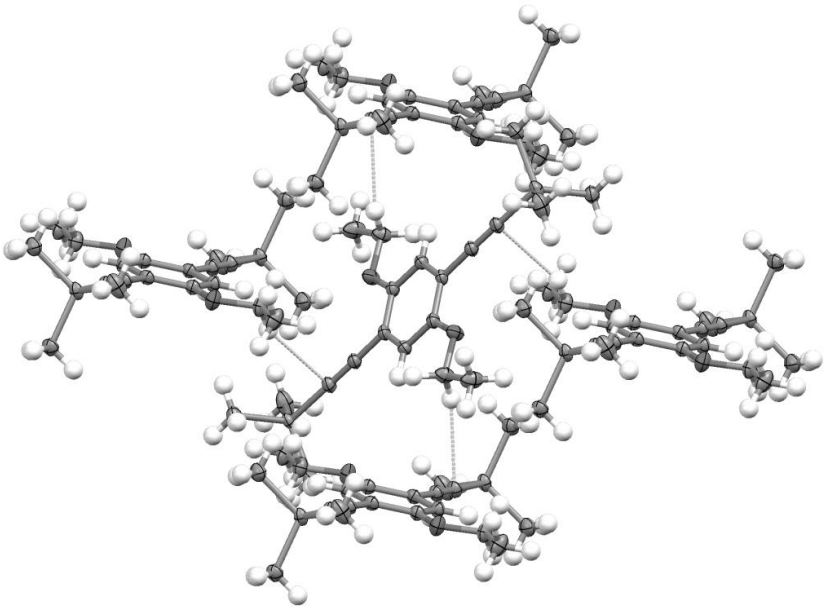

Figure 112. Packing plot[265] relative to **4c**. Only C–H···π interactions are shown.

Since **5c** does not have the bulky trimethylsilyl groups, it shows different packing behaviour. This then leads to a closer packing with interactions to eight separate molecules which are arranged in-plane with π–π interactions between the acetylenic terminal carbons of adjacent molecules. In addition to these, C–H···π interactions between the same terminal acetylenic carbon and the hydrogen from the alkoxy chain are also observed (contact distance being 2.88 Å, Figure 113).

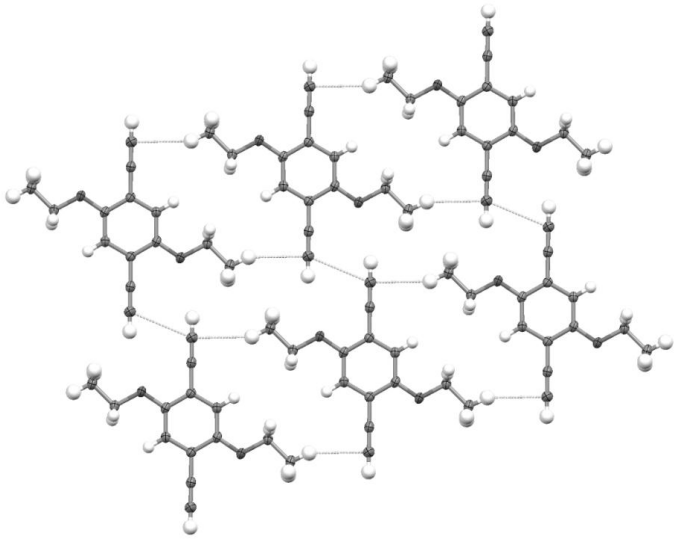

Figure 113. Packing plot[265] relative to **5c**. The in-plane interactions are shown.

The long heptoxy chains present in compound **5d** pushes the molecules apart leading to a situation where the only sufficiently short intermolecular interactions are the nonclassical hydrogen bonds (Figure 114). The contact distance between the interacting H and O atoms is 2.54 Å forming an angle of 161º and a C···O distance of 3.449 (2) Å.

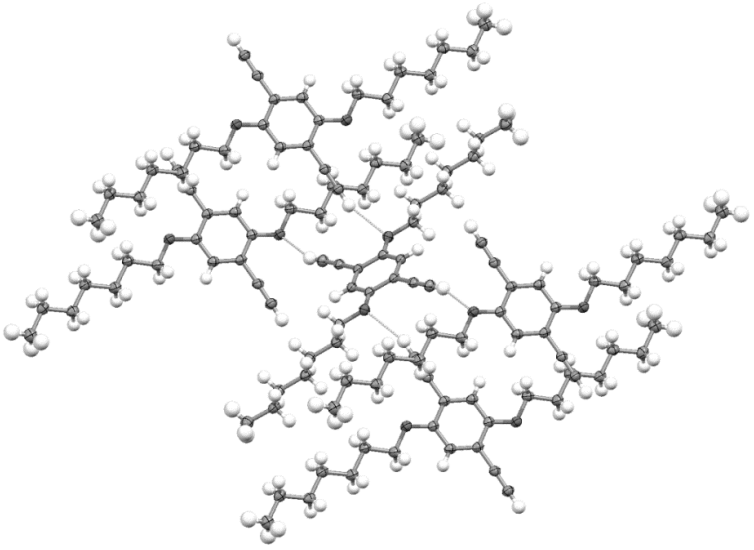

Figure 114. Packing plot[265] relative to **4c**. The C–H···π interactions are shown.

II.11.2. 1,4-bis(4-bromo-1-ethynylbenzene)-2,5-diethoxybenzene (8b)

The precursor (**8b**) used in the preparation of the tris-ringed ligand **10b** was crystallized in sufficient quality for its structure (Figure 115) to be determined by single crystal X-ray diffraction.

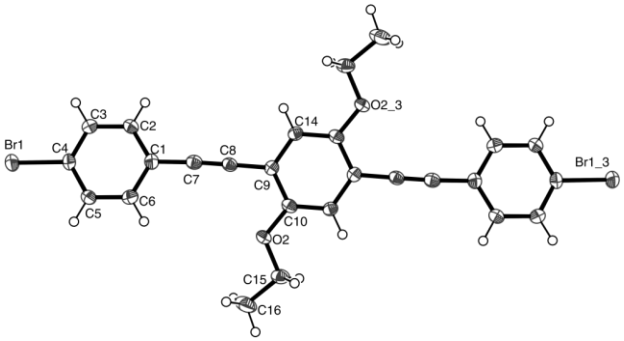

Figure 115. Perspective ORTEP-3[264] plot of **8b** (50% probability displacement ellipsoids).

As expected, the amount of reports of structures bearing this backbone (tris-PE) is relatively high (172 hits were found in the CSD with the Aug 2012 update). Surprisingly, no structure bearing terminal bromides was found. Moreover, many of these structures have quite different side chains and the ones that show similar alkoxy side chains (OC_2H_5) have different terminal group. Nevertheless, the common trend observed in the reported structures is related to the slight twisting of the planes between each ring, which is in accordance to the structure in Figure 116 as an angle of 9.64º was observed between the planes formed by the central and terminal phenyl rings.

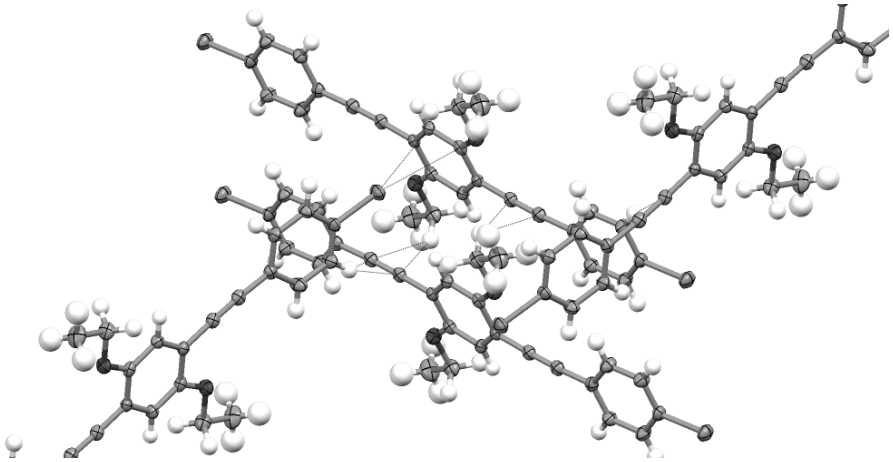

Figure 116. Mercury[265] plot of **8b** to show short contacts.

No typical hydrogen bonding was visible, but an interesting packing was found (Figure A. 37). There are short contact interactions between the terminal bromides and the π system of the central phenyl ring of another molecule situated in a perpendicular orientation. Surprisingly no interactions with the alkoxy oxygens are observed, but there are interactions of the triple bond with the CH_2 hydrogen (alkoxy chain) of an adjacent parallel molecule and the aromatic hydrogen of an adjacent perpendicular molecule.

In respect to bond distances, no deviation from the reported structures was found. The distance of Br–Ar was found to be of 1.905(2) Å which is in accordance with the literature reported range of 1.899 – 1.905 Å.[266] Furthermore, the triple bond is 1.201(4) Å and the Ar – O distance is of 1.367(3) Å which once again is in agreement with the reported[267] values of 1.188 and 1.370 Å, respectively. The value found for the Ar–O–CH_2 is of 117.9(2)º and for the

Ar(terminal)–C≡C and C≡C–Ar (central) values of 176.7(3) and 178.3(3)º were found respectively. These values are similar to those found in the literature[266-267] of 119.64º for the alkoxy angle and 175.7 and 176.2º for the triple bond angles.

II.11.3. 1,4-bis(1,4-diethynylbenzene)-2,5-dimethoxybenzene (10a)

The *tris*-ringed PE structure (**10a**) was solved and is presented in Figure 117. Following what was already observed for the previous structure (**8c**), there is a definitive difference in this case, since there is a marked angle formed between the phenyl rings. The angle is of 9.64º, in which case it would correspond to a loss of conjugation of the π system.[268] These angles are represented on the packing plot (Figure 117).

These angles could be related to the short contacts formed between the molecules. There is π–π interaction between the terminal phenyl rings of adjacent molecules as well as non-classical hydrogen bonding between the alkoxy chain's oxygen and the hydrogen from the terminal phenyl ring of one molecule and the terminal alkynyl hydrogen of another (Figure 118).

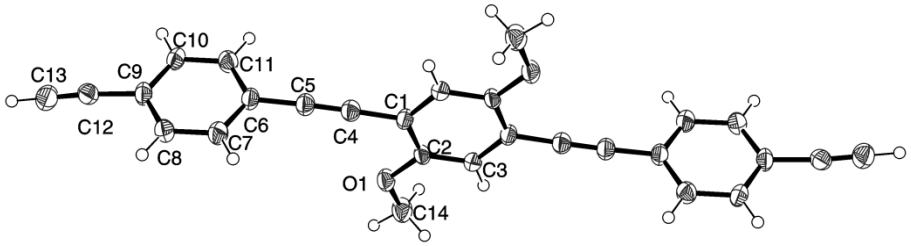

Figure 117. Perspective ORTEP-3[264] plot of **9a** (50% probability displacement ellipsoids).

As for bond lengths, inner and outer C≡C bonds show values of 1.200(4) and 1.117(5) Å, respectively. In respect to the alkoxy side chain, the Ar–O distance is of 1.369(3) Å and the O–CH_3 is of 1.425(3) Å. Regarding the bond angles, values found for Ar–O–CH_3 were 117.3(2)º, Ar(central)–C≡C of 178.6(3) º and Ar(terminal)–C≡C of 175.6(3)º for the inner triple bond and Ar(terminal)–C≡C of 174.1(3) º for the outer triple where observed. These values are in agreement to the reported distances and angles[267] as already referred for **8b**. A crystal structure for the same compound was recently published[269] and exhibits the same type of twisting found for compound **10a**.

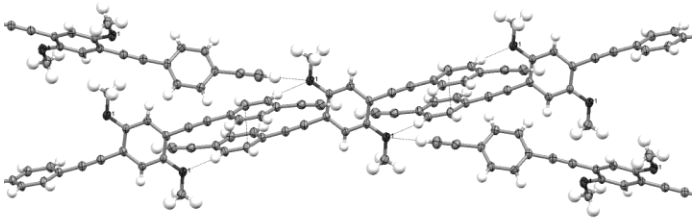

Figure 118. Mercury[265] plot of **9c** showing short contacts formed between molecules.

II.11.4. *trans*-[RuCl(H)(dppe)$_2$] (34)

A search in the CSD database surprisingly revealed that crystal structure of compound **34** is unpublished. This complex crystallizes in the triclinic *P*-1 space group (Figure 119) and the resulting geometry around the Ru(II) centre is a slightly distorted octahedral.

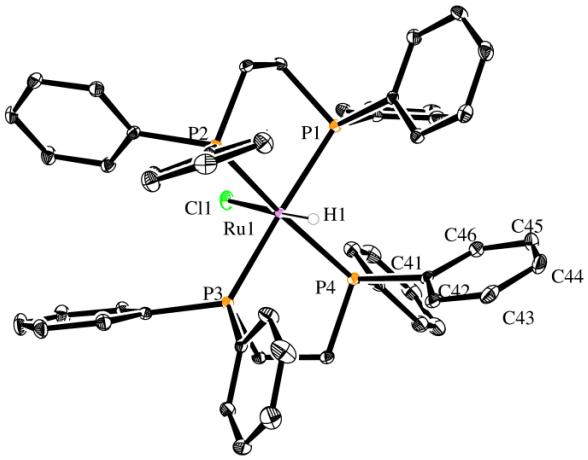

Figure 119. ORTEP-3[264] plot of the *trans*-[RuCl(H)(dppe)$_2$]·CH_2Cl_2 in perspective view. The H-atoms, apart from the hydride, as well as, the solvent molecules are excluded for clarity. Thermal displacement ellipsoids were drawn at 30% probability.

In respect to the severely different H and Cl ligands in *trans* position, the bending of the phosphine groups to the hydride side is very small (smallest H–Ru–P angle is 83.3(9)º), which translates as P–Ru–P angles of 176.75(2) and 168.19(2)º for P atoms in *trans* positions. The distances from Ru- to P-atoms show similar values (2.32-2.34 Å) as in other [Ru(L_2)(dppe)$_2$] complexes and the same is true for the Ru–Cl distance.[233] The Cl–Ru–H angle is close to linear

and the Ru–H bond distance is also found to be approximately same as reported for similar complexes like [RuCl(H)(diop)$_2$] (where diop is bis(diphenylphosphinomethyl)-2,2-dimethyl-1,3-dioxolane with Ru–H of 1.68 Å),[270] [RuCl(H)(dppm)$_2$] (dppm = $Ph_2PCH_2PPh_2$ with Cl–Ru–H of 172.74º and Ru–H of 1.484 Å),[271] [RuCl(H)($Ph_2PNMeNMePPh_2$)$_2$] (with Cl–Ru–H of 176.80º and Ru–H of 1.722 Å)[254] and [RuCl(H)(PP)]$_2$ (where the PP is (1*S*,2*S*)-1,2-trans-bis-(*O*-diphenylphosphino)cyclohexane where Cl–Ru–H is 174.21º and Ru–H is 1.535 Å).[272] However, it must be kept in mind in geometrical consideration that the determination of hydride position by X-ray diffraction is less accurate, because it contains only two electrons and even more uncertain it is when bonded to the heavy element (like Ru). Finally, the absence of a counter-ion on the asymmetric unit in conjunction with the hydride ligand (in respect to the starting material) is indicative of a neutral complex.

II.11.5. *cis*-[Ru(η^2-O_2CCH_3)(dppe)$_2$] (37)

The compound **37** was obtained during purification attempts of the ruthenium rods presented above. Its ORTEP-3[264] plot is depicted in Figure 120. The compound is *cis*-[Ru(η^2-O_2CCH_3)(dppe)$_2$] (**37**).

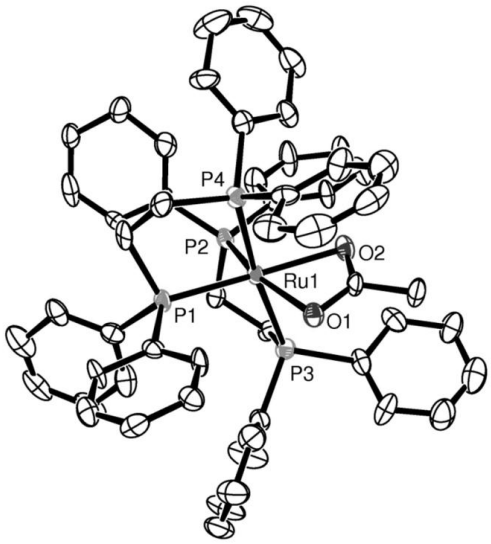

Figure 120. ORTEP-3[264] plot of *cis*-[Ru(η^2-O_2CCH_3)(dppe)$_2$][Cl] (**37**) in perspective view. H atoms, the solvent molecules and counter-ion (PF_6^-) are excluded for clarity (30% probability displacement ellipsoids).

The search in CSD for η^2 bound O_2C-R to a Ru centre yielded 18 hits. Two of them[273] are relative to a $[Ru(dppe)_2(\eta^2\text{-}O_2CCH_3)][PF_6]$ which is very similar to the obtained compound (**37**). Other reported similar structures include $[Ru(dppm)_2(\eta^2\text{-}O_2CCH_3][BH_4]$,[274] [Ru(*i*-$Pr_2PCH_2CH_2P$*i*-$Pr_2)_2(\eta^2\text{-}O_2CCH_3][O_2CCH_3]$,[275] [Ru(dppm)2($\eta^2$-$O_2CCH_3$][$PF_6$],[273a] and $[Ru(dppp)_2(\eta^2\text{-}O_2CCH_3][PF_6]$.[273a] Curiously a recurring η^2 bound CO_2 type of molecule is in fact CO_3 (η^2-O_2CO) which is reported for a number of metal centres like Co,[276] U,[277] Cu,[278] Cr,[279] Pt,[280] and also Ru.[281]

The structure of compound **37** shows similar short contacts to **34** in the sense that there are π···H interactions between phosphine phenyl rings of adjacent molecules. Furthermore, chloride atoms are observed to be part of lattice and also form short contacts with the phenyl ring's protons.

The Ru centre is separated from the acetate's oxygens by 2.202(3) and 2.191(3) Å forming an angle (O – Ru – O) of 59.2(1)º. These values are in accordance to the reported[273-275, 282] Ru – O distances of 2.173 – 2.211 Å as well as the formed angle (reported[273-275, 282] around 60 º). The phosphorus atoms all have a bond distance to the Ru of *ca.* 2.330º, being that the ones located in the *trans* position to the acetate ligand, show the shorter distances and even one of them (P2) is separated from Ru at 2.288(1)º. This difference, although not very significant is worth noting and fits perfectly in the range of 2.240 – 2.406 Å found in the literature.[273-275, 282] The shorter distances for *trans* – positioned phosphorus is also verified in the reports[273-275, 282] of similar compounds. The octahedral geometry observed for **37** is highly distorted with one of the P – Ru – P angles showing a value of 82.36(4)º. Nevertheless, this type of distortion is common for this type of complexes especially when in *cis* conformation.[233-234, 273-275, 282]

II.11.6. Palladium phenylene ethynylene rod (21b).

A crystal for compound **21b** was obtained and its structure was solved successfully. It is noteworthy that the metal's phosphine ligand as well as the chloride showed disorder only on one side of the molecule as depicted in Figure 121.

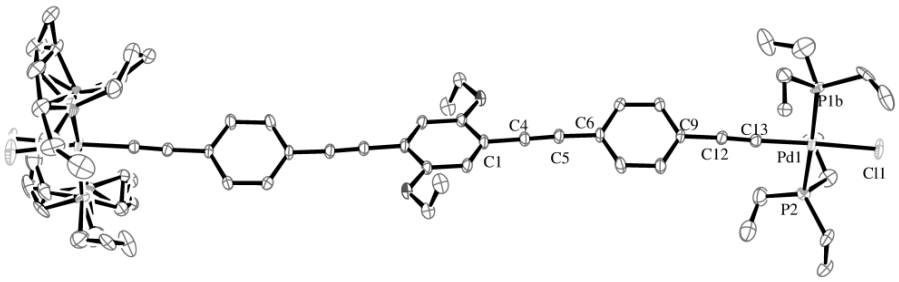

Figure 121. ORTEP-3[264] plot of *trans*-[PdCl(PEt_3)$_2$–C≡C–C_6H_4–C≡C]$_2$–C_6H_4(OC_2H_5)$_2$ (**21b**). H atoms are excluded for clarity (30% probability displacement ellipsoids). Right side of the molecules was plotted with disordered atoms.

Whilst searching the literature, only three similar structures were found[172a, 283] one of them a very recent[283] one and all of single ringed bridges. These were relative to PdCl(PR_3)$_2$ (where R = butyl, ethyl) bridged by 1,4-diethynylbenzene[172a, 283] (one of them[172a] with a single central decorated phenyl ring with OC_8H_{17} side chains). No data for a dinuclear rod bridged by a *tris*-ringed PE was found, apart from an example bearing terminal gold moiety.[269]

Curiously, the central and terminal phenyl rings do not show too much twisting between each other, with the angle formed between the corresponding planes being only 23.29 º. Nevertheless, there is an 86.56 º angle formed between the central phenyl moiety and the plane defined by Pd – P – Cl.

In regard to the bond distances, Pd – P is of 2.340(4) and 2.283(7) Å and Pd – Cl of 2.346(6) Å which are a bit longer than those of the free complex[284] 2.186(2) Å and 2.293(2) Å for Pd – P and Pd – Cl respectively. These values are in agreement with the literature reported distances of 2.306 Å for Pd – P and 2.334 Å for Pd – Cl.[172a, 283] The distance of Pd – C≡C is of 1.947(6) also close to reported values of 1.939 Å.

The triple bond lengths are of 1.184(8) for the Pd bond one and 1.200(8) Å for the internal C≡C. These are in accordance to reported[172a, 283] values (1.198 Å) and show a slightly stronger triple bond when coordinated to the Pd. Finally, the Ar – O is of 1.360(8) Å with an angle of Ar – O – CH_2 118.6(5)º are similar to the literature.[172a, 283]

Regarding the Pd centre, angles for P – Pd – Cl are of 96.5(2) º and 89.1(2) º and in the case of P – Pd – P a value of was found 171.1(2) º. Furthermore, the angle of C – Pd – Cl is 177.8(2). These values are close to the reported in the literature.[172a, 283] In comparison with the

free complex, the P – Pd – Cl are similar, but the P – Pd – P was reported[284] to be 180.00(8) º which is shows the effect of the bridging ligand on this angle.

In respect with the intermolecular interactions, it was found that two parallel molecules have both Pd centres and terminal phenyl rings interact with the other molecules phenyl and Pd centre respectively forming Pd ··· H short contacts.

There is also non-classical hydrogen bonding between the chloride and the methyls hydrogen from the ethoxy group of the adjacent. Moreover, there is π···H interaction between the hydrogens of an ethyl group of the phosphine and the inner triple bond of the adjacent molecules.

II.12. Fluorescence decay studies

Oligo(phenylene ethynylene)s as well as the thiophene counterparts are known to exhibit strong fluorescence.[267e] The ligands (bearing at least one 1,4-ethynylbenzene moiety) produced in this work all show emission by simply observing a solution of the compound under sun light. Moreover, this emission is even more accentuated under the UV light in, for example, a UV chamber (for TLC checking). As such, and taking advantage of a collaboration with Prof. Fernando Lahoz (of the La Laguna University, in Tenerife, Canary Islands, Spain), the compounds were studied for the decay of their fluorescence when the samples where excited with a pulsed laser (80 ps pulse width) at 405 nm. The results obtained for the free ligands and their respective Pd rods are shown in the Figure 122 and 123 respectively. The fluorescence decay was detected at about the maximum of the emission bands. A characteristic non-exponential decay was observed in all the cases. In order to estimate an average lifetime, the decay curves were fitted to a three exponential decay curve (Equation 6).

$$I(t) = B_1 \cdot e^{(-t/\tau_1)} + B_2 \cdot e^{(-t/\tau_2)} + B_3 \cdot e^{(-t/\tau_3)} \qquad \textbf{(6)}$$

The fitting was made using IRF ((Instrumental Response Function) deconvolution analysis with F900 software by Edinburgh Instruments. The average lifetime is then calculated as[285]:

$$\tau_{av} = \frac{B_1\tau_1^2 + B_2\tau_2^2 + B_3\tau_3^2}{B_1\tau_1 + B_2\tau_2 + B_3\tau_3} \qquad \textbf{(7)}$$

The results for the free ligands and for the Pd complexes are given in Table 11. Since the ruthenium complexes (**23c-d**, **24a-b**) proved to be a lot less fluorescent than the free ligands (**5a-d**, **10a-b**) and the Pd rods (**20a-d**, **21a-b**), decay experiments were not possible. Also and since the emission intensity tests cannot be directly compared, these are available in the Annex.

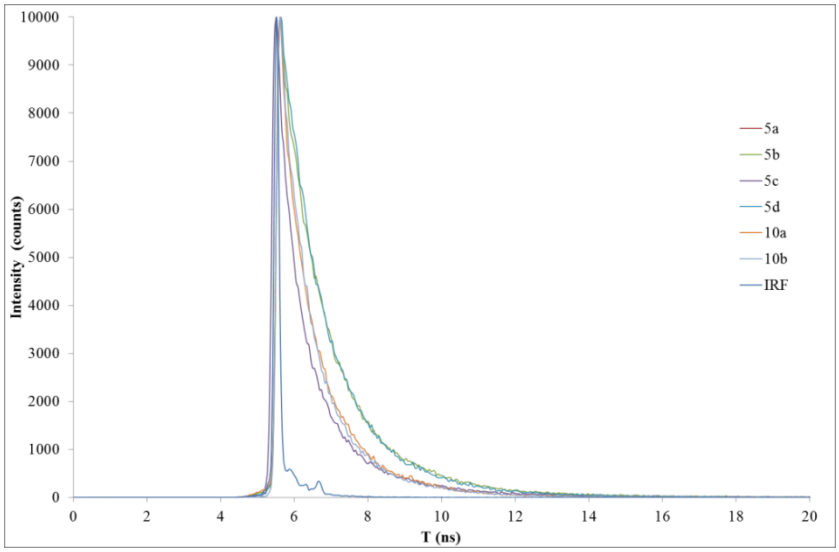

Figure 122. Decay of the fluorescence of the free ligands (**5a-d**, **10a-b**) and IRF.

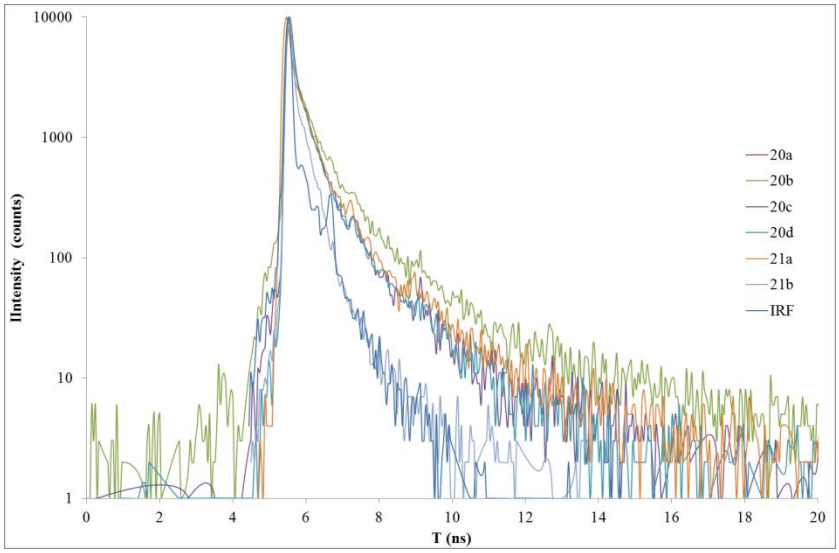

Figure 123. Decay of the fluorescence for the Pd rods (**20a-d**, **21a-b**) and IRF.

Table 11: Solid state fluorescence time-of-life values for the prepared free ligands (**5a-d**, **10a-b**) and Pd rods (**20a-d**, **21a-b**).

	Free ligands			Pd Complexes	
	λ/nm	**τ/ns**		**λ/nm**	**τ/ns**
5a	510	0.80	**20a**	454	0.24
5b	510	1.00	**20b**	510	0.60
5c	510	0.70	**20c**	510	0.30
5d	510	0.90	**20d**	510	0.30
10a	510	1.20	**21a**	450	0.05
10b	490	0.95	**21b**	510	0.40

When comparing the values in Table 11, higher life time values are found for the longer ligands (**10a-b**). Furthermore, and a trend observed for all the complexes that were analysed (**20a-d**, **21a-b**, **23c-d** and **24a-b**), there was a marked decrease in both the emission and the respective fluorescence time-of-life values when coordinating the ligands to the Pd (**20a-d**, **21a-b**) and Ru (**23c-d**, **24a-b**, fluorescence itensity values available in the Annex) centres. This could be accounted by the charge distribution (from ligand to metal centre) reducing available electronic density that would induce a non-radiative relaxation path, which would decrease the lifetime and radiative emission quantum yield.

The free ligands (**5a-d**, **10a-b**) show average lifetime values comparable to those found in the literature for the new hybrid composites composed of poly(2-methoxy-5-(2'-ethylhexyloxy)-1,4-phenylenevinylene (MEH-PPV) and clay (montmorillonite) and purposely prepared for use in optoelectronic devices (like OLEDs).[286] These nanocomposites show increased lifetimes when the concentration is higher, but values are still on the *pico* second scale. Moreover, lasing capabilities were reported[287] for *p*-(phenylene ethynylene) polymers, but in solution phase. Nevertheless in the case of small compounds, similar to these reported here, the reported[268] lifetimes values of chloroform solutions of phenylene ethynylenes bearing three rings, values of 2 ns were obtained. Furthermore, this report[268] also shows similar lifetime values for the fluorescence when comparing a tris phenylene ethynylene with its twisted (by a secondary chain) counterpart, even though significantly lower (21 fold) quantum yield was found for the twisted compound. The authors[268] do not account for this discrepancy and attribute it to the equipment's fast decay.

Chapter III – Conclusions and Future Perspectives

This work's main goal is to prepare molecular wire candidates that would then be probed for electron transfer properties. These wires were prepared using 1,4-diethynylbenzene derivatives with alkoxy side chains as bridges between homometallic metal centres of ruthenium and palladium moieties. Characterization of these compounds was performed by traditional spectroscopic techniques like ^{1}H, ^{13}C and ^{31}P NMR, MS, FTIR and UV-Vis as well as by cyclic voltammetry which allowed classifying the candidates in the Robin–Day system and determination of bridges side chain and length effects on electronic transport.

Most of the work performed in this thesis is undoubtedly related to the preparation of the **bridging ligands** and respective starting materials which entailed several cross-coupling steps. This was especially true when preparing the tris ringed ligands (**10a-b**). Palladium catalyzed cross-coupling (Sonogashira) was thus a recurring synthetic tool. Nevertheless a family of single ringed 1,4-diethynylbenzene ligands with different length alkoxy side chains (OCH_3, OC_2H_5, OC_7H_{15}) were prepared allowing for the influence of these ring decorations to be assessed. The mentioned longer ligands, tris ringed 1,4-diethynylbenzene derivatives with side chains were also helpful in probing length dependency of the electron transport properties. These studies were also performed for the ruthenium and palladium rods.

Some difficulties were encountered whilst preparing the **ruthenium binuclear rods** by the methods detailed in the numerous reports that can be found in the literature (from Bruce's pioneer work, to the immense knowledge amassed by Dixneuf's group and finally the latest developments regarding non-innocent alkynyl ligands reported by Touchard and Lavastre). As such the details regarding this synthetical method had to be further explored before satisfactory ruthenium rods were obtained.

The ruthenium binuclear rods showed communication between metal centres only when the shorter ligands were used (**22a**, **23c-d**) confirming the reports by other groups that were produced before and during this work. The longer Ru complexes (**24a-b**) show only one redox pair in CV studies which is in agreement to non-communicating metal centres. Nevertheless the effect of increased conjugation brought about the longer ligands in the latter complexes is observed in the UV-Vis spectra where a red shift of MLCT is observed.

The same typical red shift in the MLCT bands was also observed for the **Pd binuclear rods** leading to a first impression of delocalization through the complexes backbone. Nevertheless, cyclic voltammetry studies show irreversible one wave processes for these complexes (**20a-d**, **21a-b**). The Pd rods are thus molecular insulators.

The fluorescence studies performed on the rods and ligands, namely **time-of-life/decay studies** show a pattern of decreasing decay times upon coordination to the metal centres as it was observed when going from free ligands to Pd rods or even lower values for the Ru rods which can due to ligand charge redistribution upon coordination leading to non-radiative relaxation paths.

Regarding the structures obtained by **single crystal X-ray diffraction**, two new ligand related structures were obtained (**8b** and **10a**). These show significantly different torsion angles (9.64 to 83.94 º respectively) between the central phenyl rings and the terminal ones. It is, nevertheless, hard to attribute this torsion to intermolecular interactions in the crystal lattice, but this would point to significant changes in the packing structures of these compounds when only two terminal groups were changed (Br to $SiMe_3$ and OCH_3 to OCH_2CH_3). Furthermore the structure regarding, a Pd rod (**21a**), also shows some twisting (23.29 º), but not as large as in **10a**.

Finally and in respect to an important study point of this work, the effect of the **side chains**, usually only associated to solubility effects was found to be important in regard to wires electronic properties with oxidation potential values dropping when side chains were involved. The effect brought by longer chains is nevertheless almost negligible.

As **future perspectives**, the ruthenium rods discussed above should be capped with molecular alligator clips in order to study SAM properties. This would allow for further electronic characterization and some other transport mechanisms might arise in the longer rods. This could also be true for the Pd rods with a probability of tunnelling phenomena in STM experiments. Extra characterization could also be achieved by performing near infrared spectroscopy studies on the mono oxidized complexes allowing for the study of the ligands role on the process.

Regarding the general application of these rods as wires, the advantages of an organometallic approach is thus obvious in relation to a purely organic solution as the metal moieties make oxidation states easier to reach and maintain which would also be the in heteronuclear binuclear rods. These rods have the disadvantage of being length dependent which could the starting point for a new study using alternating molecular motifs of different electron donating properties.

Chapter IV – Experimental Details and Characterization

IV.1. General remarks

With the exception the Williamson substitution all reactions were carried out in dry nitrogen or dry argon (in the case of the Ru rods **23a**,**c-d** and **24a-b**) atmosphere. Special care was taken in the coupling reactions (Sonogashira and Stille) as well as in the coordination reactions (preparation of the ruthenium and palladium rods) by using standard Schlenk techniques.

Glassware was generally pre-washed with KOH/Ethanol bath prior to the normal soap and water washing. It was thoroughly rinsed with washing grade acetone (98%) and blow dried before introduced into the oven. The reaction vessels were oven-dried for a minimum of 2 h (normally overnight) at 120 ºC. They were then cooled to room temperature under vacuum (oil pump) and at least 3 purge cycles (nitrogen/vacuum) were performed.

Solvents were freshly distilled under nitrogen. Triethylamine (NEt_3) and diethylamine ($NHEt_2$) were distilled over potassium hydroxide; *n*-hexane and dichloromethane (CH_2Cl_2) over calcium hydride; tetrahydrofuran (THF), diethyl ether (Et_2O) and toluene over sodium/benzophenone ketyl. Dimethyl sulfoxide (DMSO) and glacial acetic acid (AcOH) were used as received and degassed under nitrogen (with stirring or sonication). Methanol (MeOH) was degassed under argon (with sonication). Solvents used in column chromatography were used as received and re-used when collected from the rotary evaporator.

KOH (used in the Williamson substitution) was grinded using a mortar as well as the NaOH used in the 2-methyl-3-butyn-2-ol deprotection.

The reagents 2-methyl-3-butyn-2-ol, the alkyl bromides (ethyl and heptyl bromide), ammonium chloride (NH_4Cl), ammonium hexafluorophosphate (NH_4PF_6), barium hydroxide ($Ba(OH)_2.8H_2O$), bromine (Br_2), caesium fluoride (CsF), copper chloride (CuCl), copper iodide (CuI), ethanol (EtOH), hydroquinone, iodine (I_2), magnesium and sodium sulphate ($MgSO_4$ and Na_2SO_4), potassium carbonate (K_2CO_3), potassium hydroxide (KOH), potassium fluoride (KF), potassium iodate (KIO_3), potassium *tert*-butoxide (*t*-BuOK), sodium thiosulfate ($Na_2S_2O_3$), sulphuric acid (H_2SO_4), *tert*-butyl lithium (*t*-BuLi), thallium sulphate ($TlSO_4$), trismethylsilylacetylene (TMSA), trimethyltin chloride ($SnCl(CH_3)_3$). Alumina (neutral), celite and silica gel (neutral) were used as received. palladium catalysts ($[PdCl_2(PPh_3)_2]$, $[Pd(PPh_3)_4]$) and the palladium starting material $[PdCl_2(PEt_3)_2]$ were also used as received taking special care

in controlling their color (both should be yellow[192]) and their storage (argon flushing and 0 ºC in the case of $[Pd(PPh_3)_4]$).

The ruthenium moiety *cis*-$[RuCl_2(dppe)_2]$, and its activated 16 electron product $[RuCl(dppe)_2][PF_6]$ were prepared by the author using optimized procedures established in the working laboratory (detailed in the Annexes). *trans*-$[RuCl_2(dppe)_2]$ (used for UV-Vis spectra comparison) was also prepared in this laboratory.

CuI and CuCl were pre-dried at 120ºC for at least 2h (usually overnight) before usage.

All measurements were performed at room temperature (25 ºC) unless otherwise noted.

IV.2. Preparation and characterization of the 1,4-diethynylbenzene and the 2,5-thiophene derivatives

The free ligands were prepared according to the discussed synthetic pathways described in Chapter II. The intermediary compounds – **3b-d**, **4a-d**, **6a-b**, **7a-b**, **8a-b**, **9a-b** – will not be detailed but were prepared in accordance to the methods described in Chapter II and controlled *via* ^1H and ^{13}C NMR. Target ligands are detailed next with each compound's ^1H NMR spectrum. The FTIR and UV-Vis spectra as well as the cyclic voltammograms are collected after each group of compounds. ^{13}C NMR and MS spectra are annexed.

IV.2.1. 1,4-diethynylbenzene, 5a

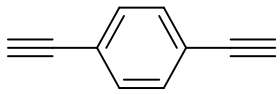

5a

1,4-bis((trimethylsilyl)ethynyl)benzene (**4a**, 200 mg, 0.73 mmol) was dissolved in CH_2Cl_2/MeOH (40 mL, 1:1) and K_2CO_3 (613 mg, 4.43 mmol) was added in one portion. The reaction mixture was stirred for 2 h at room temperature and then filtrated through a celite/silica plug. The resulting solution was evaporated under low pressure resulting in a white powder (71 mg, 77.2 %). This compound was reported by Dixneuf and co-workers.[288]

^{1}H NMR ($CDCl_3$): δ 3.14 (*s*, 2H, C≡C-*H*), 7.56 (*d*, 4H, Ar-*H*, $J_{H,H}$ =8.168 Hz) ppm;

$^{13}C\{^1H\}$ NMR ($CDCl_3$): δ 83.4, 121.5, 126.9, 132.7, 140.6 ppm;

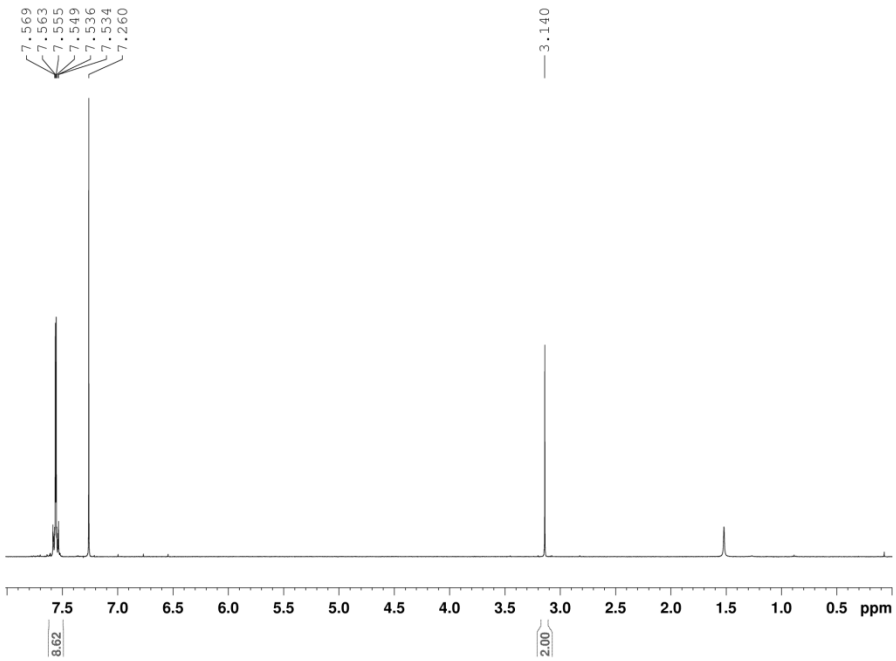

Figure 124. ^{1}H NMR ($CDCl_3$, 400 MHz) spectrum of **5a**.

IV.2.2. 1,4-dimethoxy-2,5-diethynylbenzene, 5b

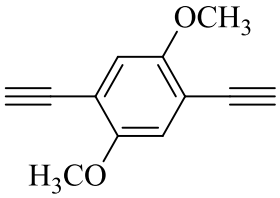

5b

1,4-bis((trimethylsilyl)ethynyl)-2,5-dimethoxybenzene (**4b**, 437 mg, 1.32 mmol) was dissolved in CH_2Cl_2/MeOH (50 mL, 1:1) and K_2CO_3 (456 mg, 3.30 mmol) was added in one portion. The reaction mixture was stirred for 2 h at room temperature and then filtrated through a celite/silica plug. The resulting solution was evaporated under low pressure resulting in a white powder (199 mg, 81.2 %). This compound was reported by Dirk *et al.*.[209]

^{1}H NMR ($CDCl_3$): δ 3.40 (*s*, 2H, C≡C-*H*), 3.87 (*s*, 6H, OCH_3), 6.98 (*s*, 2H, Ar-*H*) ppm;
^{13}C{^{1}H} NMR ($CDCl_3$): δ 56.4, 79.6, 82.7, 116.2, 113.0, 130.6, 132.2, 154.4 ppm;
FTIR: $\tilde{\nu}$ = 3257 (s, $\nu_{C\equiv C-H}$), 2106 (vw, $\nu_{C\equiv C}$), 655 (s, $\delta_{C\equiv C-H}$), 1495 (m), 1464 (m), 1455 (m), 1445 (m), (ar. $\nu_{C=C}$) cm^{-1};

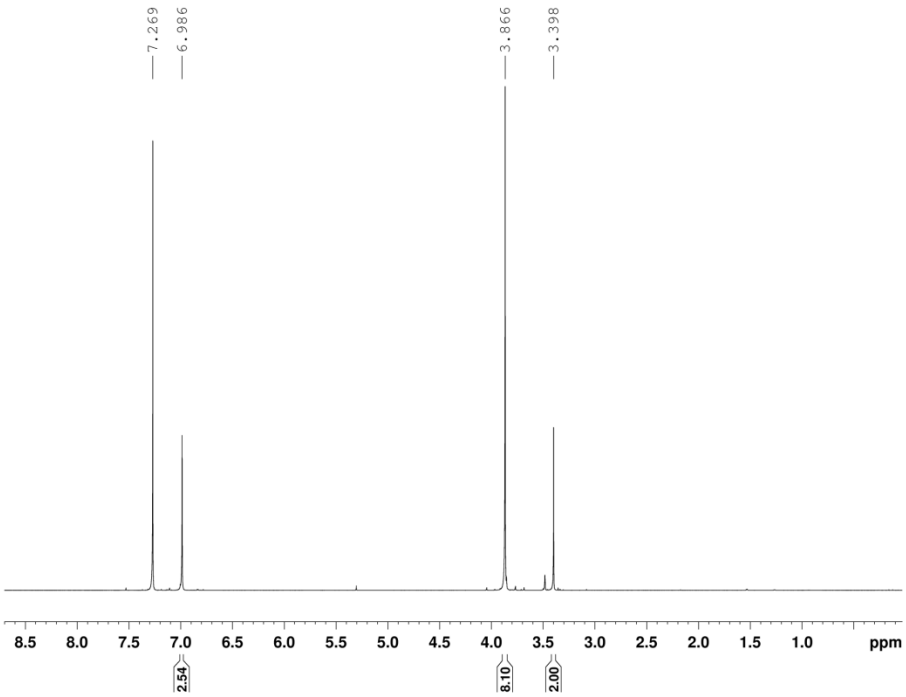

Figure 125. ^{1}H NMR ($CDCl_3$, 400 MHz) spectrum of **5b**.

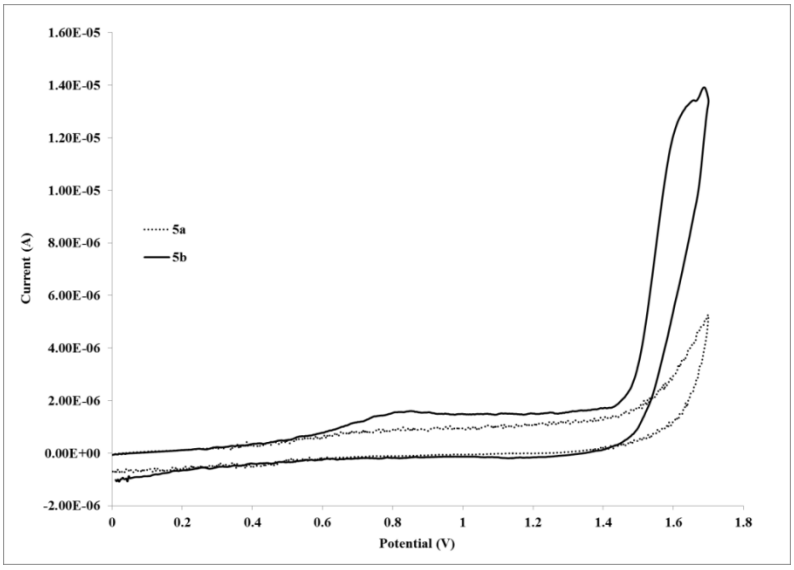

Figure 126. Cyclic voltammograms for the single ringed PE free ligands **5a-b**.

IV.2.3. 1,4-diethoxy-2,5-diethynylbenzene, 5c

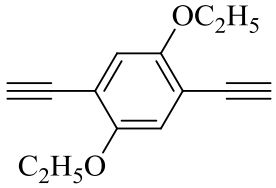

5c

1,4-bis((trimethylsilyl)ethynyl)-2,5-diethoxybenzene (**4c**, 1.91 g, 5.30 mmol) was dissolved in CH_2Cl_2/MeOH (70 mL, 7:3) and K_2CO_3 (1.61 g, 11.60 mmol) was added in one portion. The reaction mixture was stirred for 2 h at room temperature and then filtrated through a celite/silica plug. The resulting solution was evaporated under low pressure resulting in a white powder (1,13 g, 73.8 %). This compound was reported by the author in ref. [210].

^{1}H NMR ($CDCl_3$): δ 1.43 (*t*, 6*H*, CH_3, J_{HH} = 14 Hz), 3.40 (*s*, 2*H*, C≡C-*H*), 4.07 (*q*, 4*H*, CH_2, J_{HH} = 14 Hz), 6.89 (*s*, 2*H*, Ar) ppm;

^{13}C{^{1}H} NMR ($CDCl_3$): δ 14.6, 65.2, 79.8, 82.4, 113.4, 117.9, 153.8 ppm;

TOF-MS (ESI+): *m/z* = 158 $[M-(C_2H_5)_2 + H_2]^+$, 214 $[M]^+$;

FTIR: $\tilde{\nu}$ = 3265(*s*), 2927 (*s*), 2932 (*s*), 2866 (*s*), 2105 (w), 1497 (*s*), 1275 (*m*);

Melting point = 74–75 °C.

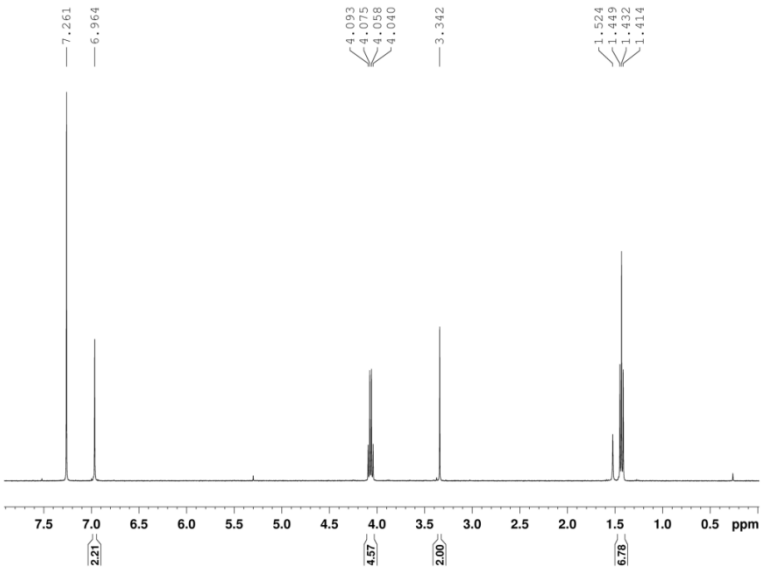

Figure 127. ^{1}H NMR ($CDCl_3$, 400 MHz) spectrum of **5c**.

IV.2.4. 1,4-diheptoxy-2,5-diethynylbenzene, 5d

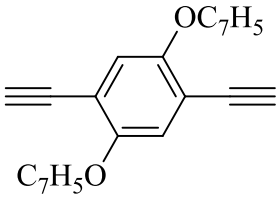

5d

4,4'-(2,5-bis(heptyloxy)-1,4-phenylene)bis(2-methylbut-3-yn-2-ol) (**7d**, 499 mg, 1.06 mmol) was refluxed in toluene (300 mL) with high excess of NaOH (~ 15 g, 375 mmol) for four hours. After this, the still hot solution was filtered and concentrated under vacuum. The resulting solution was evaporated under low pressure resulting in a white powder (495 mg, 99 %). This compound was reported by the author in ref. [210].

^{1}H NMR ($CDCl_3$): δ 0.89 (*d*, 3*H*, CH_3, J_{HH} = 9), 1.47–1.26 (16*H*, $(CH_2)_4$), 1.76 (*quint*, 4*H*, CH_2, J_{HH} = 27 Hz), 3.32 (*s*, 2*H*, C≡C-*H*), 3.97 (*t*, 4*H*, CH_2, J_{HH} = 27 Hz), 6.95 (2*H*, *s*, Ar) ppm;
^{13}C{^{1}H} NMR ($CDCl_3$): δ 13.9, 22.4, 25.7, 28.9, 28.9, 31.6, 69.5, 79.7, 82.2, 113.2, 117.6, 153.9 ppm;
TOF-MS (ESI+): *m/z* = 158 $[M-(C_2H_5)_2 + H_2]^+$, 354 $[M]^+$;
FTIR: $\tilde{\nu}$ = 3262 (s, $\nu_{C\equiv C-H}$), 1500 (m), 1469 (m), 1387 (m) (ar. $\nu_{C=C}$), 661 (s, $\delta_{C\equiv C-H}$)
Melting point = 73–74 °C.

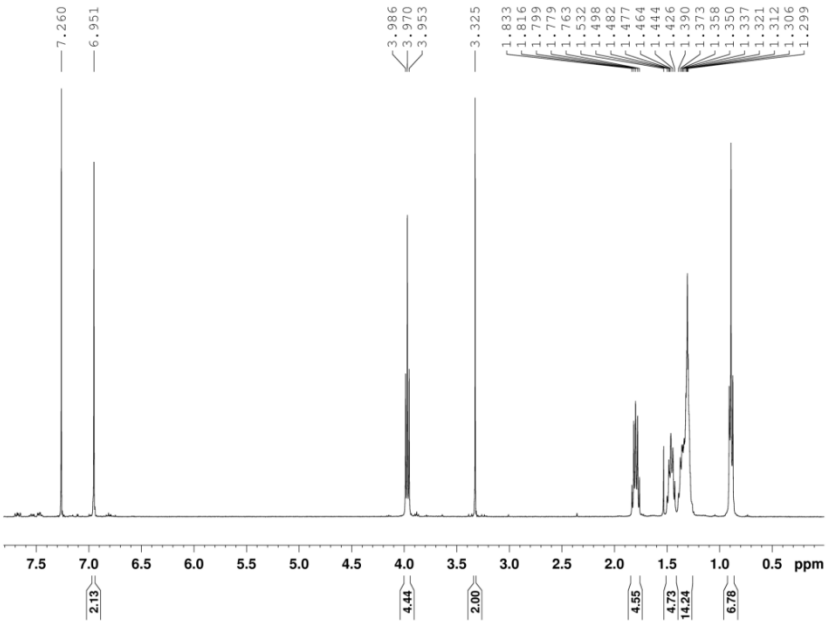

Figure 128. ^{1}H NMR ($CDCl_3$, 400 MHz) spectrum of **5d**.

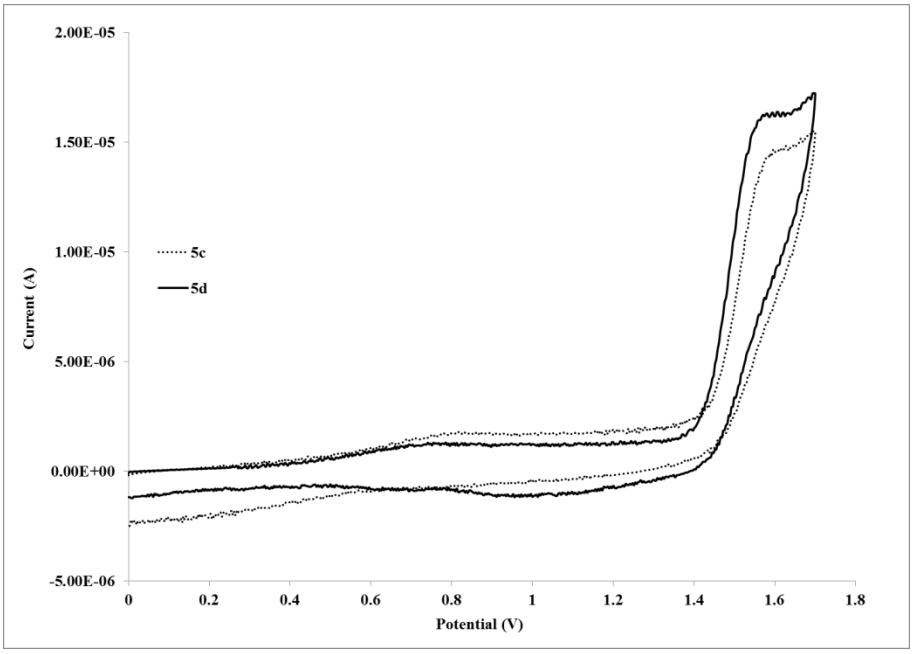

Figure 129. Cyclic voltammograms for the single ringed PE free ligands **5c-d**.

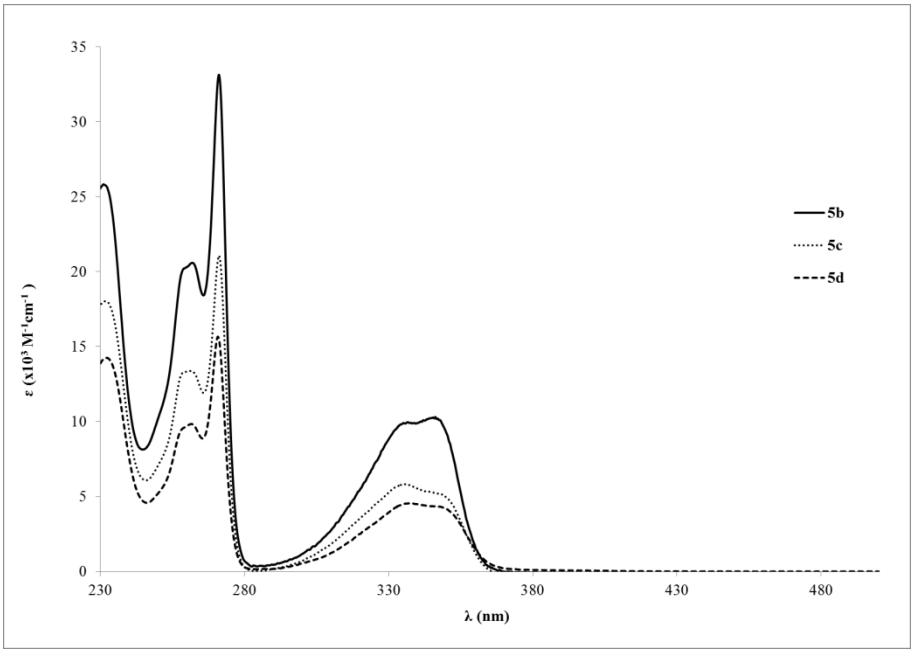

Figure 130. UV-Vis spectra of the mono ringed PE ligands (**5b-d**) bearing side chains in CH_2Cl_2 at *ca.* $1x10^{-5}$ M.

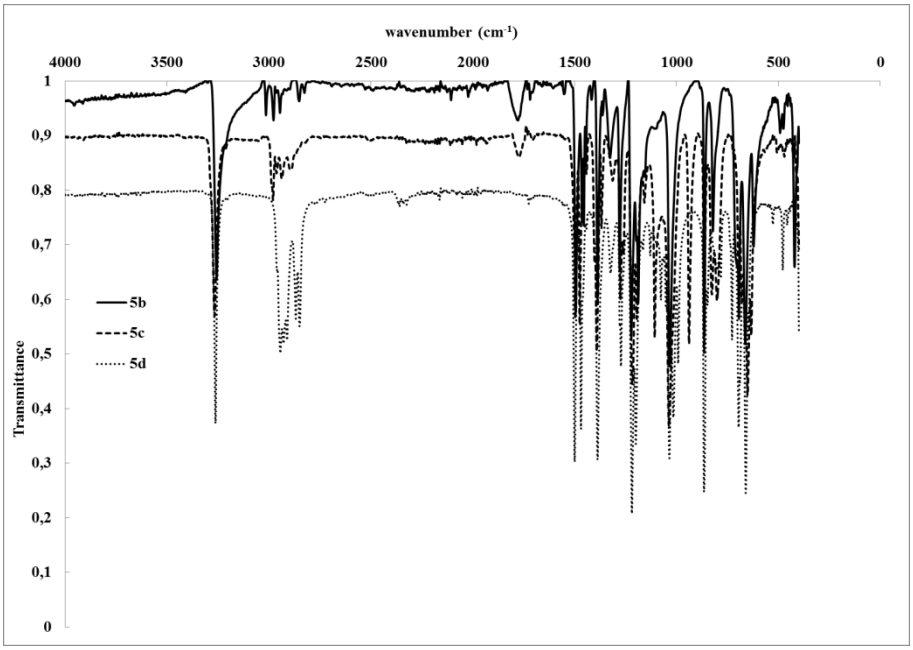

Figure 131. FTIR spectra for the single ringed PE ligands (**5b-d**).

IV.2.5. 1,4-dimethoxy-2,5-bis((4-ethynylphenyl)ethynyl)benzene, 10a

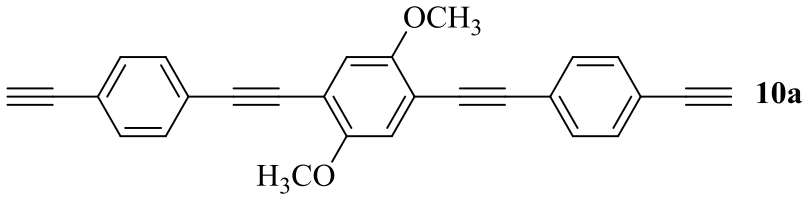

10a

1,4-dimethoxy-2,5-bis((4-trimethylsilylethynylphenyl)ethynyl)benzene (**9a**, 350 mg, 0.65 mmol) was dissolved in CH_2Cl_2/MeOH (60 mL, 1:1) and K_2CO_3 (211 mg, 1.52 mmol) was added in one portion. The reaction mixture was stirred for 16 h at room temperature and then filtrated. The resulting solution was evaporated under low pressure and purified by column chromatography (neutral alumina, petroleum ether (40-60) and 5% diethyl ether). Compound **10a** was obtained as a yellow powder (200 mg, 78.5 %).

^{1}H NMR ($CDCl_3$): δ 3.18 (*s*, 2H, C≡C-*H*), 3.91 (*s*, 6H, OCH_3), 7.03 (*s*, Ar-*H*, centre ring) 7.47 (*d*, 4H, Ar-*H* outer ring, $J_{H,H}$= 8.20 Hz), 7.52 (*d*, 4H, Ar-*H* outer ring, $J_{H,H}$ =8.28 Hz) ppm;

$^{13}C\{^{1}H\}$ NMR ($CDCl_3$): δ 56.9 (*s*, O*C*H_3), 79.3, 83.7, 88.0, 94.9 (*s*, C≡C, internal and external), 113.8, 116.0, 122.4, 124.1, 131.9, 132.4 (*s*, Ar. Inner and outer rings), 154.4 (*s*, Ar. *C*–O–CH_3) ppm;

TOF-MS (ESI+): 409.12 $[M+Na]^+$, 441.13 $[M+Na+CH_3OH]^+$, 493.13 $[M+K+Cl+CH_3OH+H]^+$, 795.23 $[2M+Na]^+$;

FTIR: $\tilde{\nu}$ = 3271 (m, $\nu_{C\equiv C-H}$), 2102 (vw, $\nu_{C\equiv C}$), 655 (s, $\delta_{C\equiv C-H}$), 1510 (w), 1500 (w), 1492 (w), 1461 (w), 1936 (m) (ar. $\nu_{C=C}$) cm^{-1};

Melting point = 212-215 ºC;

EA: $C_{28}H_{18}O_2 \cdot 1.9\ CH_3OH \cdot 1.4\ CH_2Cl_2$ (573.21): calcd. C 66.39, H 5.06; found C 66.5, H 5.17;

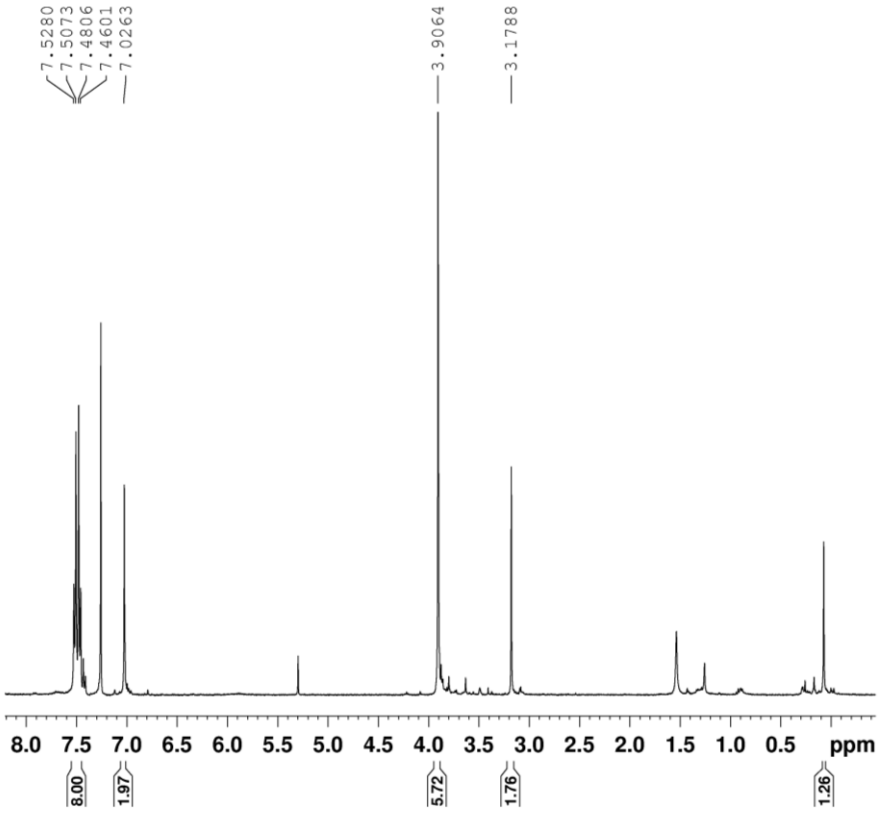

Figure 132. ^{1}H NMR ($CDCl_3$, 400 MHz) spectrum of **10a**.

IV.2.6. 1,4-diethoxy-2,5-bis((4-ethynylphenyl)ethynyl)benzene, 10b

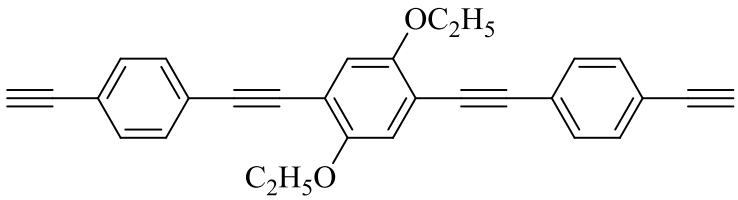

10b

1,4-dimethoxy-2,5-bis((4-trimethylsilylethynylphenyl)ethynyl)benzene (**9b**, 25 mg, 0.44 mmol) was dissolved in CH_2Cl_2/MeOH (50 mL, 1:1) and K_2CO_3 (15 mg, 0.10 mmol) was added in one portion. The reaction mixture was stirred for 16 h at room temperature and then filtrated. The resulting solution was evaporated under low pressure and purified by column chromatography (neutral alumina, petroleum ether (40-60) and 5% diethyl ether). Compound **10b** was obtained as a yellow powder (14 mg, 75.5 %).

^{1}H NMR ($CDCl_3$): δ 1.48 (t, 6H, OC*H*$_3$, $J_{H,H}$ =6.97 Hz), 3.17 (s, 2H, C≡C-*H*), 4.11 (s, 6H, OC*H*$_2$), 7.01 (s, 2H, Ar-*H*, centre ring), 7.47 (d, 4H, Ar-*H* outer ring, $J_{H,H}$ =8.56 Hz), 7.49 (d, 4H, Ar-*H* outer ring, $J_{H,H}$ =8.60 Hz) ppm;

^{13}C{^{1}H} NMR ($CDCl_3$): δ 15.1 (s, OCH_2CH_3), 65.5 (s, OCH_2CH_3), 79.1, 83.5, 88.1, 94.6 (s, C≡C, internal and external) 117.4, 122.1, 124.1, 131.6, 132.2 (s, Ar. Inner and outer rings), 153.7 (s, Ar. *C*–O–CH_2CH_3) ppm;

TOF-MS (ESI+): *m/z* = 437.203 $[M+Na]^+$, 469.217 $[M+Na+CH_3OH]^+$, 851.374 $[2M+Na]^+$;

FTIR: $\tilde{\nu}$ = 3275 (m, $\nu_{C\equiv C-H}$), 2105 (vw, $\nu_{C\equiv C}$), 661 (s, $\delta_{C\equiv C-H}$), 1516 (m), 1499 (w), 1490 (w), 1474 (w), 1417 (m), 1403 1392 (m) (ar. $\nu_{C=C}$) cm^{-1};

Melting point = 212-215 ºC;

EA: $C_{30}H_{22}O_2$ (414.5): calcd. C 86.9, H 5.35; found C 85.2, H 5.56.

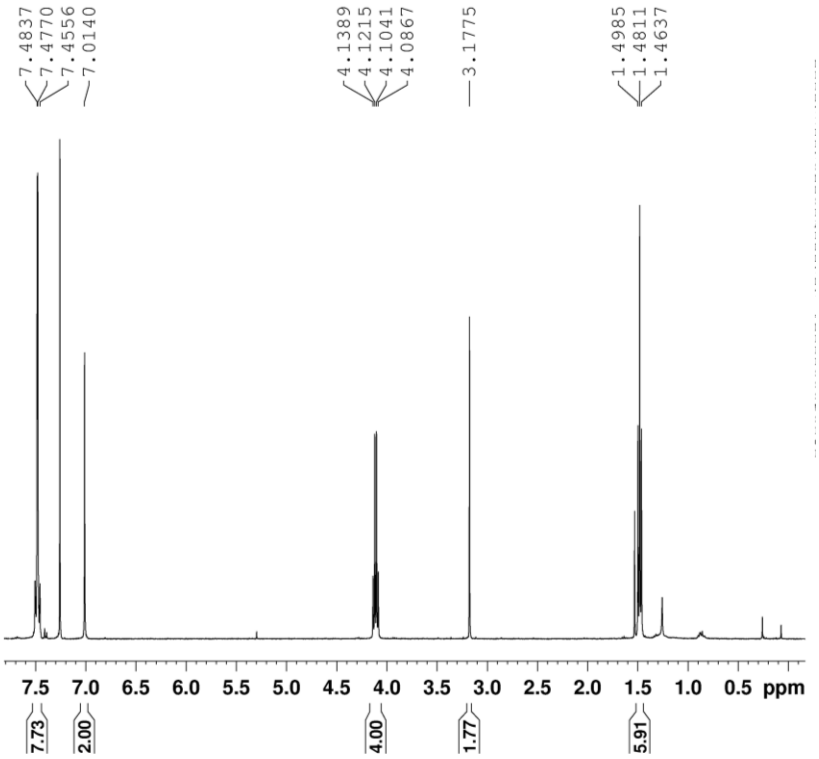

Figure 133. ^{1}H NMR ($CDCl_3$, 400MHz) spectrum of **10b**.

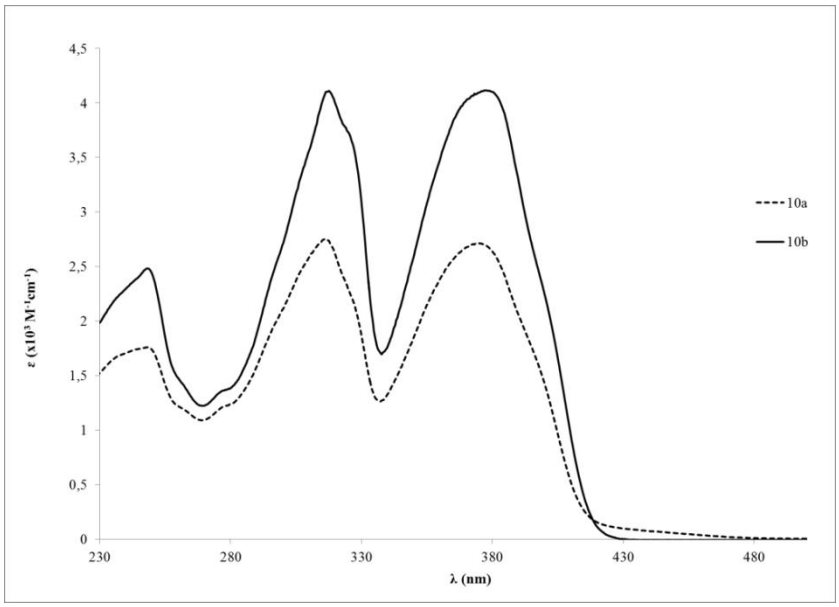

Figure 134. UV-Vis spectra of the *tris* ringed PE ligands (**10a-b**) bearing side chains in CH_2Cl_2 at *ca.* $1x10^{-5}$ M.

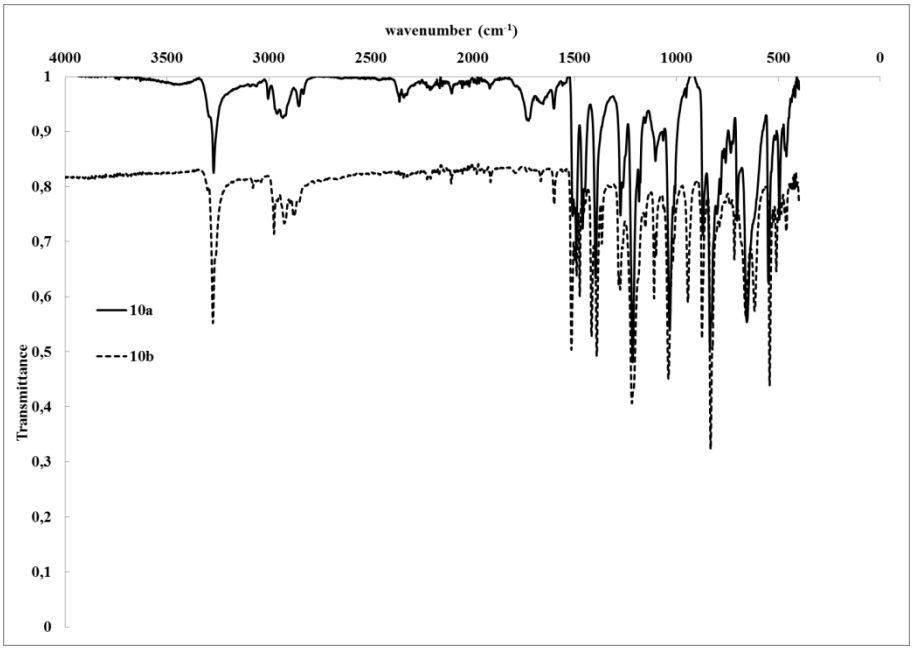

Figure 135. FTIR spectra for the tris ringed PE ligands (**10a-b**).

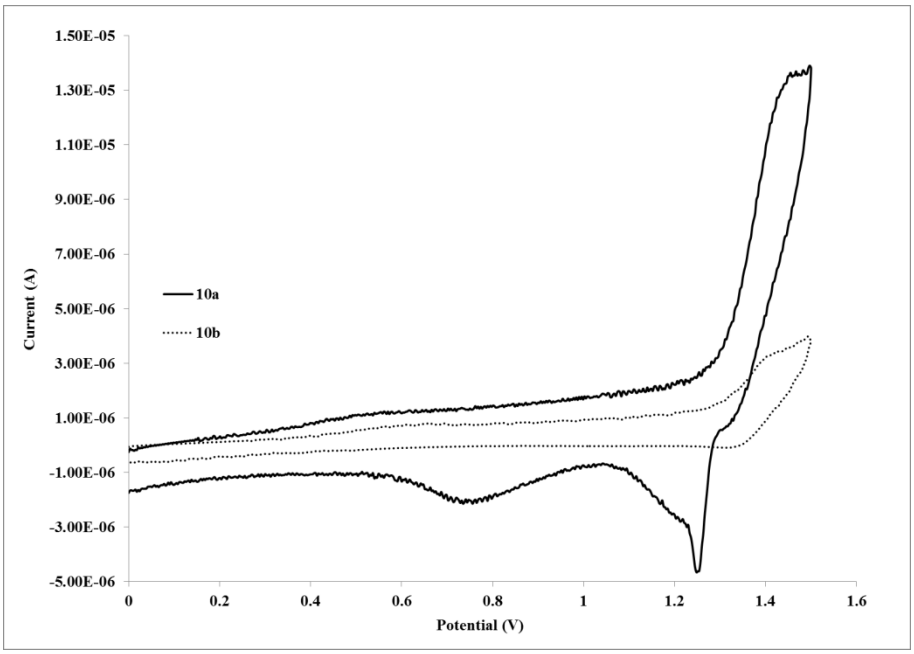

Figure 136. Cyclic voltammograms for the tris ringed PE free ligands (**10a-b)**.

IV.2.7. 2,5-bis(4-ethynylphenyl)thiophene, 14b

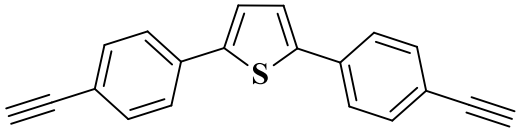

14b

2,5-bis(4-((trimethylsilyl)ethynyl)phenyl)thiophene (**14a**, 70 mg, 0.16 mmol) was dissolved in CH_2Cl_2/MeOH (20 mL, 1:1) and K_2CO_3 (56 mg, 0.41 mmol) was added in one portion. The reaction mixture was stirred overnight at room temperature and then filtrated through a celite/silica plug. The resulting solution was evaporated under low pressure resulting in a yellow powder (40 mg, 86%).

^{1}H NMR ($CDCl_3$): δ 3.19 (s, 2H, C≡C-*H*), 7.17 (s, 2H, thiophene), 7.47 (s, 8H, Ar.) ppm;
^{13}C{^{1}H} NMR ($CDCl_3$): 78.2, 83.4, 121.2, 124.8, 125.4, 127.1, 132.1, 132.7, 143.4 ppm;
FTIR: $\tilde{\nu}$ = 3292 (m, $\nu_{C\equiv C-H}$), 666 (m, $\delta_{C\equiv C-H}$), 1488 (w), 1449 (w), 1406 (w), (ar. $\nu_{C=C}$) cm^{-1};
Melting point = 184-187 ºC.

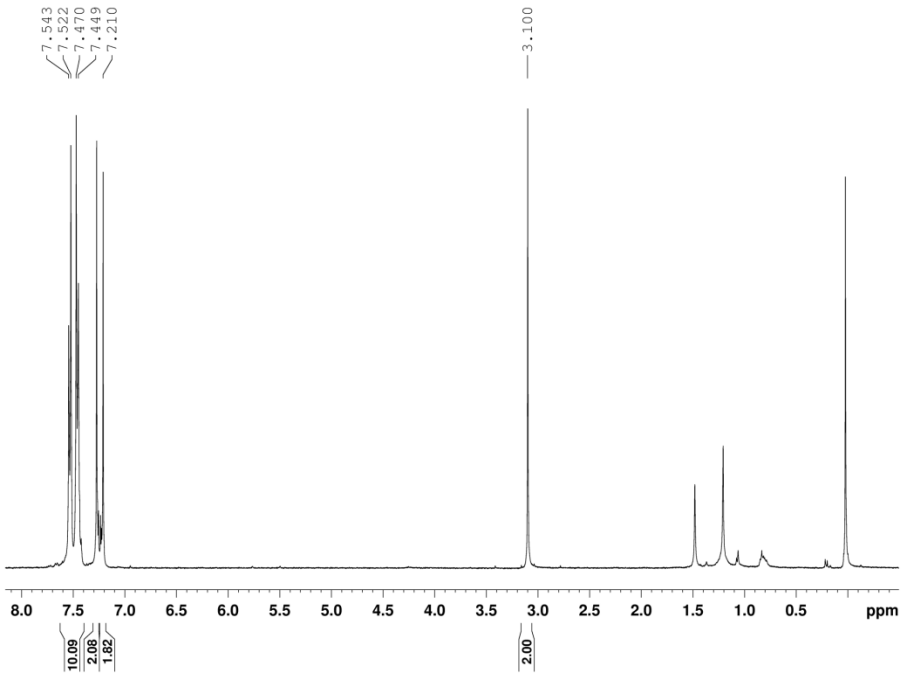

Figure 137. ^{1}H NMR ($CDCl_3$, 400 MHz) spectrum of **14b**.

IV.2.8. 2,5-bis((4-ethynylphenyl)ethynyl)thiophene, 18b

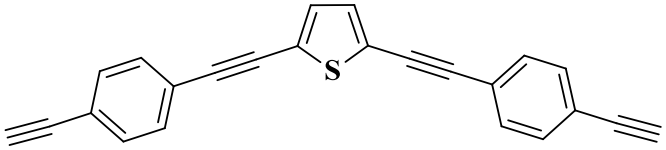

18b

2,5-bis((4-trimethylsilylethynylphenyl)ethynyl)thiophene (**18a**, 90 mg, 0.18 mmol) was dissolved in CH_2Cl_2/MeOH (50 mL, 1:1) and K_2CO_3 (100 mg, 0.72 mmol) was added in one portion. The reaction mixture was stirred overnight at room temperature and then filtrated through a celite/silica plug. The resulting solution was evaporated under low pressure resulting in a yellow powder (100 mg, 0.72 mmol).

^{1}H NMR ($CDCl_3$): δ 3.19 (s, 2H, C≡C-*H*), 7.17 (s, 2H, Ar-*H* thiop), 7.47 (s, 8H, Ar-*H*) ppm;
^{13}C{^{1}H} NMR ($CDCl_3$): δ 79.3, 83.2, 84.2, 93.8, 122.4, 122.9, 124.7, 131.3, 132.1, 132.2, 132.9 ppm;
FTIR: $\tilde{\nu}$ = 3284 (s, $\nu_{C\equiv C-H}$), 644 (s, $\delta_{C\equiv C-H}$), 2201 (w, br), 2106 (w) ($\nu_{C\equiv C}$), 1525 (w), 1484 (w), (ar. $\nu_{C=C}$) cm^{-1};
Melting point = 135-137 ºC.

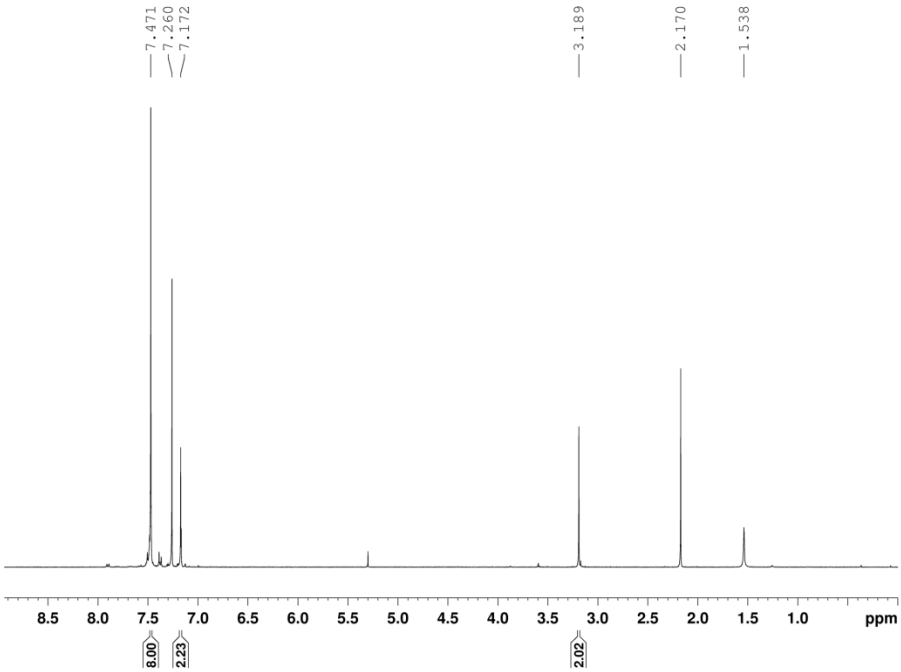

Figure 138. ^{1}H NMR ($CDCl_3$, 400 MHz) spectrum of **18b**.

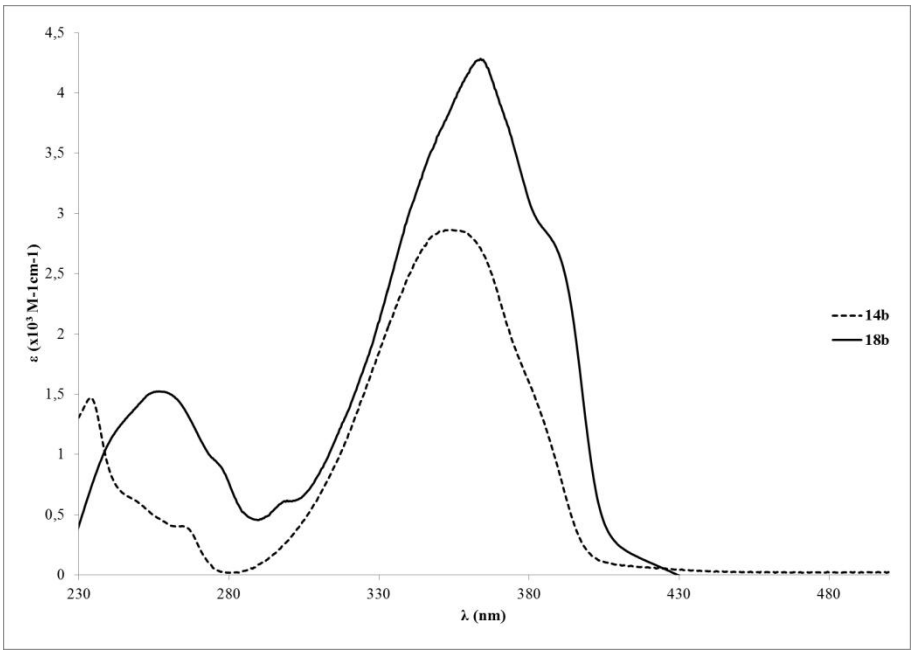

Figure 139. UV-Vis spectra of the thiophene based ligands (**14b**, **18b**) in CH_2Cl_2 at *ca.* $1x10^{-5}$ M.

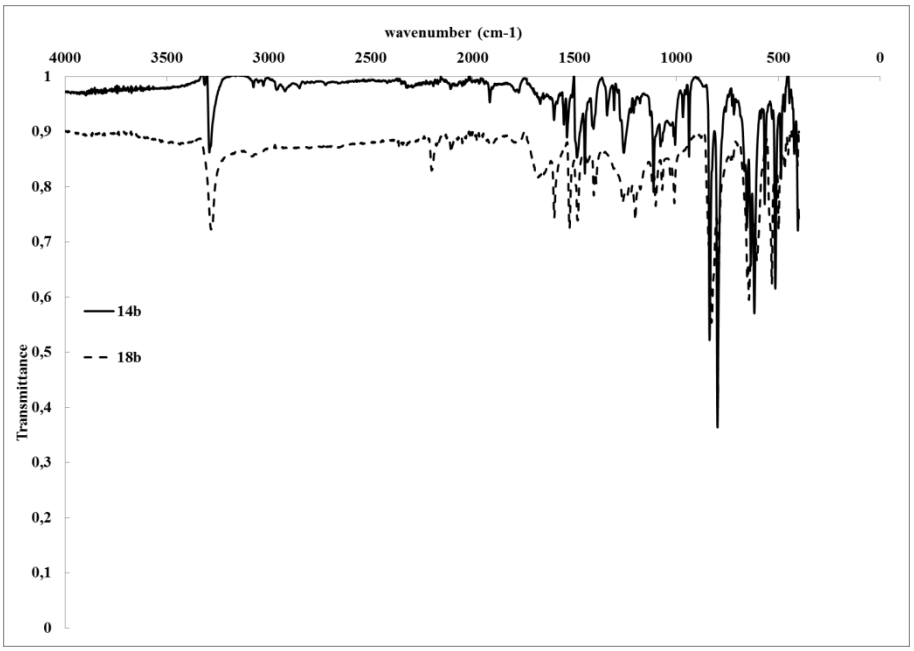

Figure 140. FTIR spectra for the thiophene based ligands (**14b** and **18b**).

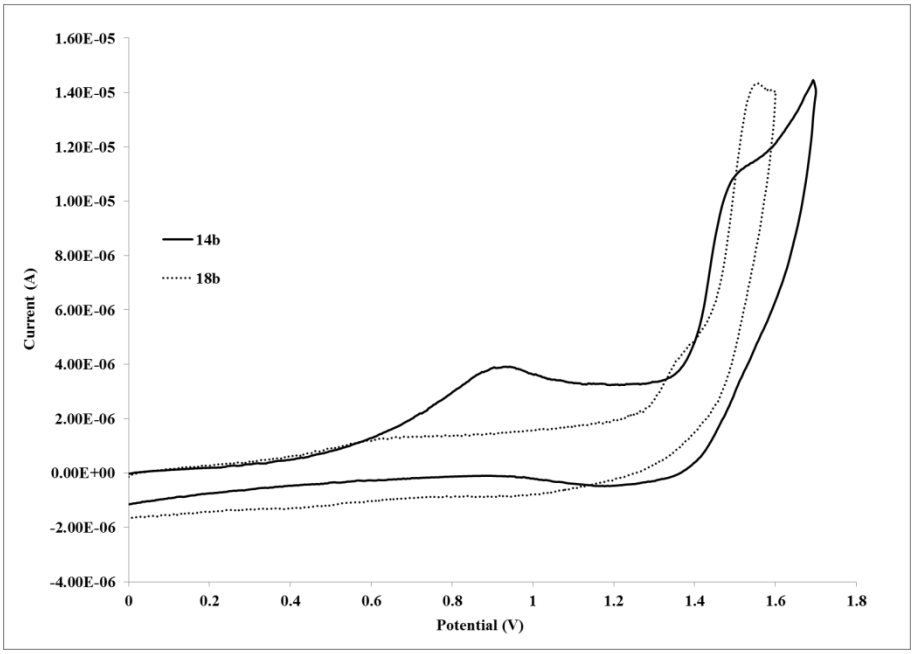

Figure 141. Cyclic voltammograms for the thiophene based free ligands **(14b** and **18b)**.

IV.3. Preparation and characterization of the palladium rods bridged with 1,4-diethynylbenzene derivatives.

The following Pd rods (**20a-d**, **21a-b**) were all prepared following the procedure as discussed in Chapter II by coordination of the free ligands to the palladium moiety *via* CuCl catalysis in diethylamine. The preparation and characterization of each complex is detailed below with the respective ^{1}H and ^{31}P NMR spectrum. The FTIR and UV-Vis spectra as well as the cyclic voltammograms are collected after each group of compounds. ^{13}C NMR and MS spectra are annexed.

IV.3.1. 1,4-bis[*trans*-(ethynyl)Pd(PEt_3)$_2$(Cl)]benzene, 20a

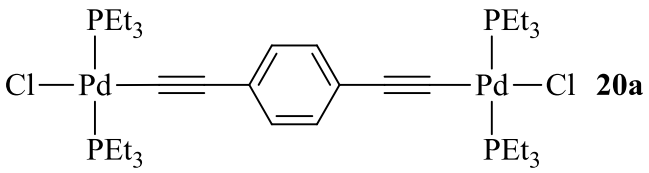

20a

The starting material *trans*-[$PdCl_2(PEt_3)_2$] (**19**, 200 mg, 0.48 mmol) and **5a** (41 mg, 0.32 mmol) were dissolved in $NHEt_2$ (20 mL). CuCl (1 mg, 0.01 mmol) was added in one portion and

the mix was stirred at room temperature for 14 h. It was then evaporated and redissolved in CH_2Cl_2. The resulting solution was washed with water, dried over Na_2SO_4 and evaporated under reduced pressure. Obtained a yellow powder (142 mg, 49.6 %). This compound was reported very recently by Bar *et al.*.[283]

^{1}H NMR ($CDCl_3$): δ 1.51 (t, *J* = 21Hz, 36H, PCH_2–C*H*$_3$), 1.92 (q, *J* = 8Hz, 24H, PC*H*$_2$), 7.07 (s, 4H, Ar-*H*) ppm;

^{13}C{^{1}H} NMR ($CDCl_3$): δ 8.3 (PCH_2*C*H_3), 15.4 (vt, $J_{C\text{-}P}$= 13.80Hz, P*C*H_2CH_3), 125.1, 130.4 ppm;

^{31}P{^{1}H} NMR ($CDCl_3$): δ 18 ppm;

TOF-MS (ESI+): *m/z* = 727.0 $[M\text{-}Cl\text{-}PEt_3+H]^+$, 845.1 $[M\text{-}Cl]^+$, 903.1 $[M+Na]^+$;

FTIR: $\tilde{\nu}$ = 2118 (w, $\nu_{C\equiv C}$); 1498 (m), 1452 (m), 1409 (m), 1378 (m) (ar. $\nu_{C=C}$) cm^{-1};

Melting point = 119 ºC (decomp.).

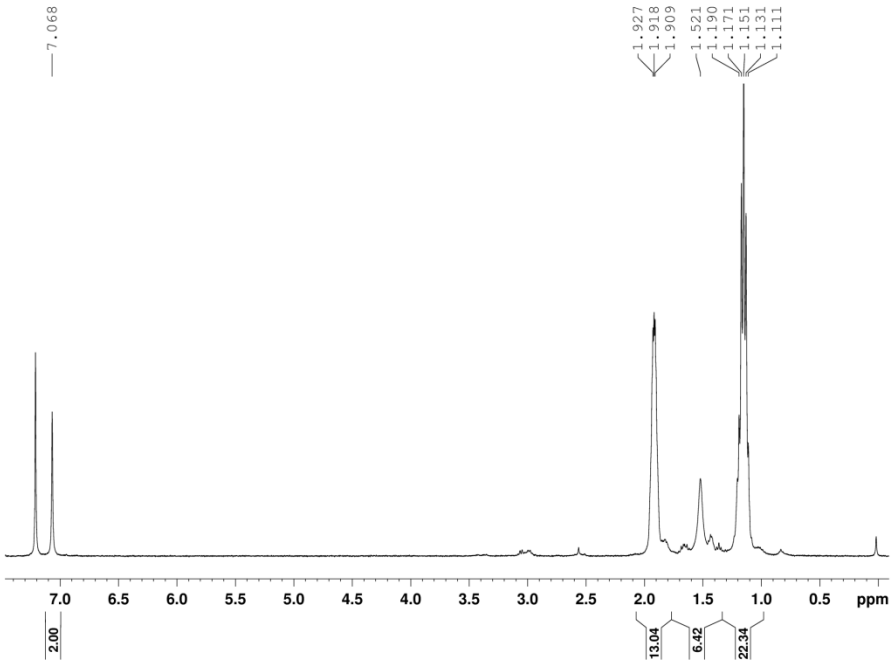

Figure 142. ^{1}H NMR ($CDCl_3$, 400 MHz) spectrum of **20a**.

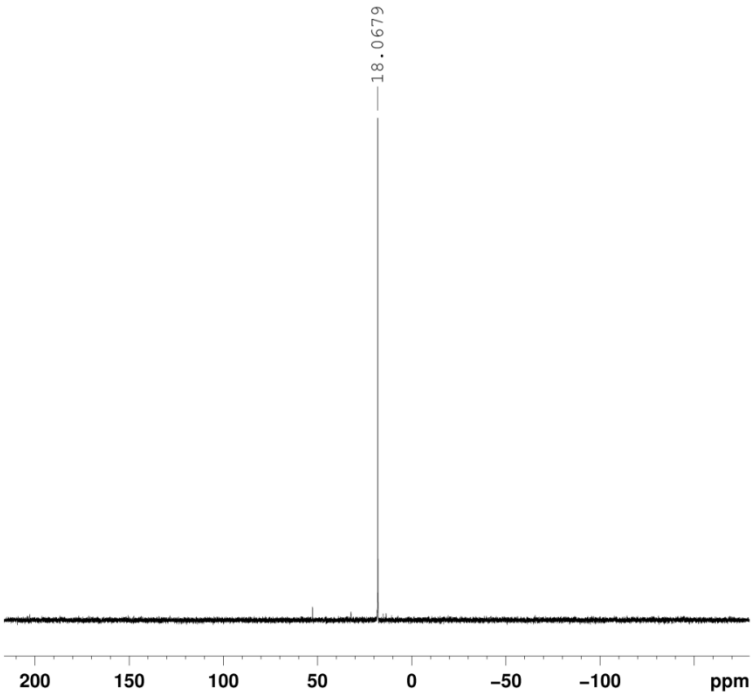

Figure 143. $^{31}P\{^{1}H\}$ NMR ($CDCl_3$, 161 MHz) spectrum of **20a**.

IV.3.2. 1,4-bis[*trans*-(ethynyl)Pd(PEt_3)$_2$(Cl)]-2,5-dimethoxybenzene, 20b

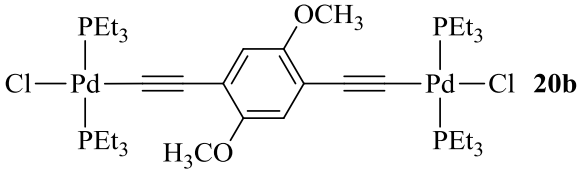

The starting material *trans*-[$PdCl_2(PEt_3)_2$] (**19**, 200 mg, 0.48 mmol) and **5b** (40 mg, 0.12 mmol) were dissolved in $NHEt_2$ (20 mL). CuCl (1 mg, 0.01 mmol) was added in one portion and the mix was stirred at room temperature for 14 h. It was then evaporated and redissolved in CH_2Cl_2. The resulting solution was washed with water, dried over Na_2SO_4 and evaporated under reduced pressure. Obtained yellow powder (198 mg, 83.7 %).

^{1}H NMR ($CDCl_3$): δ 1.21 (t, *J* = 21Hz, 36H, PCH_2–C*H*$_3$), 2.02 (q, *J* = 8Hz, 24H, PC*H*$_2$), 3.75 (s, 6H, OC*H*$_3$), 6.69 (s, 2H, Ar-*H*) ppm;

^{13}C{^{1}H} NMR ($CDCl_3$): δ 8.0 (PCH_2CH_3), 15.3 (vt, $J_{C\text{-}P}$= 13.80Hz, P*C*H_2CH$_3$), 30.9 (Pd-*C*≡C), 42.2 (Pd-C≡*C*), 56.2, 115.7, 154.3 ppm;

^{31}P{^{1}H} NMR ($CDCl_3$): δ 18 ppm;

TOF-MS (ESI+): *m/z* = 907.704 $[M\text{-}Cl]^+$, 963.089 $[M+Na]^+$;

FTIR: $\tilde{\nu}$ = 2115 (s, $\nu_{C\equiv C}$), 1493 (m), 1454 (m), 1409 (m), 1385 (m) (ar. $\nu_{C=C}$) cm^{-1};

Melting point = 153 ºC (decomp.);

EA: $C_{36}H_{68}Cl_2O_2P_4Pd_2 \cdot 1.05H_2O$ (969.46): calcd. C 45.07, H 7.36; found C 44.74, H 7.03.

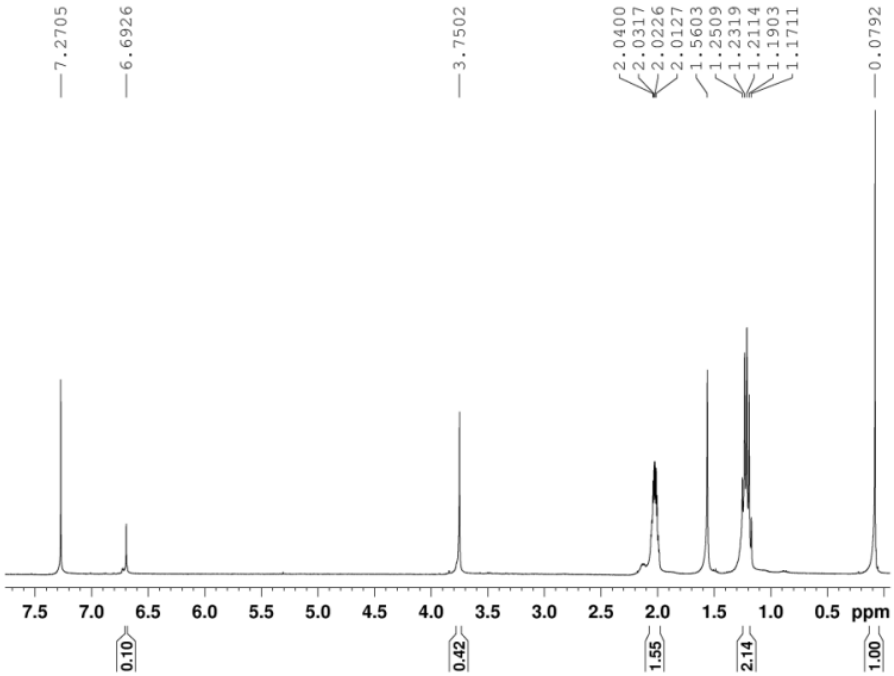

Figure 144. ^1H NMR ($CDCl_3$, 400 MHz) spectrum of **20b**.

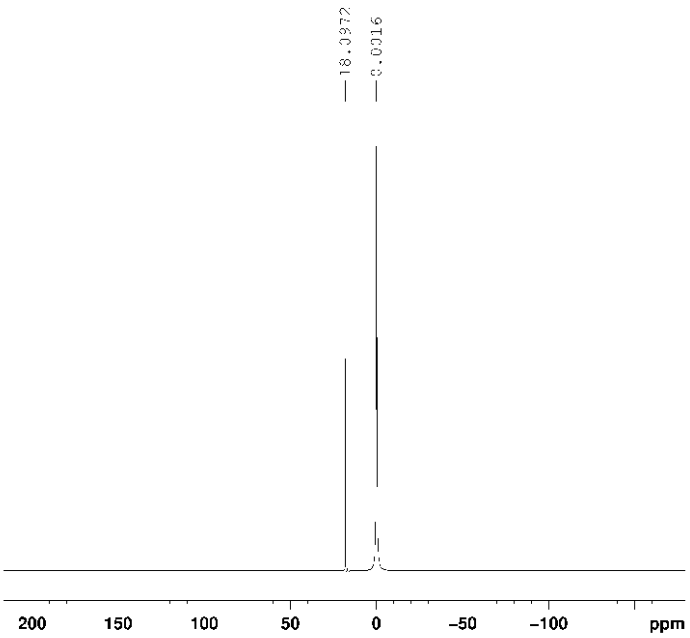

Figure 145. $^{31}P\{^{1}H\}$ NMR ($CDCl_3$, 161 MHz) spectrum of **20b** using H_3PO_4 (85% aq.) as external reference.

IV.3.3. 1,4-bis[*trans*-(ethynyl)Pd(PEt_3)$_2$(Cl)]-2,5-diethoxybenzene, 20c

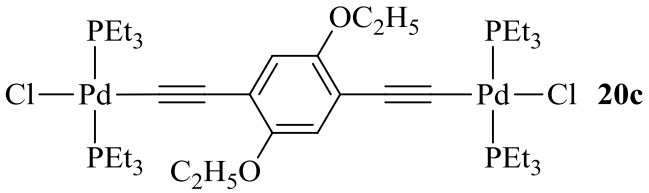

20c

The starting material *trans*-[$PdCl_2(PEt_3)_2$] (**19**, 250 mg, 0.60 mmol) and **5c** (58 mg, 0.27 mmol) were dissolved in $NHEt_2$ (20 mL). CuCl (1 mg, 0.01 mmol) was added in one portion and the mix was stirred at room temperature for 14 h. It was then evaporated and redissolved in CH_2Cl_2. The resulting solution was washed with water, dried over Na_2SO_4 and evaporated under reduced pressure. Obtained yellow powder (214 mg, 81.2%).

^{1}H NMR ($CDCl_3$): δ 1.19 (t, *J* = 20Hz, 36H, PCH_2–C*H*$_3$), 1.46 (t, *J* = 18Hz, 6H, OCH_2–C*H*$_3$), 2.01 (q, *J* = 18Hz, 24H, PC*H*$_2$), 3.97 (q, *J* = 18Hz, 4H, OC*H*$_2$), 6.69 (s, 2H, Ar–*H*) ppm;

$^{13}C\{^{1}H\}$ NMR ($CDCl_3$): δ 8.7 ($PCH_2\mathit{C}H_3$), 15.5 (s, $OCH_2\mathit{C}H_3$), 15.7 (t, $J_{C\text{-}P}$= 13.97Hz, $P\mathit{C}H_2CH_3$), 64.8 (s, $O\mathit{C}H_2CH_3$), 100.1 (t, $J_{C\text{-}P}$ = 16.06 Hz, Pd-*C*≡C), 102.9 (t, $J_{C\text{-}P}$ = 5.83 Hz, Pd-C≡*C*), 116.0 (s, C_1), 117.4 (s, Ar.), 153.2 (s, Ar. *C*–O–CH_3) ppm;

$^{31}P\{^{1}H\}$ NMR ($CDCl_3$): δ 18 ppm;

TOF-MS (ESI+): *m/z* = 933.136 $[M\text{-}Cl]^+$, 991.104 $[M+Na]^+$;

FTIR: $\tilde{\nu}$ = 2113 (w, $\nu_{C\equiv C}$), 1498 (m), 1478 (m), 1410 (m), 1389 (m, ar. $\nu_{C=C}$)cm^{-1};

Melting point = 145 ºC (decomp.);

EA: $C_{38}H_{72}Cl_2O_2P_4Pd_2{\cdot}0.75CH_2Cl_2{\cdot}0.35H_2O$ (1038.59): calcd. C 44.81, H 7.20; found: C 44.85, H 7.24.

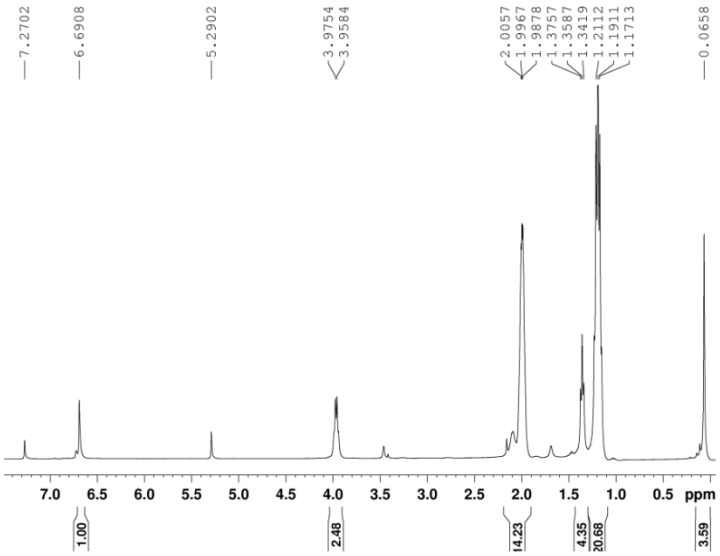

Figure 146. ^{1}H NMR ($CDCl_3$, 400 MHz) spectrum of **20c**.

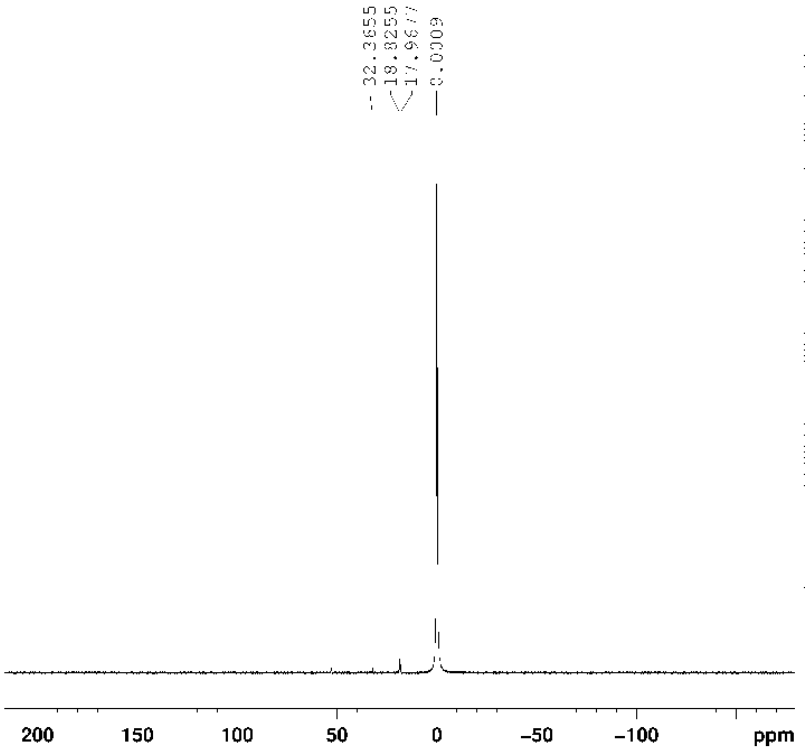

Figure 147. $^{31}P\{^{1}H\}$ NMR ($CDCl_3$, 161 MHz) spectrum of **20c** using H_3PO_4 (85% aq.) as external reference.

IV.3.4. 1,4-bis[*trans*-(ethynyl)Pd(PEt_3)$_2$(Cl)]-2,5-dihethoxybenzene, 20d

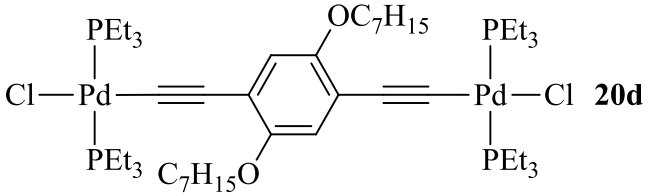

The starting material *trans*-[$PdCl_2(PEt_3)_2$] (**19**, 250 mg, 0.60 mmol) and **5d** (96 mg, 0.27 mmol) were dissolved in $NHEt_2$ (20 mL). CuCl (1 mg, 0.01 mmol) was added in one portion and the mix was stirred at room temperature for 14 h. It was then evaporated and redissolved in CH_2Cl_2. The resulting solution was washed with water, dried over Na_2SO_4 and evaporated under reduced pressure. Obtained a yellow powder (193 mg, 63.9%).

^{1}H NMR ($CDCl_3$): δ 0.89 (t, J= 6.86 Hz, 6H, $O(CH_2)_6CH_3$)), 1.19−1.31 (m, 52H, $PCH_2–CH_3$, $O(CH_2)_2(CH_2)_4CH_3$), 1.48-1.93 (m, 2H $OCH_2CH_2(CH_2)_4CH_3$), 3.89 (t, J=6.82 Hz, 4H, $OCH_2(CH_2)_5CH_3$), 2.03 (q, *J* = 7.4Hz, 24H, PCH_2), 6.69 (s, 2H, Ar-*H*) ppm;

^{13}C{^{1}H} NMR ($CDCl_3$): δ 8.0 (PCH_2CH_3), 15.3 (t, J_{C-P}= 13.80Hz, PCH_2CH_3), 5.7, 13.8, 22.6, 26.1, 29.2, 29.7, 31.8 $(OCH_2)_6CH_3$), 99.6 (s, Pd-*C*≡C, J_{C-P} = 16.13Hz), 102.7 (s, Pd-C≡*C*, J_{C-P} = 5.50Hz), 115.6, 117.1 (s, Ar. *C*), 152.8 (s, Ar. *C*–O–CH_2) ppm;

^{31}P{^{1}H} NMR ($CDCl_3$): δ 18 ppm;

TOF-MS (ESI+): *m/z* = 933.136 $[M-Cl]^+$, 991.104 $[M+Na]^+$;

FTIR: $\tilde{\nu}$ = 2113 (w, $\nu_{C\equiv C}$), 1498 (m), 1478 (m), 1409 (m), 1389.39 (m) (ar. $\nu_{C=C}$) cm^{-1};

Melting point = 98.9 ºC (decomp.);

EA: Found: $C_{48}H_{92}Cl_2O_2P_4Pd_2{\cdot}2H_2O$ (1144.90): calcd. C 50.36, H 8.45; found: C 48.83, H 8.21.

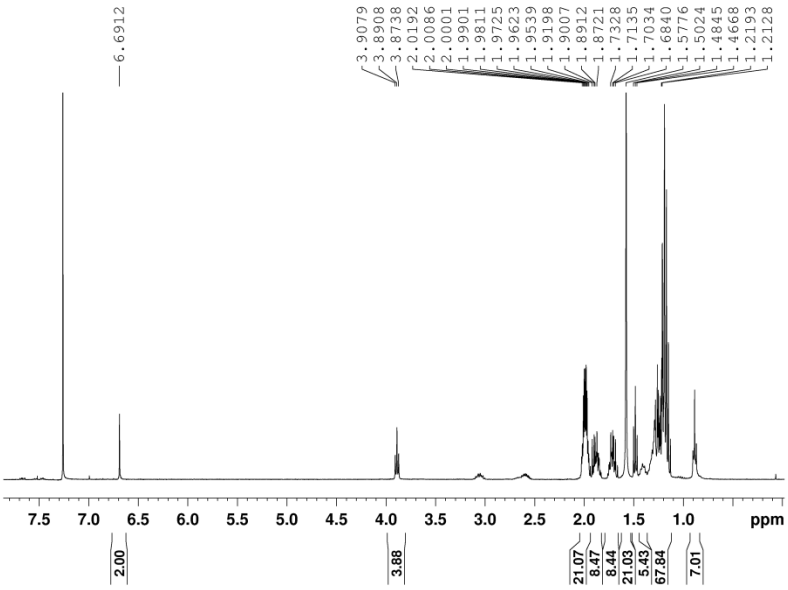

Figure 148. ^{1}H NMR ($CDCl_3$, 400 MHz) spectrum of **20d**.

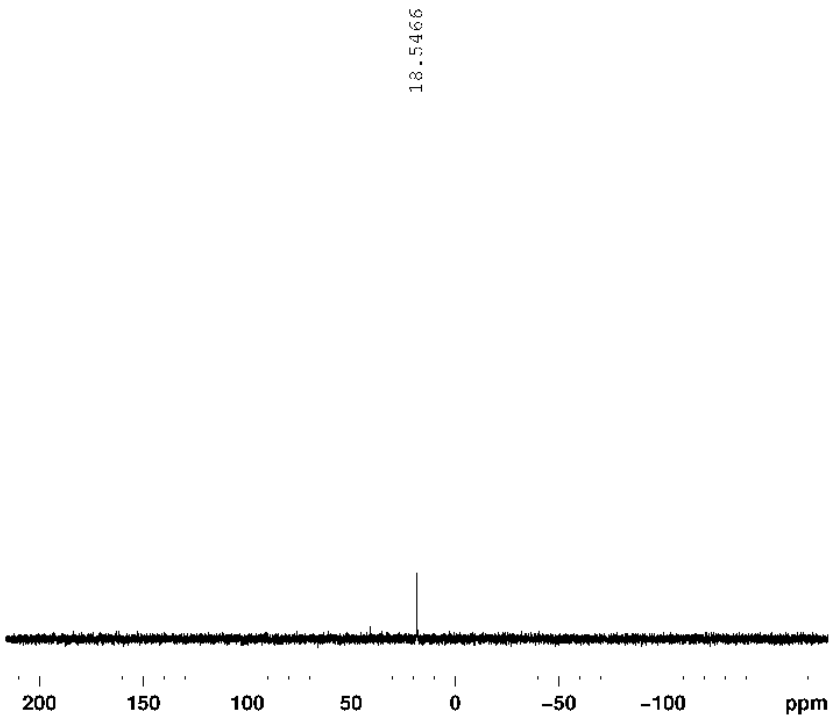

Figure 149. $^{31}P\{^{1}H\}$ NMR ($CDCl_3$, 161 MHz) spectrum of **20d**.

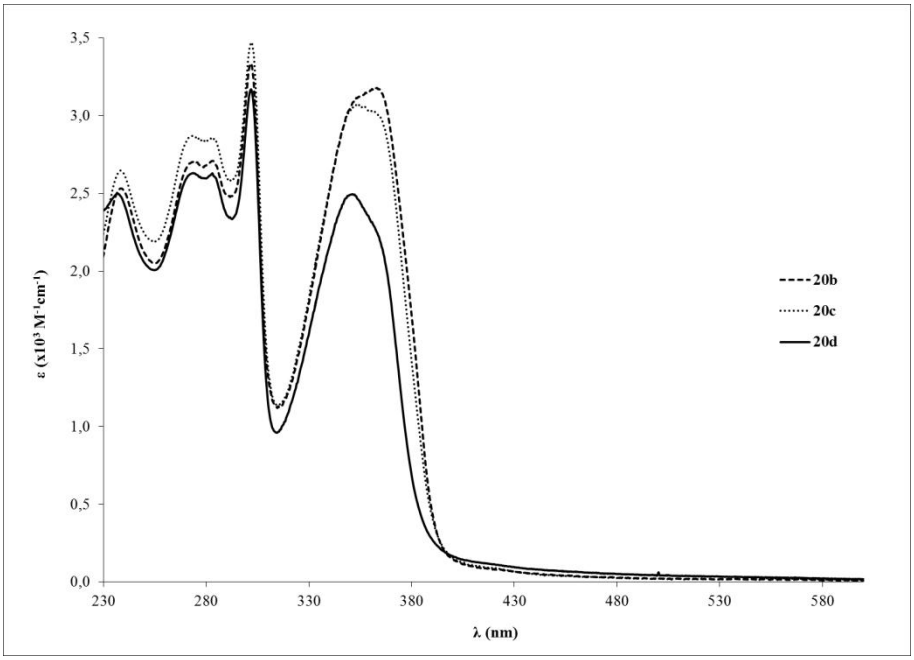

Figure 150. UV-Vis spectra of the single ringed PE based palladium binuclear rods (**20b-d**) bearing side chains in CH_2Cl_2 at *ca.* $1x10^{-5}$ M.

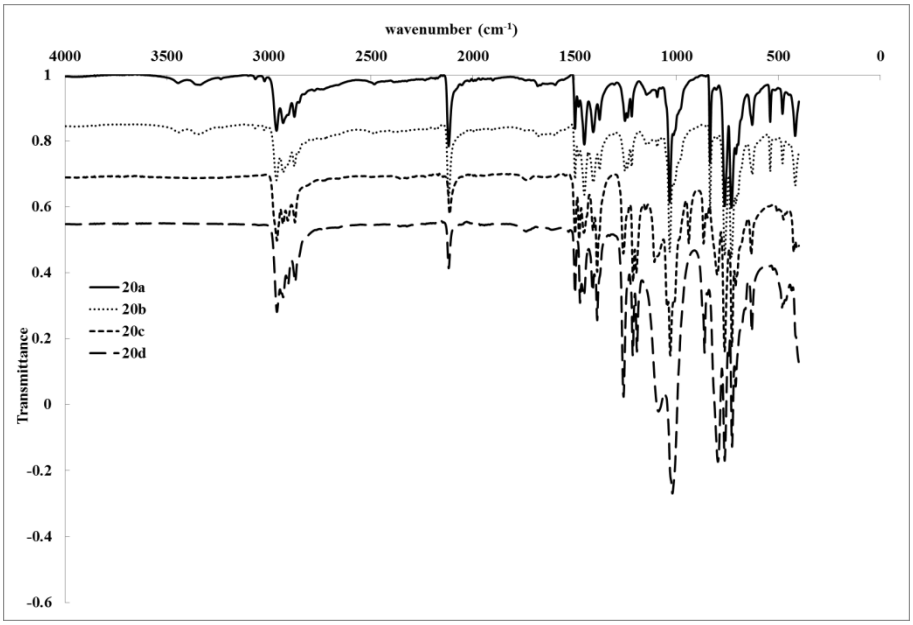

Figure 151. FTIR spectra for the single ringed PE based palladium Rods (**20a-d**).

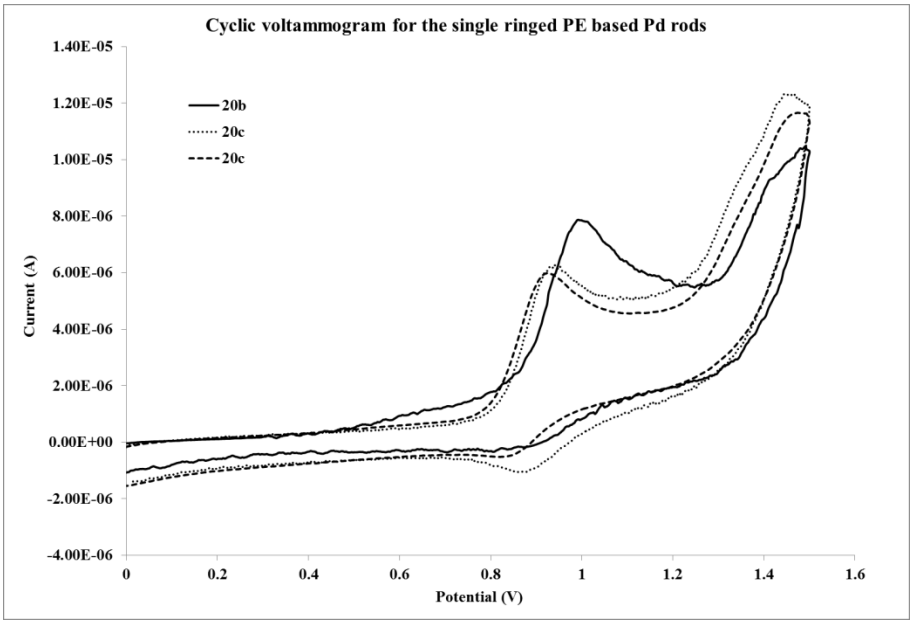

Figure 152. Cyclic voltammograms for Pd rods bridged by the shorter ligands (**20b-d**).

IV.3.5. 1,4-bis[*trans*-((4-ethynylphenyl)ethynylethynyl)Pd(PEt_3)$_2$(Cl)]-2,5-dimethoxybenzene, 21a

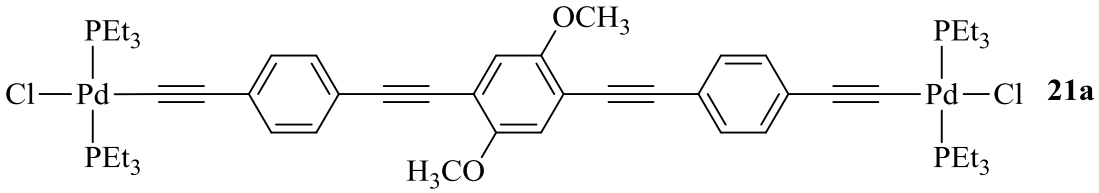

21a

The starting material *trans*-[$PdCl_2(PEt_3)_2$] (**19**, 250 mg, 0.60 mmol) and **10a** (126 mg, 0.32 mmol) were dissolved in $NHEt_2$ (30 mL). CuCl (1 mg, 0.01 mmol) was added in one portion and the mix was stirred at room temperature for 14 h. It was then evaporated and redissolved in CH_2Cl_2. The resulting solution was washed with water, dried over Na_2SO_4 and evaporated under reduced pressure. Obtained yellow powder (273 mg, 73.3%).

^{1}H NMR ($CDCl_3$): δ 1.22 (t, *J* = 8.18Hz, 36H, PCH_2–C*H*$_3$), 1.98 (q, *J* = 3.61Hz, 24H, PC*H*$_2$), 3.90 (s, 6H, OC*H*$_3$), 7.01 (s, 2H, Ar-*H*), 7.21 (d, 4H, $^3J_{H,H}$ = 8.08 Hz), 7.42 (d, 4H, $^3J_{H,H}$ = 8.12 Hz) ppm;

^{13}C{^{1}H} NMR ($CDCl_3$): δ 8.7 (s, PCH_2*C*H_3), 15.8 (t, $J_{C\text{-}P}$= 13.97 Hz, P*C*H_2CH_3), 56.69 (s, O*C*H_3), 86.8, 95.8 (s, C≡C, internal), 99.5 (t, Pd-C≡*C*, $J_{C\text{-}P}$ = 16.13Hz), 107.1 (t, Pd-*C*≡C, $J_{C\text{-}P}$ = 5.87Hz), 113.9, 116.0, 120.5, 128.3, 130.9 (s, Ar. Inner and outer rings), 154.3 (s, Ar. *C*–O–CH_3) ppm;

^{31}P{^{1}H} NMR ($CDCl_3$): δ 18 ppm;

TOF-MS (ESI+): *m/z* = 1105.264 $[M\text{-}Cl_2]^+$, 987.148 $[M\text{-}Cl\text{-}PEt_3]^+$, 881.259 $[M\text{-}(Pd(PEt_3)_2Cl)+PEt_3]^+$, 763.195 $[M\text{-}(Pd(PEt_3)_2Cl)]^+$;

FTIR: $\tilde{\nu}$ = 2110 (w, $\nu_{C\equiv C}$), 1508 (m), 1488 (m), 1457 (m), 1396 (m) (ar. $\nu_{C=C}$) cm^{-1};

Melting point = 155 ºC (decomp.);

EA: $C_{52}H_{76}Cl_2O_2P_4Pd_2 \cdot 0.35H_2O$ (1147.09): calcd. C 54.45, H 6.74; found: C 54.33, H 6.59.

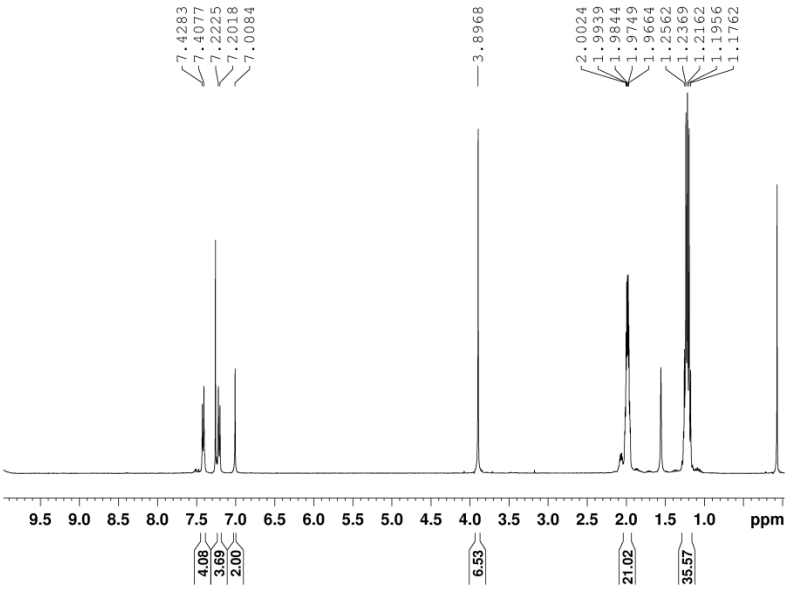

Figure 153. ^{1}H NMR ($CDCl_3$, 400 MHz) spectrum of **21a**.

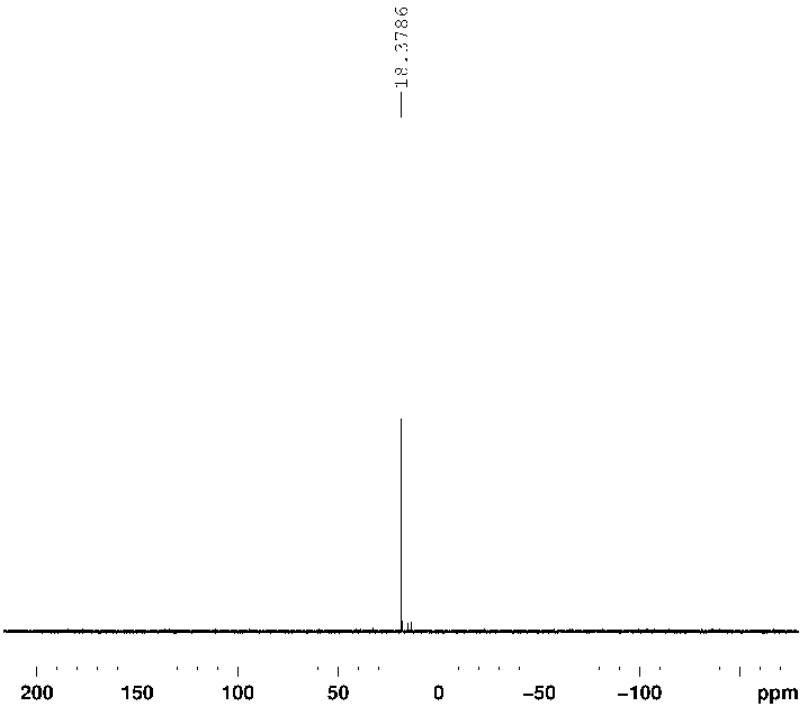

Figure 154. $^{31}P\{^{1}H\}$ NMR ($CDCl_3$, 161 MHz) spectrum of **21a**.

IV.3.6. 1,4-bis[*trans*-((4-ethynylphenyl)ethynylethynyl)Pd(PEt_3)$_2$(Cl)]-2,5-diethoxybenzene, 21b

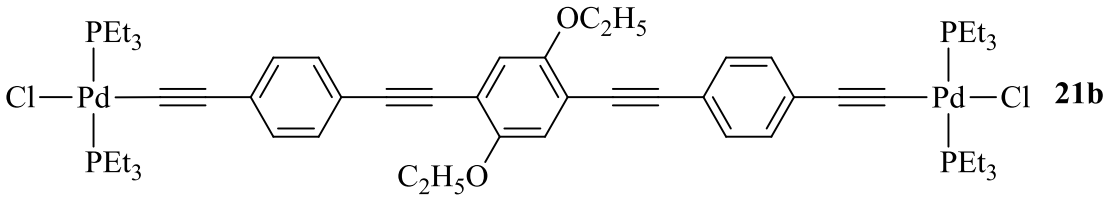

21b

The starting material *trans*-[$PdCl_2(PEt_3)_2$] (**19**, 250 mg, 0.60 mmol) and **10b** (100 mg, 0.24 mmol) were dissolved in $NHEt_2$ (30 mL). CuCl (1 mg, 0.01 mmol) was added in one portion and the mix was stirred at room temperature for 14 h. It was then evaporated and redissolved in CH_2Cl_2. The resulting solution was washed with water, dried over Na_2SO_4 and evaporated under reduced pressure. Obtained yellow powder (241 mg, 85.3%).

^{1}H NMR ($CDCl_3$): δ 1.22 (t, *J* = 8.02Hz, 36H, PCH_2–C*H*$_3$), 1.48 (t, 6H, OCH_2CH_3) 1.98 (q, *J* = 3.61Hz, 24H, PCH_2), 4.10 (s, 4H, OCH_2CH_3), 6.95 (s, 2H, Ar-*H*), 7.21 (d, 4H, $^3J_{H,H}$ = 8.44 Hz), 7.40 (d, 4H, $^3J_{H,H}$ = 8.44 Hz) ppm;

^{13}C{^{1}H} NMR ($CDCl_3$): δ 8.7 (s, PCH_2CH_3), 15.3 (s, OCH_2CH_3) 15.8 (t, $J_{C\text{-}P}$= 13.93 Hz, PCH_2CH_3), 65.7 (s, OCH_3), 87.1, 95.6 (s, C≡C, internal), 99.4 (t, Pd-C≡C, $J_{C\text{-}P}$ = 15.80Hz), 107.1 (t, Pd-C≡C, $J_{C\text{-}P}$ = 5.53Hz), 114.6, 117.6, 120.5, 128.2, 130.9 (s, Ar. Inner and outer rings), 153.9 (s, Ar. *C*–O–CH_3) ppm;

^{31}P{^{1}H} NMR ($CDCl_3$): δ 18 ppm;

TOF-MS (ESI+): *m/z* = 1133.330 $[M\text{-}Cl]^+$;

FTIR: $\tilde{\nu}$ = 2112 (w, $\nu_{C\equiv C}$), 1510 (m), 1487 (m), 1454 (m), 1413 (m) 1377 (m) (ar. $\nu_{C=C}$) cm^{-1};

Melting point = 150 ºC (decomp.);

EA: $C_{54}H_{80}Cl_2O_2P_4Pd_2$ (1168.83): calcd. C 55.49, H 6.90; found: C 56.10, H 6.74.

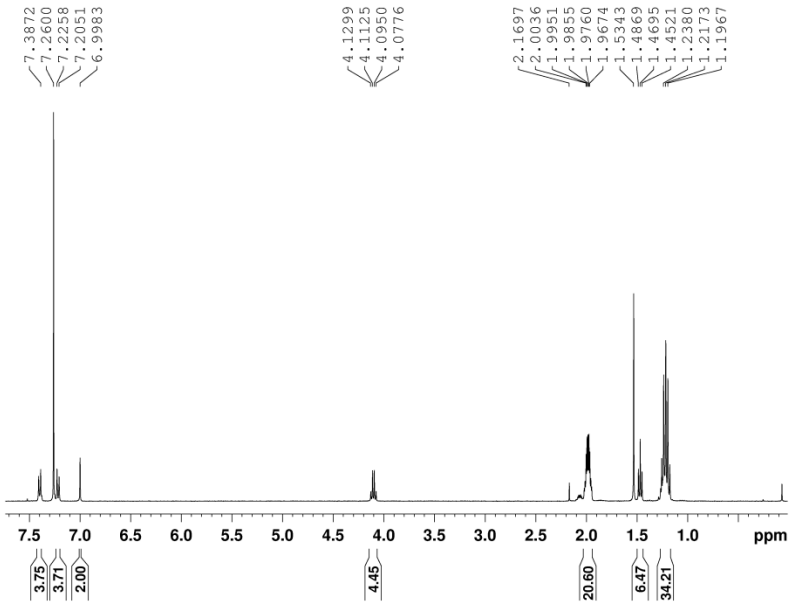

Figure 155. ^{1}H NMR ($CDCl_3$, 400 MHz) spectrum of **21b**.

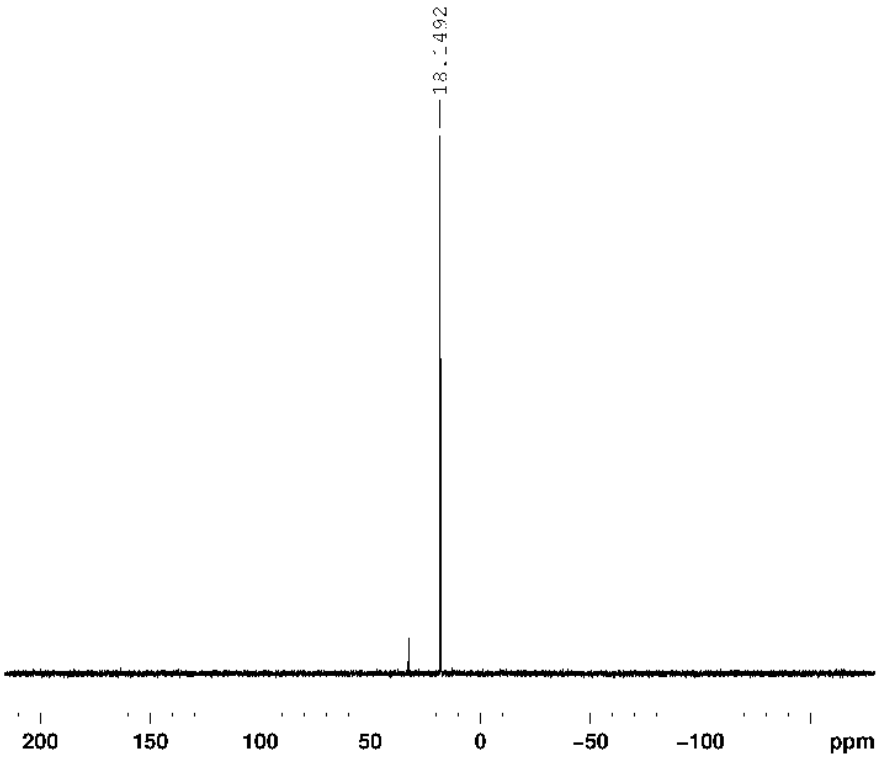

Figure 156. $^{31}P\{^{1}H\}$ NMR ($CDCl_3$, 161 MHz) spectrum of **21b**.

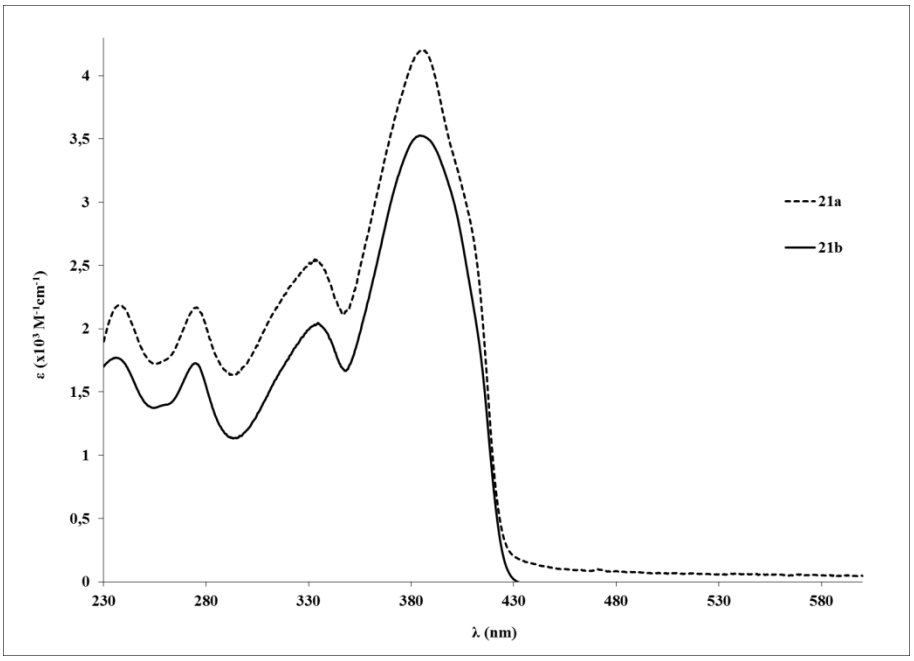

Figure 157. UV-Vis spectra of the tris ringed PE based palladium binuclear rods (**21a-b**) bearing side chains in CH_2Cl_2 at *ca.* $1x10^{-6}$ M.

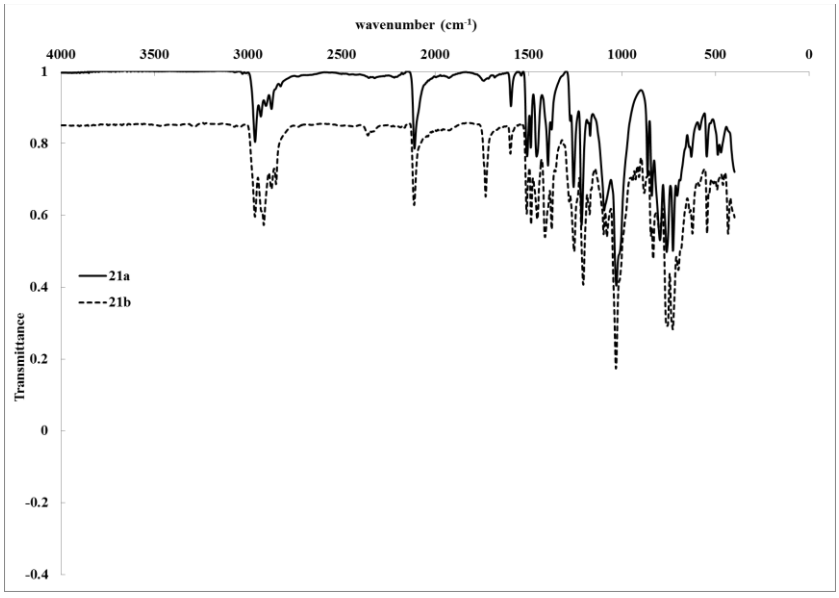

Figure 158. FTIR spectra for the *tris* ringed PE based palladium Rods (**21a-b**).

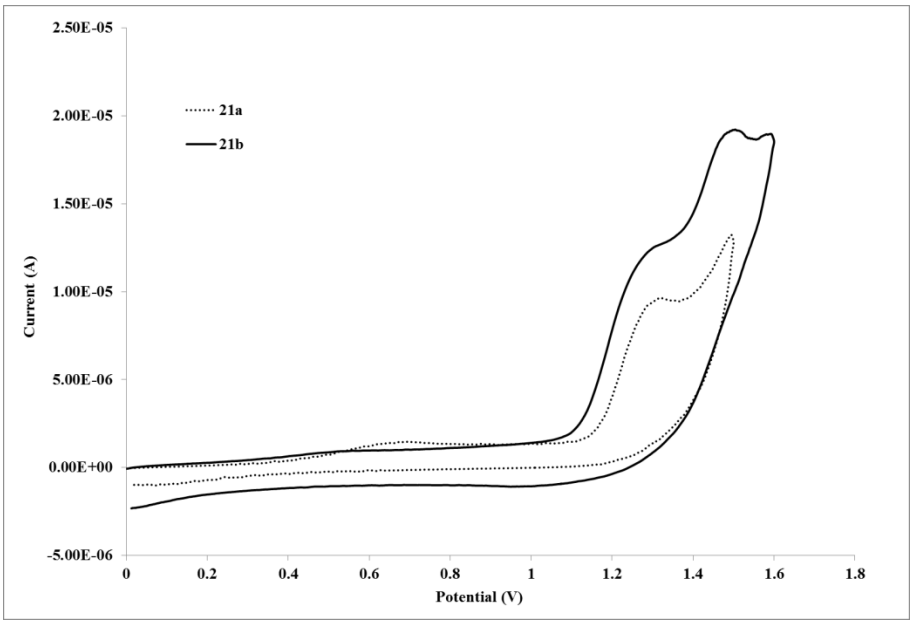

Figure 159. Cyclic voltammograms for Pd rods bridged by the longer ligands (**21a-b**).

IV.4. Preparation and characterization of the ruthenium rods bridged with 1,4-diethynylbenzene and 2,5-thiophene derivatives.

The phenylene based Ru rods (**23a**,**c-d**, **24a-b**, **27** and **28**) were all prepared following the procedure as discussed in Chapter II by coordination of the free ligands to the ruthenium moiety. The preparation and characterization of each complex is detailed below with the respective ^{1}H and ^{31}P NMR spectrum. The FTIR and UV-Vis spectra as well as the cyclic voltammograms are collected after each group of compounds. ^{13}C NMR and MS spectra are annexed.

IV.4.1. $[Cl(dppe)_2Ru–C\equiv C]_2–C_6H_4$, 23a

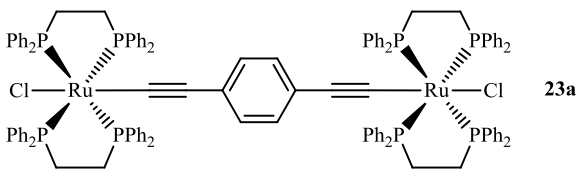

23a

cis-[Ru(dppe)$_2$Cl][PF$_6$] (**22**, 483mg, 0.34 mmol) was loaded into a Schlenk. THF (30 mL) is then added dissolving most of the starting material. The free ligand **5a** (20 mg, 0.15 mmol) is then added and a dark reddish suspension is formed. The mix is left to react overnight and then NEt$_3$ (5mL, high excess) is added prompting the immediate color change of the mix to dark orange. Solvent is removed under vacuum (oil pump) and washed with MeOH/CH$_2$Cl$_2$ (30:1) until the ^{31}P NMR signal is free of the starting material which usually coincides with the disappearance of the red color from the washing fractions. Obtained yellow powder (149 mg, 51.2%). This compound was reported by Lavastre and co-workers.[171b]

^{31}P{^{1}H} NMR (CD$_2$Cl$_2$): δ 48 (s, *P*CH$_2$-CH$_2$-*P*) ppm.
TOF-MS (ESI+): *m/z* = 960.3 [M-Cl$_2$]$^{2+}$, 1025.4 [(dppe)$_2$Ru-C≡C+P]$^+$;
FTIR: $\tilde{\nu}$ = 2049 (w, $\nu_{C\equiv C}$), 14856 (w), 1433 (m) (ar. $\nu_{C=C}$) cm^{-1};

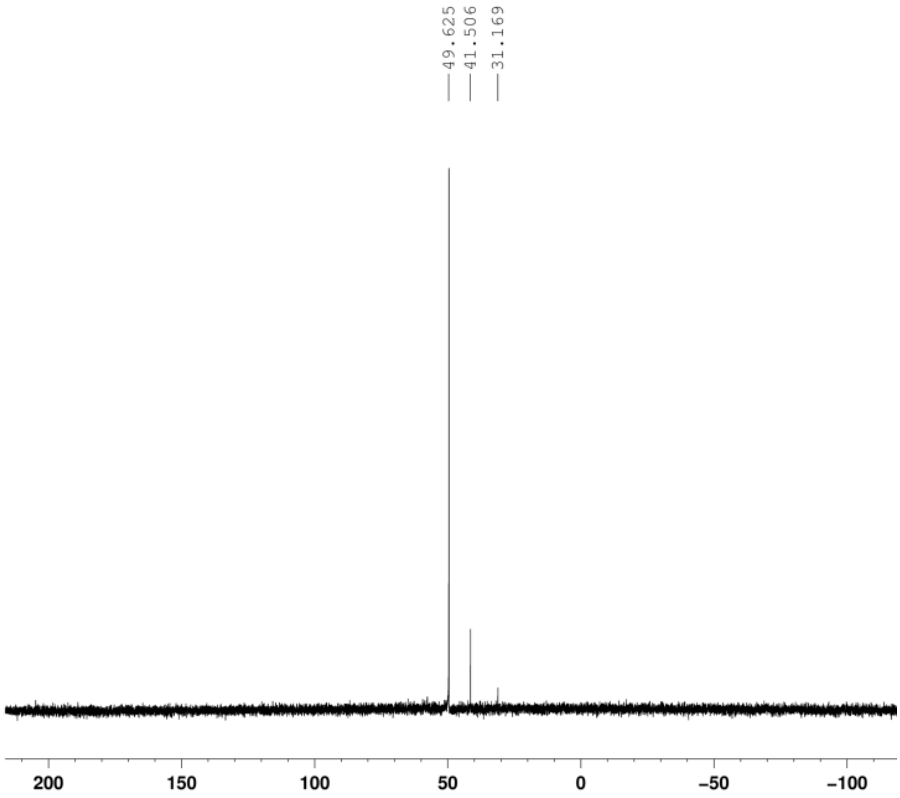

Figure 160. ^{31}P{^{1}H} NMR (CDCl$_3$, 161 MHz) spectrum of **23a**.

IV.4.2. $[Cl(dppe)_2Ru–C\equiv C]_2–C_6H_4(OC_2H_5)_2$, 23c

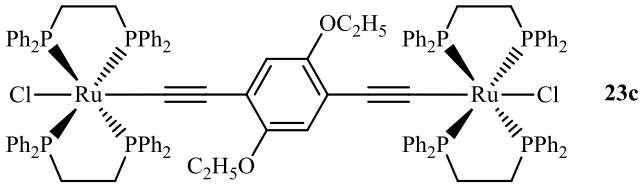

23c

cis-$[Ru(dppe)_2Cl][PF_6]$ (**22**, 427 mg, 0.30 mmol) was loaded into a Schlenk. THF (20 mL) is then added dissolving most of the starting material. The free ligand **5c** (30 mg, 0.14 mmol) is then added and a dark reddish suspension is formed. The mix is left to react overnight and then NEt_3 (5mL, high excess) is added prompting the immediate color change of the mix to dark orange. Solvent is removed under vacuum (oil pump) and washed with $MeOH/CH_2Cl_2$ (30:1) until the ^{31}P NMR signal is free of the starting material which usually coincides with the disappearance of the red color from the washing fractions. Obtained a yellow powder (139 mg, 47.8%).

^{1}H NMR (CD_2Cl_2): δ 1.82 (t, OCH_2CH_3 6H, $J_{H,H}$ = 6.60 Hz), 2.72–3.00 (br. 8H + 8H, PCH_2-CH_2-P), 3.68 (q, 4H, OCH_2CH_3, $J_{H,H}$ = 6.60 Hz), 6.92 – 7.47 (m, 82H, PPh_2, C_6H_2) ppm;
^{13}C{^{1}H} NMR (CD_2Cl_2): δ 15.8 (OCH_2CH_3), 30.9 (PCH_2-CH_2-P), 127.3, 128.7, 129.3, 135.0 (Ar, CC-Ru) ppm;
^{31}P{^{1}H} NMR (CD_2Cl_2): δ 48 ppm;
TOF-MS (ESI+): *m/z* = 2078.67 $[M]^+$, 1021.84 $[M\text{-}Cl]^{2+}$:
FTIR: $\tilde{\nu}$ = 2057 ($\nu_{C\equiv C}$), 1485 (w), 1432 (m), 1437 (m) 1392 (w) (ar. $\nu_{C=C}$) cm^{-1};
Melting point = 176 ºC (decomp.).

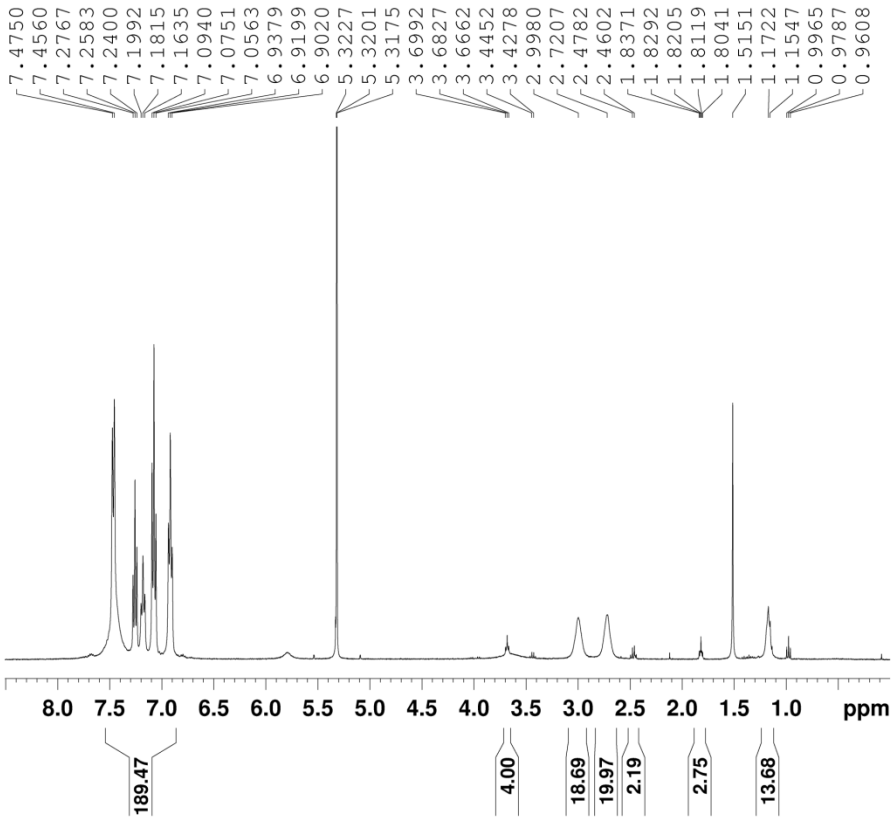

Figure 161. ^{1}H NMR($CDCl_3$, 400 MHz) spectrum of **23c**.

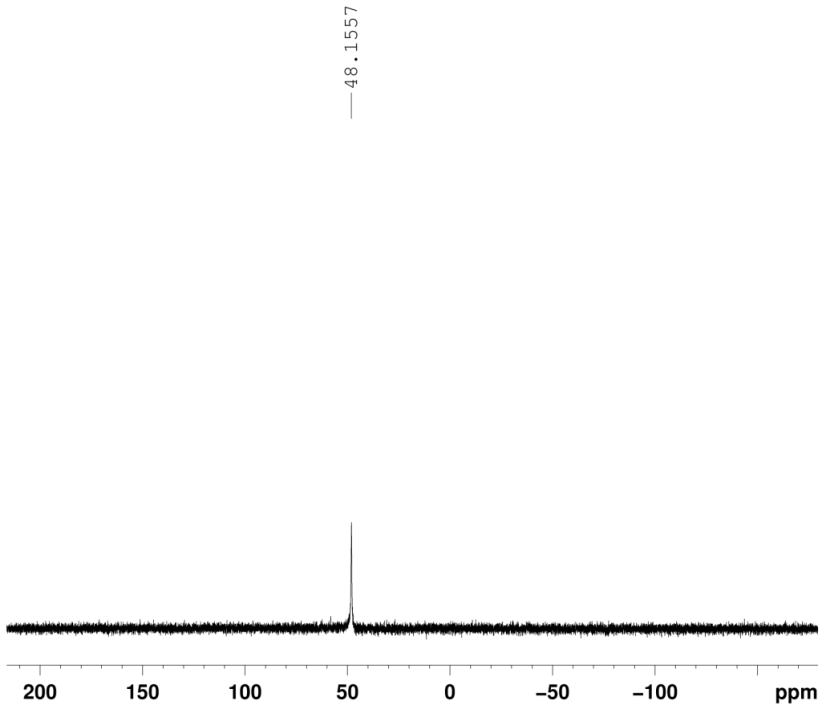

Figure 162. $^{31}P\{^{1}H\}$ NMR($CDCl_3$, 161 MHz) spectrum of **23c**.

IV.4.3. $[Cl(dppe)_2Ru–C\equiv C]_2–C_6H_4(OC_7H_{15})_2$, 23d

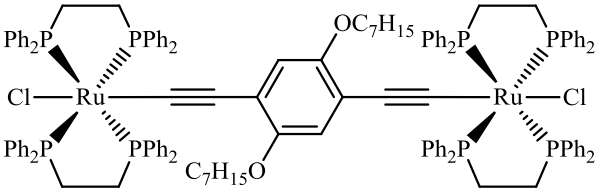

cis-[Ru(dppe)$_2$Cl][PF$_6$] (**22**, 583 mg, 0.12 mmol) was loaded into a Schlenk. THF (20 mL) is then added dissolving most of the starting material. The free ligand **5d** (20 mg, 0.07 mmol) is then added and a dark reddish suspension is formed. The mix is left to react overnight and then NEt_3 (5mL, high excess) is added prompting the immediate color change of the mix to dark orange. Solvent is removed under vacuum (oil pump) and washed with MeOH/CH_2Cl_2 (30:1) until the ^{31}P NMR signal is free of the starting material which usually coincides with the disappearance of the red color from the washing fractions. Obtained a yellow powder (70 mg, 55.9%).

^{1}H NMR (CD_2Cl_2): δ 0.80, (t, $OCH_2(CH_2)_5CH_3$ 6H, $J_{H,H}$ = 6.60 Hz), 1.19–1.57 (m, 16H $OCH_2(CH_2)_5CH_3$), 2.72–2.99 (br. 8H + 8H, PCH_2-CH_2-P), 3.73 (q, 4H, OCH_2CH_3, $J_{H,H}$ = 6.60 Hz), 6.92 – 7.46 (m, 82H, PPh_2, C_6H_2) ppm;

^{13}C{^{1}H} NMR (CD_2Cl_2): δ 23.1, 26.6, 29.6, 32.3 (m, $O(CH_2)_6CH_3$), 30.9 (PCH_2-CH_2-P), 127.3, 128.8, 129.3, 134.9 (Ar, CC-Ru) ppm;

^{31}P{^{1}H} NMR (CD_2Cl_2): δ 48 ppm;

TOF-MS (ESI+): *m/z* = 2218.95 $[M]^+$;

FTIR: $\tilde{\nu}$ = 2064 (w, $\nu_{C\equiv C}$), 1486 (m), 1432 (w), 1383 (w) (ar. $\nu_{C=C}$) cm^{-1};

Melting point = 179 ºC (decomp.).

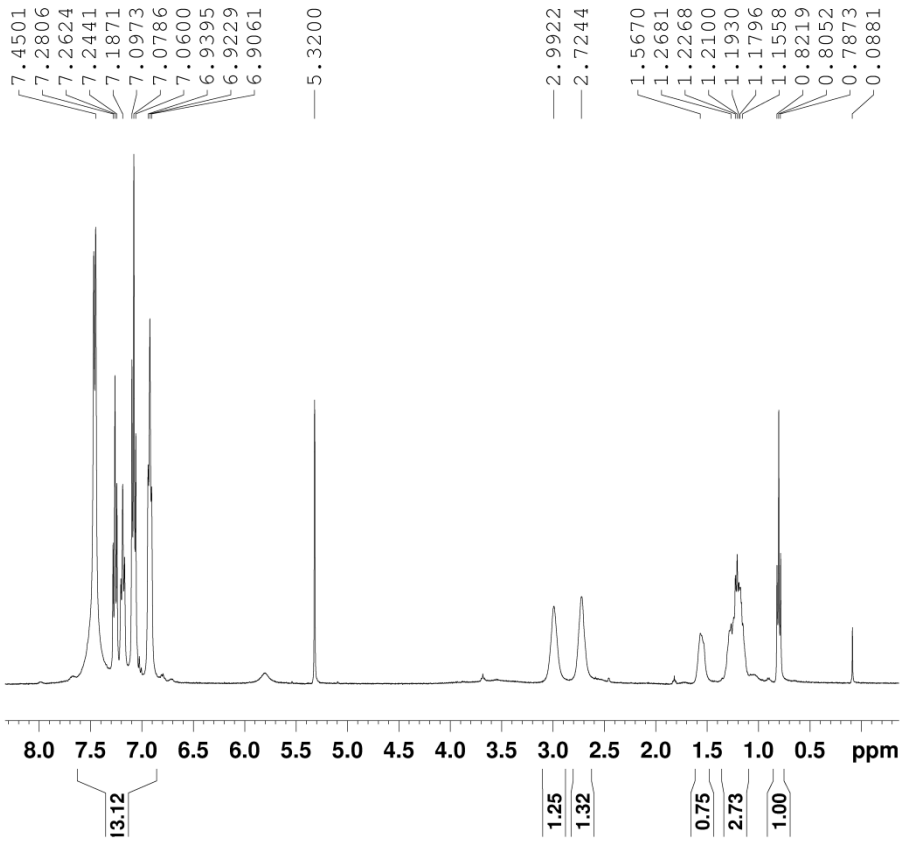

Figure 163. ^{1}H NMR($CDCl_3$, 400 MHz) spectrum of **23d**.

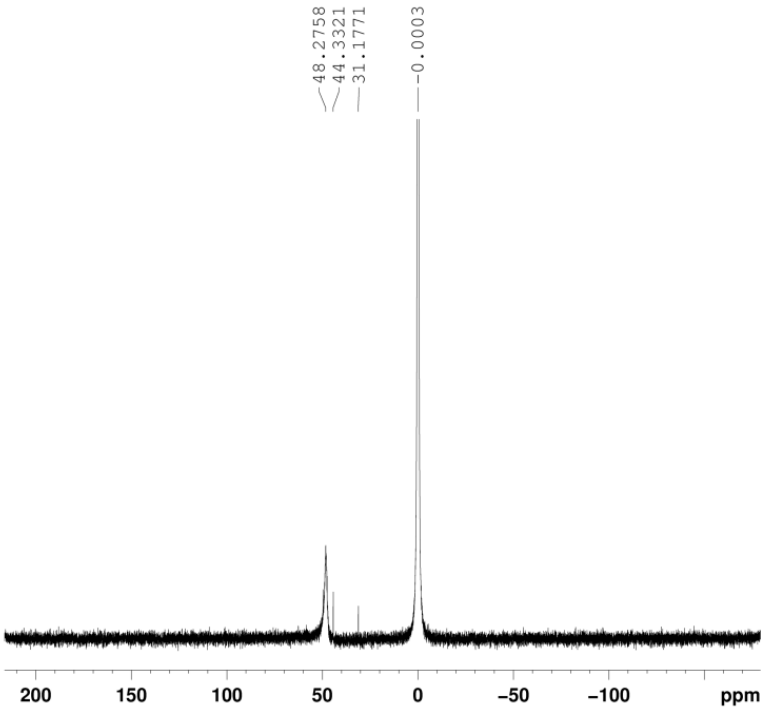

Figure 164. $^{31}P\{^{1}H\}$ NMR($CDCl_3$, 161 MHz) spectrum of **23d**.

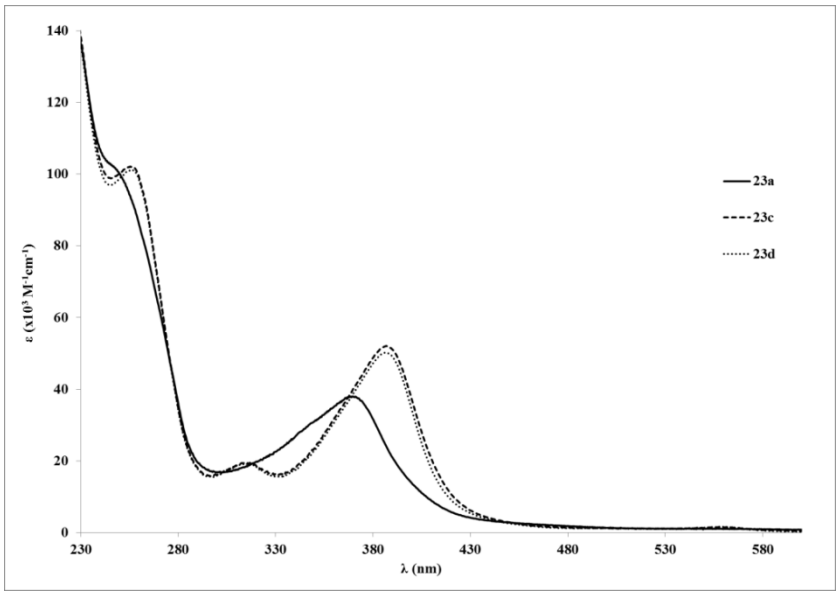

Figure 165. UV-Vis spectra of the single ringed PE based ruthenium rods (**23a**,**c-d**) in CH_2Cl_2 at *ca.* $6x10^{-6}$ M.

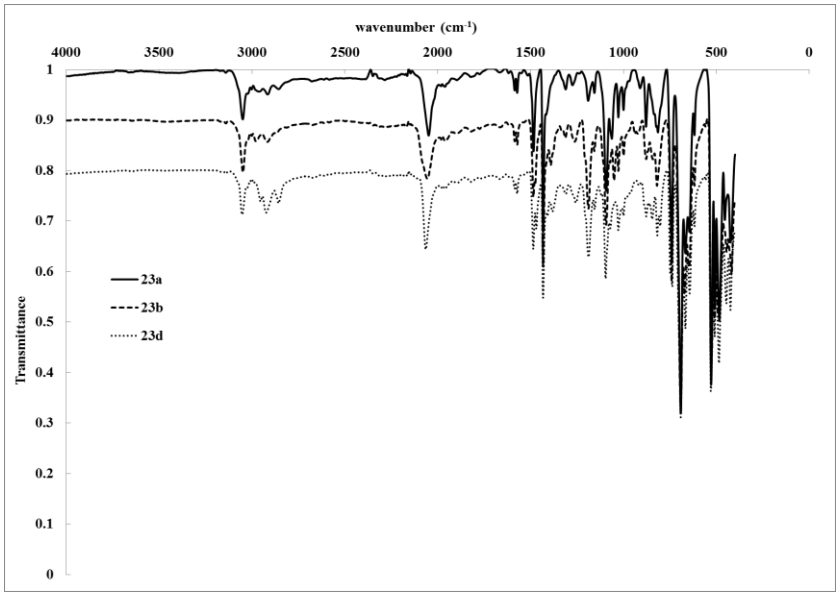

Figure 166. FTIR spectra for the single ringed PE based ruthenium rods (**23a**,**c-d**).

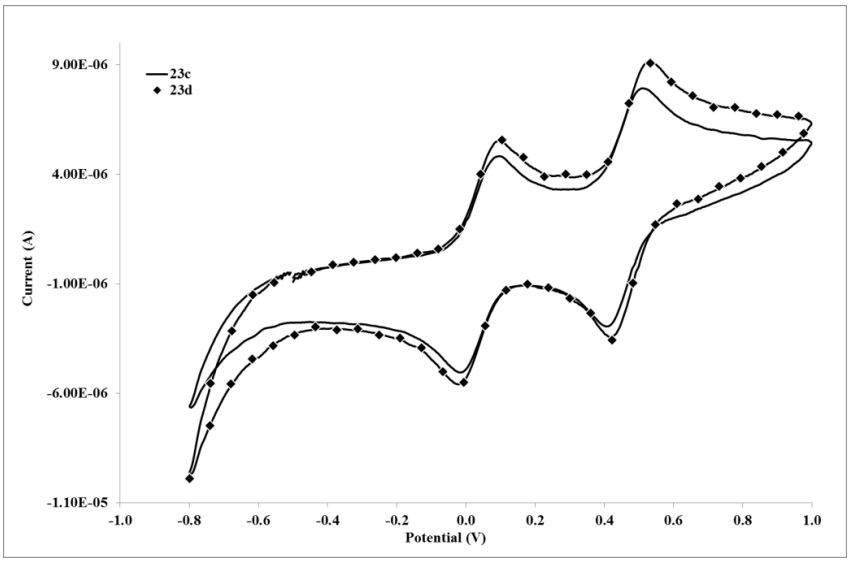

Figure 167. Cyclic voltammograms for Ru rods bridged by the shorter ligands (**23c-d**).

IV.4.4. $[Cl(dppe)_2Ru–C\equiv C–C_6H_4–C\equiv C]_2–C_6H_4(OCH_3)_2$, 24a

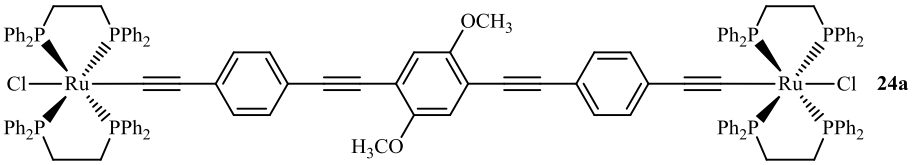

24a

cis-$[Ru(dppe)_2Cl][PF_6]$ (**22**, 468 mg, 0.43 mmol) was loaded into a Schlenk. THF (30 mL) is then added dissolving most of the starting material. The free ligand **10a** (70 mg, 0.19 mmol) is then added and a dark reddish suspension is formed. The mix is left to react overnight and then NEt_3 (5mL, high excess) is added prompting the immediate color change of the mix to dark orange. Solvent is removed under vacuum (oil pump) and washed with $MeOH/CH_2Cl_2$ (30:1) until the ^{31}P NMR signal is free of the starting material which usually coincides with the disappearance of the red color from the washing fractions. Obtained a yellow powder (219 mg, 49.3%).

^{1}H NMR (CD_2Cl_2): δ 2.72 (br. 8H + 8H, PCH_2-CH_2-P), 3.68 (q, 6H, OCH_3, $J_{H,H}$ = 4.88 Hz), 6.55 – 7.44 (m, 90H, PPh_2, C_6H_2, C_6H_4) ppm;

^{13}C{^{1}H} NMR (CD_2Cl_2): δ 11.5 (OCH_3), 30.6 (PCH_2-CH_2-P), 46.2, 56.5, 67.8 126.9, 127.2, 128.8, 129.0, 130.1, 130.7, 133.9, 134.6 (Ar, CC-Ru) ppm;

^{31}P{^{1}H} NMR (CD_2Cl_2): δ 48 ppm;

TOF-MS (ESI+): *m/z* = 1283.46 $[M\text{-}RuCl(dppe)_2\text{-}Cl]^+$, 1090.35 $[M\text{-}Cl_2]^{2+}$;

FTIR: $\tilde{\nu}$ = 2061 (w, $\nu_{C\equiv C}$), 1509 (w), 1485 (m), 1433 (w) 1432 (m) 1396 (w) (ar. $\nu_{C=C}$) cm^{-1};

Melting point = 175 ºC (decomp.).

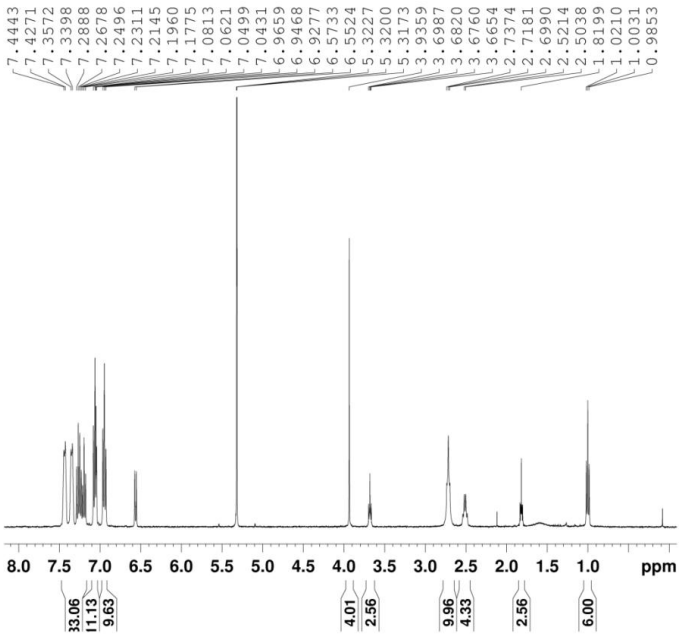

Figure 168. ^1H NMR($CDCl_3$, 400 MHz) spectrum of **24a**.

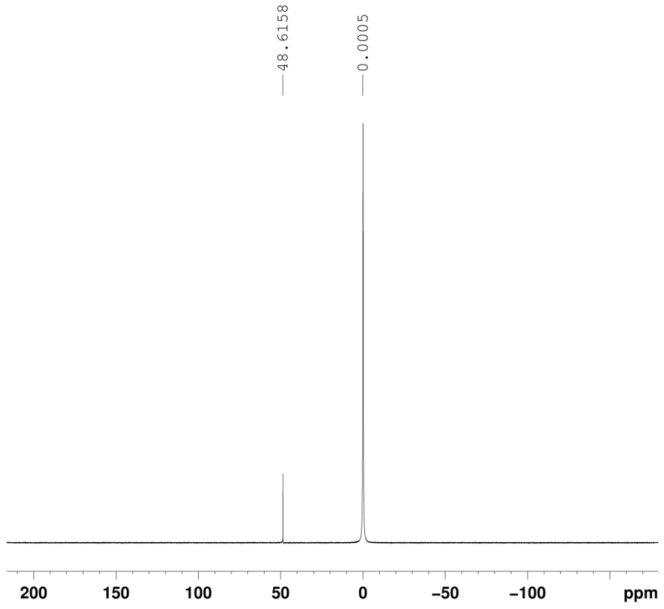

Figure 169. $^{31}P\{^1H\}$ NMR($CDCl_3$, 161 MHz) spectrum of **24a** using H_3PO_4 (85% aq.) as external reference.

IV.4.5. $[Cl(dppe)_2Ru–C\equiv C–C_6H_4–C\equiv C]_2–C_6H_4(OC_2H_5)_2$, 24b

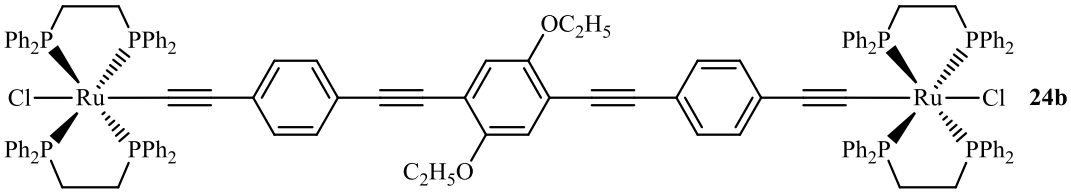

24b

cis-[Ru(dppe)$_2$Cl][PF$_6$] (**22**, 500 mg, mmol) was loaded into a Schlenk. THF (30 mL) is then added dissolving most of the starting material. The free ligand **10b** (87 mg, 21 mmol) is then added and a dark reddish suspension is formed. The mix is left to react overnight and then *t*-BuOK (104 mg, 0.92 mmol) is added in one portion prompting the immediate color change of the mix to dark orange. Solvent is removed under vacuum (oil pump) and washed with MeOH/CH_2Cl_2 (30:1) until the ^{31}P NMR signal is free of the starting material which usually coincides with the disappearance of the red color from the washing fractions. Obtained a yellow powder (110 mg, 37.7 %).

^{1}H NMR (CD_2Cl_2): δ 1.48 (t, 6H, OCH$_2$C*H*$_3$, $J_{H,H}$ = 6.94 Hz), 2.71 (br. 8H + 8H, PC*H*$_2$-C*H*$_2$-P), 4.11 (q, 6H, OC*H*$_3$, $J_{H,H}$ = 6.96 Hz), 6.55 – 7.44 (m, 90H, P*Ph*$_2$, C$_6$*H*$_2$, C$_6$*H*$_4$) ppm;

^{13}C{^{1}H} NMR (CD_2Cl_2): δ 15.2 (O*C*H$_3$), 31.0 (P*C*H$_2$-*C*H$_2$-P), 65.7 (s, CC), 114.5, 117.4, 127.4, 127.6, 129.4, 130.5, 131.1, 134.4, 135.0, 136.4, 136.8, 153.7 (Ar, CC-Ru) ppm;

^{31}P{^{1}H} NMR (CD_2Cl_2): δ 49 ppm;

TOF-MS (ESI+): *m/z* = 1311.29 [M-RuCl(dppe)$_2$-Cl]$^+$, 1105.76 [M-Cl$_2$]$^{2+}$;

FTIR: $\tilde{\nu}$ =2061 (w, $\nu_{C\equiv C}$), 1509 (w), 1485 (m), 1413 (w) 1432 (m), 1412 (w) (ar. $\nu_{C=C}$) cm^{-1};

Melting point = 174 ºC (decomp.).

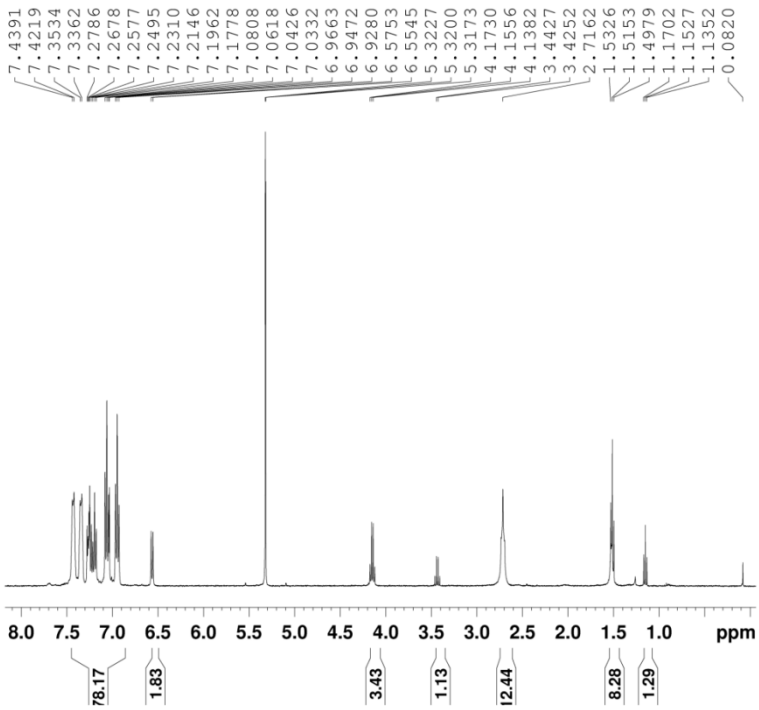

Figure 170. ^{1}H NMR($CDCl_3$, 400 MHz) spectrum of **24b**.

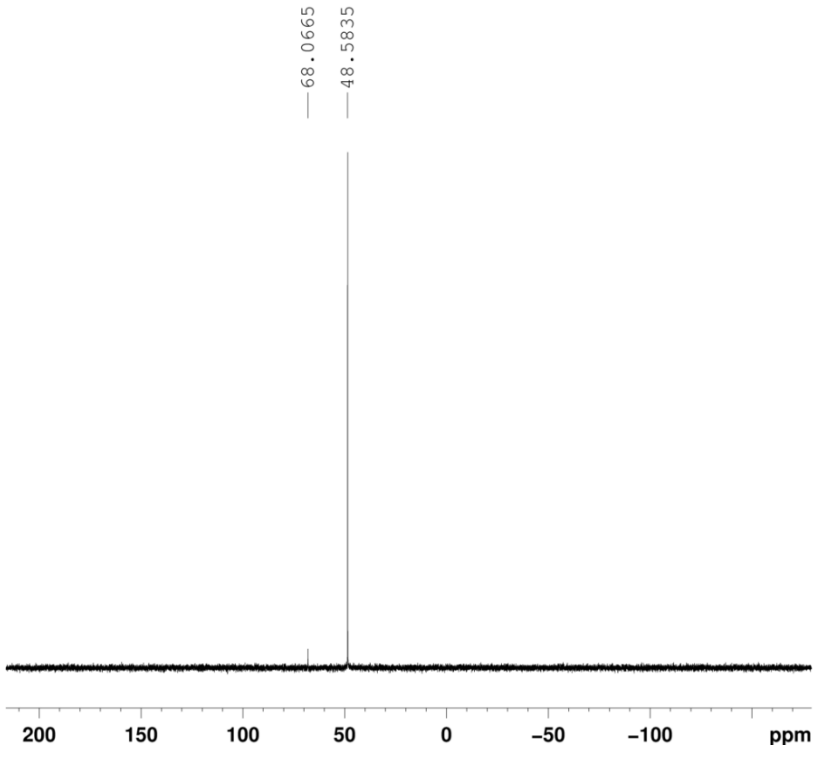

Figure 171. $^{31}P\{^{1}H\}$ NMR($CDCl_3$, 161 MHz) spectrum of **24b**.

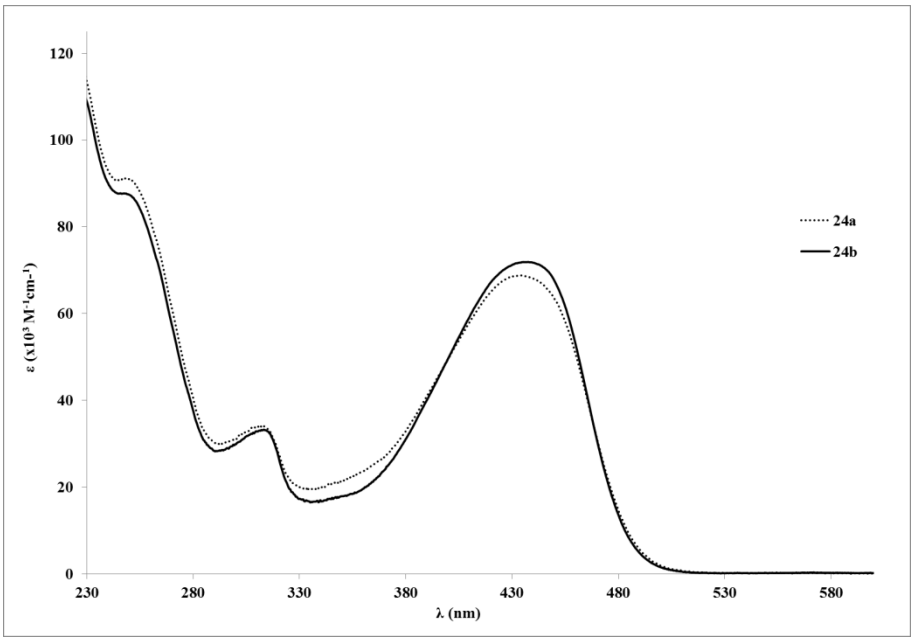

Figure 172. UV-Vis Spectra of the tris ringed PE based ruthenium binuclear rods (**24a-b**) in CH_2Cl_2 at *ca.* $6x10^{-6}$ M.

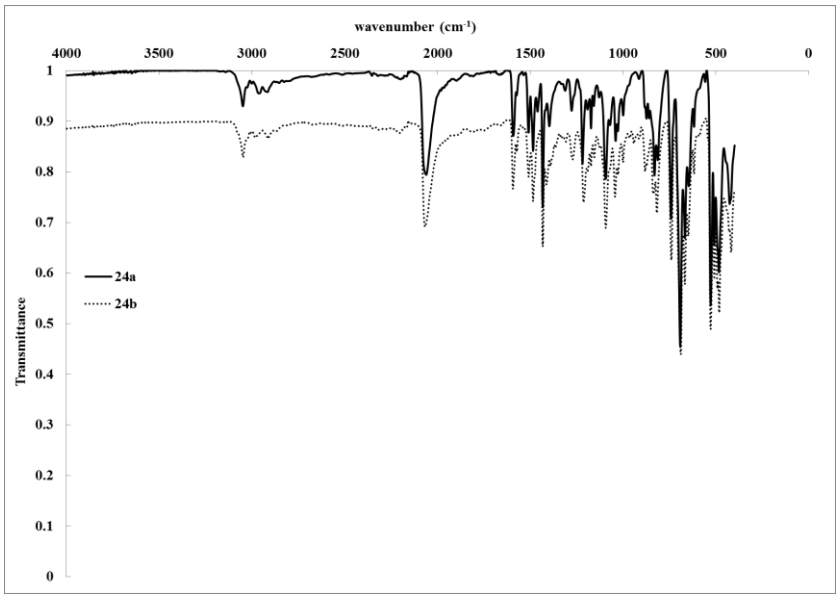

Figure 173. FTIR spectra for the tris ringed PE based ruthenium rods (**24a-b**).

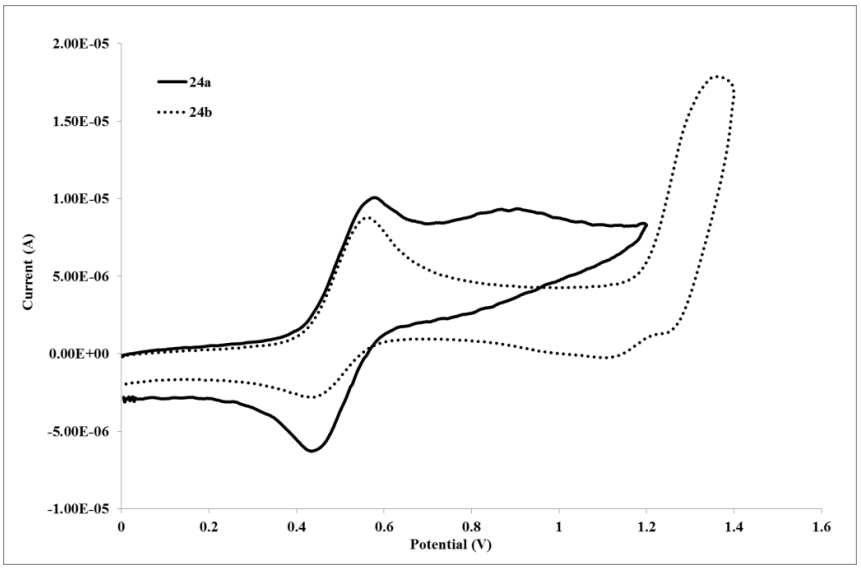

Figure 174. Cyclic voltammograms for Pd rods bridged by the longer ligands (**24a-b**).

IV.4.6. $[Cl(dppe)_2Ru–C\equiv C–C_6H_4]_2–C_5H_4S$, 27

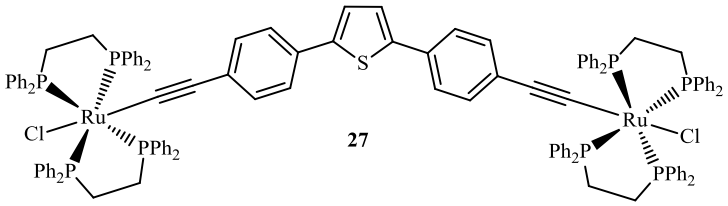

The free ligand **14b** (23 mg, 0.08 mmol) is dissolved in dry diethyl ether (20 mL) and the solution is cooled down with an EtOH/Liquid nitrogen bath. *t*-BuLi (0.5 mL, excess) is added drop-wise to the solution forming a dark brown mix. A freshly prepared solution *cis*-[Ru(dppe)$_2$Cl][OTf] (223mg, 0.2 mmol), in dry CH_2Cl_2 (20 mL) is then added *via* cannula. The mix is left to react overnight. It is then filtrated and concentrated. *n*-hexane is added to precipitate the resulting yellow powder (98 mg, 55.2 %).

^{1}H NMR (CD_2Cl_2): δ 6.64 – 7.42 (m, 80H + 8H + 2H, P*Ph*$_2$, C_6H_4, C_4H_2S) ppm;

^{13}C{^{1}H} NMR (CD_2Cl_2): δ 31.3 (P*C*H$_2$-*C*H$_2$-P), 127.4, 127.6, 129.3, 130.8, 134.5, 134.8, 135.0 (Ar, CC-Ru) ppm;

^{31}P{^{1}H} NMR ($CD2Cl_2$): δ 49 ppm;

TOF-MS (ESI+): *m/z* = 2148.59[M]$^+$, 2113.62 [M-Cl]$^+$;

FTIR: $\tilde{\nu}$ = 2058 (m, $\nu_{C\equiv C}$), 1489 (m), 1435 (m) (ar. $\nu_{C=C}$) cm^{-1};

Melting point = 181 ºC (decomp.).

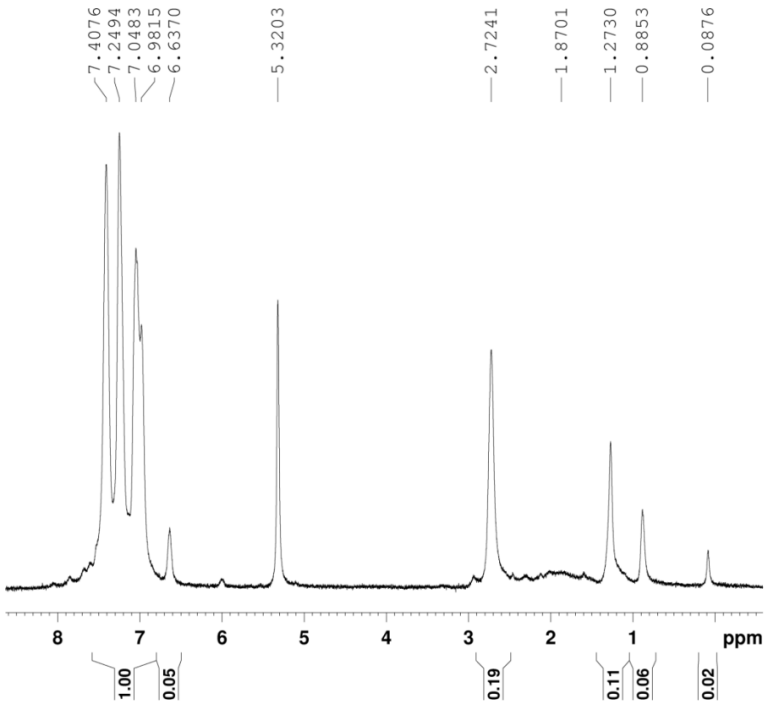

Figure 175. ^{1}H NMR($CDCl_3$, 400 MHz) spectrum of **27**.

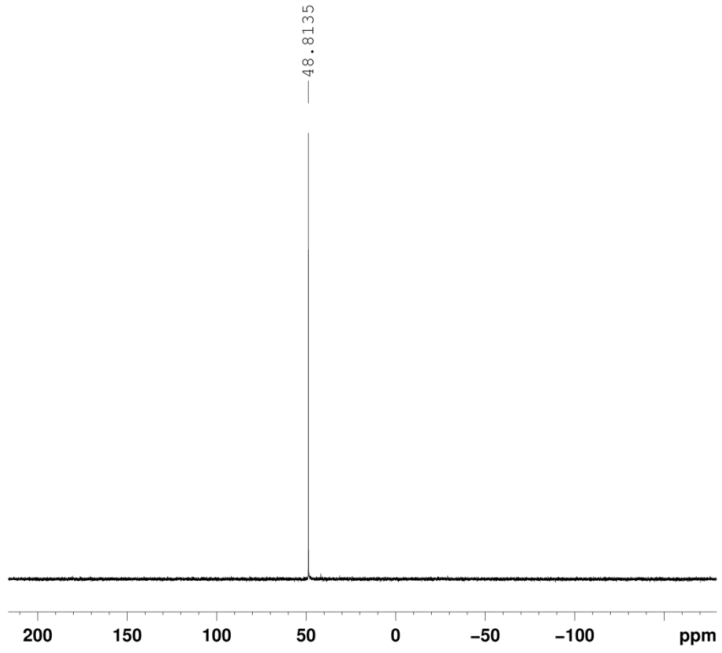

Figure 176. $^{31}P\{^{1}H\}$ NMR($CDCl_3$, 161 MHz) spectrum of **27**.

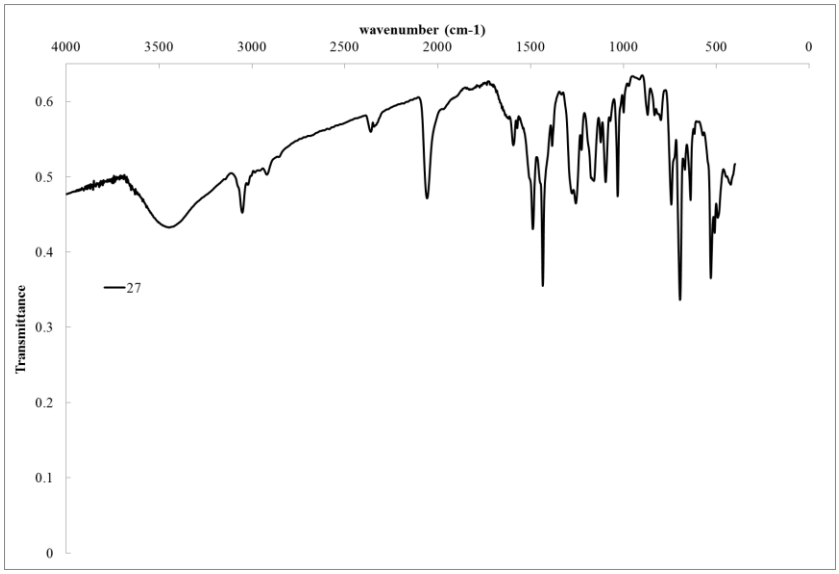

Figure 177. FTIR spectra for the thiophene based ruthenium rod **27** in KBr pellet.

IV.4.7. $[Cl(dppe)_2Ru–C\equiv C–C_6H_4–C\equiv C]_2–\ C_5H_4S$, 28

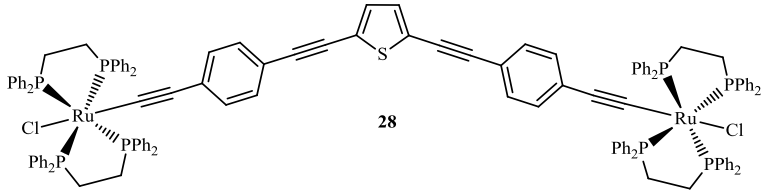

The free ligand **15b** (40 mg, 0.12 mmol) is dissolved in dry diethyl ether (20 mL) and the solution is cooled down with an EtOH/Liquid nitrogen bath. *t*-BuLi (0.5 mL, excess) is added drop-wise to the solution forming a dark brown mix. A freshly prepared solution *cis*-$[Ru(dppe)_2Cl][OTf]$ (279 mg, 0.2 mmol), in dry CH_2Cl_2 (20 mL) is then added *via* cannula. The mix is left to react overnight. It is then filtrated and concentrated. *n*-hexane is added to precipitate the resulting yellow powder (170 mg, 64.3 %).

^{1}H NMR (CD_2Cl_2): δ 6.54 – 7.53 (m, 80H + 8H + 2H, P*Ph*$_2$, C_6H_4, C_4H_2S) ppm;

^{13}C{^{1}H} NMR (CD_2Cl_2): δ 30.1 (P*C*H_2-*C*H_2-P), 127.5, 129.3, 134.78 (Ar, CC-Ru);

^{31}P{^{1}H} NMR (CD_2Cl_2): δ 49 ppm;

TOF-MS (ESI+): *m/z* = 1081.41 $[M\text{-}Cl]^{2+}$, 1063.42 $[M\text{-}Cl_2]^{2+}$, $[M\text{-}(RuCl(dppe)_2)+P+C]^+$;

FTIR: $\tilde{\nu}$ = 2191 (w), 2060 (s) ($\nu_{C\equiv C}$) cm^{-1};

Melting point = 162 ºC (decomp.).

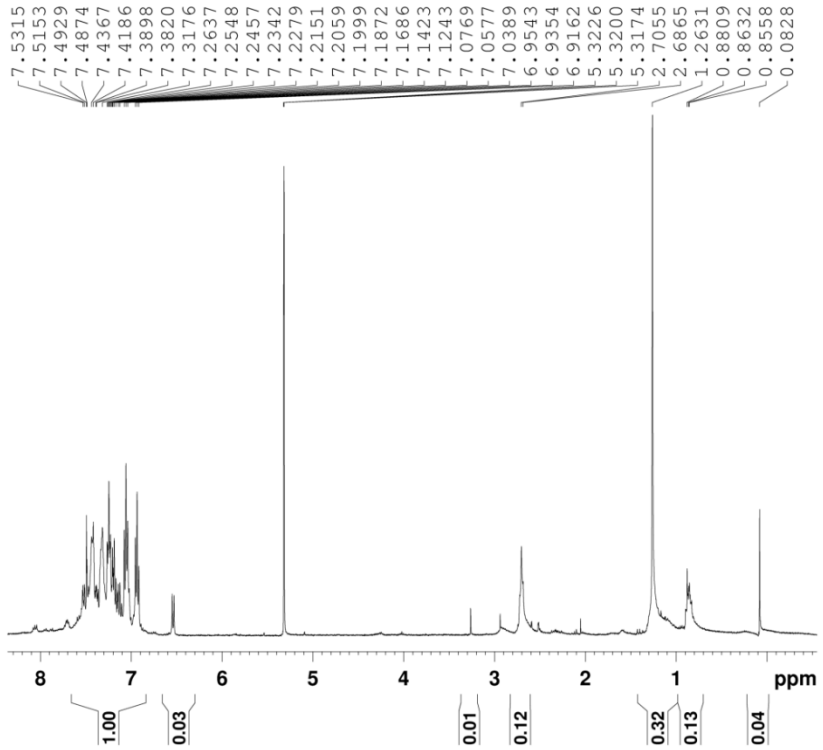

Figure 178. ^{1}H NMR($CDCl_3$, 400 MHz) spectrum of **28**.

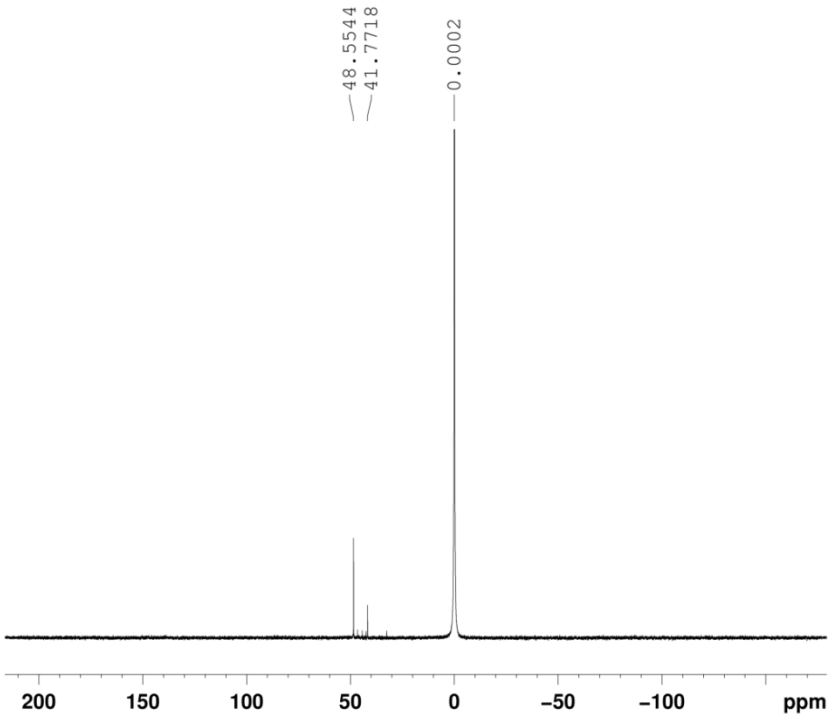

Figure 179. $^{31}P\{^{1}H\}$ NMR($CDCl_3$, 161 MHz) spectrum of **28** using H_3PO_4 (85% aq.) as external reference.

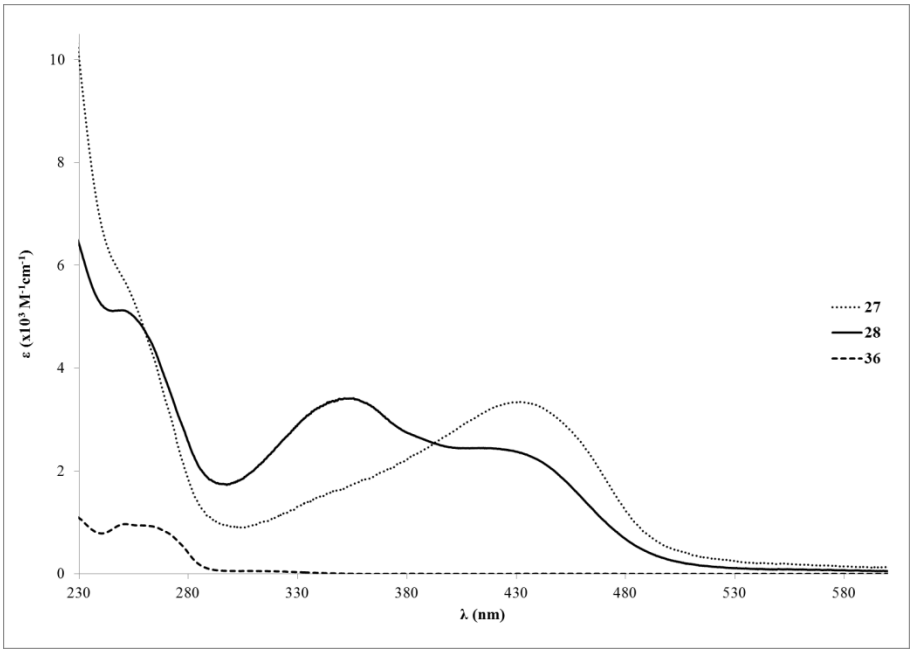

Figure 180. UV-Vis Spectra of the thiophene based ruthenium binuclear rods (**27**, **28**) and *trans*-[$RuCl_2(dppe)_2$] (**36**) in CH_2Cl_2 at *ca.* $1x10^{-6}$M.

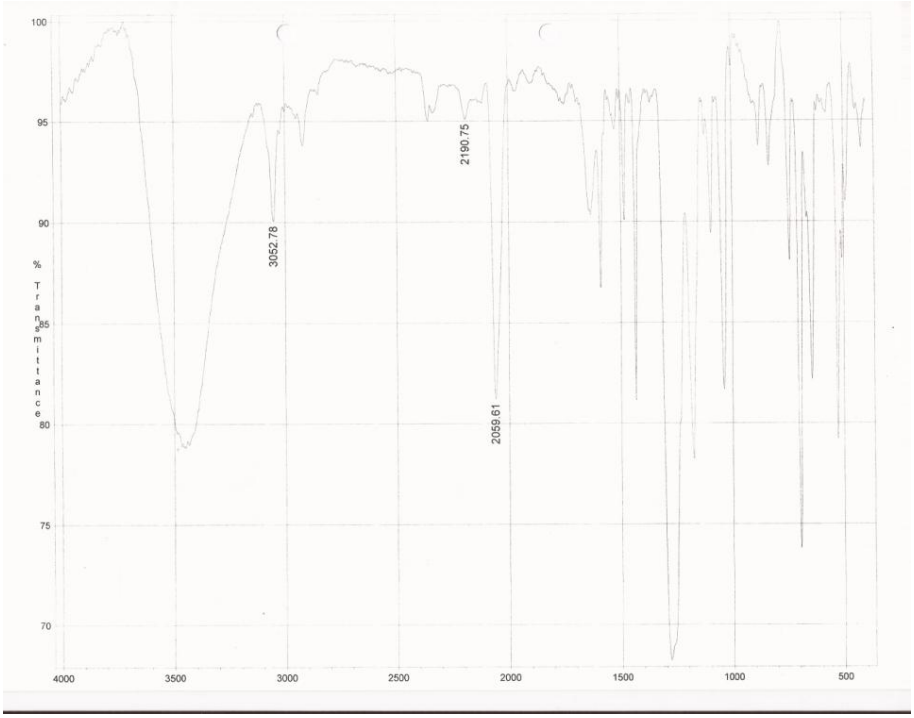

Figure 181. FTIR spectra for the thiophene based ruthenium rod **28** in KBr pellet.

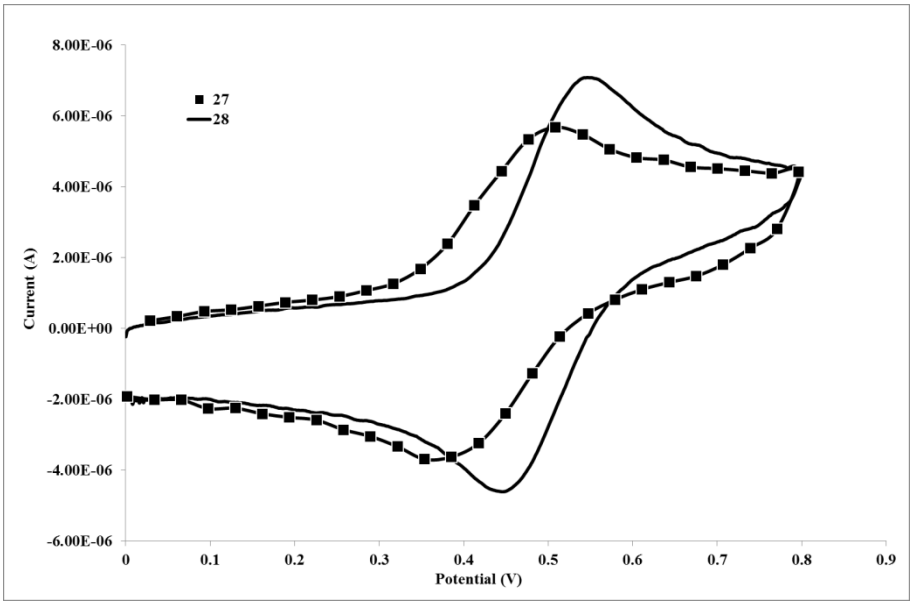

Figure 182. Cyclic voltammograms for Pd rods bridged by the longer ligands (**27** and **28**).

IV.5. Preparation and characterization of other compounds.

IV.5.1. *trans*-[RuCl(H)(dppe)$_2$] (34)

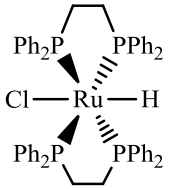

34

As discussed in Chapter II, compound **34** was obtained first serendipitously as a single crystal (**Method 1**). Tests were performed to access the viability of the hydride migration from methanol to the Ru centre (**Method 2**) and finally, the compound was prepared to complete all the characterization (**Method 3**).

Method 1:

trans-[RuCl(H)(dppe)$_2$], (**34**) was serendipitously obtained in a very small quantity as an unexpected product that resulted from the reaction of *cis*-[RuCl(dppe)$_2$][PF_6] with excess *t*-BuOK in methanol. Upon recrystallization of the reaction mixture from a mixture of dichloromethane and diethyl ether yellow crystals formed suitable for single crystal X-ray diffraction analysis. $^{13}C\{^1H\}$ NMR, FTIR spectroscopy and elemental analysis of the crystals were due to a minute amount of it, but the structure obtained from the crystal structure determination as well as the ^1H, ^{31}P NMR and ESI-MS (Ion trap) data unambiguously identified it as compound **34**.

^{1}H NMR (400 MHz, $CDCl_3$): δ = 7.39 – 6.97 (m, 40 H, P*Ph*$_2$), 2.59 and 2.05 (br., 8 H, PC*H*$_2$C*H*$_2$P), - 19.2 (quint, Ru*H*, $^2J_{(H,P)}$ = 19.4Hz) ppm;

$^{31}P\{^1H\}$ NMR (161 MHz, $CDCl_3$): δ = 62.7 (s) ppm;

ESI-MS (Ion Trap): *m/z* = 899.1 $[M - Cl]^+$, 949.0 $[RuCl(dppe)_2(O)]^+$, 1074.1 $[Ru(OMe)(dppe)+PF_6]^+$, 1269.2 $[Ru(C_{24}H_{34}O_2)(dppe)_2] + H_2O]^+$.

Method 2:

Small scale NMR experiment (in the NMR tube) was performed to support the hypothesis of reaction of *cis*-[RuCl(dppe)$_2$][PF_6] with methanol and *t*-BuOK as reported in Method 1. The reaction was performed in a 5 mm NMR tube using 600 μL of $CDCl_3$, 10 mg of *cis*-[RuCl(dppe)$_2$][PF_6] ($7.21x10^{-3}$ mmol) and 100 μL of methanol (24.71 mmol). To the same tube, 10 mg of *t*-BuOK ($8.9x10^{-2}$ mmol) was added in one portion prompting the immediate change in color from red to pale yellow and the formation of a small white precipitate. ^{31}P NMR analysis (161 MHz, $CDCl_3$): δ = 63.8 (br) ppm confirmed the formation of **34**.

^{31}P NMR (161 MHz, $CDCl_3$): δ = 63.8 (br) ppm;

Method 3:

Large scale synthesis in a Schlenk tube. A solution of 100 mg of *t*-BuOK (0.8 mmol) in 10 mL of MeOH was added *via* cannula to a solution of 200 mg of *cis*-[RuCl(dppe)$_2$][PF_6] (0.2 mmol) in 10 mL of $CHCl_3$ under argon atmosphere until the color of the *cis*-[RuCl(dppe)$_2$][PF_6]

solution changed completely from red to pale yellow and a white precipitate was formed. This took approximately 3 mL of the *t*-BuOK/MeOH solution and around 3 minutes. The mixture was then filtrated and the formed white precipitate was discarded. The solution was evaporated to dryness yielding a pale yellow crystalline solid (164 mg, 95%).

^{1}H NMR ($CDCl_3$): δ 7.39 – 7.07 (m, 40 H, P*Ph*$_2$), 2.59 and 2.05 (br., 8 H, PC*H*$_2$C*H*$_2$P), - 19.2 (quint, Ru*H*, $^{2}J_{(H,P)}$ = 19.4Hz) ppm.

^{31}P{^{1}H} NMR ($CDCl_3$): δ 63 ppm;

^{1}H NMR (CD_2Cl_2): δ 7.31 – 7.07 (m, 40 H, P*Ph*$_2$), 2.61 and 2.07 (br., 8 H, PC*H*$_2$C*H*$_2$P), - 18.9 (quint, Ru*H*, $^{2}J_{(H,P)}$ = 19.3Hz) ppm;

^{13}C{^{1}H} NMR (CD_2Cl_2): δ 133.7, 132.9, 128.2, 128.2, 126.8, 126.5, 31.9 ppm;

^{31}P{^{1}H} NMR (CD_2Cl_2): 63 ppm;

TOF-MS (ESI+): *m/z* = 899.211 $[M - Cl]^+$, 931.214 $[M - Cl + MeOH]^+$, 959.270 $[Ru(OMe)_2(dppe) - H]^+$, 1003.312 $[Ru(dppe)_2(Cl)(MeO) + K]^+$;

FTIR: $\tilde{\nu}$ = ν 3056 (w), 1974 (w), 1585 (m), 1486 (m), 1090 (m), 738 (s), 526 (s) cm^{-1};

Melting point = 270 ºC (decomp. in closed capillary);

EA: $C_{52}H_{49}ClP_4Ru$ (1144.90) : calcd. C 66.84, H 5.29; found: C 65.84, H 5.30.

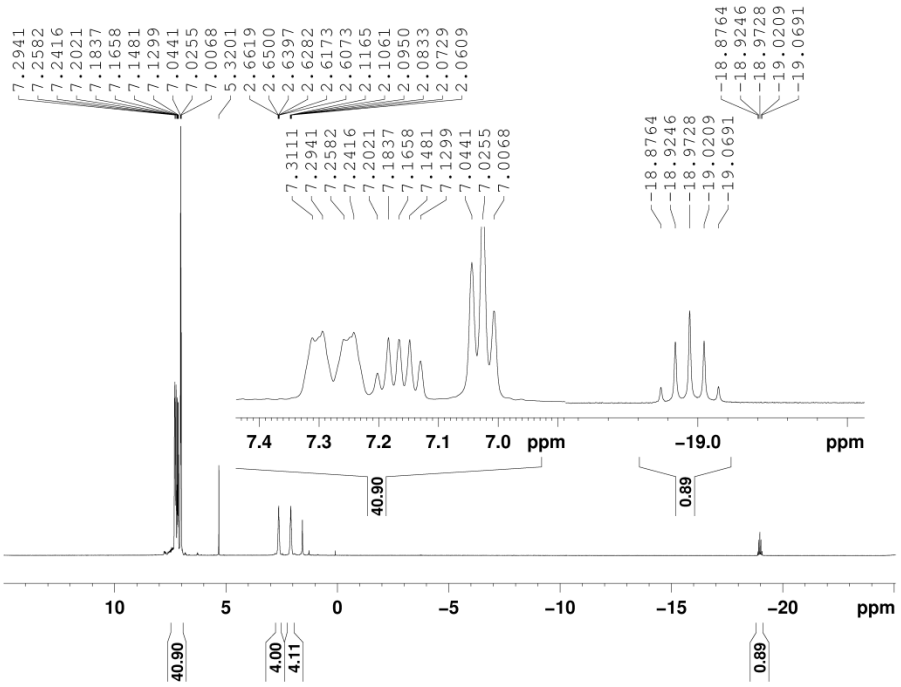

Figure 183. ^{1}H NMR (CD_2Cl_2, 400 MHz) of compound **34**.

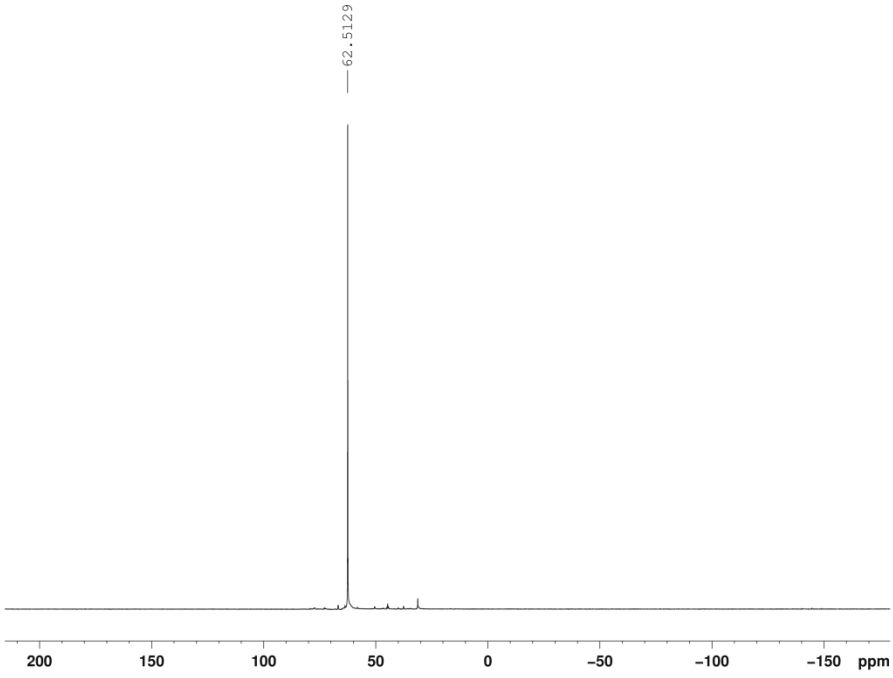

Figure 184. $^{31}P\{^{1}H\}$ NMR (CD_2Cl_2, 161 MHz) of compound **34**.

Annexes

A.1. Characterization techniques

A.1.1. UV-Vis spectroscopy

The UV-Vis studies (absorption spectra) were performed using a GBC-Cintra 40 double-beam UV-Vis spectrometer with 1 cm quartz stoppered cuvettes. Solutions were prepared using dry and argon degassed (with sonication) CH_2Cl_2 unless otherwise noted. The analysed samples did not exceed a maximum absorption of 1 u.a. which meant, for the studied samples, a concentration of $1x10^{-5}$ to $1x10^{-6}$M. Molar extinction (ε, $M^{-1}cm^{-1}$) was calculated in accordance to the Beer–Lambert law, $\varepsilon = \frac{A}{lC}$, where A is the absorption (u.a.), l is the cuvette length (1 cm) and C is the sample's concentration (M or mol dm^{-3}).

A.1.2. FTIR spectroscopy

The Infra-red spectra were collected using a Bruker Tensor 27 FTIR spectrophotometer equipped with an ATR (Attenuated Total Reflectance) add-on which permitted to use powder samples of the tested compounds without any requirement for a matrix. Samples were collected at a resolution of 2 cm^{-1} using a spectral range of 4000 to 400 cm^{-1}. For compounds **27** and **28**, KBr sample pellets were used in a Nicolet Avatar 360 FTIR spectrometer, calibrated with polystyrene.

A.1.3. NMR spectroscopy

NMR spectra plot were obtained and treated in Bruker's ® TopSin 3.2 ® software. ^{1}H, $^{13}C\{^{1}H\}$ and $^{31}P\{^{1}H\}$ NMR spectra were recorded with a Bruker Avance II+ 400 at 299 K (probe temperature) at 400, 100 and 161 MHz. The chemical shifts (δ) are reported in ppm and referenced to residual solvent peaks for ^{1}H and ^{13}C. ^{31}P NMR is referenced to external 85% H_3PO_4.

A.1.4. MS spectroscopy

ESI-TOF spectra were collected with a Micro-mass LCT spectrometer by direct infusion of a Methanol/CH_2Cl_2 solution prepared in the following manner: very low concentration 1 mL solution of the sample (0.5 mg for 1mL) was prepared in CH_2Cl_2 as the stock solution; dilution of 50µL of this sample in 1mL of methanol was then prepared and injected. The methanol contained 0.1% of formic acid. The same sample preparation was used for the MS Ion trap acquisition on a Bruker Esquire 6000. ESI-TOF samples were collected in Jyväskylä by Mirja Lahtiperä or by the author. ESI-Ion trap was run in CQM by Dr. Ying Lu.

A.1.5. Cyclic voltammetry

The cyclic voltammetry studies were performed by Prof. José Carlos Mesquita (CQM). The voltammograms are presented at 100 mV s^{-1} and were collected starting at 0.0 V unless otherwise noted. Half-wave potentials were calculated based on the following equation:[259]

$$E_{1/2} = \frac{E_{pc} + E_{pa}}{2}$$

A sample concentration of 1×10^{-3} M in dry and degassed (N_2) CH_2Cl_2 was used and the support electrolyte was NBu_4PF_6 at 0.1 M For the working electrode, a platinum disk was used. The reference electrode was Ag/AgCl saturated in KCl. Finally, the secondary electrode was also platinum, in this case a platinum flag with a surface area larger than that of the working electrode and all tests were carried out at room temperature (*ca.* 20 ºC). Table values may also include data referenced to the ferrocene (Fc) half-wave potential which was determined through the analysis of several voltammograms (in solution with just support electrolyte) various scan rates..

A.1.6. Single crystal X-ray diffraction

The data collection, structure resolving and refining, either performed by the author, by Acad. Prof. Kari Rissasen, Dr. Kalle Nättinen, Dr. Luca Russo or Dr. Arto Valkonen, which

were or are still working in the department of chemistry in Jyväskylä University. A collection of suitable crystals were usually sent from the University of Madeira by mail and sorted in Finland.

Collection was performed using a Nonius KappaCCD diffractometer at 123(2) K with Mo *K*α radiation. All displacement ellipsoids are represented at 50% probability unless otherwise noted in the plot's caption.

A.1.7. Fluorescence decay studies

The samples were measured Prof. Fernando Lahoz, at La Lagun University (Tenerife, Spain) in the form of powder by putting them between two microscope slides. The measurements were then performed using LifeSpec II Spectrophotometer with a pulsed 406 nm diode laser with 80 ps of pulse duration as the excitation source. Furthermore, measurements were performed in different days and sometimes with different excitation wavelengths. Moreover, as the powders did not present all the same particle size and sample size was different, integrated fluorescence spectra can only be compared by orders of magnitude of difference. Samples are compared in accordance to their times of life which is independent of the factors referred above.

A.1.8. Elemental Analysis

Elemental analyses were carried out by using a VariolEL instrument from Elementar Analysensysteme with three samples of at least 3 mg at the University of Jyväskylä, Finland.

A.1.9. Melting point determination

Melting points were obtained with Electrothermal 9200 equipment using sealed capillary tubes unless otherwise noticed.

A.2. General experimental procedures

A.2.1. Williamson substitution

In a double necked flask, degassed DMSO was inserted, followed by the ground KOH (high excess, *ca.* 10 eq). Hydroquinone was then added to this KOH suspension and dissolved readily. The alkyl bromide was finally added and the mix was allowed to stir at r.t., under positive pressure of nitrogen for 3-4 hours. The mixture was then filtrated and water was added to the resulting solution prompting the precipitation of the desired alkoxybenzene which was further washed with water to remove any remaining DMSO and then recrystallized from hot EtOH. Adapted from ref. [130].

A.2.2. Iodination of the 1,4-bis(alkoxy)benzenes

The starting dialkoxybenzene (*e.g.* 1,4-diethoxybenzene, limiting reagent) is added to a three-necked flask that contained glacial acetic acid (enough to dissolve the starting material). KIO_3 (0.2 eq per reaction site) and I_2 (1 eq). Finally, concentrated sulphuric acid (excess, *ca.* 6mL) is added to the mix, which is then left under reflux overnight. Constant stirring and positive nitrogen pressure are always maintained. It is then left to cool down to room temperature. Sodium thiosulfate ($Na_2S_2O_3$) is added to remove the unreacted iodine and followed by extraction with CH_2Cl_2. This organic phase is then re-washed with a solution of $Na_2S_2O_3$, water and finally dried off with Na_2SO_4. Filtration through a celite/silica plug is performed before column chromatography is started (Neutral Silica Gel and a gradient of *n*-hexane/CH_2Cl_2 starting from pure *n*-hexane). Adapted from ref. [130].

A.2.3. Bromination of the 1,4-bis(alkoxy)benzenes

Typical acid catalyzed bromination was performed on dialkoxybenzenes. The starting dialkoxybenzenes are suspended in glacial acetic acid and a solution of Br_2 (2 eq, also in glacial acetic acid) is added *via* an addition funnel. The mix is left to stir overnight. Sodium thiosulfate

($Na_2S_2O_3$) is added to remove the unreacted bromine and then extraction with CH_2Cl_2 follows. This organic phase was re-washed with a solution of $Na_2S_2O_3$, water and finally dried off with Na_2SO_4. Filtration through a celite/silica plug is performed before the column chromatography (Neutral Silica Gel and a gradient of *n*-hexane/CH_2Cl_2 starting from pure *n*-hexane). Adapted from ref. [211].

A.2.4. Sonogashira coupling reactions

The halogenated starting material(*e.g.* 1,4-diethoxy-2,5-dibromobenzene, limiting reagent) and the palladium Catalyst (5% eq) are introduced to the Schlenk and left under vacuum for 30 min. Addition of the solvent (THF) and base ($NHEt_2$ or NEt_3) follows in a 1:1 ratio until the limiting reagent is completely dissolved. CuI (10% eq.) is then added in one portion and vigorous stirring is initiated. TMSA or 2-methyl-3-butyn-2-ol, (1.1 eq by reaction site on the halogenated material) is then added drop-wise to the mix. A final purging is performed before rising the temperature (if necessary) to 45 ºC for iodinated starting materials or to 55 ºC for brominated starting materials. The reaction is generally left overnight under a positive pressure of nitrogen and protected from sun light. The solvent is then removed under reduced pressure (normally using the rotary evaporator) and the resulting solid is re-dissolved in CH_2Cl_2 and washed with a solution of NH_4Cl. Washing with water followed by drying of the organic phase with Na_2SO_3 precedes the column chromatography which is performed using Neutral Silica Gel and a gradient of *n*-hexane/CH_2Cl_2 (starting from pure *n*-hexane). Based on the work of Tour and modified according other reports.[130, 142, 198, 210, 212-214]

A.2.5. Deprotection of "Acetone Protected" ligands

Protected starting material (*e.g.* 1,4-bis(3-hydroxy-3-methylbut-1-ynyl)-2,5-diethoxybenzene) is dissolved in dry toluene. Ground KOH is added and the mix is left under reflux overnight. Before the toluene cools down to r.t., filtration is performed (through a sintered glass disc funnel). It is then evaporated and the resulting solid is re-dissolved in *n*-hexane and filtered through a celite/silica plug. If further purification is required, a small flash

chromatography using neutral silica gel and *n*-hexane is performed. Adapted from ref. [142, 214, 221a].

A.2.6. Deprotection of trimethylsilyl protected ligands

Protected starting material (*e.g.* 1,4-bis(trimethylsilylethynyl)-2,5-diethoxybenzene) is dissolved in a degassed mix of CH_2Cl_2/MeOH (1:1, dried solvents aren not required). K_2CO_3 is then added (high excess is usually used, *ca.* 6 eq) for the single PEs. KF (same eq)[215] is preferred for the tris-ringed PEs. The reaction is normally run overnight for the longer PEs to make sure it is finished. The mix is then filtered through a celite/silica plug which generally is enough to yield the pure compound. Further purification is achieved with a small flash chromatography using neutral silica gel and *n*-hexane. Adapted from ref. [130, 142, 198, 210, 212-214].

A.2.7. Palladium binuclear complexes.

Both the free ligand and the starting complex $[PdCl_2(PEt_3)_2]$ are loaded into the Schlenk and left under vacuum for 30min prior to vacuum/nitrogen purging. The base (acting also as solvent), diethylamine, is then introduced using a syringe and another purge is performed. The CuCl is finally added to the mix under positive pressure of nitrogen and the reaction is left to progress during the night. Volatiles are removed under reduced pressure (oil pump) and the solid is re-dissolved in CH_2Cl_2 and then washed with a saturated aqueous solution of NH_4Cl and finally with water. The organic phase is dried with Na_2SO_4 and the solid is precipitated by adding diethyl ether. Adapted from ref. [222a].

A.2.8. Ruthenium phenylene ethynylene binuclear rods.

Freshly prepared $[RuCl(dppe)_2][PF_6]$ (1.1 eq by terminal alkynyl on the free ligand) was loaded into a Schlenk. THF is then added dissolving most of the starting material. The free ligand (*e.g.* 1,4-diethynyl-2,5-diethoxybenzene) is then added and a dark reddish suspension is

formed. The mix is left to react overnight and then *t*-BuOK (1.1 eq by terminal alkynyl on the free ligand) is added in one portion prompting the immediate color change of the mix to dark orange. Solvent is removed under vacuum (oil pump) and washed with MeOH/CH_2Cl_2 (30:1) until the ^{31}P NMR signal is free of the starting material which usually coincides with the disappearance of the red color from the washing fractions. Adapted from refs. [16, 66f, 224b, 289].

A.2.9. Ruthenium thiophenylene ethynylene binuclear rods.

The free ligand is dissolved in dry diethyl ether and the solution is cooled down with an EtOH/Liquid nitrogen bath. *t*-BuLi (1 eq per alkynyl site) is added drop-wise to the solution forming a dark brown mix. A freshly prepared solution [RuCl(dppe)$_2$][OTf] (OTf = Trifluoromethanesulfonate, 1.1 eq by terminal alkynyl on the free ligand, in dry CH_2Cl_2, prepared freshly from AgOTf and *cis/trans*-[$RuCl_2$(dppe)$_2$] as in Annex A.3.5) is then added *via* cannula. The mix is left to react overnight. It is then filtrated and concentrated. *n*-hexane is added to precipitate the resulting orange solid. Adapted from refs. [235-237].

A.3. Preparation of general starting materials

A.3.1. $RuCl_2(DMSO)_4$ (DMSO = dimethylsulfoxide)

$RuCl_3.xH_2O$ (3 g) is loaded in a 3-necked flask under positive pressure of nitrogen. Addition of degassed DMSO (*ca.* 100 mL), forms a dark red solution which is brought to reflux (140º) and kept at that temperature for 4h. The resulting red solution is concentrated under vacuum (oil pump) and dry acetone is added to precipitate the product which is filtrated and washed with cold acetone. Usual reaction yield for 3g of starting salt is around 5 g of the $RuCl_2(DMSO)_4$ (*cis*-dichlorotetrakis(dimethyl sulfoxide)ruthenium(II)).[290]

A.3.2. *cis*-[$RuCl_2(dppe)_2$]

$RuCl_2(DMSO)_4$ (500 mg, 1 mmol) is dissolved in 10 mL of CH_2Cl_2 forming an orange solution to which another solution of dppe (1,2-bis(diphenylphosphino)ethane, also in CH_2Cl_2) is added *via* cannula. The resulting mix is left to stir for approximately 1h before removing the solvent. The resulting yellow solid is washed twice to remove excess phosphine and re-dissolved in CH_2Cl_2. Filtration (also using a cannula) is performed before adding about half the amount (in volume, relative to CH_2Cl_2) of *n*-hexane. The biphasic mix is left at -20 ºC until a good amount of yellow precipitate is formed. This solid is filtrated and the mother liquor is loaded with more *n*-hexane. This process is repeated until the filtrate starts showing ^{31}P NMR signals of the *trans* isomer. Obtained yellow powder (322 mg, 31.2 %). Adapted from ref. [291].

$^{31}P\{^1H\}$ NMR ($CDCl_3$): 53.02 (t, $J_{P,P}$ = 14.7 Hz), 38 (t, $J_{P,P}$ = 14.7 Hz) ppm.

A.3.3. *trans*-[$RuCl_2(dppe)_2$]

The *trans* isomer of *cis*-[$RuCl_2(dppe)_2$] was obtained from the later fractions of the purification process used to obtain the *cis* isomer, as explained in Annex A.3.2 or by the a modified procedure.[224c]

$^{31}P\{^1H\}$ NMR ($CDCl_3$): 44.05 (s) ppm;

A.3.4. $TlPF_6$

$Ba(OH)_2.8H_2O$ (3.23 g; 10.2 mmol) was completely dissolved in 50 mL of distilled water that was heated to boiling point in a two necked flask. $TlSO_4$ (5.3 g, 17.6 mmol) was dissolved separately in a 100 mL by the same heating method. The $TlSO_4$ was added, under vigorous stirring and heating, to the $Ba(OH)_2$ solution immediately forming a white precipitate. The mix was left under stirring for another 2h before turning both the stirring and heating off during the night. Stirring and heating was once again restarted and NH_4PF_6 (3.36 g, 20.6 mmol) was added. After 10 min, stirring and heating were stopped and the mix was left that way for

another 2 h. The white precipitate was removed by filtration and the aqueous solution was evaporated to yield the pure $TlPF_6$ (4.86 g, 79.1 %).

A.3.5. *cis*-[RuCl(dppe)$_2$][PF$_6$]

Initially prepared from pure *cis*-[$RuCl_2(dppe)_2$], [$RuCl(dppe)_2$][PF_6] started to be prepared from the *cis*/*trans* mix obtained from the preparation of *cis*-[$RuCl_2(dppe)_2$] (before separation of the isomers by crystallization). As such, the *cis*/*trans* mix (4.5 g, 4.64 mmol) is dissolved in *ca.* 20mL of CH_2Cl_2 forming a pale yellow solution. $TlPF_6$ (1.95 g, 5.57 mmol) is then added and the mix is heated to reflux during the night to ensure full reaction. The now dark red mix is left to cool down to room temperature before filtration is performed (cannula). The resulting solution is concentrated under vacuum to half volume and n-hexane is added to precipitate the desired compound (4.45 g, 89.1%). Adapted from ref. [225].

^{31}P{^{1}H} NMR ($CDCl_3$): 84.61 (t, $J_{P,P}$ = 12.1 Hz), 57.3 (t, $J_{P,P}$ = 12.3 Hz), -143.58 (hept, $J_{P,P}$ = 711.4 Hz) ppm;

A.4. NMR Studies

A.4.1. Free ligands

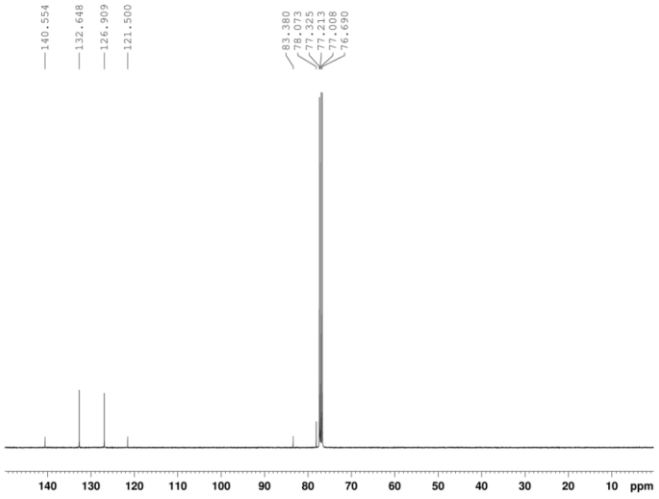

Figure A. 1: $^{13}C\{^1H\}$ NMR($CDCl_3$, 100 MHz) spectrum of **5a**.

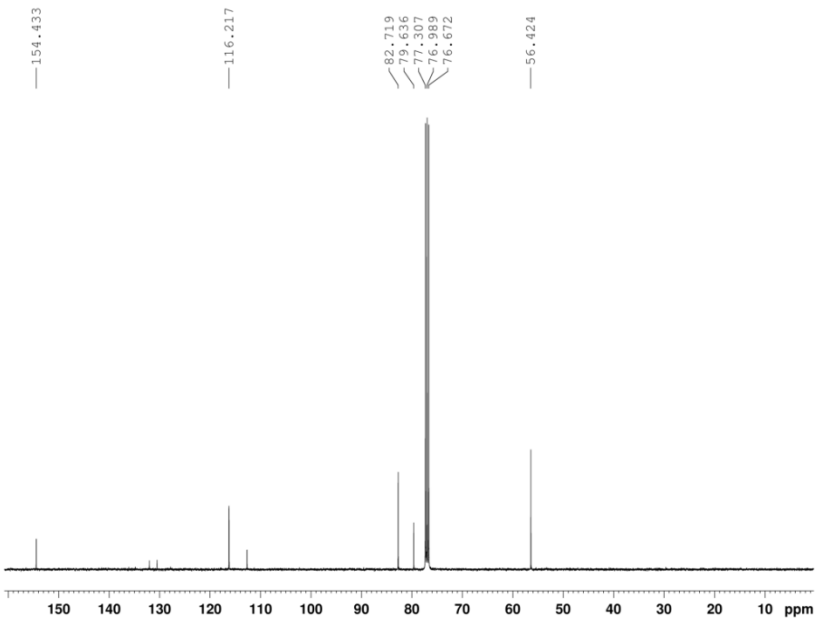

Figure A. 2: $^{13}C\{^{1}H\}$ NMR($CDCl_3$, 100 MHz) spectrum of **5b**.

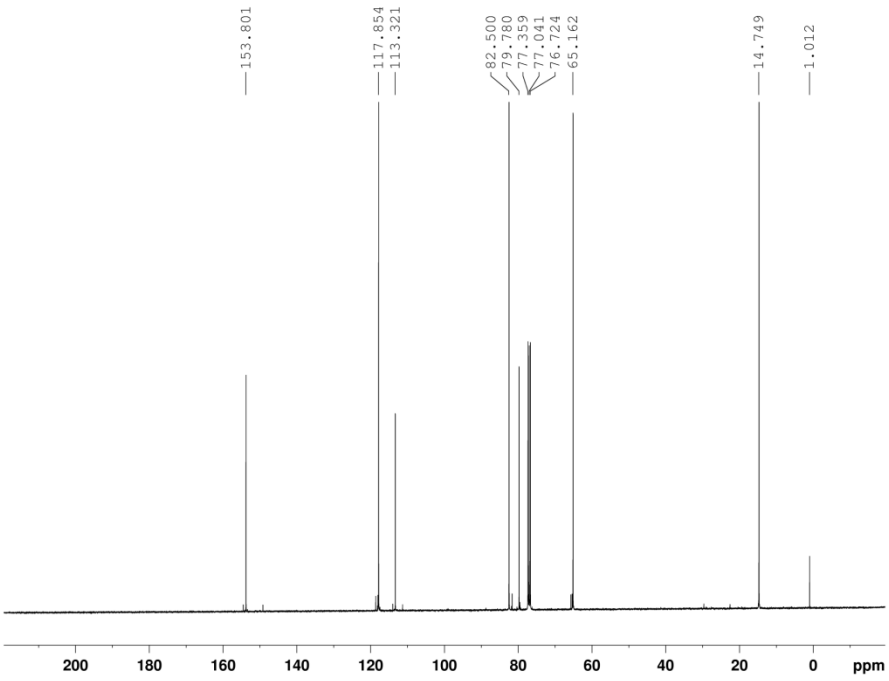

Figure A. 3: $^{13}C\{^{1}H\}$ NMR($CDCl_3$, 100 MHz) spectrum of **5c**.

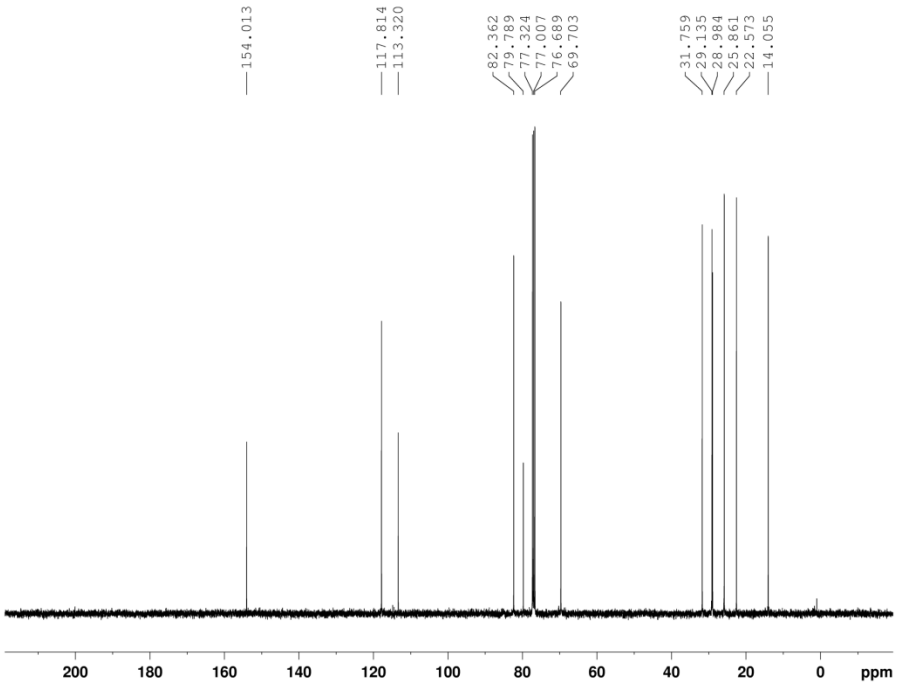

Figure A. 4: $^{13}C\{^{1}H\}$ NMR($CDCl_3$, 100 MHz) spectrum of **5d**.

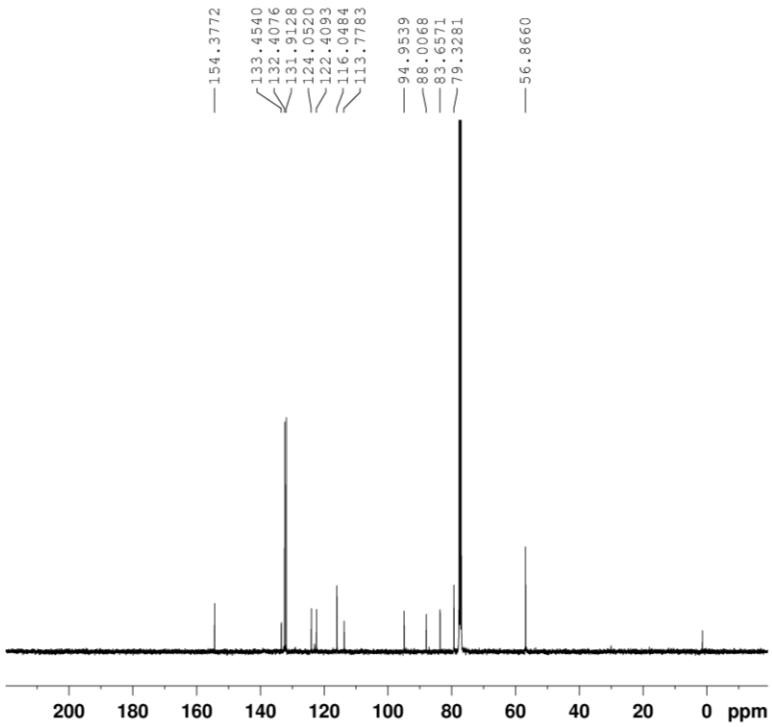

Figure A. 5: $^{13}C\{^{1}H\}$ NMR($CDCl_3$, 100 MHz) spectrum of **10a**.

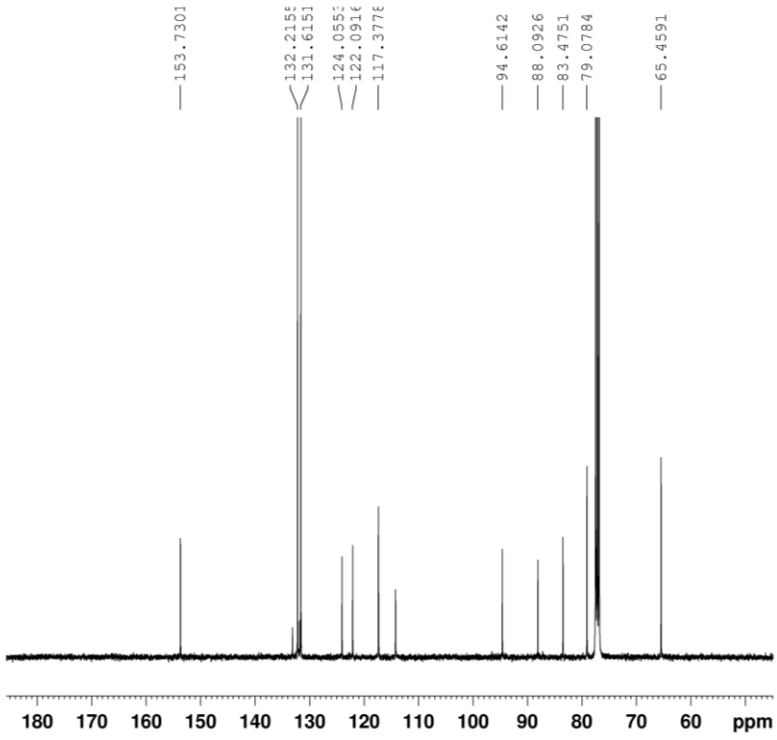

Figure A. 6: $^{13}C\{^{1}H\}$ NMR($CDCl_3$, 100 MHz) spectrum of **10b**.

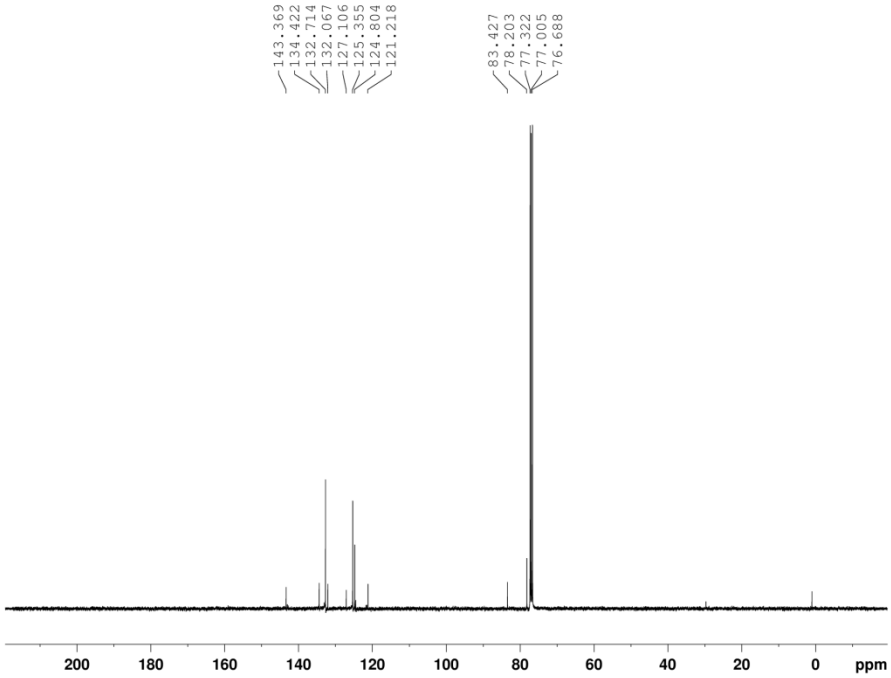

Figure A. 7: $^{13}C\{^{1}H\}$ NMR($CDCl_3$, 100 MHz) spectrum of **14b**.

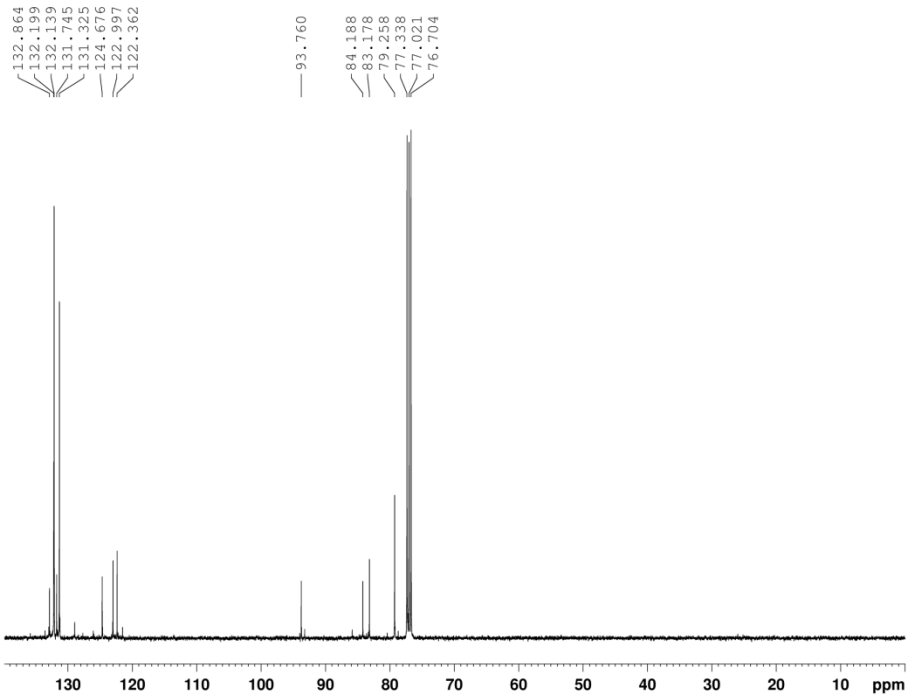

Figure A. 8: $^{13}C\{^{1}H\}$ NMR($CDCl_3$, 100 MHz) spectrum of **18b**.

A.4.2. Palladium rods

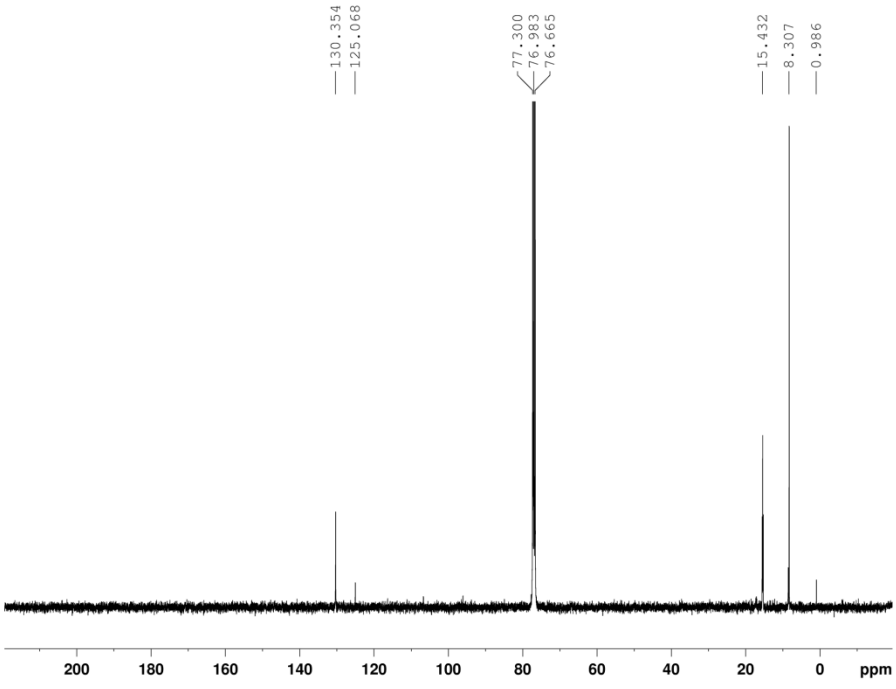

Figure A. 9: $^{13}C\{^{1}H\}$ NMR($CDCl_3$, 100 MHz) spectrum of **20a**.

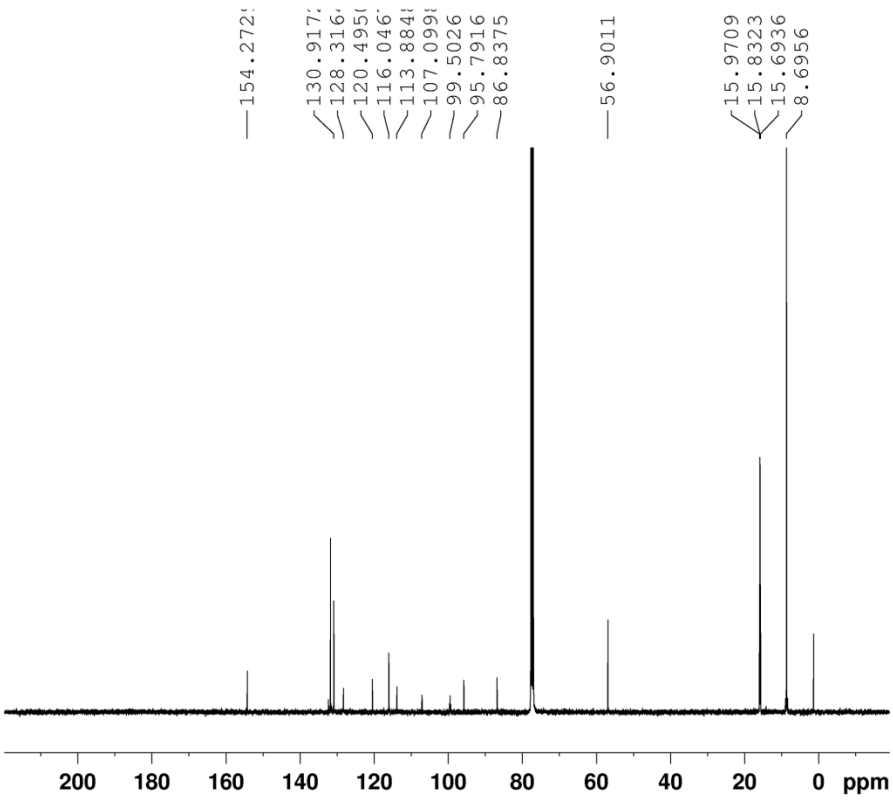

Figure A. 10: $^{13}C\{^{1}H\}$ NMR($CDCl_3$, 100 MHz) spectrum of **20b**.

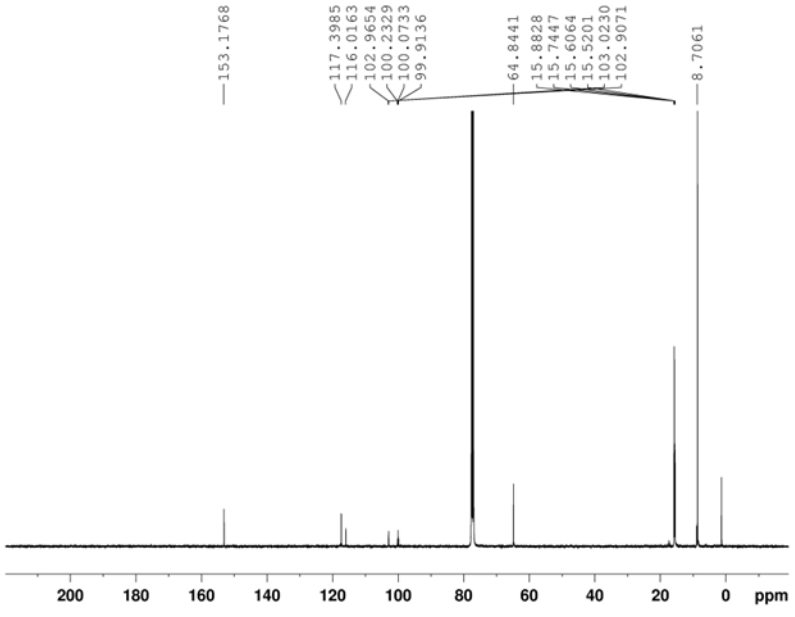

Figure A. 11: $^{13}C\{^{1}H\}$ NMR($CDCl_3$, 100 MHz) spectrum of **20c**.

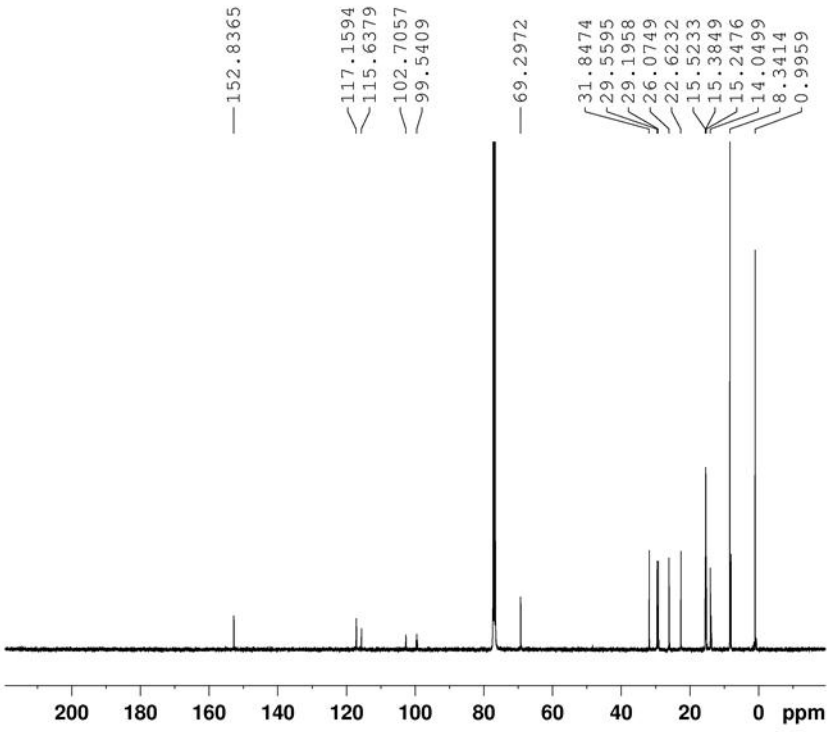

Figure A. 12: $^{13}C\{^{1}H\}$ NMR($CDCl_3$, 100 MHz) spectrum of **20d**.

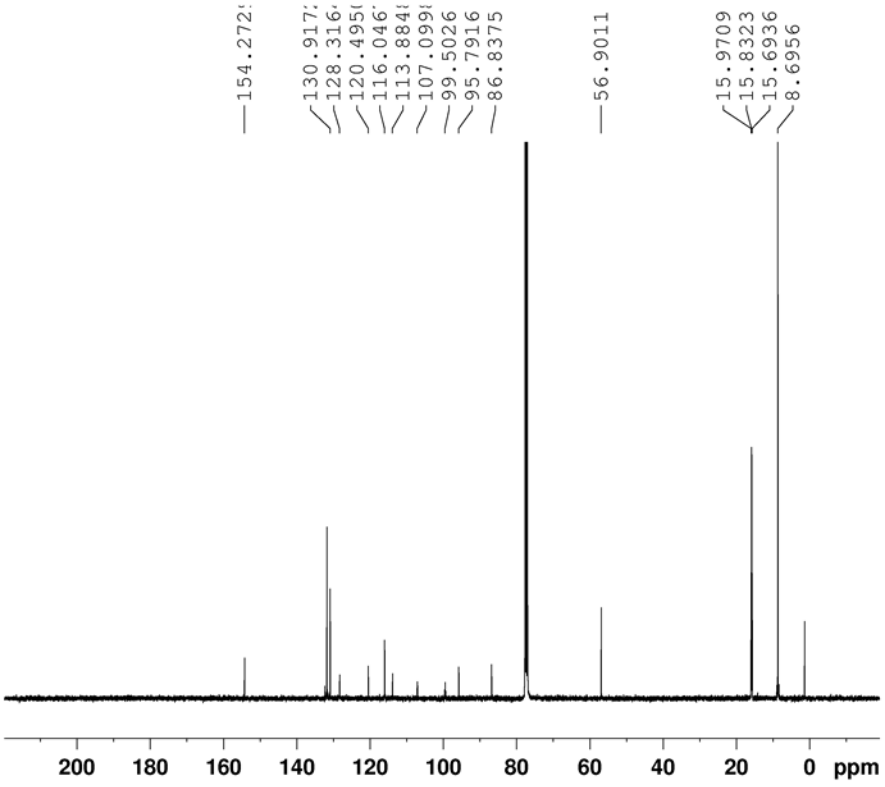

Figure A. 13: $^{13}C\{^{1}H\}$ NMR($CDCl_3$, 100 MHz) spectrum of **21a**.

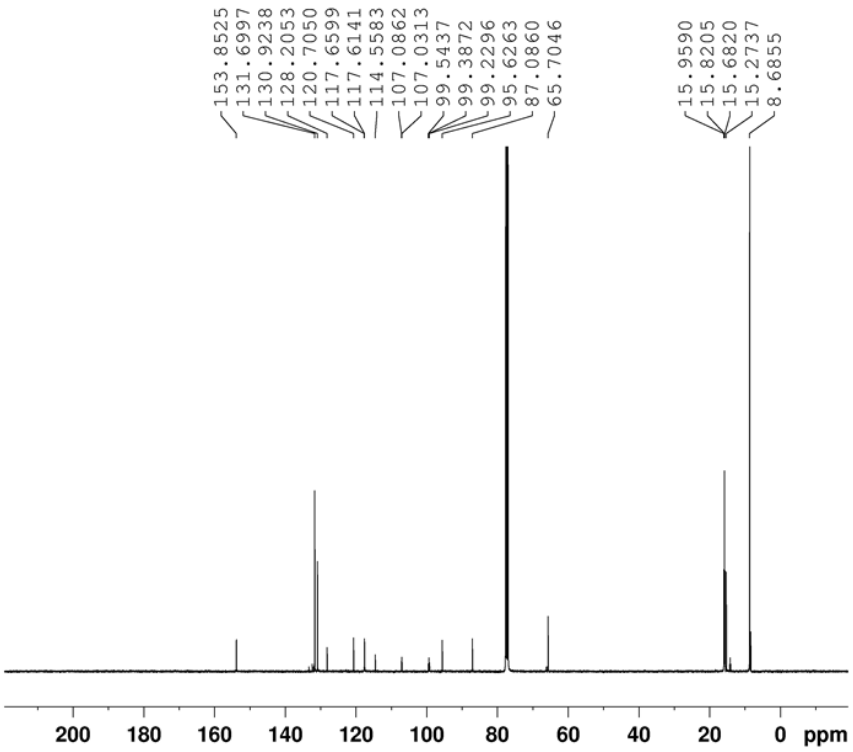

Figure A. 14: $^{13}C\{^{1}H\}$ NMR($CDCl_3$, 100 MHz) spectrum of **21b**.

A.4.3. Ruthenium rods

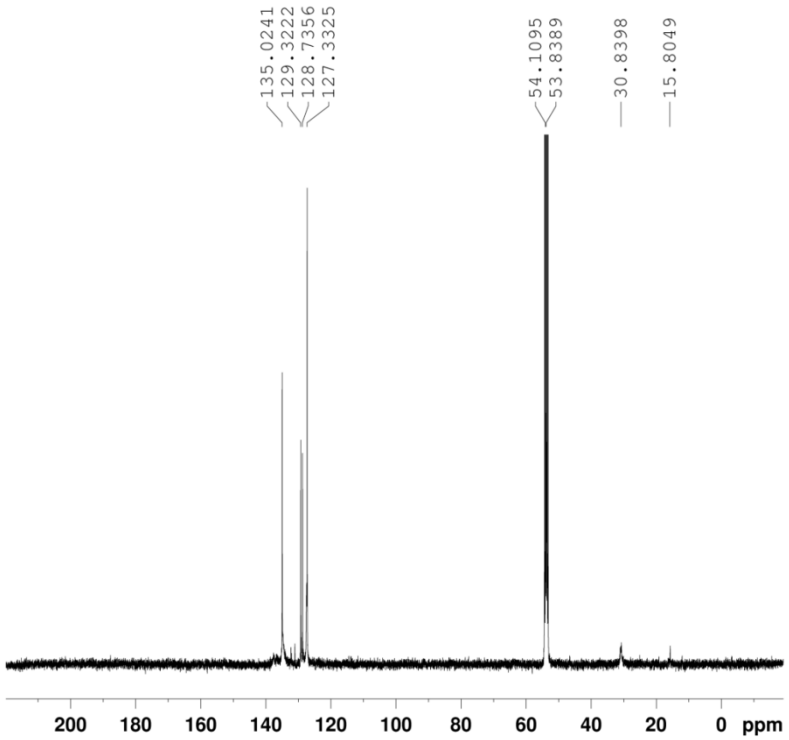

Figure A. 15: $^{13}C\{^{1}H\}$ NMR(CD_2Cl_2, 100 MHz) spectrum of **23c**.

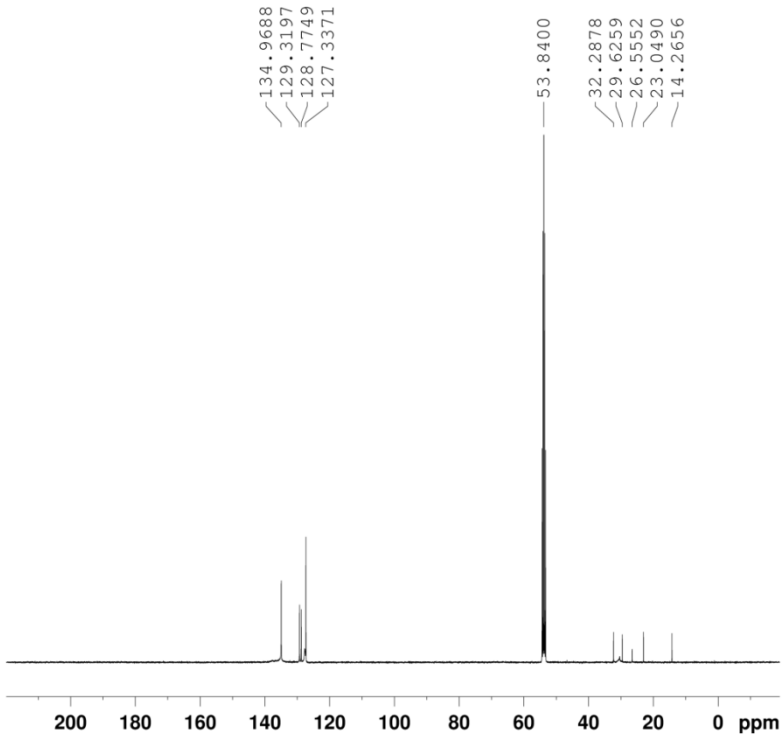

Figure A. 16: $^{13}C\{^{1}H\}$ NMR(CD_2Cl_2, 100 MHz) spectrum of **23d**.

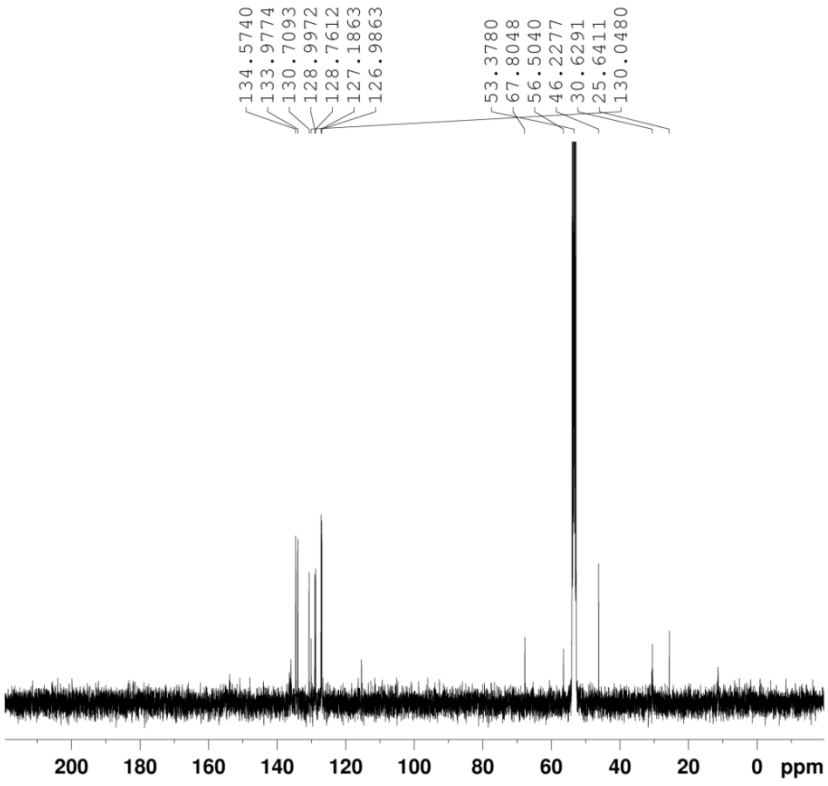

Figure A. 17: $^{13}C\{^{1}H\}$ NMR(CD_2Cl_2, 100 MHz) spectrum of **24a**.

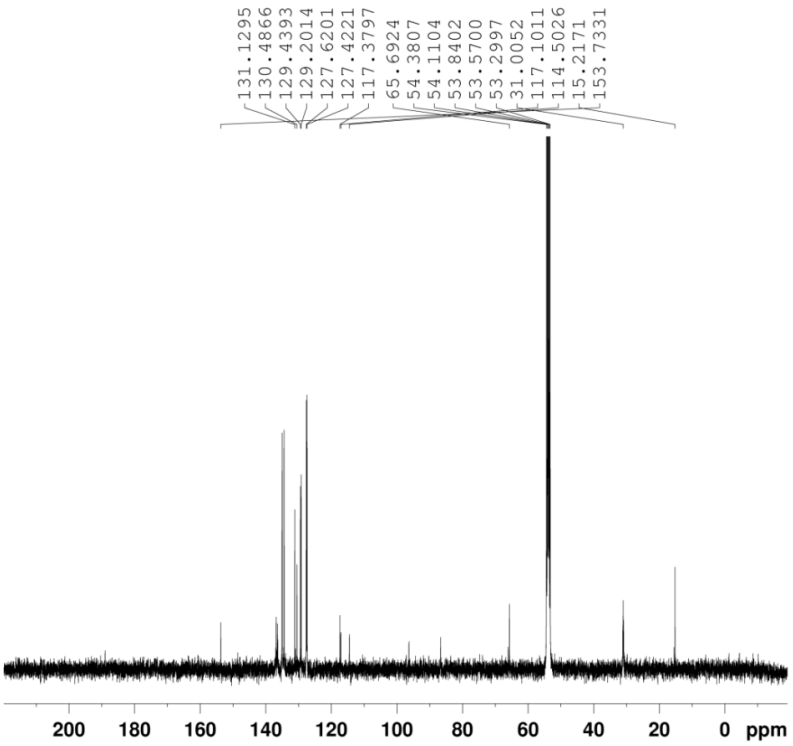

Figure A. 18: $^{13}C\{^{1}H\}$ NMR(CD_2Cl_2, 100 MHz) spectrum of **24b**.

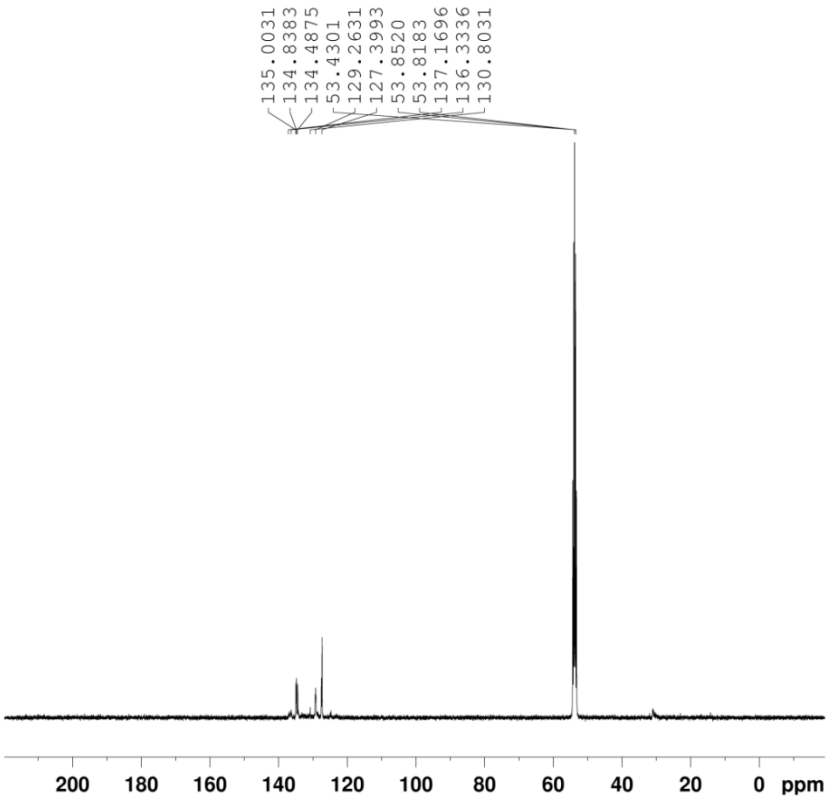

Figure A. 19: $^{13}C\{^{1}H\}$ NMR(CD_2Cl_2, 100 MHz) spectrum of **27**.

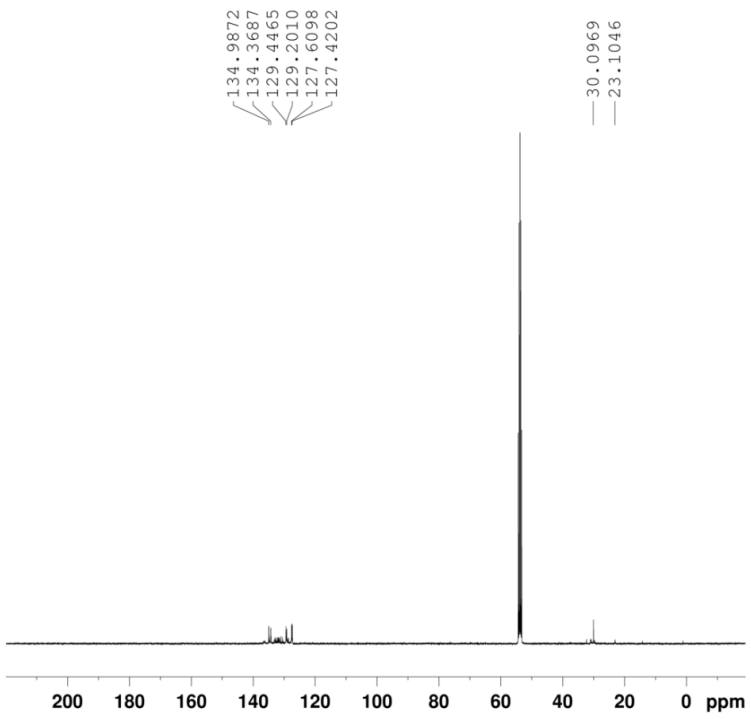

Figure A. 20: $^{13}C\{^{1}H\}$ NMR(CD_2Cl_2, 100 MHz) spectrum of **28**.

A.5. MS Studies

A.5.1. Free ligands

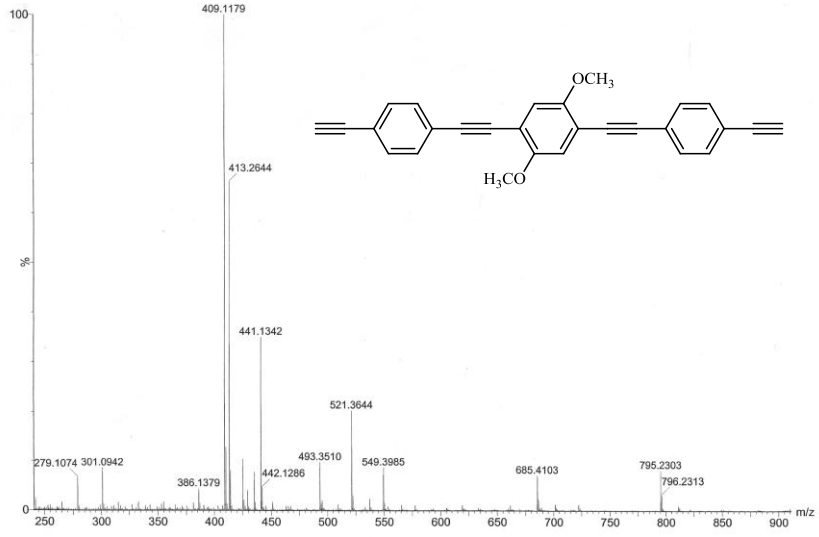

Figure A. 21: ESI-MS(TOF+) spectrum of **10a**.

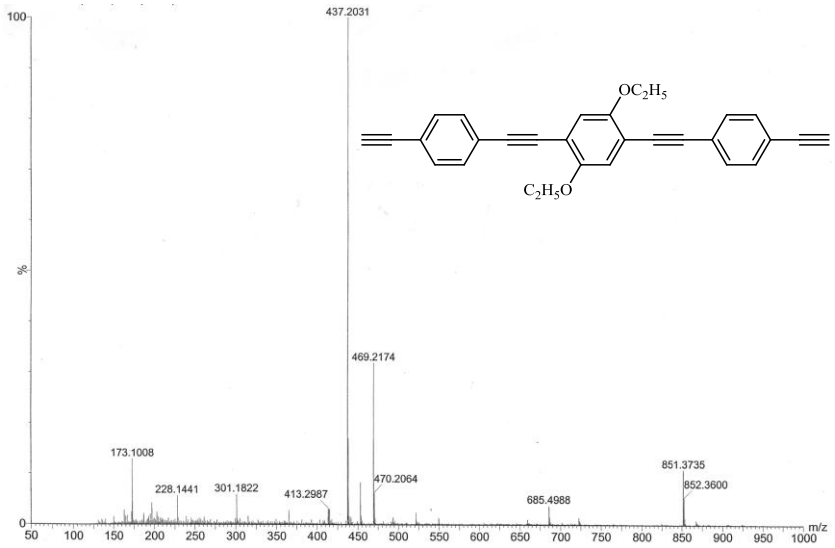

Figure A. 22: ESI-MS(TOF+) spectrum of **10b**.

A.5.2. Palladium rods

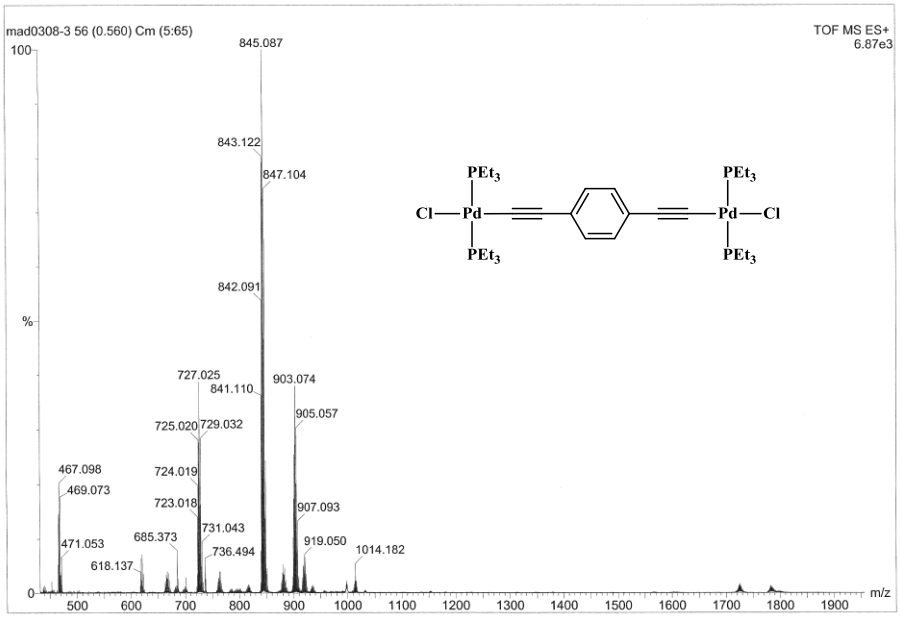

Figure A. 23: ESI-MS(TOF+) spectrum of **20a**.

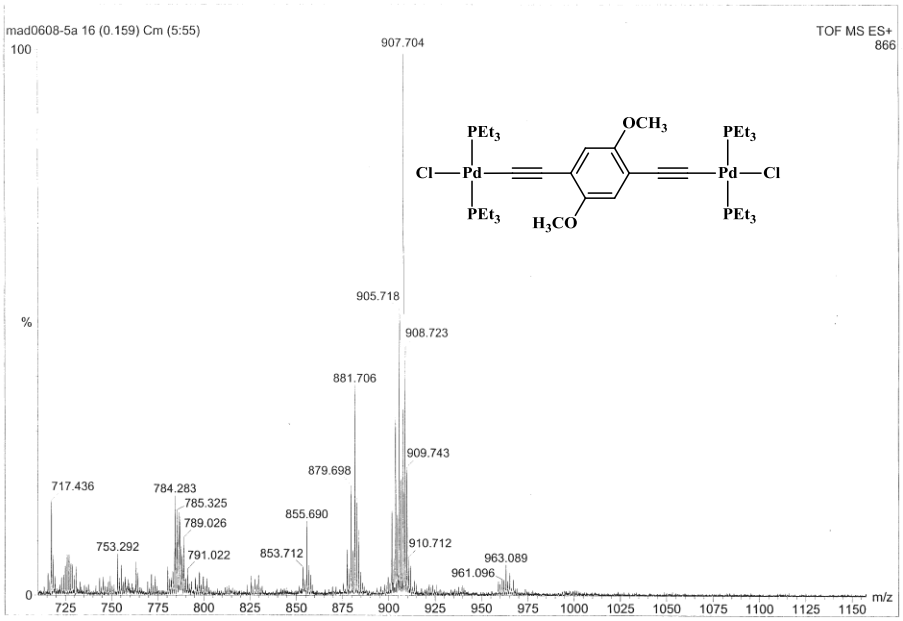

Figure A. 24: ESI-MS(TOF+) spectrum of **20b**.

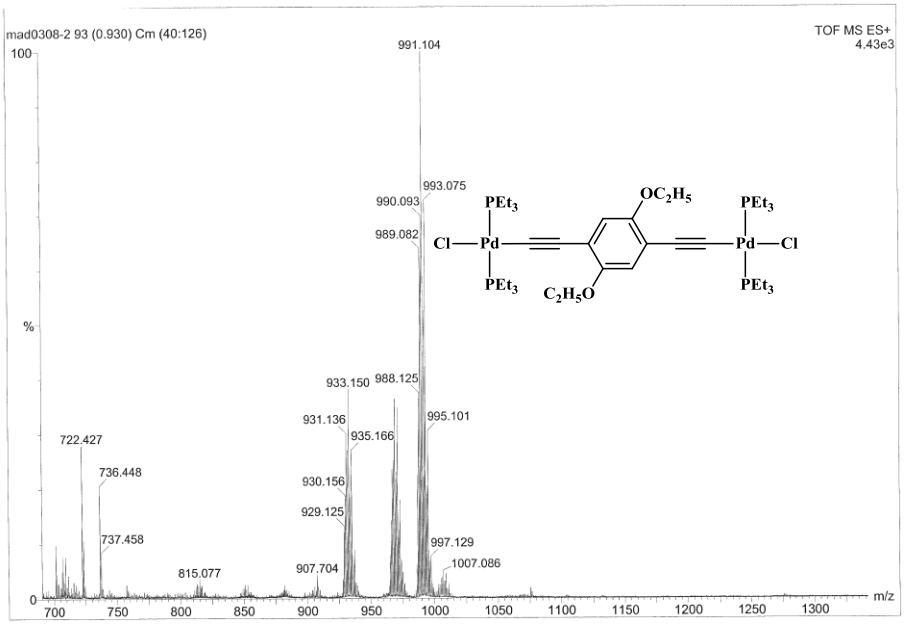

Figure A. 25: ESI-MS(TOF+) spectrum of **20c**.

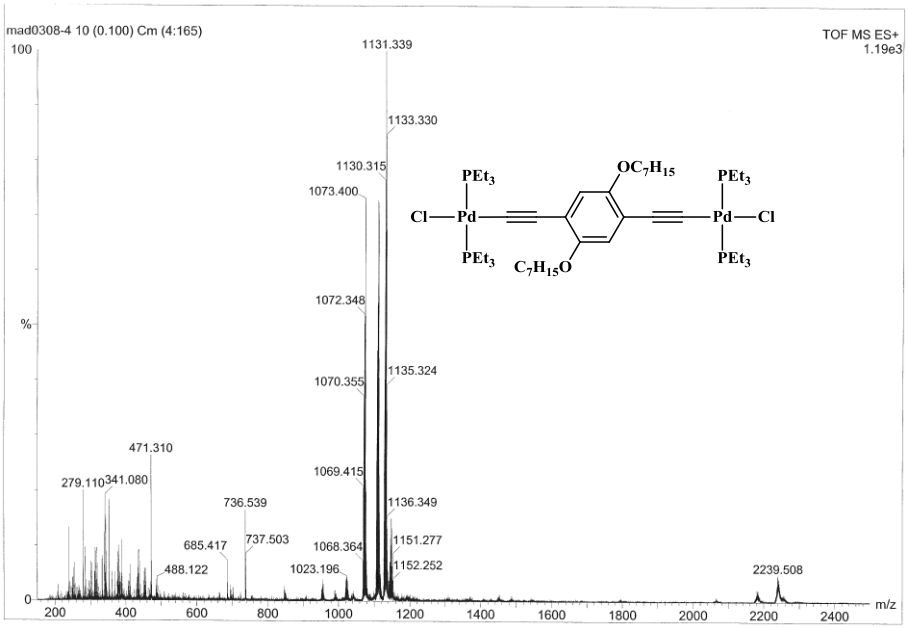

Figure A. 26: ESI-MS(TOF+) spectrum of **20d**.

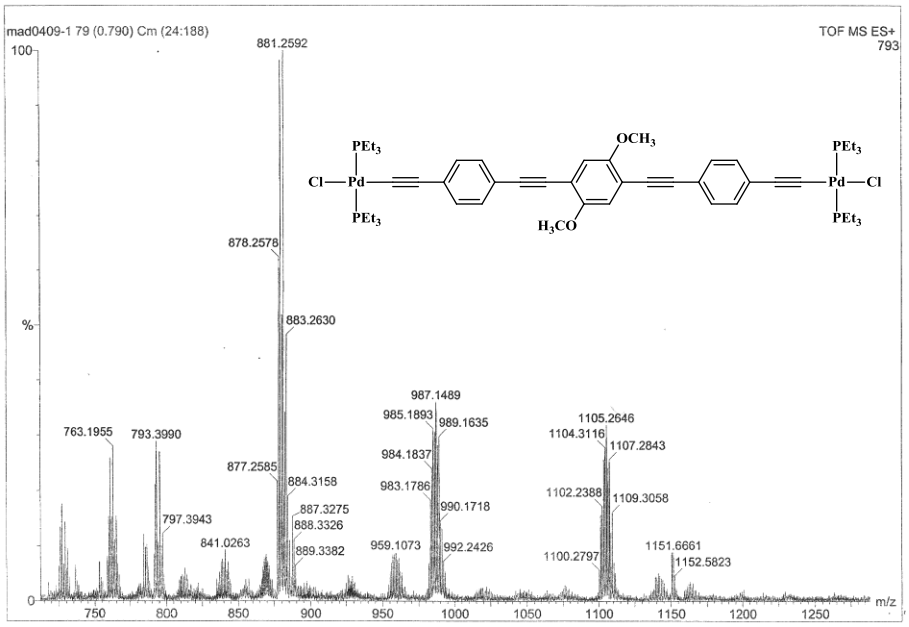

Figure A. 27: ESI-MS(TOF+) spectrum of **21a**.

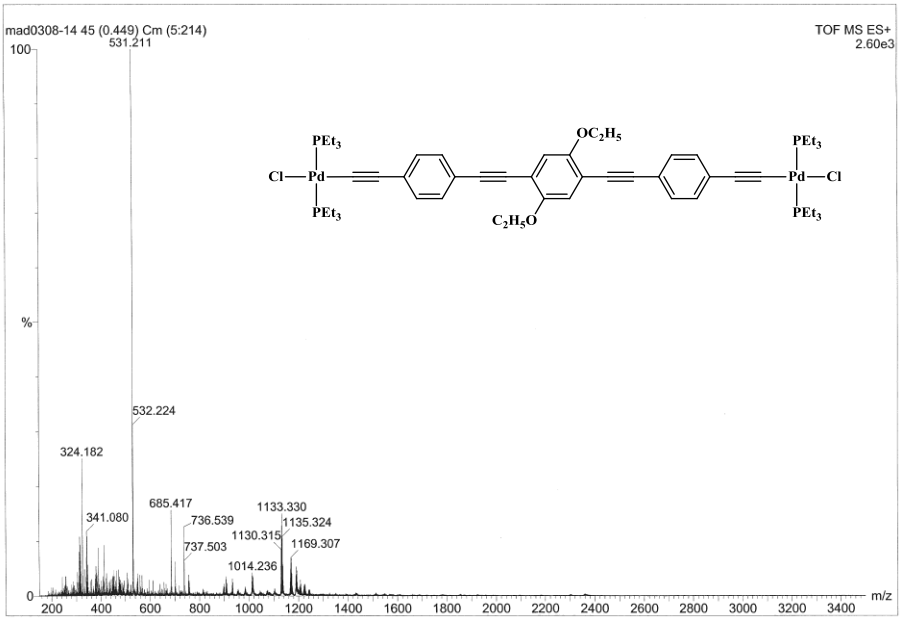

Figure A. 28: ESI-MS(TOF+) spectrum of **21b**.

A.5.3. Ruthenium rods

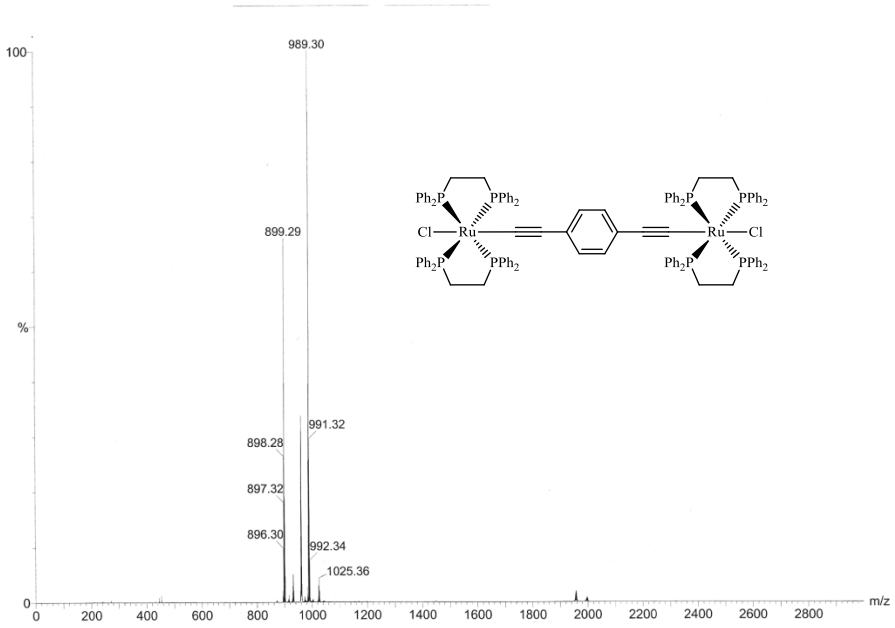

Figure A. 29: ESI-MS(TOF+) Spectrum of **23a**.

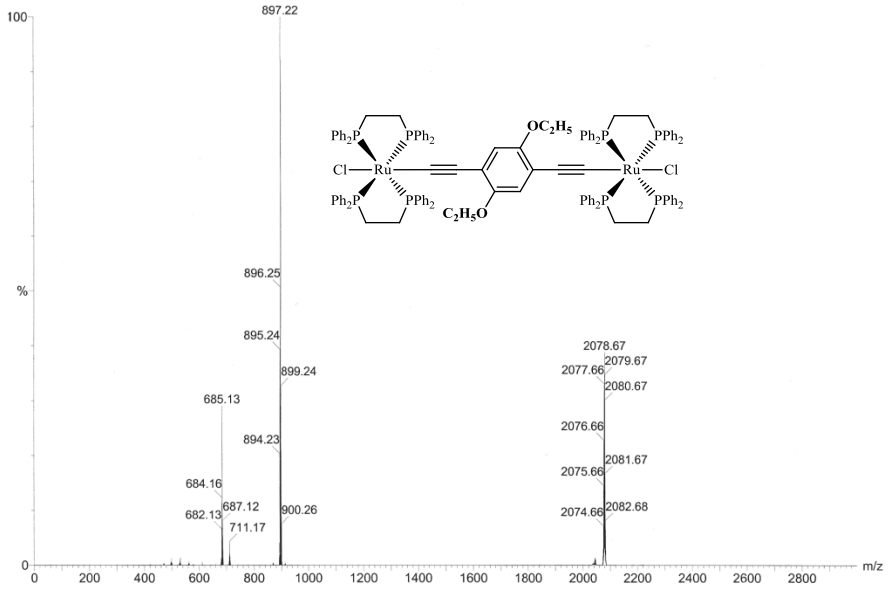

Figure A. 30: ESI-MS(TOF+) Spectrum of **23c**.

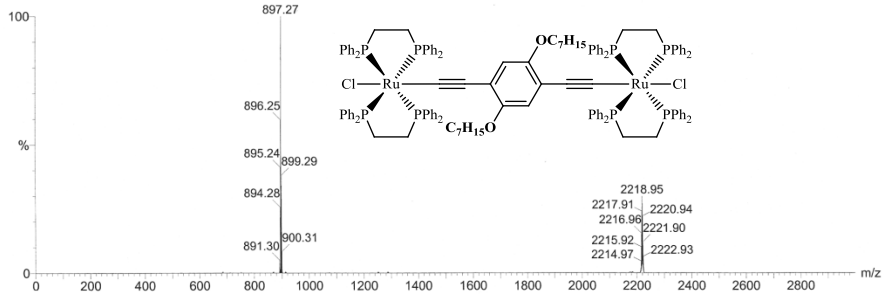

Figure A. 31: ESI-MS(TOF+) Spectrum of **23d**.

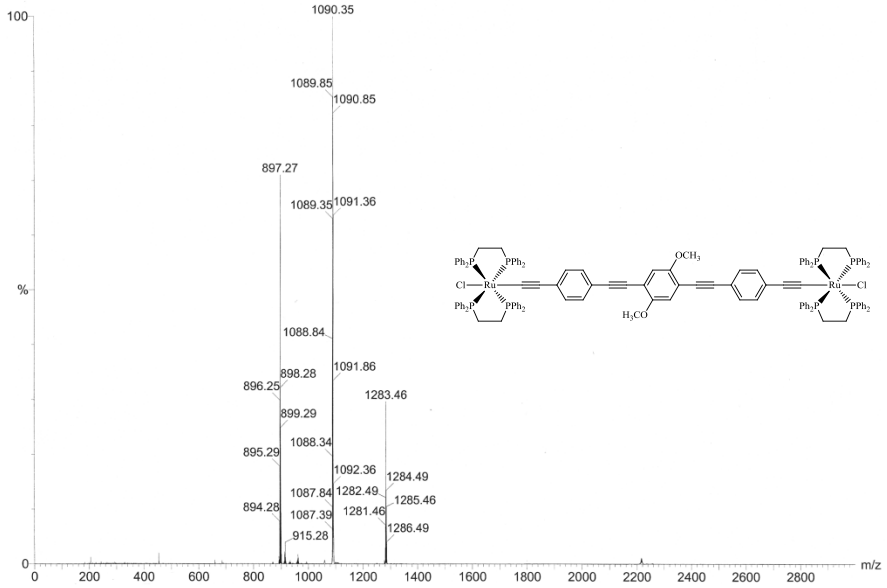

Figure A. 32: ESI-MS(TOF+) Spectrum of **24a**.

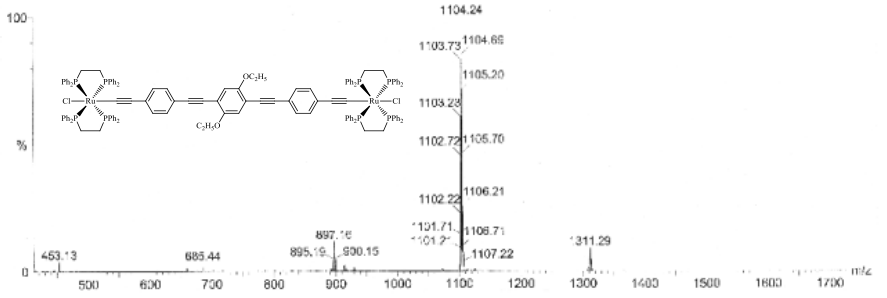

Figure A. 33: ESI-MS(TOF+) Spectrum of **24b**.

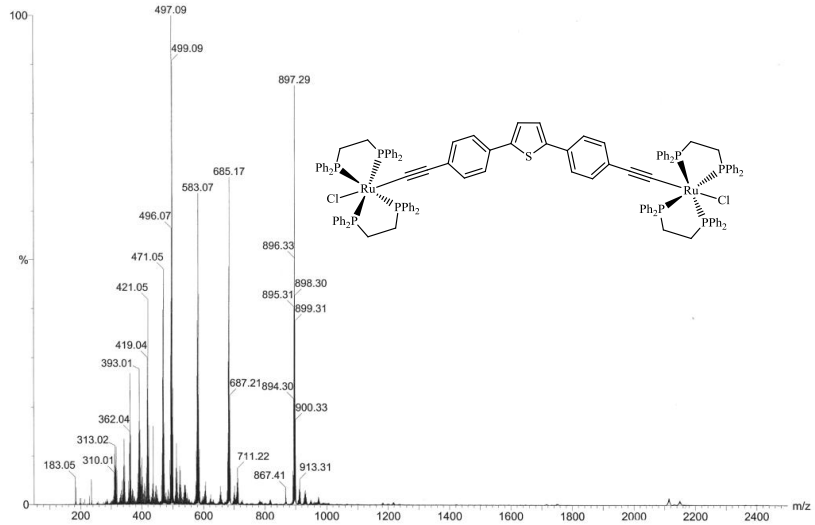

Figure A. 34: ESI-MS(TOF+) Spectrum of **27**.

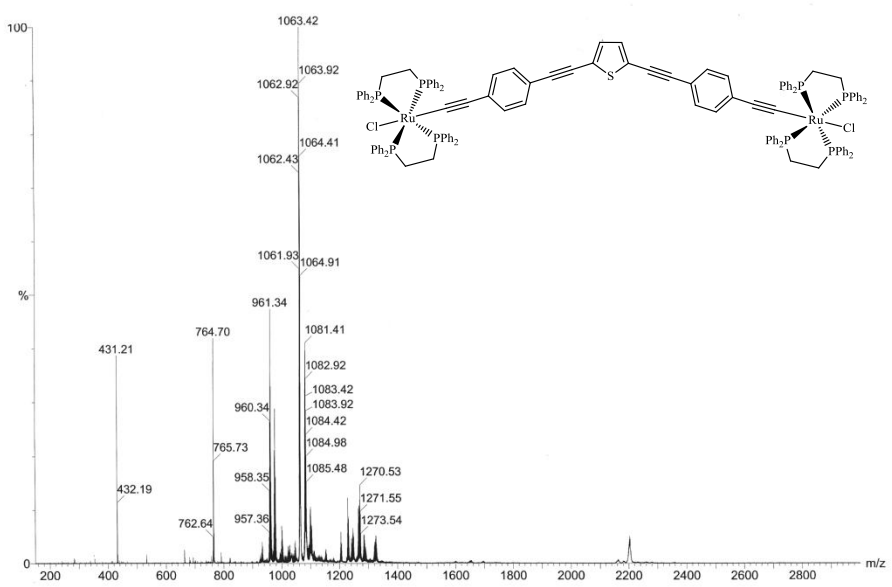

Figure A. 35: ESI-MS(TOF+) Spectrum of **28**.

A.6. CV Studies

Table A. 1: Selected values for the cyclic voltammetry studies of **23c-d**.

			First Redox Pair						
	v **/ mVs^{-1}**	**(*v*/V s^{-1})$^{1/2}$**	**E_{pa} / mV (*vs.* E_{ref})**	**E_{pc} / mV (*vs.* E_{ref})**	**$E_{1/2}$ / mV (*vs.* E_{ref})**	**E_{pa} / mV (*vs.* Fc)**	**E_{pc} / mV (*vs.* Fc)**	**$E_{1/2}$ / mV (*vs.* Fc)**	**(E_{pa} - E_{pc})/mV**
23c	100	0.3162	96.7	-12.8	41.9	-390.7	-500.3	-445.5	109.5
			Second redox Pair						
			E_{pa} / mV (*vs.* E_{ref})	**E_{pc} / mV (*vs.* E_{ref})**	**$E_{1/2}$ / mV (*vs.* E_{ref})**	**E_{pa} / mV (*vs.* Fc)**	**E_{pc} / mV (*vs.* Fc)**	**$E_{1/2}$ / mV (*vs.* Fc)**	**(E_{pa} - E_{pc})/mV**
			510.3	407.4	458.9	22.9	-80.0	-28.6	102.9
			Second redox Pair						
	v **/ mVs^{-1}**	**(*v*/V s^{-1})$^{1/2}$**	**E_{pa} / mV (*vs.* E_{ref})**	**E_{pc} / mV (*vs.* E_{ref})**	**$E_{1/2}$ / mV (*vs.* E_{ref})**	**E_{pa} / mV (*vs.* Fc)**	**E_{pc} / mV (*vs.* Fc)**	**$E_{1/2}$ / mV (*vs.* Fc)**	**(E_{pa} - E_{pc})/mV**
23d	100	0.3162	103.3	-17.4	43.0	-384.1	-504.8	-444.5	120.7
			Second redox Pair						
			E_{pa} / mV (*vs.* E_{ref})	**E_{pc} / mV (*vs.* E_{ref})**	**$E_{1/2}$ / mV (*vs.* E_{ref})**	**E_{pa} / mV (*vs.* Fc)**	**E_{pc} / mV (*vs.* Fc)**	**$E_{1/2}$ / mV (*vs.* Fc)**	**(E_{pa} - E_{pc})/mV**
			535.7	423.7	479.7	48.3	-63.7	-7.7	112.0

A.7. XRD Studies

Table A. 2: Selected crystal data for the structures of **4c**, **5c-d**,[210, 292] **8b**, **10a**, **21b, 34, 37, 38**.

	Crystal Data	
4c	Monoclinic $P2_1/c$ a = 10.132 (1) Å b = 9.887 (2) Å c = 12.169 (4) Å β = 107.46 (2) º	V = 1162.9 (5) Å^3 Z = 2
5c	Monoclinic $P2_1/c$ a = 9.748 (2) Å b = 8.890 (2) Å c = 7.566 (2) Å β = 112.74 (3) º	V = 604.7 (3) Å^3 Z = 2
5d	Monoclinic $P2_1/a$ a = 6.7246 (2) Å b = 16.7456 (5) Å c = 9.8026 (3) Å β = 97.320 (2) º	V = 1094.85 (6) Å^3 Z = 2
8b	Monoclinic $P2_1/n$ a = 5.2993 (2) Å b = 20.2161 (7) Å c = 10.8196 (3) Å β = 101.404 (2) º	V = 1136.23 (7) Å^3 Z = 2
10a	Monoclinic $P2_1/c$ a = 12.0422 (7) Å b = 7.1249 (4) Å c = 12.7028 (8) Å β = 115.178 (3) º	V = 986.34 (10) Å^3 Z = 2
34	Triclinic P -1 a = 10.7656(2) Å b = 13.1367(2) Å c = 17.5851(3) Å α = 106.316(1) º β = 101.404 (2) º γ = 93.499(1) º	V = 2364.37(7) Å^3 Z = 2
37	Orthorhombic *Pbca* a = 15.7463(2) Å b = 21.8914(3) Å c = 28.6122(4) Å	V = 9862.9(2) Å^3 Z = 2
20b	Monoclinic $P2_1/n$ a = 13.4614(3) Å b = 11.7059(3) Å c = 18.7397(4) Å β = 103.7050(10) º	V = 2868.89(12) Å^3 Z = 2
38	Monoclinic $P2_1/n$ a = 5.4557 (11) Å b = 19.467 (4) Å c = 15.592 (3) Å β = 91.89 (3) º	V = 1655.1 (6) Å^3 Z = 4

1,4-bis(4-bromo-1-ethynylbenzene)-2,5-diethoxybenzene (8b)

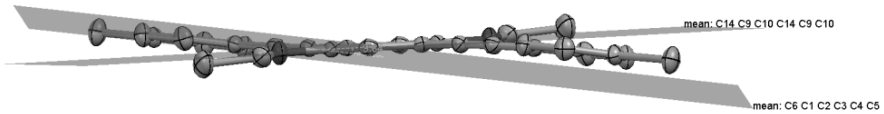

Figure A. 36: Mercury[265] plot of **8c** to show angle formed by the planes of the central and terminal phenyl moieties. Hydrogen atoms omitted for clarity.

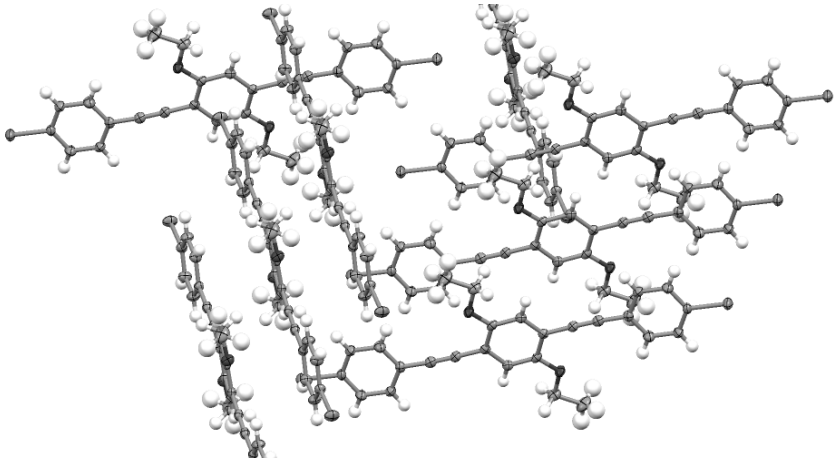

Figure A. 37: Mercury[265] plot of **8b** to show packing.

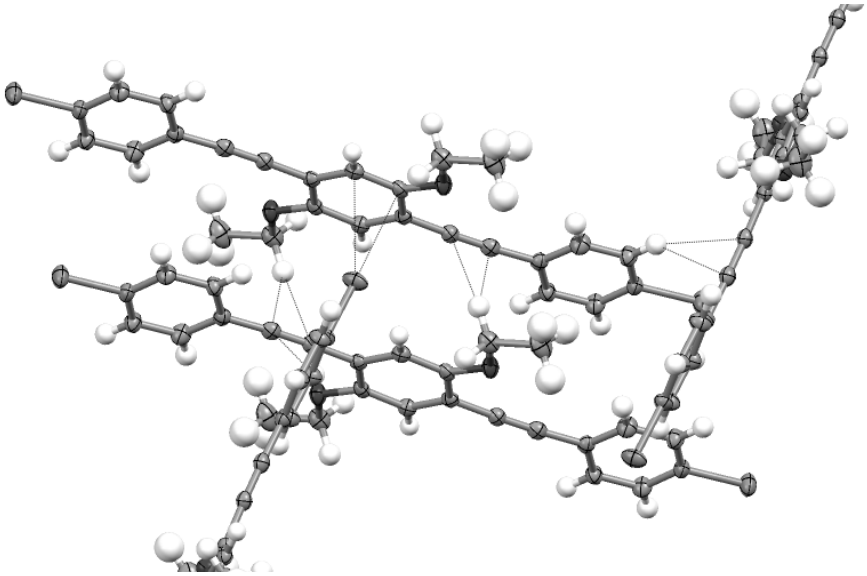

Figure A. 38: Mercury[265] plot of **8b** to show short contacts in a different perspective.

Table A. 3: Selected bond (Å) and angle (º) values for **8b**.

Br1 – C4	1.905(2)
C7 – C8	1.201(4)
C1 – C7	1.431(4)
C8 – C9	1.424(3)
C10 – O2	1.367(3)
C10 – O2 – C15	117.8(2)
C1 – C7 – C8	176.7(3)
C7 – C8 – C9	178.3(3)

1,4-bis(1,4-diethynylbenzene)-2,5-diethoxybenzene (10a)

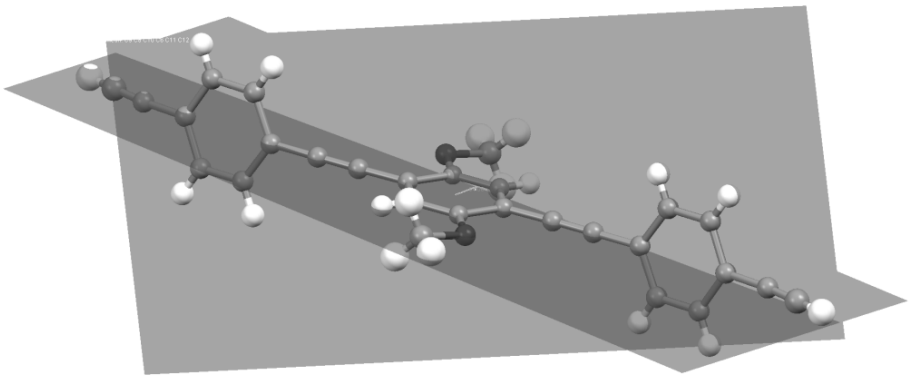

Figure A. 39: Mercury[265] plot of **10a** showing the angle formed between phenyl ring planes.

Table A. 4: Selected bond (Å) and angle (º) values for **10a**.

C13 – C12	1.117(5)
C5 – C4	1.200(4)
C2 – O1	1.369(3)
O1 – C14	1.425(3)
C5 – C4 – C1	178.6(3)
C6 – C5 – C4	175.6(3)
C9 – C12 – C13	174.9(3)
C2 – O1 – C14	117.3(2)

***trans*-[RuCl(H)(dppe)$_2$] (34)**

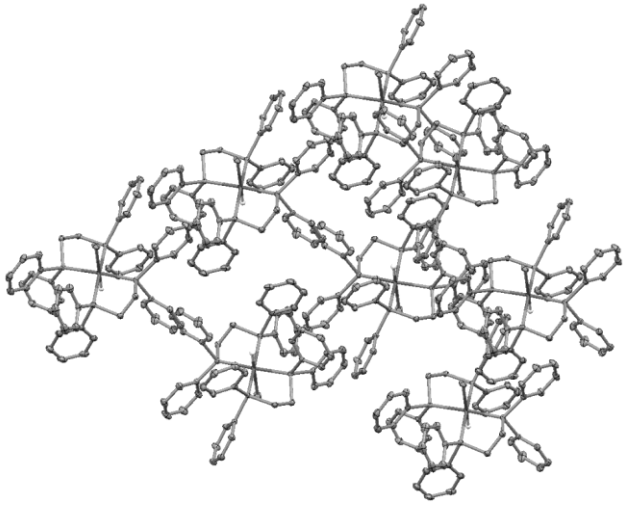

Figure A. 40: Mercury[265] plot of **34** showing packing.

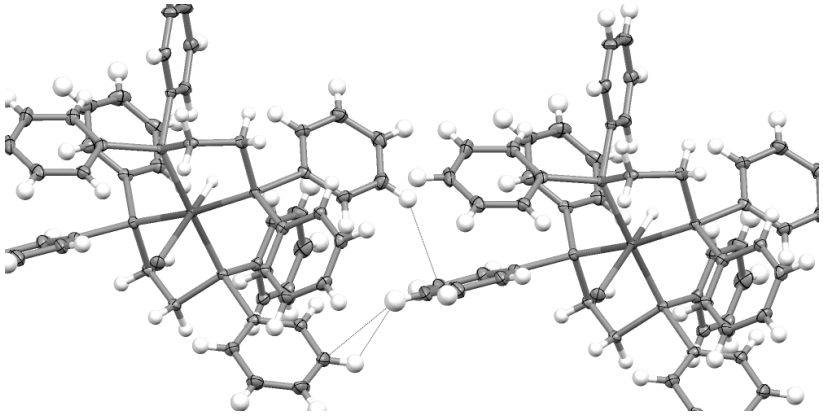

Figure A. 41: Mercury[265] plot of **34** showing short contacts.

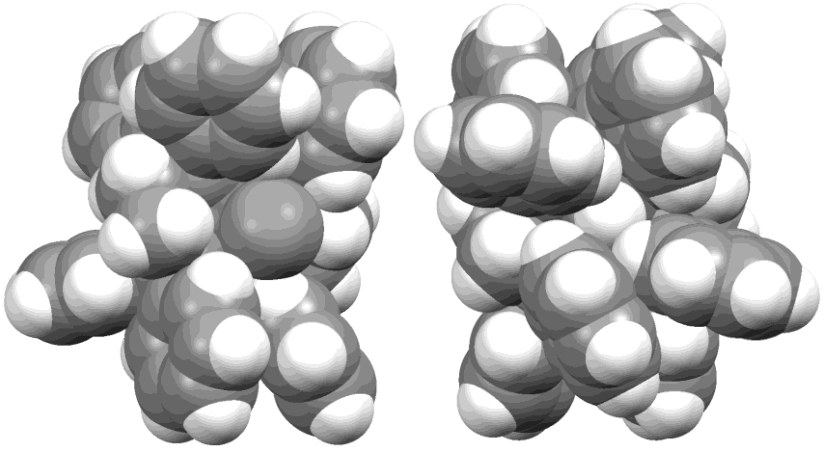

Figure A. 42: Mercury[265] plot of **34** showing CPK model. Chloride perspective (left), hydride perspective (right).

Table A. 5: Selected bond (Å) and angle (º) values for **34**.

Ru1 – Cl1	2.5697(6)
Ru1 – H1	1.53(2)
P4 – Ru1	2.3389(8)
Ru1 – P3	2.3222(6)
Ru1 – P2	2.3383(8)
Ru1 – P1	2.3203(6)
Cl1 – Ru1 – H1	178.3(9)
H1 – Ru1 – P2	83.4(9)
H1 – Ru1 – P1	87.9(9)
H1 – Ru1 – P3	89.0(9)
P4 – Ru1 – H1	84.8(9)
P3 – Ru1 – P1	176.75(2)
P4 – Ru1 – P2	168.19(2)

cis-[RuCl(η^2-O_2CCH_3)(dppe)$_2$] (37)

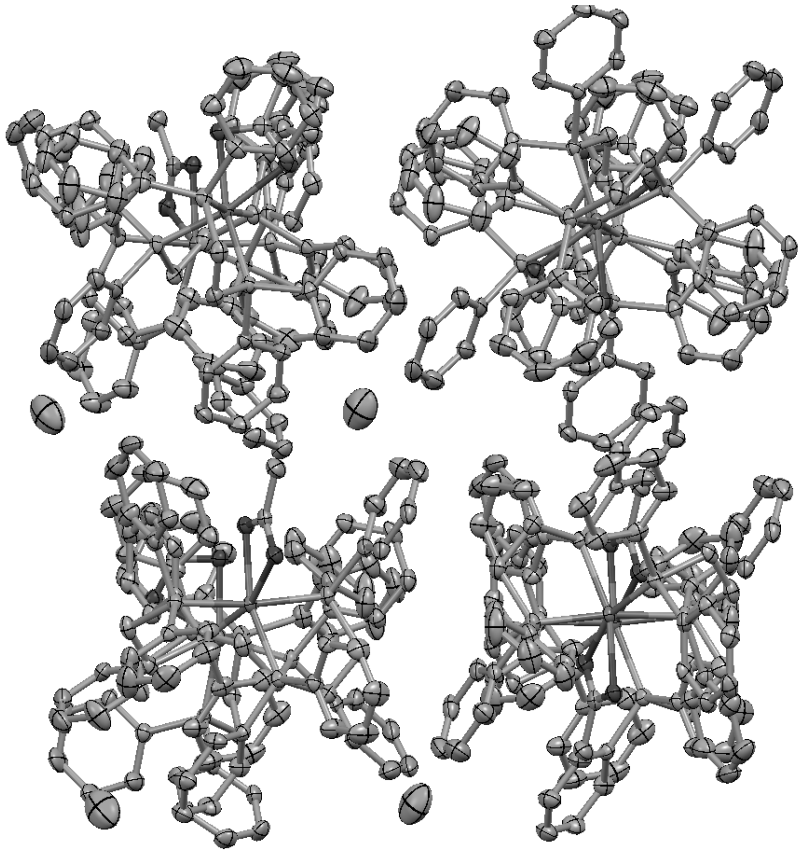

Figure A. 43: Mercury[265] plot of **37** showing packing.

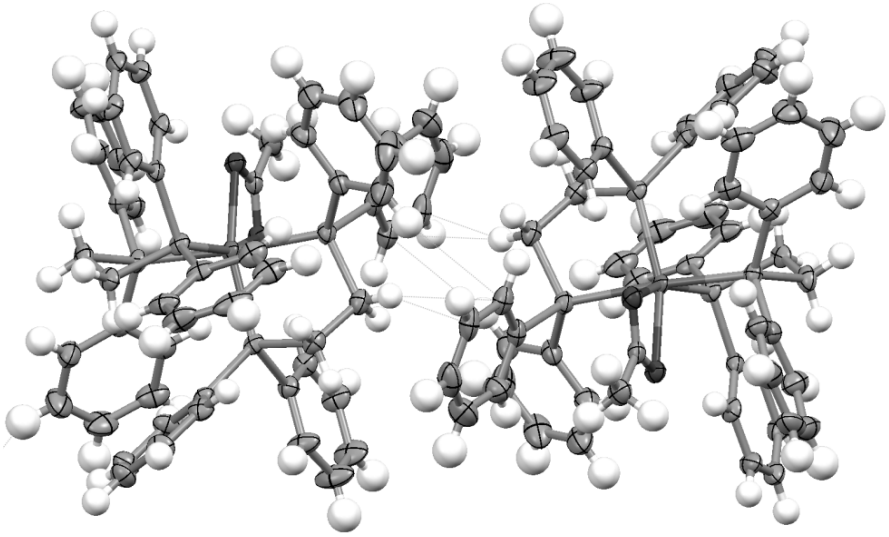

Figure A. 44: Mercury[265] plot of **37** showing short contacts.

Table A. 6: Selected bond (Å) and angle (º) values for **37**.

Ru1 – O2	2.202(3)
Ru1 – O1	2.191(3)
O2 – C210	1.262(6)
O1 – C210	1.268(6)
Ru1 – P3	2.379(1)
Ru1 – P1	2.321(1)
Ru1 – P2	2.288(1)
Ru1 – P4	2.368(1)
P2 – Ru1 – P4	101.65(5)
P1 – Ru1 – P3	102.89(5)
P2 – Ru1 – P3	83.44(5)
P1 – Ru1 – P4	82.36(4)
O2 – Ru1 – O1	59.2(1)

Palladium phenylene ethynylene rod (20b)

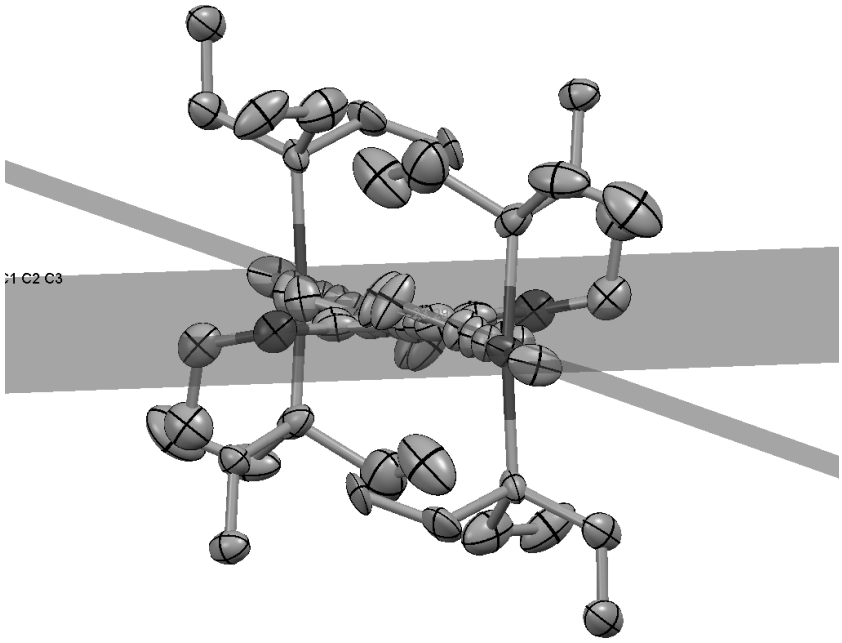

Figure A. 45: Mercury[265] plot of angle formed between the phenyl moieties in **20c**.

Short contacts plot (Figure A.46) had do not show hydrogens because of disordering which resulted from 0.6 occupancy of the atoms that constitute the phosphine groups.

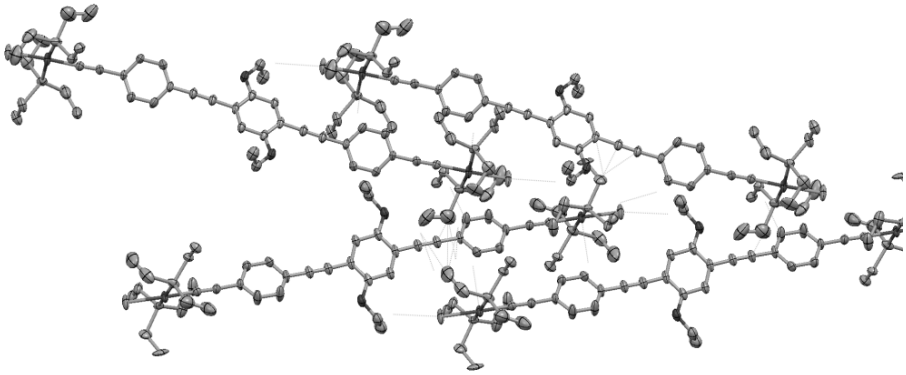

Figure A. 46: Mercury[265] plot of **20b** showing short contacts.

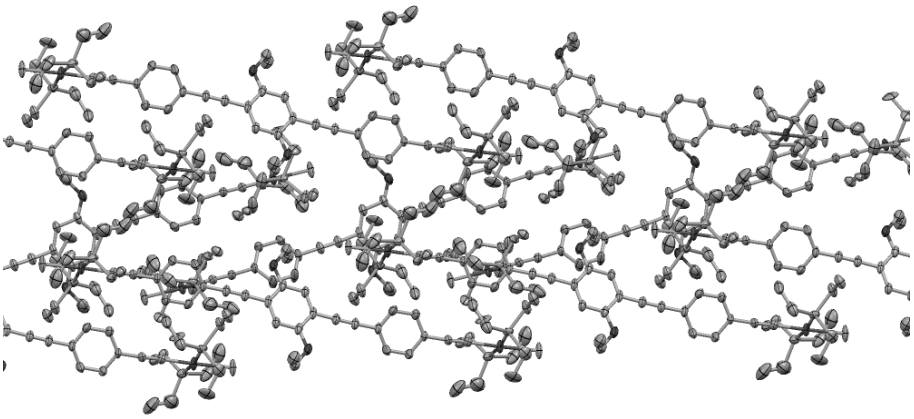

Figure A. 47: Mercury[265] plot of **20b** showing packing.

Table A. 7: Selected bond (Å) and angle (º) values for **20b**.

Pd1 – Cl1	2.346(6)
Pd1 – P2	2.340(4)
Pd1 – P1	2.283(7)
Pd1 – C13	1.947(6)
C13 – C12	1.184(8)
C12 – C9	1.444(8)
C6 – C5	1.430(8)
C4 – C5	1.200(8)
C4 – C1	1.429(8)
C2 – O1	1.360(8)
C2 – O1 – C26	118.6(5)
C1 – C4 – C5	175.9(7)
C4 – C5 – C6	176.8(7)
C9 – C12 – C13	177.0(7)
C12 – C13 – Pd1	178.1(6)
C13 – Pd1 – Cl1	177.8(2)
P1 – Pd1 – P2	171.1(2)
P1 – Pd1 – Cl1	96.5(2)
P2 – Pd1 – Cl1	89.1(2)

Nitrile terminated thiophenylene ethynylene (38)

Although not a part of the described ligands that were used in the work, this compound, 4,4'-[Thiophene-2,5-diylbis(ethyne-2,1-diyl)]dibenzonitrile[292] (**38**) was prepared in other attempts to produce the a rod similar to **28** but with nitrile coordination to the Ru centre.

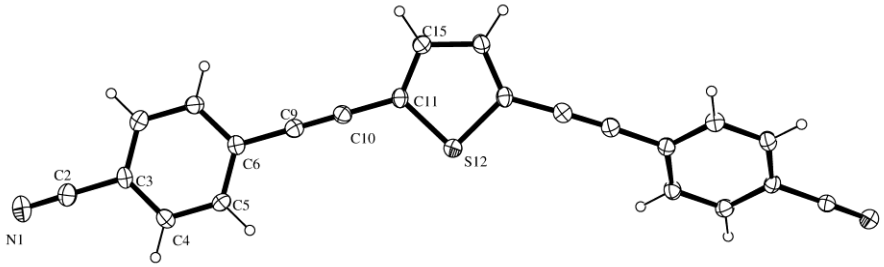

Figure A. 48: Perspective ORTEP-3[264] plot of **38**[292] (50% probability displacement ellipsoids).

The ligand shows some deviation from planarity with the first and second phenyl rings presenting dihedral angles with the thiophene with values of 7.21 (16) º and 39.58 (9) º respectively (Figure A.49). Some hydrogen bonding can be found between the terminal nitrogen atom and a hydrogen atom from the adjacent molecule's phenyl or thiophene ring (illustrated in Figure A.50).

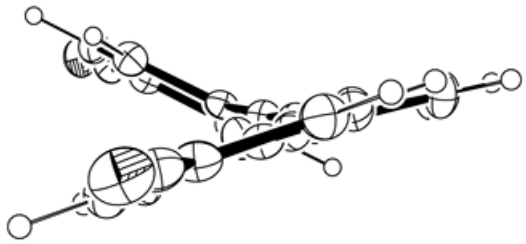

Figure A. 49: Perspective ORTEP-3[264] plot of **38**.

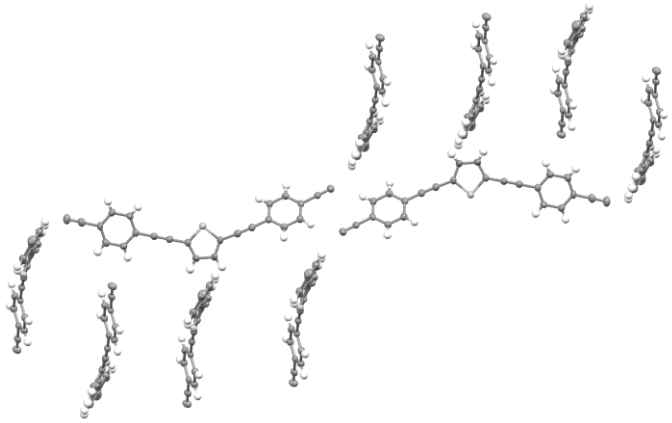

Figure A. 50: Mercury[265] plot of **38** to show hydrogen bonding between terminal nitrogen and aromatic hydrogen atoms.

A.8. Fluorescence decay studies

Available integrated fluorescence values are presented in Table A. 8.

Table A. 8: Fluorescence decay data for some of the starting materials (**4a-b** and **9b**), some free ligands (**10b**), some Pd rods (**20c** and **21a**) and some Ru rods (**23c-d**, **24a-b** and **39**).

Protected Ligands		**Free ligands**		**Pd rods**		**Ru rods**	
	Int. [b]		**Int.** [b]		**Int.** [b]		**Int.** [b]
4a	215052.03	–	–	**19a**	44288.98	–	–
4b	2170000.00	–	–	–	–	–	–
–	–	–	–	–	–	**22c**	7341.31
–	–	–	–	–	–	**22d**	5047.80
–	–	–		**20b**	278525.93	**23b**	11598.63
9c	9320000.00	**10c**	3830000.00	–	–	**23c**	17767.77
–	–	–	–	–	–	**39** [c]	12230.86

[a] Detection wavelength in nm; [b] average time-of-life in ns; [c] 39 is *trans*-[$(dppe)_2$ClRu–C≡C–Ph]

References

[1] G. E. Moore, *Proceedings of the IEEE* **1998**, *86*, 82-85.

[2] a) W. A. Goddard, *Handbook of nanoscience, engineering, and technology*, 2nd ed., CRC Press, Boca Raton, FL, **2007**; b) M. C. Petty, *Molecular electronics : from principles to practice*, John Wiley & Sons, Chichester, England; Hoboken, NJ, **2007**; c) P. J. Low, *Dalton Trans.* **2005**, 2821-2824.

[3] a) R. Chau, B. Doyle, J. Kavalieros, D. Barlage, A. Murthy, M. Doczy, R. Arghavani, S. Datta, in *International Conference on Solid-State Devices and Materials (SSDM)*, Nagoya, Japan, **2002**, pp. 68-69; b) F. Paul, C. Lapinte, *Coord. Chem. Rev.* **1998**, *178-180*, 431-509.

[4] http://www.ausairpower.net/OSR-0700.html (26/08/12).

[5] D. James, J. Tour, Molecular Wires in *Molecular Wires and Electronics*, *Vol. 257*, Springer Berlin / Heidelberg, **2005**, pp. 784-785.

[6] R. P. Feynman, *Eng. Sci.* **1960**, *23*, 22-36.

[7] R. F. Service, *Science* **2001**, *294*, 2442-2443.

[8] a) W. A. Reinerth, L. Jones, T. P. Burgin, C. W. Zhou, C. J. Muller, M. R. Deshpande, M. A. Reed, J. M. Tour, *Nanotech.* **1998**, *9*, 246-250; b) A. Coskun, J. M. Spruell, G. Barin, W. R. Dichtel, A. H. Flood, Y. Y. Botros, J. F. Stoddart, *Chem. Soc. Rev.* **2012**, *41*, 4827-4859.

[9] W. B. Culbertson, R. Amerson, R. J. Carter, P. Kuekes, G. Snider, in *1996 IEEE International Symposium on Defect and Fault Tolerance in Vlsi Systems, Proceedings*, **1996**, pp. 2-10.

[10] J.-M. Lehn, *Supramolecular Chemistry: Concepts and Perspectives*, VCH, Wiley, **2005**.

[11] L. Luo, S. H. Choi, C. D. Frisbie, *Chem. Mat.* **2011**, *23*, 631-645.

[12] A. Aviram, M. A. Ratner, *Chem. Phys. Lett.* **1974**, *29*, 277-283.

[13] a) J. S. Schumm, D. L. Pearson, J. M. Tour, **1994**, *33*, 1360-1363; b) F. Paul, C. Lapinte, *Coord. Chem. Rev.* **1998**, *178-180*, 431-509.

[14] a) M. F. García-Parajó, J. Hernando, G. S. Mosteiro, J. P. Hoogenboom, E. M. H. P. van Dijk, N. F. van Hulst, *Chem. Phys. Chem.* **2005**, *6*, 819-827; b) N. Robertson, C. A. McGowan, *Chem. Soc. Rev.* **2003**, *32*, 96-103.

[15] M. J. Crossley, P. L. Burn, *J. Chem. Soc., Chem. Comm.* **1991**, 1569-1571.

[16] A. Klein, O. Lavastre, J. Fiedler, *Organometallics* **2006**, *25*, 635-643.

[17] F. C. Grozema, L. D. A. Siebbeles, J. M. Warman, S. Seki, S. Tagawa, U. Scherf, *Adv. Mat.* **2002**, *14*, 228-231.

[18] A. Mishchenko, D. Vonlanthen, V. Meded, M. Bürkle, C. Li, I. V. Pobelov, A. Bagrets, J. K. Viljas, F. Pauly, F. Evers, M. Mayor, T. Wandlowski, *Nano Lett.* **2009**, *10*, 156-163.

[19] J. Rotzler, D. Vonlanthen, A. Barsella, A. Boeglin, A. Fort, M. Mayor, *Eur. J. Org. Chem.* **2010**, 1096-1110.

[20] A. Mishchenko, L. A. Zotti, D. Vonlanthen, M. Bürkle, F. Pauly, J. C. Cuevas, M. Mayor, T. Wandlowski, *J. Am. Chem. Soc.* **2010**, *133*, 184-187.

[21] a) H. D. Sikes, *Science* **2001**, *291*, 1519-1523; b) W. B. Davis, M. A. Ratner, M. R. Wasielewski, *J. Am. Chem. Soc.* **2001**, *123*, 7877-7886.

[22] a) Z. Shuai, J. Brédas, *Phys. Rev. B* **1992**, *46*, 4395-4404; b) J. L. Brédas, G. B. Street, B. Thémans, J. M. André, *J. Chem. Phys.* **1985**, *83*, 1323-1329; c) M. Belletete, L. Mazerolle, N. Desrosiers, M. Leclerc, G. Durocher, *Macromolecules* **1995**, *28*, 8587-8597; d) H. Chan, *Prog. Polym. Sci.* **1998**, *23*, 1167-1231; e) T. Noda, H. Ogawa, N. Noma, Y. Shirota, *J. Mater. Chem.* **1999**, *9*, 2177-2181; f) J. J. Apperloo, R. A. J. Janssen, P. R. L. Malenfant, J. M. J. Fréchet, *J. Am. Chem. Soc.* **2001**, *123*, 6916-6924; g) C. Rothe, S. Hintschich, A. P. Monkman, M. Svensson, M. R. Anderson, *J. Chem. Phys.* **2002**, *116*, 10503; h) G. Barbarella, *Chem. Eur. J.* **2002**, *8*, 5072-5077.

[23] T. Izumi, S. Kobashi, K. Takimiya, Y. Aso, T. Otsubo, *J. Am. Chem. Soc.* **2003**, *125*, 5286-5287.

[24] T. A. Skotheim, *Handbook of Conducting Polymers*, M. Dekker, New York, **1986**.

[25] D. A. M. Egbe, L. H. Nguyen, B. Carbonnier, D. Mühlbacher, N. S. Sariciftci, *Polymer* **2005**, *46*, 9585-9595.

[26] D. Egbe, L. Huongnguyen, D. Muhlbacher, H. Hoppe, K. Schmidtke, N. Serdarsariciftci, *Thin Solid Films* **2006**, *511-512*, 486-488.

[27] L. Jones, D. L. Pearson, J. S. Schumm, J. M. Tour, *Pure Appl. Chem.* **1996**, *68*, 145-148.

[28] D. L. Pearson, J. M. Tour, *J. Org. Chem.* **1997**, *62*, 1376-1387.

[29] E. L. Dane, S. B. King, T. M. Swager, *J. Am. Chem. Soc.* **2010**, *132*, 7758-7768.

[30] a) M. Lindgren, B. Minaev, E. Glimsdal, R. Vestberg, R. Westlund, E. Malmström, *J. Lumin.* **2007**, *124*, 302-310; b) R. Vestberg, R. Westlund, A. Eriksson, C. Lopes, M. Carlsson, B. Eliasson, E. Glimsdal, M. Lindgren, E. Malmström, *Macromolecules* **2006**, *39*, 2238-2246.

[31] A. Kraft, A. C. Grimsdale, A. B. Holmes, *Angew. Chem. Int. Ed.* **1998**, *37*, 402-428.
[32] H. Detert, E. Sugiono, *Synthetic Met.* **2000**, *115*, 89-92.
[33] C. Joachim, S. Roth, *Atomic and Molecular Wires*, Springer, **1997**.
[34] C. Wang, A. S. Batsanov, M. R. Bryce, I. Sage, *Org. Lett.* **2004**, *6*, 2181-2184.
[35] G. Seifert, T. Köhler, T. Frauenheim, *App. Phys. Lett.* **2000**, *77*, 1313–1315.
[36] C. W. Marquardt, S. Grunder, A. Błaszczyk, S. Dehm, F. Hennrich, H. v. Löhneysen, M. Mayor, R. Krupke, *Nature Nanotech.* **2010**, *5*, 863-867.
[37] K. S. Novoselov, *Science* **2004**, *306*, 666-669.
[38] http://www.quirkyscience.com/wp-content/uploads/2012/05/LBL-graphene_sheet1.jpg (28-08-2012).
[39] Y. M. Lin, A. Valdes-Garcia, S. J. Han, D. B. Farmer, I. Meric, Y. Sun, Y. Wu, C. Dimitrakopoulos, A. Grill, P. Avouris, K. A. Jenkins, *Science* **2011**, *332*, 1294-1297.
[40] http://www.technologyreview.com/computing/24482/ (14/05/2011).
[41] D. V. Kosynkin, W. Lu, A. Sinitskii, G. Pera, Z. Sun, J. M. Tour, *ACS Nano* **2011**, *5*, 968-974.
[42] T. Ren, *Organometallics* **2005**, *24*, 4854-4870.
[43] M. Akita, T. Koike, *Dalton Trans.* **2008**, 3523-3530.
[44] Y. Tanaka, T. Koike, M. Akita, *Eur. J. Inorg. Chem.* **2010**, *2010*, 3571-3575.
[45] D. Touchard, P. H. Dixneuf, *Coord. Chem. Rev.* **1998**, *178-180*, 409-429.
[46] C. Olivier, K. Costuas, S. Choua, V. Maurel, P. Turek, J.-Y. Saillard, D. Touchard, S. Rigaut, *J. Am. Chem. Soc.* **2010**, *132*, 5638-5651.
[47] C. Creutz, H. Taube, *J. Am. Chem. Soc.* **1969**, *91*, 3988-3989.
[48] A. Ceccon, S. Santi, L. Orian, A. Bisello, *Coord. Chem. Rev.* **2004**, *248*, 683-724.
[49] P. J. Low, N. J. Brown, *J. Clust. Sci.* **2010**, *21*, 235-278.
[50] J. Park, A. N. Pasupathy, J. I. Goldsmith, C. Chang, Y. Yaish, J. R. Petta, M. Rinkoski, J. P. Sethna, H. D. Abruña, P. L. McEuen, D. C. Ralph, *Nature* **2002**, *417*, 722-725.
[51] W. Liang, M. P. Shores, M. Bockrath, J. R. Long, H. Park, *Nature* **2002**, *417*, 725-729.
[52] a) M. C. B. Colbert, J. Lewis, N. J. Long, P. R. Raithby, A. J. P. White, D. J. Williams, *J. Chem. Soc., Dalton Trans.* **1997**, 99-104; b) Y. Zhu, O. Clot, M. O. Wolf, G. P. A. Yap, *J. Am. Chem. Soc.* **1998**, *120*, 1812-1821; c) C. Lebreton, D. Touchard, L. L. Pichon, A. Daridor, L. Toupet, P. H. Dixneuf, *Inorg. Chim. Acta* **1998**, *272*, 188-196; d) W.-Y. Wong, G.-L. Lu, K.-F. Ng, K.-H. Choi, Z. Lin, *J. Chem. Soc., Dalton Trans.* **2001**, 3250-3260; e) J.-L. Zuo, E. Herdtweck, F. Fabrizi de Biani, A. M. Santos, F. E. Kühn, *New J. Chem.* **2002**, *26*, 889-894; f) J. H. K. Yip, J. Wu, K.-Y. Wong, K. P. Ho, C. So-Ngan Pun, J. J. Vittal, *Organometallics* **2002**, *21*, 5292-5300; g) G.-L. Xu, M. C. DeRosa, R. J. Crutchley, T. Ren, *J. Am. Chem. Soc.* **2004**, *126*, 3728-3729; h) J. F. Berry, F. A. Cotton, C. A. Murillo, *Organometallics* **2004**, *23*, 2503-2506; i) T. Sheng, H. Vahrenkamp, *Eur. J. Inorg. Chem.* **2004**, *2004*, 1198-1203; j) R. D. Dewhurst, A. F. Hill, A. C. Willis, *Organometallics* **2004**, *23*, 1646-1648; k) G.-L. Xu, R. J. Crutchley, M. C. DeRosa, Q.-J. Pan, H.-X. Zhang, X. Wang, T. Ren, *J. Am. Chem. Soc.* **2005**, *127*, 13354-13363; l) C.-K. Kuo, J.-C. Chang, C.-Y. Yeh, G.-H. Lee, C.-C. Wang, S.-M. Peng, *Dalton Trans.* **2005**, 3696-3701; m) A. Albinati, F. Fabrizi de Biani, P. Leoni, L. Marchetti, M. Pasquali, S. Rizzato, P. Zanello, *Angew. Chem. Int. Ed.* **2005**, *44*, 5701-5705; n) Y.-C. Lin, W.-T. Chen, J. Tai, D. Su, S.-Y. Huang, I. Lin, J.-L. Lin, M. M. Lee, M. F. Chiou, Y.-H. Liu, K.-S. Kwan, Y.-J. Chen, H.-Y. Chen, *Inorg. Chem.* **2009**, *48*, 1857-1870.
[53] a) A. Benameur, P. Brignou, E. Di Piazza, Y.-M. Hervault, L. Norel, S. Rigaut, *New J. Chem.* **2011**, *35*, 2105-2113; b) M. Mayor, C. von Hänisch, H. B. Weber, J. Reichert, D. Beckmann, *Angew. Chem. Int. Ed.* **2002**, *41*, 1183-1186; c) K. Liu, X. Wang, F. Wang, *ACS Nano* **2008**, *2*, 2315-2323; d) A. S. Blum, T. Ren, D. A. Parish, S. A. Trammell, M. H. Moore, J. G. Kushmerick, G.-L. Xu, J. R. Deschamps, S. K. Pollack, R. Shashidhar, *J. Am. Chem. Soc.* **2005**, *127*, 10010-10011; e) A. K. Mahapatro, J. Ying, T. Ren, D. B. Janes, *Nano Lett.* **2008**, *8*, 2131-2136; f) B. S. Kim, J. M. Beebe, C. Olivier, S. Rigaut, D. Touchard, J. G. Kushmerick, X. Y. Zhu, C. D. Frisbie, *J. Phys. Chem. C* **2007**, *111*, 7521-7526; g) B. Xi, G.-L. Xu, P. E. Fanwick, T. Ren, *Organometallics* **2009**, *28*, 2338-2341.
[54] a) Y. Li, M. Josowicz, L. M. Tolbert, *J. Am. Chem. Soc.* **2010**, *132*, 10374-10382; b) E. A. Weiss, M. J. Ahrens, L. E. Sinks, A. V. Gusev, M. A. Ratner, M. R. Wasielewski, *J. Am. Chem. Soc.* **2004**, *126*, 5577-5584; c) E. G. Petrov, V. May, *J. Phys. Chem. A* **2001**, *105*, 10176-10186.
[55] A. A. Kocherzhenko, F. C. Grozema, L. D. A. Siebbeles, *Phys. Chem. Chem. Phys.* **2011**, *13*, 2096-2110.
[56] N. G. Connelly, W. E. Geiger, *Chem. Rev.* **1996**, *96*, 877-910.
[57] C. Olivier, B. Kim, D. Touchard, S. Rigaut, *Organometallics* **2008**, *27*, 509-518.
[58] P. Aguirre-Etcheverry, D. O'Hare, *Chem. Rev.* **2010**, *110*, 4839-4864.
[59] M. B. Robin, P. Day, *Adv. Inorg. Chem. Radiochem.* **1968**, *10*, 247-422.

[60] a) N. S. Hush, *Prog. Inorg. Chem.* **1967**, *8*, 391-444; b) N. S. Hush, *Electrochim. Acta* **1968**, *13*, 1005-1023; c) N. S. Hush, *Coord. Chem. Rev.* **1985**, *64*, 135-157.
[61] K. D. Demadis, C. M. Hartshorn, T. J. Meyer, *Chem. Rev.* **2001**, *101*, 2655-2686.
[62] a) C. E. B. Evans, M. L. Naklicki, A. R. Rezvani, C. A. White, V. V. Kondratiev, R. J. Crutchley, *J. Am. Chem. Soc.* **1998**, *120*, 13096-13103; b) S. F. Nelsen, *Chem. Eur. J.* **2000**, *6*, 581-588.
[63] D. M. D'Alessandro, F. R. Keene, *Chem. Soc. Rev.* **2006**, 424-440.
[64] O. F. Koentjoro, R. Rousseau, P. J. Low, *Organometallics* **2001**, *20*, 4502-4509.
[65] a) D. Pilette, K. Ouzzine, H. Le Bozec, P. H. Dixneuf, C. E. F. Rickard, W. R. Roper, *Organometallics* **1992**, *11*, 809-817; b) H. Le Bozec, K. Ouzzine, P. H. Dixneuf, *J. Chem. Soc., Chem. Commun.* **1989**, 219-221.
[66] a) S. Rigaut, C. Olivier, K. Costuas, S. Choua, O. Fadhel, J. Massue, P. Turek, J.-Y. Saillard, P. H. Dixneuf, D. Touchard, *J. Am. Chem. Soc.* **2006**, *128*, 5859-5876; b) P. Hamon, F. Justaud, O. Cador, P. Hapiot, S. Rigaut, L. Toupet, L. Ouahab, H. Stueger, J.-R. Hamon, C. Lapinte, *J. Am. Chem. Soc.* **2008**, *130*, 17372-17383; c) A. Vacher, A. Benameur, C. M. Ndiaye, D. Touchard, S. Rigaut, *Organometallics* **2009**, *28*, 6096-6100; d) F. Pevny, E. Di Piazza, L. Norel, M. Drescher, R. F. Winter, S. Rigaut, *Organometallics* **2010**, *29*, 5912-5918; e) K. Costuas, S. Rigaut, *Dalton Trans.* **2011**, *40*, 5643-5658; f) N. Gauthier, N. Tchouar, F. Justaud, G. Argouarch, M. P. Cifuentes, L. Toupet, D. Touchard, J.-F. o. Halet, S. Rigaut, M. G. Humphrey, K. Costuas, F. Paul, *Organometallics* **2009**, *28*, 2253-2266.
[67] a) M. I. Bruce, P. J. Low, K. Costuas, J.-F. Halet, S. P. Best, G. A. Heath, *J. Am. Chem. Soc.* **2000**, *122*, 1949-1962; b) M. Brady, W. Weng, Y. Zhou, J. W. Seyler, A. J. Amoroso, A. M. Arif, M. Böhme, G. Frenking, J. A. Gladysz, *J. Am. Chem. Soc.* **1997**, *119*, 775-788; c) S. Záliš, R. F. Winter, W. Kaim, *Coord. Chem. Rev.* **2010**, *254*, 1383-1396.
[68] C. K. Jørgensen, *Coord. Chem. Rev.* **1966**, *1*, 164-178.
[69] N. Gauthier, N. Tchouar, F. d. r. Justaud, G. Argouarch, M. P. Cifuentes, L. Toupet, D. Touchard, J.-F. o. Halet, S. p. Rigaut, M. G. Humphrey, K. Costuas, F. r. Paul, *Organometallics* **2009**, *28*, 2253-2266.
[70] L. Luo, A. Benameur, P. Brignou, S. H. Choi, S. Rigaut, C. D. Frisbie, *J. Phys. Chem. C* **2011**, *115*, 19955-19961.
[71] E. Wuttke, F. Pevny, Y.-M. Hervault, L. Norel, M. Drescher, R. F. Winter, S. Rigaut, *Inorg. Chem.* **2012**, *51*, 1902-1915.
[72] T. Bartik, B. Bartik, M. Brady, R. Dembinski, J. A. Gladysz, *Angew. Chem. Int. Ed.* **1996**, *35*, 414-417.
[73] I. Alkorta, J. Elguero, *Struct. Chem.* **2005**, *16*, 77-79.
[74] B. Bildstein, M. Schweiger, H. Kopacka, K. Wurst, *J. Organomet. Chem.* **1998**, *553*, 73-81.
[75] S. Guesmi, D. Touchard, P. H. Dixneuf, *Chem. Comm.* **1996**, 2773-2774.
[76] B. Bildstein, O. Loza, Y. Chizhov, *Organometallics* **2004**, *23*, 1825-1835.
[77] L.-B. Gao, S.-H. Liu, L.-Y. Zhang, L.-X. Shi, Z.-N. Chen, *Organometallics* **2006**, *25*, 506-512.
[78] a) S. Rigaut, D. Touchard, P. H. Dixneuf, *J. Organomet. Chem.* **2003**, *684*, 68-76; b) S. Rigaut, L. Le Pichon, D. Touchard, P. H. Dixneuf, J.-C. Daran, *Chem. Comm.* **2001**, 1206-1207.
[79] M. I. Bruce, B. G. Ellis, B. W. Skelton, A. H. White, *J. Organomet. Chem.* **2005**, *690*, 1772-1783.
[80] J. V. Ortega, B. Hong, S. Ghosal, J. C. Hemminger, B. Breedlove, C. P. Kubiak, *Inorg. Chem.* **1999**, *38*, 5102-5112.
[81] S. Rigaut, D. Touchard, P. H. Dixneuf, *Coord. Chem. Rev.* **2004**, *248*, 1585-1601.
[82] Y. Matsuura, Y. Tanaka, M. Akita, *J. Organomet. Chem.* **2009**, *694*, 1840-1847.
[83] a) R. Dembinski, T. Bartik, B. Bartik, M. Jaeger, J. A. Gladysz, *J. Am. Chem. Soc.* **2000**, *122*, 810-822; b) W. Weng, T. Bartik, M. Brady, B. Bartik, J. A. Ramsden, A. M. Arif, J. A. Gladysz, *J. Am. Chem. Soc.* **1995**, *117*, 11922-11931.
[84] T. B. Peters, J. C. Bohling, A. M. Arif, J. A. Gladysz, *Organometallics* **1999**, *18*, 3261-3263.
[85] a) N. Le Narvor, L. Toupet, C. Lapinte, *J. Am. Chem. Soc.* **1995**, *117*, 7129-7138; b) F. Coat, M.-A. Guillevic, L. Toupet, F. Paul, C. Lapinte, *Organometallics* **1997**, *16*, 5988-5998; c) M. Guillemot, L. Toupet, C. Lapinte, *Organometallics* **1998**, *17*, 1928-1930.
[86] F. Coat, C. Lapinte, *Organometallics* **1996**, *15*, 477-479.
[87] A. Sakurai, M. Akita, Y. Moro-oka, *Organometallics* **1999**, *18*, 3241-3244.
[88] M. Akita, M.-C. Chung, A. Sakurai, S. Sugimoto, M. Terada, M. Tanaka, Y. Moro-oka, *Organometallics* **1997**, *16*, 4882-4888.
[89] M. I. Bruce, L. I. Denisovich, P. J. Low, S. M. Peregudova, N. A. Ustynyuk, *Mendeleev Comm.* **1996**, *6*, 200-201.
[90] S. Kheradmandan, K. Heinze, H. W. Schmalle, H. Berke, *Angew. Chem.* **1999**, *111*, 2412-2415.

[91] M. J. Powers, T. J. Meyer, *J. Am. Chem. Soc.* **1978**, *100*, 4393-4398.
[92] C. Levanda, K. Bechgaard, D. O. Cowan, *J. Org. Chem.* **1976**, *41*, 2700-2704.
[93] N. D. Jones, M. O. Wolf, D. M. Giaquinta, *Organometallics* **1997**, *16*, 1352-1354.
[94] M. I. Bruce, P. J. Low, F. Hartl, P. A. Humphrey, F. de Montigny, M. Jevric, C. Lapinte, G. J. Perkins, R. L. Roberts, B. W. Skelton, A. H. White, *Organometallics* **2005**, *24*, 5241-5255.
[95] M.-C. Chung, X. Gu, B. A. Etzenhouser, A. M. Spuches, P. T. Rye, S. K. Seetharaman, D. J. Rose, J. Zubieta, M. B. Sponsler, *Organometallics* **2003**, *22*, 3485-3494.
[96] P. Yuan, X.-h. Wu, G.-a. Yu, D. Du, S. H. Liu, *J. Organomet. Chem.* **2007**, *692*, 3588-3592.
[97] S. H. Liu, Q. Y. Hu, P. Xue, T. B. Wen, I. D. Williams, G. Jia, *Organometallics* **2005**, *24*, 769-772.
[98] L.-B. Gao, J. Kan, Y. Fan, L.-Y. Zhang, S.-H. Liu, Z.-N. Chen, *Inorg. Chem.* **2007**, *46*, 5651-5664.
[99] L. Bonniard, S. Kahlal, A. K. Diallo, C. Ornelas, T. Roisnel, G. Manca, J. Rodrigues, J. Ruiz, D. Astruc, J.-Y. Saillard, *Inorg. Chem.* **2011**, *50*, 114-124.
[100] N. Le Narvor, C. Lapinte, *Organometallics* **1995**, *14*, 634-639.
[101] A. Barbieri, B. Ventura, L. Flamigni, F. Barigelletti, G. Fuhrmann, P. Bäuerle, S. Goeb, R. Ziessel, *Inorg. Chem.* **2005**, *44*, 8033-8043.
[102] A. De Nicola, Y. Liu, K. S. Schanze, R. Ziessel, *Chem. Commun.* **2003**, 288-289.
[103] a) F. A. Cotton, N. S. Dalal, C. Y. Liu, C. A. Murillo, J. M. North, X. P. Wang, *J. Am. Chem. Soc.* **2003**, *125*, 12945-12952; b) M. H. Chisholm, N. J. Patmore, *Acc. Chem. Res.* **2007**, *40*, 19-27.
[104] M. Ruben, A. Landa, E. Lörtscher, H. Riel, M. Mayor, H. Görls, H. B. Weber, A. Arnold, F. Evers, *Small* **2008**, *4*, 2229-2235.
[105] A. Harriman, A. Mayeux, A. De Nicola, R. Ziessel, *Phys. Chem. Chem. Phys.* **2002**, *4*, 2229-2235.
[106] J.-W. Ying, I. P.-C. Liu, B. Xi, Y. Song, C. Campana, J.-L. Zuo, T. Ren, *Angew. Chem. Int. Ed.* **2010**, 954–957.
[107] W. Y. Wong, W. K. Wong, P. R. Raithby, *J. Chem. Soc. Dalton.* **1998**, 2761-2766.
[108] P. K. Eggers, H. M. Zareie, M. N. Paddon-Row, J. J. Gooding, *Langmuir* **2009**, *25*, 11090-11096.
[109] J. M. Beebe, V. B. Engelkes, J. Liu, J. J. Gooding, P. K. Eggers, Y. Jun, X. Zhu, M. N. Paddon-Row, C. D. Frisbie, *J. Phys. Chem. B* **2005**, *109*, 5207-5215.
[110] M. A. Fox, R. L. Roberts, T. E. Baines, B. Le Guennic, J.-F. Halet, F. Hartl, D. S. Yufit, D. Albesa-Jové, J. A. K. Howard, P. J. Low, *J. Am. Chem. Soc.* **2008**, *130*, 3566-3578.
[111] S. Hbaieb, N. Amdouni, H. Parrot-Lopez, R. Kalfat, Y. Chevalier, *New. J. Chem.* **2011**, *35*, 36-40.
[112] a) M. J. Frampton, H. L. Anderson, *Angew. Chem. Int. Ed.* **2007**, *46*, 1028-1064; b) M. Hanack, A. Hirsch, A. Lange, M. Rein, G. Renz, P. Vermehren, *J. Mater. Res.* **1991**, *6*, 385-392.
[113] K. Jang, I. G. Jung, H. J. Nam, D.-Y. Jung, S. U. Son, *J. Am. Chem. Soc.* **2009**, *131*, 12046-12047.
[114] F. Cacialli, J. S. Wilson, J. J. Michels, C. Daniel, C. Silva, R. H. Friend, N. Severin, P. Samorì, J. P. Rabe, M. J. O'Connell, P. N. Taylor, H. L. Anderson, *Nat. Mater.* **2002**, *1*, 160-164.
[115] M. H. Chang, M. J. Frampton, H. L. Anderson, L. M. Herz, *Appl. Phys. Lett.* **2006**, *89*, 232110-232113.
[116] a) J. Terao, Y. Tanaka, S. Tsuda, N. Kambe, M. Taniguchi, T. Kawai, A. Saeki, S. Seki, *J. Am. Chem. Soc.* **2009**, *131*, 18046-18047; b) J. Terao, S. Tsuda, Y. Tanaka, K. Okoshi, T. Fujihara, Y. Tsuji, N. Kambe, *J. Am. Chem. Soc.* **2009**, *131*, 16004-16005.
[117] D. M. Guldi, B. M. Illescas, C. M. Atienza, M. Wielopolski, N. Martín, *Chem. Soc. Rev.* **2009**, *38*, 1587.
[118] J. R. Lakowicz, *Principles of fluorescence spectroscopy*, 2nd ed., Kluwer Academic/Plenum, New York, **1999**.
[119] R. Rudolf, M. Mongillo, R. Rizzuto, T. Pozzan, *Nat. Rev. Mol. Cell Bio.* **2003**, *4*, 579-586.
[120] M. Jurow, A. E. Schuckman, J. D. Batteas, C. M. Drain, *Coord. Chem. Rev.* **2010**, *254*, 2297-2310.
[121] J. Fortage, J. Boixel, E. Blart, L. Hammarström, H. C. Becker, F. Odobel, *Chem.-Eur. J.* **2008**, *14*, 3467-3480.
[122] A. Molina-Ontoria, M. Wielopolski, J. Gebhardt, A. Gouloumis, T. Clark, D. M. Guldi, N. Martín, *J. Am. Chem. Soc.* **2011**, *133*, 2370-2373.
[123] A. Ambroise, C. Kirmaier, R. W. Wagner, R. S. Loewe, D. F. Bocian, D. Holten, J. S. Lindsey, *J. Org. Chem.* **2002**, *67*, 3811-3826.
[124] B. Schlicke, P. Belser, L. De Cola, E. Sabbioni, V. Balzani, *J. Am. Chem. Soc.* **1999**, *121*, 4207-4214.
[125] a) A. C. Benniston, A. Harriman, P. Li, P. V. Patel, C. A. Sams, *J. Org. Chem.* **2006**, *71*, 3481-3493; b) A. Helms, D. Heiler, G. McLendon, *J. Am. Chem. Soc.* **1991**, *113*, 4325-4327.
[126] M. Moroni, J. Le Moigne, T. A. Pham, J. Y. Bigot, *Macromolecules* **1997**, *30*, 1964-1972.
[127] N. Zhou, Y. Zhao, *J. Org. Chem.* **2010**, *75*, 1498-1516.
[128] Y. Liu, M. S. Liu, X.-c. Li, A. K. Y. Jen, *Chem. Mater.* **1998**, *10*, 3301-3304.

[129] D. A. M. Egbe, A. Wild, E. Birckner, U.-W. Grummt, U. S. Schubert, *Macromol. Symp.* **2008**, *268*, 25-27.
[130] C. Weder, M. S. Wrighton, *Macromolecules* **1996**, *29*, 5157-5165.
[131] U. Mitschke, P. Bäuerle, *J. Mater. Chem.* **2000**, *10*, 1471-1507.
[132] B. Friedel, C. R. McNeill, N. C. Greenham, *Chem. Mater.* **2010**, 3389–3398.
[133] Z. Xu, D. Fichou, G. Horowitz, F. Garnier, *J. Electroanal. Chem.* **1989**, *267*, 339-342.
[134] N. Sumi, H. Nakanishi, S. Ueno, K. Takimiya, Y. Aso, T. Otsubo, *Bull. Chem. Soc. Jpn.* **2001**, *74*, 979-988.
[135] J. Bargon, S. Mohmand, R. J. Waltman, *IBM J. Res. Develop* **1983**, *27*, 330-331.
[136] F. Meyers, A. J. Heeger, J. L. Brédas, *J. Chem. Phys.* **1992**, *97*, 2750-2758.
[137] M. Akita, Y. Tanaka, C. Naitoh, T. Ozawa, N. Hayashi, M. Takeshita, A. Inagaki, M.-C. Chung, *Organometallics* **2006**, *25*, 5261-5275.
[138] a) L. Medei, L. Orian, O. V. Semeikin, M. G. Peterleitner, N. A. Ustynyuk, S. Santi, C. Durante, A. Ricci, C. Lo Sterzo, *Eur. J. Inorg. Chem.* **2006**, *2006*, 2582-2597; b) C. Lapinte, *J. Organomet. Chem.* **2008**, *693*, 793-801; c) F. de Montigny, G. Argouarch, K. Costuas, J.-F. Halet, T. Roisnel, L. Toupet, C. Lapinte, *Organometallics* **2005**, *24*, 4558-4572; d) F. de Montigny, G. Argouarch, T. Roisnel, L. Toupet, C. Lapinte, S. C.-F. Lam, C.-H. Tao, V. W.-W. Yam, *Organometallics* **2008**, *27*, 1912-1923; e) F. Justaud, G. Argouarch, S. I. Ghazala, L. Toupet, F. Paul, C. Lapinte, *Organometallics* **2008**, *27*, 4260-4264; f) S. I. Ghazala, F. Paul, L. Toupet, T. Roisnel, P. Hapiot, C. Lapinte, *J. Am. Chem. Soc.* **2006**, *128*, 2463-2476.
[139] A. K. Flatt, S. M. Dirk, J. C. Henderson, D. E. Shen, J. Su, M. A. Reed, J. M. Tour, *Tetrahedron Letters* **2003**, *59*, 8555-8570.
[140] I. Fratoddi, C. Battocchio, A. Furlani, P. Mataloni, G. Polzonetti, M. V. Russo, *J. Organomet. Chem.* **2003**, *674*, 10-23.
[141] M. S. Khan, M. R. A. Al-Mandhary, M. K. Al-Suti, T. C. Corcoran, Y. Al-Mahrooqi, J. P. Attfield, N. Feeder, W. I. F. David, K. Shankland, R. H. Friend, A. Köhler, E. A. Marseglia, E. Tedesco, C. C. Tang, P. R. Raithby, J. C. Collings, K. P. Roscoe, A. S. Batsanov, L. M. Stimson, T. B. Marder, *New J. Chem.* **2003**, *27*, 140-149.
[142] X. H. Wu, S. Jin, J. H. Liang, Z. Y. Li, G.-a. Yu, S. H. Liu, *Organometallics* **2009**, *28*, 2450-2459.
[143] X.-H. Wu, J. H. Liang, J.-L. Xia, S. Jin, G.-A. Yu, S. H. Liu, *Organometallics* **2010**, *29*, 1150-1156.
[144] X. H. Wu, J. H. Liang, J. L. Xia, J. Yin, S. Jin, G.-a. Yu, S. H. Liu, *Inorg. Chim. Acta* **2011**, *370*, 286-291.
[145] a) J. Ulrich, D. Esrail, W. Pontius, L. Venkataraman, D. Millar, L. H. Doerrer, *J. Phys. Chem. B* **2006**, *110*, 2462-2466; b) J. M. Seminario, A. G. Zacarias, J. M. Tour, *J. Am. Chem. Soc.* **1999**, *121*, 411-416; c) S. Grunder, R. Huber, S. Wu, C. Schönenberger, M. Calame, M. Mayor, *Eur. J. Org. Chem.* **2010**, 833-845; d) C. H. Xue, G. Arumugam, K. Palaniappan, S. A. Hackney, H. Y. Liu, J. Liu, *Chem. Comm.* **2005**, 1055-1057; e) D. T. Gryko, C. Clausen, K. M. Roth, N. Dontha, D. F. Bocian, W. G. Kuhr, J. S. Lindsey, *J. Org. Chem.* **2000**, *65*, 7345-7355.
[146] S. Dirk, *Tetrahedron* **2001**, *57*, 5109-5121.
[147] S. M. Dirk, J. M. Tour, *Tetrahedron* **2003**, *59*, 287-293.
[148] a) J.-C. Lin, J.-H. Kim, J. A. Kellar, M. C. Hersam, S. T. Nguyen, M. J. Bedzyk, *Langmuir* **2010**, *26*, 3771-3773; b) J. M. Notestein, C. Canlas, J. Siegfried, J. S. Moore, *Chem. Mater.* **2010**, *22*, 5319-5327.
[149] a) L. Venkataraman, J. E. Klare, I. W. Tam, C. Nuckolls, M. S. Hybertsen, M. L. Steigerwald, *Nano Lett.* **2006**, *6*, 458-462; b) F. Chen, X. Li, J. Hihath, Z. Huang, N. Tao, *J. Am. Chem. Soc.* **2006**, *128*, 15874-15881; c) Y. S. Park, A. C. Whalley, M. Kamenetska, M. L. Steigerwald, M. S. Hybertsen, C. Nuckolls, L. Venkataraman, *J. Am. Chem. Soc.* **2007**, *129*, 15768-15769; d) M. Kiguchi, S. Miura, T. Takahashi, K. Hara, M. Sawamura, K. Murakoshi, *J. Phys. Chem. C* **2008**, *112*, 13349-13352.
[150] a) C. A. Martin, D. Ding, J. K. Sørensen, T. Bjørnholm, J. M. van Ruitenbeek, H. S. J. van der Zant, *J. Am. Chem. Soc.* **2008**, *130*, 13198-13199; b) Y. Shirai, J. M. Guerrero, T. Sasaki, T. He, H. Ding, G. Vives, B.-C. Yu, L. Cheng, A. K. Flatt, P. G. Taylor, Y. Gao, J. M. Tour, *J. Org. Chem.* **2009**, *74*, 7885-7897.
[151] a) Z. Li, D. S. Kosov, *J. Phys. Chem. B* **2006**, *110*, 9893-9898; b) F. von Wrochem, D. Gao, F. Scholz, H.-G. Nothofer, G. Nelles, J. M. Wessels, *Nat. Nanotechnol.* **2010**, *5*, 618-624.
[152] a) B. Fabre, *Acc. Chem. Res.* **2010**, *43*, 1509-1518; b) M. Lu, T. He, J. M. Tour, *Chem. Mater.* **2008**, *20*, 7352-7355.
[153] S. T. Schneebeli, M. Kamenetska, Z. Cheng, R. Skouta, R. A. Friesner, L. Venkataraman, R. Breslow, *J. Am. Chem. Soc.* **2011**, *133*, 2136-2139.
[154] W. Chen, J. R. Widawsky, H. Vázquez, S. T. Schneebeli, M. S. Hybertsen, R. Breslow, L. Venkataraman, *J. Am. Chem. Soc.* **2011**, *133*, 17160-17163.
[155] a) E. Leary, M. T. González, C. van der Pol, M. R. Bryce, S. Filippone, N. Martín, G. Rubio-Bollinger, N. s. Agraït, *Nano Lett.* **2011**, *11*, 2236-2241; b) Y. Ie, T. Hirose, A. Yao, T. Yamada, N. Takagi, M. Kawai, Y.

Aso, *Phys. Chem. Chem. Phys.* **2009**, *11*, 4949-4951; c) Y. Ie, T. Hirose, H. Nakamura, M. Kiguchi, N. Takagi, M. Kawai, Y. Aso, *J. Am. Chem. Soc.* **2011**, *133*, 3014-3022.
[156] http://hyperphysics.phy-astr.gsu.edu/hbase/solids/fermi.html (08-03-2011).
[157] N. Prokopuk, K.-A. Son, *J. Phys.: Condens. Matter.* **2008**, *20*, 374116-374137.
[158] a) J. G. Kushmerick, A. S. Blum, D. P. Long, *Anal. Chim. Acta* **2006**, *568*, 20-27; b) J. G. Kushmerick, J. Lazorcik, C. H. Patterson, R. Shashidhar, D. S. Seferos, G. C. Bazan, *Nano Lett.* **2004**, *4*, 639-642.
[159] M. A. Rampi, O. J. A. Schueller, G. M. Whitesides, *Appl. Phys. Lett.* **1998**, *72*, 1781-1783.
[160] a) E. Tran, M. A. Rampi, G. M. Whitesides, *Angew. Chem. Int. Ed.* **2004**, *43*, 3835-3839; b) E. Tran, C. Grave, G. M. Whitesides, M. A. Rampi, *Electrochim. Acta* **2005**, *50*, 4850-4856.
[161] F. Giacalone, M. A. Herranz, L. Gruter, M. T. Gonzalez, M. Calame, C. Schonenberger, C. R. Arroyo, G. Rubio-Bollinger, M. Velez, N. Agrait, N. Martin, *Chem. Commun.* **2007**, 4854-4856.
[162] Xiao, Xu, N. J. Tao, *Nano Lett.* **2004**, *4*, 267-271.
[163] A. Busiakiewicz, S. Karthauser, M. Homberger, P. Kowalzik, R. Waser, U. Simon, *Phys. Chem. Chem. Phys.* **2010**, *12*, 10518-10524.
[164] a) F. Matino, G. Schull, F. Kohler, S. Gabutti, M. Mayor, R. Berndt, *P. Natl. Acad. Sci. USA* **2011**, *108*, 961-964; b) A. Blaszczyk, M. Chadim, C. von Hanisch, M. Mayor, *Eur. J. Org. Chem.* **2006**, 3809-3825; c) A. Blaszczyk, M. Fischer, C. von Hanisch, M. Mayor, *Eur J Org Chem* **2007**, 2630-2642; d) N. Weibel, S. Grunder, M. Mayor, *Org. Biomol. Chem.* **2007**, *5*, 2343-2353; e) E. Lortscher, M. Elbing, M. Tschudy, C. von Hanisch, H. B. Weber, M. Mayor, H. Riel, *Chemphyschem* **2008**, *9*, 2252-2258; f) R. Huber, M. T. González, S. Wu, M. Langer, S. Grunder, V. Horhoiu, M. Mayor, M. R. Bryce, C. Wang, R. Jitchati, C. Schönenberger, M. Calame, *J. Am. Chem. Soc.* **2007**, *130*, 1080-1084; g) M. Mayor, *Angew. Chem. Int. Ed.* **2009**, *48*, 5583-5585; h) Z. Mu, L. Shu, H. Fuchs, M. Mayor, L. Chi, *Langmuir* **2011**, *27*, 1359-1363.
[165] Y. Noguchi, T. Nagase, R. Ueda, T. Kamikado, T. Kubota, S. Mashiko, *Jpn. J. Appl. Phys.* **2007**, *46*, 2683-2686.
[166] S. Kronholz, S. Karthauser, A. van der Hart, T. Wandlowski, R. Waser, *Microelectron. J.* **2006**, *37*, 591-594.
[167] F. Chen, Q. Qing, L. Ren, Z. Y. Wu, Z. F. Liu, *Appl. Phys. Lett.* **2005**, *86*, 123105-123107.
[168] a) K. Shigeto, M. Kawamura, A. Y. Kasumov, K. Tsukagoshi, K. Kono, Y. Aoyagi, *Microelectron. Eng.* **2006**, *83*, 1471-1473; b) M. D. Fischbein, M. Drndic, *Appl. Phys. Lett.* **2006**, *88*, 063116-063118.
[169] a) A. Hatzor, P. S. Weiss, *Science* **2001**, *291*, 1019-1020; b) R. Negishi, T. Hasegawa, K. Terabe, M. Aono, H. Tanaka, T. Ogawa, H. Ozawa, *Appl. Phys. Lett.* **2007**, *90*, 223112-223114.
[170] a) S. Takahashi, H. Morimoto, E. Murata, S. Kataoka, K. Sonogashira, N. Hagihara, *J. Polym. Sci. Polym. Chem. Ed.* **1982**, *20*, 565-573; b) V. W. W. Yam, L. J. Zhang, C. H. Tao, K. M. C. Wong, K. K. Cheung, *J. Chem. Soc. Dalton Trans.* **2001**, 1111-1116; c) S. Takahashi, E. Murata, M. Kariya, K. Sonogashira, N. Hagihara, *Macromolecules* **1979**, *12*, 1016-1018; d) S. Takahashi, M. Kariya, T. Yatake, K. Sonogashira, N. Hagihara, *Macromolecules* **1978**, *11*, 1063-1066; e) D. Taher, B. Walfort, G. Van Koten, H. Lang, *Inorg. Chem. Commun.* **2006**, *9*, 955-958; f) D. Taher, B. Walfort, H. Lang, *Inorg. Chim. Acta* **2006**, *359*, 1899-1906; g) J. Lewis, N. J. Long, P. R. Raithby, G. P. Shields, W. Y. Wong, M. Younus, *J. Chem. Soc. Dalton Trans.* **1997**, 4283-4288.
[171] a) O. Lavastre, M. Even, P. H. Dixneuf, A. Pacreau, J.-P. Vairon, *Organometallics* **1996**, *15*, 1530-1531; b) O. Lavastre, J. Plass, P. Bachmann, S. Guesmi, C. Moinet, P. H. Dixneuf, *Organometallics* **1997**, *16*, 184-189.
[172] a) A. La Groia, A. Ricci, M. Bassetti, D. Masi, C. Bianchini, C. Lo Sterzo, *J. Organomet. Chem* **2003**, *683*, 406-420; b) H. Lang, D. Taher, B. Walfort, H. Pritzkow, *J. Organomet. Chem.* **2006**, *691*, 3834-3845; c) H. Lang, K. Doring, D. Taher, U. Siegert, B. Walfort, T. Ruffer, R. Holze, *J. Organomet. Chem.* **2009**, *694*, 27-35; d) H. Ogawa, K. Onitsuka, T. Joh, S. Takahashi, Y. Yamamoto, H. Yamazaki, *Organometallics* **1988**, *7*, 2257-2260.
[173] C. Battocchio, I. Fratoddi, M. V. Russo, V. Carravetta, S. Monti, G. Iucci, F. Borgatti, G. Polzonetti, *Surf. Sci.* **2007**, *601*, 3943-3947.
[174] K. Onitsuka, S. Yamamoto, S. Takahashi, *Ang. Chem. Int. Ed.* **1999**, *38*, 174-176.
[175] a) J. M. Tour, *Chem. Rev.* **1996**, *96*, 537-553; b) M. A. Reed, C. Zhou, C. J. Muller, T. P. Burgin, J. M. Tour, *Science* **1997**, *278*, 252-254; c) J. M. Seminario, A. G. Zacarias, J. M. Tour, *J. Am. Chem. Soc.* **1998**, *120*, 3970-3974; d) D. J. Wold, C. D. Frisbie, *J. Am. Chem. Soc.* **2000**, *122*, 2970-2971; e) X. D. Cui, A. Primak, X. Zarate, J. Tomfohr, O. F. Sankey, A. L. Moore, T. A. Moore, D. Gust, G. Harris, S. M. Lindsay, *Science* **2001**, *294*, 571-574; f) D. J. Wold, C. D. Frisbie, *J. Am. Chem. Soc.* **2001**, *123*, 5549-5556.

[176] T. L. Schull, J. G. Kushmerick, C. H. Patterson, C. George, M. H. Moore, S. K. Pollack, R. Shashidhar, *J. Am. Chem. Soc.* **2003**, *125*, 3202-3203.

[177] P. Siemsen, U. Gubler, C. Bosshard, P. Gunter, F. Diederich, *Chem. Eur. J.* **2001**, *7*, 1333-1341.

[178] D. Osella, L. Milone, C. Nervi, M. Ravera, *J. Organomet. Chem.* **1995**, *488*, 1-7.

[179] J. A. Kramer, D. N. Hendrickson, *Inorg. Chem.* **1980**, *19*, 3330-3337.

[180] Q. Ge, G. T. Dalton, M. G. Humphrey, M. Samoc, T. S. A. Hor, *Chem. Asian J.* **2009**, *4*, 998-1005.

[181] S. C. Jones, V. Coropceanu, S. Barlow, T. Kinnibrugh, T. Timofeeva, J.-L. Brédas, S. R. Marder, *J. Am. Chem. Soc.* **2004**, *126*, 11782-11783.

[182] C. Lambert, G. Nöll, *J. Am. Chem. Soc.* **1999**, *121*, 8434-8442.

[183] M. Koch, J. A. Garg, O. Blacque, K. Venkatesan, *J. Organomet. Chem.* **2012**, *700*, 154-159.

[184] W.-Y. Wong, K.-Y. Ho, S.-L. Ho, Z. Lin, *J. Organomet. Chem.* **2003**, *683*, 341-353.

[185] M. Shiotsuka, N. Nishiko, K. Keyaki, K. Nozaki, *Dalton Trans.* **2010**, *39*, 1831.

[186] a) C. Liao, J. E. Yarnell, K. D. Glusac, K. S. Schanze, *J. Phys. Chem. B* **2010**, *114*, 14763-14771; b) J. M. Keller, K. D. Glusac, E. O. Danilov, S. McIlroy, P. Sreearuothai, A. R. Cook, H. Jiang, J. R. Miller, K. S. Schanze, *J. Am. Chem. Soc.* **2011**, *133*, 11289-11298.

[187] a) T.-Y. Dong, S.-W. Chang, S.-F. Lin, M.-C. Lin, Y.-S. Wen, L. Lee, *Organometallics* **2006**, *25*, 2018-2024; b) T.-Y. Dong, M.-C. Lin, S.-W. Chang, C.-C. Ho, S.-F. Lin, L. Lee, *J. Organomet. Chem.* **2007**, *692*, 2324-2333; c) T.-Y. Dong, H.-Y. Lin, S.-F. Lin, C.-C. Huang, Y.-S. Wen, L. Lee, *Organometallics* **2008**, *27*, 555-562; d) C.-H. Tao, N. Zhu, V. W.-W. Yam, **2009**, *207*, 94-101; e) C.-H. Tao, V. W.-W. Yam, *J. Photochem. Photobiol. C: Photochem. Rev.* **2009**, *10*, 130-140; f) E. G. Tennyson, R. C. Smith, *Inorg. Chem.* **2009**, *48*, 11483-11485; g) C. K. M. Chan, C.-H. Tao, H.-L. Tam, N. Zhu, V. W.-W. Yam, K.-W. Cheah, *Inorg. Chem.* **2009**, *48*, 2855-2864; h) Z. Ji, S. Li, Y. Li, W. Sun, *Inorg. Chem.* **2010**, *49*, 1337-1346; i) V. W.-W. Yam, K. K.-W. Lo, Luminescence Behavior & Photochemistry of Organotransition Metal Compounds in *Encyclopedia of Inorganic and Bioinorganic Chemistry*, Wiley, **2011**; j) K.-Q. Wu, J. Guo, J.-F. Yan, L.-L. Xie, F.-B. Xu, S. Bai, P. Nockemann, Y.-F. Yuan, *Dalton Trans.* **2012**, *41*, 11000-11008.

[188] a) R. F. Heck, J. P. Nolley, *J. Org. Chem.* **1972**, *37*, 2320-2322; b) R. J. Lundgren, M. Stradiotto, *Chem. Eur. J.* **2012**, *18*, 9758-9769.

[189] a) N. Miyaura, A. Suzuki, *Chem.Rev.* **1995**, *95*, 2457-2483; b) E.-i. Negishi, Q. Hu, Z. Huang, M. Qian, G. Wang, *Aldrichim. Acta* **2005**, *38*, 71-88; c) R. Jana, T. P. Pathak, M. S. Sigman, *Chem. Rev.* **2011**, *111*, 1417-1492; d) R. Chinchilla, C. Nájera, *Chem. Rev.* **2007**, *107*, 874-922; e) C. Barnard, *Platinum Metals Rev.* **2008**, *52*, 38-45.

[190] A. Organics", *Palladium-Catalysed Coupling Chemistry*, **2011**.

[191] C. A. Tolman, *Chem. Rev.* **1977**, *77*, 313-348.

[192] A. de Meijere, F. Diederich, *Metal-catalyzed cross-coupling reactions*, 2nd ed., Wiley-VCH, Weinheim, **2004**.

[193] K. Sonogashira, Y. Tohda, N. Hagihara, *Tetrahedron Lett.* **1975**, *16*, 4467-4470.

[194] A. O. King, N. Okukado, E.-i. Negishi, *J. Chem. Soc., Chem. Commun.* **1977**, 683-684.

[195] N. Miyaura, *Tetrahedron Lett.* **1979**, *20*, 3437-3440.

[196] D. Milstein, J. K. Stille, *J. Am. Chem. Soc.* **1978**, *100*, 3636-3638.

[197] a) R. D. Stephens, C. E. Castro, *J. Org. Chem.* **1963**, *28*, 3313-3315; b) D. C. Owsley, C. E. Castro, *Org. Synth.* **1988**, *Coll. Vol. 6*, 916-918.

[198] U. H. F. Bunz, *Chem. Rev.* **2000**, *100*, 1605-1644.

[199] V. Polshettiwar, C. Len, A. Fihri, *Coord. Chem. Rev.* **2009**, *253*, 2599-2626.

[200] B. Liang, M. Dai, J. Chen, Z. Yang, *J. Org. Chem.* **2005**, *70*, 391-393.

[201] M. Kosugi, K. Sasazawa, Y. Shimizu, T. Migita, *Chem. Lett.* **1977**, 301-302.

[202] M. I. Bruce, B. G. Ellis, P. J. Low, B. W. Skelton, A. H. White, *Organometallics* **2003**, *22*, 3184-3198.

[203] a) K. Ouzzine, H. Le Bozec, P. H. Dixneuf, *J. Organomet. Chem.* **1986**, *317*, C25-C27; b) C. Olivier, S. Choua, P. Turek, D. Touchard, S. Rigaut, *Chem. Commun.* **2007**, 3100-3102; c) S. Rigaut, J. Massue, D. Touchard, J.-L. Fillaut, S. Golhen, P. H. Dixneuf, *Angew. Chem. Int. Ed.* **2002**, *41*, 4513-4517; d) M. I. Bruce, R. C. Wallis, *Aust. J. Chem.* **1979**, *32*, 1471-1485.

[204] a) A. Davison, J. P. Selegue, *J. Am. Chem. Soc.* **1978**, *100*, 7763-7765; b) A. Davison, J. Solar, *J. Organomet. Chem.* **1978**, *155*, C8-C12; c) T. Weyland, K. Costuas, A. Mari, J.-F. Halet, C. Lapinte, *Organometallics* **1998**, *17*, 5569-5579.

[205] a) M. I. Bruce, J. Davy, B. C. Hall, Y. J. van Galen, B. W. Skelton, A. H. White, *Appl. Organomet. Chem.* **2002**, *16*, 559-568; b) C. Battocchio, I. Fratoddi, R. Vitaliano, M. V. Russo, G. Polzonetti, *Solid State Sci.* **2010**, *12*, 1881-1885.
[206] V. Wing-Wah Yam, L. Zhang, C.-H. Tao, K. Man-Chung Wong, K.-K. Cheung, *J. Chem. Soc. Dalton Trans.* **2001**, 1111-1116.
[207] F. Kessler, B. Weibert, H. Fischer, *Organometallics* **2010**, *29*, 5154-5161.
[208] O. Lavastre, L. Ollivier, P. H. Dixneuf, S. Sibandhit, *Tetrahedron* **1996**, *52*, 5495-5504.
[209] S. M. Dirk, D. W. Price, S. Chanteau, D. V. Kosynkin, J. M. Tour, *Tetrahedron* **2001**, *57*, 5109-5121.
[210] J. Figueira, J. Rodrigues, L. Russo, K. Rissanen, *Acta Cryst. C.* **2008**, *64*, O33-O36.
[211] a) A. Palmgren, A. Thorarensen, J.-E. Bäckvall, *J. Org. Chem.* **1998**, *63*, 3764-3768; b) Q. Hua Cheng, *Tetrahedron: Asymmetry* **1996**, *7*, 3083-3086.
[212] J. M. Tour, *Molecular electronics: commercial insights, chemistry, devices, architecture, and programming*, World Scientific, River Edge, N.J., **2003**.
[213] K. Sonogashira, *Tetrahedron Lett.* **1975**, *16*, 4467-4470.
[214] a) A. Nagy, Z. Novák, A. Kotschy, *J. Organomet. Chem* **2005**, *690*, 4453-4461; b) K. L. Chandra, S. Zhang, C. B. Gorman, *Tetrahedron* **2007**, *63*, 7120-7132.
[215] P. G. Gassman, T. L. Guggenheim, *J. Am. Chem. Soc.* **1982**, *104*, 5849-5850.
[216] E. C. Minnihan, S. L. Colletti, F. D. Toste, H. C. Shen, *J. Org. Chem.* **2007**, *72*, 6287-6289.
[217] W. M. Seganish, P. DeShong, *J. Org. Chem.* **2004**, *69*, 6790-6795.
[218] S. Ma, L. Lu, J. Zhang, *J. Am. Chem. Soc.* **2004**, *126*, 9645-9660.
[219] S. P. H. Mee, V. Lee, J. E. Baldwin, *Angew. Chem. Int. Ed.* **2004**, *43*, 1132-1136.
[220] R. D. Kimbrough, *Environ. Health Perspect.* **1976**, *14*, 51-56.
[221] a) T. X. Neenan, G. M. Whitesides, *J. Org. Chem.* **1988**, *53*, 2489-2496; b) K. D. Ley, Y. Li, J. V. Johnson, D. H. Powell, K. S. Schanze, *Chem. Commun.* **1999**, 1749-1750.
[222] a) K. Onitsuka, H. Ogawa, T. Joh, S. Takahashi, Y. Yamamoto, H. Yamazaki, *J. Chem. Soc. Dalton Trans.* **1991**, 1531-1536; b) N. Ohshiro, F. Takei, K. Onitsuka, S. Takahashi, *J. of Organometallic Chem.* **1998**, *569*, 195-202; c) S. Takahashi, Y. Takai, H. Morimoto, K. Sonogashira, *J. Chem. Soc., Chem. Commun.* **1984**, 3; d) S. Takahashi, Y. Takai, H. Morimoto, K. Sonogashira, N. Hagihara, *Mol. Cryst. Liq. Cryst.* **1982**, *82*, 139-143; e) K. Sonogashira, S. Takahashi, N. Hagihara, *Macromolecules* **1977**, *10*, 879-880; f) K. Sonogashira, *J. Organomet. Chem.* **1978**, *145*, 101-108; g) K. Sonogashira, *J. Organomet. Chem.* **1978**, *160*, 319-327.
[223] R. Nast, A. Beyer, *J. Organomet. Chem.* **1980**, *194*, 125-130.
[224] a) P. Haquette, *J. Org. Chem.* **1998**, *565*, 63-73; b) S. Hurst, *Inorg. Chim. Acta* **2003**, *350*, 62-76; c) M. A. Fox, J. E. Harris, S. Heider, V. Pérez-Gregorio, M. E. Zakrzewska, J. D. Farmer, D. S. Yufit, J. A. K. Howard, P. J. Low, *J. Organomet. Chem.* **2009**, *694*, 2350-2358.
[225] B. Chin, A. J. Lough, R. H. Morris, C. T. Schweitzer, C. D'Agostino, *Inorg. Chem.* **1994**, *33*, 6278-6288.
[226] B. P. Sullivan, T. J. Meyer, *Inorg. Chem.* **1982**, *21*, 1037-1040.
[227] M. Ponikvar, *J. Fluorine Chem.* **2003**, *123*, 217-220.
[228] a) R. Fernandez-Galan, B. R. Manzano, A. Otero, M. Lanfranchi, M. A. Pellinghelli, *Inorg. Chem.* **1994**, *33*, 2309-2312; b) M. G. Freire, C. M. S. S. Neves, I. M. Marrucho, J. o. A. P. Coutinho, A. M. Fernandes, *J. Phys. Chem. A* **2010**, *114*, 3744-3749.
[229] a) Cheng, Y.-C. Kuo, S.-H. Chang, Y.-C. Lin, Y.-H. Liu, Y. Wang, *J. Am. Chem. Soc.* **2007**, *129*, 14974-14980; b) K.-H. Chen, Y. J. Feng, H.-W. Ma, Y.-C. Lin, Y.-H. Liu, T.-S. Kuo, *Organometallics* **2010**, *29*, 6829-6836; c) H.-H. Chou, Y.-C. Lin, S.-L. Huang, Y.-H. Liu, Y. Wang, *Organometallics* **2008**, *27*, 5212-5220.
[230] H. Le Bozec, K. Ouzzine, P. H. Dixneuf, *Organometallics* **1991**, *10*, 2768-2772.
[231] S.-M. Yang, M. C.-W. Chan, K.-K. Cheung, C.-M. Che, S.-M. Peng, *Organometallics* **1997**, *16*, 2819-2826.
[232] Y. Zhu, D. B. Millet, M. O. Wolf, S. J. Rettig, *Organometallics* **1999**, *18*, 1930-1938.
[233] L. Russo, J. Figueira, J. Rodrigues, K. Rissanen, *Acta Cryst. E* **2006**, *62*, M699-M701.
[234] a) J. Figueira, J. Rodrigues, K. Rissanen, *Acta Cryst. E* **2006**, *62*, m3594-m3596; b) L. Russo, J. Figueira, J. Rodrigues, K. Rissanen, *Acta Cryst. E* **2006**, *62*, M1154-M1155.
[235] S. Rigaut, J. Perruchon, L. Le Pichon, D. Touchard, P. H. Dixneuf, *J. Organomet. Chem.* **2003**, *670*, 37-44.
[236] N. J. Long, C. K. Williams, *Angew. Chem. Int. Ed.* **2003**, *42*, 2586-2617.
[237] G. Albertin, S. Antoniutti, E. Bordignon, *J. Organomet. Chem.* **1996**, *513*, 147-153.
[238] D. James, J. M. Tour, *Aldrichim. Acta* **2006**, *39*, 47-56.

[239] a) S. Percec, R. Getty, W. Marshall, G. Skidd, R. French, *J. Pol. Sci.: Part A: Pol. Chem.* **2004**, *42*, 541-550; b) J. P. Collman, M. Zhong, S. Costanzo, C. J. Sunderland, A. Aukauloo, K. Berg, L. Zeng, *Synthesis* **2001**, *2001*, 0367-0369.

[240] R. P. Hsung, C. E. D. Chidsey, L. R. Sita, *Organometallics* **1995**, *14*, 4808-4815.

[241] a) L. Norel, K. Bernot, M. Feng, T. Roisnel, A. Caneschi, R. Sessoli, S. Rigaut, *Chem. Comm.* **2012**, *48*, 2105-2113; b) E. Di Piazza, L. Norel, K. Costuas, A. Bourdolle, O. Maury, S. Rigaut, *J. Am. Chem. Soc.* **2011**, *133*, 6174-6176.

[242] G. Grelaud, M. P. Cifuentes, T. Schwich, G. Argouarch, S. Petrie, R. Stranger, F. Paul, M. G. Humphrey, *Eur. J. Inorg. Chem.* **2012**, 65-75.

[243] a) B. G. Bharate, A. N. Jadhav, S. S. Chavan, *Polyhedron* **2012**, *33*, 179-184; b) N. Gauthier, G. Argouarch, F. Paul, L. Toupet, A. Ladjarafi, K. Costuas, J.-F. Halet, M. Samoc, M. P. Cifuentes, T. C. Corkery, M. G. Humphrey, *Chem. Eur. J.* **2011**, *17*, 5561-5577; c) M. Samoc, T. C. Corkery, A. M. McDonagh, M. P. Cifuentes, M. G. Humphrey, *Aust. J. Chem.* **2011**, *64*, 1267-1271.

[244] F. R. Pavan, G. V. Poelhsitz, M. I. F. Barbosa, S. R. A. Leite, A. A. Batista, J. Ellena, L. S. Sato, S. G. Franzblau, V. Moreno, D. Gambino, C. Q. F. Leite, *Eur. J. Med. Chem.* **2011**, *46*, 5099-5107.

[245] a) M. G. Jardim, K. Rissanen, J. Rodrigues, *Eur. J. Inorg. Chem.* **2010**, 1729-1735; b) J. Rodrigues, M. G. Jardim, J. Figueira, M. Gouveia, H. Tomas, K. Rissanen, *New J. Chem.* **2012**, *35*, 1938–1943; c) D. G. Branzea, A. Fihey, T. Cauchy, A. El-Ghayoury, N. Avarvari, *Inorg. Chem.* **2012**, *51*, 8545-8556.

[246] J. Chatt, R. G. Hayter, *J. Chem. Soc.* **1961**, 772-774.

[247] P. S. Hallman, D. Evans, J. A. Osborn, G. Wilkinson, *Chem. Comm.* **1967**, 305-306.

[248] a) S.-I. Murahashi, H. Takaya, T. Naota, *Pure Appl. Chem.* **2002**, *74*, 19-24; b) T. Naota, H. Takaya, S.-I. Murahashi, *Chem. Rev.* **1998**, *98*, 2599-2660; c) B. Bosnich, *Aldrichchim. Acta* **1998**, *31*, 76-83; d) T. Naota, Y. Shichijo, S.-I. Murahashi, *J. Chem. Soc., Chem. Commun.* **1994**, 1359-1360; e) S. Murahashi, T. Naota, E. Saito, *J. Am. Chem. Soc.* **1986**, *108*, 7846-7847; f) T. Naota, H. Taki, M. Mizuno, S. Murahashi, *J. Am. Chem. Soc.* **1989**, *111*, 5954-5955; g) S.-I. Murahashi, T. Naota, H. Taki, M. Mizuno, H. Takaya, S. Komiya, Y. Mizuho, N. Oyasato, M. Hiraoka, *J. Am. Chem. Soc.* **1995**, *117*, 12436-12451; h) A. Mutch, M. Leconte, F. Lefebvre, J.-M. Basset, *J. Mol. Cat. A: Chem.* **1998**, *133*, 191-199.

[249] a) H. Hayashi, S. Ogo, T. Abura, S. Fukuzumi, *J. Am. Chem. Soc.* **2003**, *125*, 14266-14267; b) S. Ogo, T. Abura, Y. Watanabe, *Organometallics* **2002**, *21*, 2964-2969; c) C. P. Casey, N. A. Strotman, S. E. Beetner, J. B. Johnson, D. C. Priebe, I. A. Guzei, *Organometallics* **2006**, *25*, 1236-1244; d) C. P. Casey, N. A. Strotman, S. E. Beetner, J. B. Johnson, D. C. Priebe, T. E. Vos, B. Khodavandi, I. A. Guzei, *Organometallics* **2006**, *25*, 1230-1235.

[250] X.-Y. Yi, H.-Y. Ng, I. D. Williams, W.-H. Leung, *Inorg. Chem.* **2011**, *50*, 1161-1163.

[251] a) C. L. Lund, M. J. Sgro, R. Cariou, D. W. Stephan, *Organometallics* **2012**, *31*, 802-805; b) S. E. Clapham, A. Hadzovic, R. H. Morris, *Coord. Chem. Rev.* **2004**, *248*, 2201-2237.

[252] P. S. Hallman, B. R. McGarvey, G. Wilkinson, *J. Chem. Soc. A* **1968**, 3143-3150.

[253] M. Jimenez-Tenorio, M. C. Puerta, P. Valerga, *Inorg. Chem.* **1994**, *33*, 3515-3520.

[254] J. Shen, E. D. Stevens, S. P. Nolan, *Organometallics* **1998**, *17*, 3875-3882.

[255] S. P. Nolan, T. R. Belderrain, R. H. Grubbs, *Organometallics* **1997**, *16*, 5569-5571.

[256] E. Pretsch, P. Bühlmann, M. Badertscher, *Structure determination of organic compounds: tables of spectral data*, 4th ed., Springer, Berlin, **2009**.

[257] S. Nakatsuji, K. Matsuda, Y. Uesugi, K. Nakashima, S. Akiyama, W. Fabian, *J. Chem. Soc. Perkin Trans. 1* **1992**, 755-758.

[258] a) C. L. Choi, Y. F. Cheng, C. Yip, D. L. Phillips, V. W.-W. Yam, *Organometallics* **2000**, *19*, 3192-3196; b) W. M. Kwok, D. L. Phillips, P. K. Y. Yeung, V. W. W. Yam, *Chem. Phys. Lett.* **1996**, *262*, 699-708; c) H. Masai, K. Sonogashira, N. Hagihara, *Bull. Chem. Soc. Jpn.* **1971**, *44*, 2226-2230; d) W. M. Kwok, D. L. Phillips, P. K. Y. Yeung, V. W. W. Yam, *J. Phys. Chem. A* **1997**, *101*, 9286-9295; e) V. W.-W. Yam, C.-H. Tao, L. Zhang, K. M.-C. Wong, K.-K. Cheung, *Organometallics* **2001**, *20*, 453-459.

[259] R. B. Jordan, *Reaction Mechanisms Of Inorganic And Organometallic Systems*, 2nd ed., Oxford University Press, New York, **1998**.

[260] Y. Suenaga, Y. Hirano, Y. Umehata, K. Kamei, M. Maekawa, *RIST, Science and Technology* **2011**, *2011/2012*, 23-33.

[261] H. Günther, *NMR Spectroscopy: Basic Principles, Concepts, and Applications in Chemistry*, 2nd ed., **1996**.

[262] K. Ohmura, M. Kijima, H. Shirakawa, *Synthetic Met.* **1997**, *84*, 417-418.

[263] C. E. Powell, M. P. Cifuentes, M. G. Humphrey, A. C. Willis, J. P. Morrall, M. Samoc, *Polyhedron* **2007**, *26*, 284-289.

[264] L. J. Farrugia, *J. Appl. Cryst.* **1997**, *30*, 565-565.
[265] C. F. Macrae, I. J. Bruno, J. A. Chisholm, P. R. Edgington, P. McCabe, E. Pidcock, L. Rodriguez-Monge, R. Taylor, J. van de Streek, P. A. Wood, *J. Appl. Crystallogr.* **2008**, *41*, 466-470.
[266] a) Z.-L. Cheng, Q.-Y. Chen, *J. Fluor. Chem.* **2005**, *126*, 39-43; b) Z.-L. Cheng, Q.-Y. Chen, *J. Fluor. Chem.* **2005**, *126*, 93-97; c) J. M. Gu, X. R. Hu, M. S. Xu, *Acta Cryst. E* **2004**, *60*, o1224-o1225; d) K. Costuas, F. Paul, L. Toupet, J.-F. Halet, C. Lapinte, *Organometallics* **2004**, *23*, 2053-2068.
[267] a) T. Iijima, S.-I. Kuroda, T. Yamamoto, *Macromolecules* **2008**, *41*, 1654-1662; b) O. J. Dautel, G. Wantz, D. Flot, J.-P. Lere-Porte, J. J. E. Moreau, J.-P. Parneix, F. Serein-Spirau, L. Vignau, *J. Mat. Chem.* **2005**, *15*, 4446; c) C. Xue, F.-T. Luo, *Tetrahedron* **2004**, *60*, 6285-6294; d) R. Thomas, S. Varghese, G. U. Kulkarni, *J. Mat. Chem.* **2009**, *19*, 4401; e) H. Li, D. R. Powell, R. K. Hayashi, R. West, *Macromolecules* **1998**, *31*, 52-58; f) W. Haiss, C. Wang, I. Grace, A. S. Batsanov, D. J. Schiffrin, S. J. Higgins, M. R. Bryce, C. J. Lambert, R. J. Nichols, *Nature Mater.* **2006**, *5*, 995-1002; g) A. R. Ramesh, K. G. Thomas, *Chem. Commun.* **2010**, *46*, 3457.
[268] H. Nakayama, S. Kimura, *J. Phys. Chem. A* **2011**, *115*, 8960-8968.
[269] W. M. Khairul, M. A. Fox, P. A. Schauer, D. S. Yufit, D. Albesa-Jové, J. A. K. Howard, P. J. Low, *Dalton Trans.* **2010**, *39*, 11605-11615.
[270] R. G. Ball, B. R. James, J. Trotter, D. K. W. Wang, K. R. Dixon, *J. Chem. Soc., Chem. Commun.* **1979**, 460-461.
[271] B. Delavaux, B. Chaudret, J. Devillers, F. Dahan, G. Commenges, R. Poilblanc, *J. Am. Chem. Soc.* **1986**, *108*, 3703-3711.
[272] G. R. Clark, A. Falshaw, G. J. Gainsford, C. Lensink, A. T. Slade, L. James Wright, *J. Coord. Chem.* **2010**, *63*, 373-393.
[273] a) I. W. Wyman, T. J. Burchell, K. N. Robertson, T. S. Cameron, M. A. S. Aquino, *Organometallics* **2004**, *23*, 5353-5364; b) N. T. Lucas, C. E. Powell, M. G. Humphrey, *Acta Cryst. C* **2000**, *56*, e392-e393.
[274] E. B. Boyar, P. A. Harding, S. D. Robinson, C. P. Brock, *J. Chem. Soc., Dal. Trans.* **1986**, 1771-1778.
[275] S. Holle, P. W. Jolly, J. Kuhnigk, *J. Organomet. Chem.* **1997**, *543*, 255-258.
[276] a) T. D. Keene, M. B. Hursthouse, D. J. Price, *Acta Cryst. E* **2004**, *60*, m381-m383; b) S. García-Granda, V. Calvo-Pérez, F. Gómez-Beltrán, **1993**, *49*, 322-324.
[277] A. G. Beirakhov, I. M. Orlova, Z. R. Ashurov, G. M. Lobanova, Y. N. Mikhailov, R. N. Shchelokov, *Russ. J. Inorg. Chem.* **1981**, *26*, 718-719.
[278] M.-S. Wang, G.-C. Guo, L.-Z. Cai, G.-W. Zhou, J.-S. Huang, *Chin. J. Struct. Chem.* **2003**, *22*, 427-428.
[279] L. Dobrzańska, *Acta Cryst. E* **2005**, *61*, m1625-m1627.
[280] S. Scholz, H.-W. Lerner, M. Bolte, *Acta Cryst. E* **2006**, *62*, m312-m313.
[281] a) T. Kimura, T. Sakurai, M. Shima, T. Nagai, K. Mizumachi, T. Ishimori, *Acta Cryst. B* **1982**, *38*, 112-115; b) B. Demerseman, M. D. Mbaye, D. Sémeril, L. Toupet, C. Bruneau, P. H. Dixneuf, *Eur. J. Inorg. Chem.* **2006**, *2006*, 1174-1181; c) D. B. Dell'Amico, F. Calderazzo, L. Labella, F. Marchetti, *J. Organomet. Chem.* **2000**, *596*, 144-151; d) P. W. Blosser, J. C. Gallucci, A. Wojcicki, *J. Mol. Catal. A: Chem.* **2004**, *224*, 133-144; e) O. R. Allen, S. J. Dalgarno, L. D. Field, P. Jensen, A. C. Willis, *Organometallics* **2009**, *28*, 2385-2390; f) C. E. Ellul, O. Saker, M. F. Mahon, D. C. Apperley, M. K. Whittlesey, *Organometallics* **2008**, *27*, 100-108.
[282] a) T. V. Ashworth, M. J. Nolte, E. Singleton, *J. Chem. Soc., Dal. Trans.* **1976**, 2184; b) G. Albertin, S. Antoniutti, A. Bacchi, E. Bordignon, P. Matteo Dolcetti, *J. Chem. Soc., Dalt. Trans.* **1997**, 4435-4444; c) A. H. Murray, Z. Yue, A. I. Wallbank, T. S. Cameron, R. Vadavi, B. J. MacLean, M. A. S. Aquino, *Polyhedron* **2008**, *27*, 1270-1279; d) I. W. Wyman, K. N. Robertson, T. S. Cameron, J. C. Swarts, M. A. S. Aquino, *Organometallics* **2005**, *24*, 6055-6058; e) I. W. Wyman, K. N. Robertson, T. S. Cameron, J. C. Swarts, M. A. S. Aquino, *Inorg. Chim. Acta* **2006**, *359*, 3092-3096.
[283] A. K. Bar, S. Shanmugaraju, K.-W. Chi, P. S. Mukherjee, *Dalton Trans.* **2011**, *40*, 2257-2267.
[284] O. E. Woisetschlager, W. Beck, K. Polburn, *Private Communication* **2005**, CCDC: 267609.
[285] J. R. Lakowicz, *Principles of fluorescence spectroscopy*, 4rd ed., Springer, New York, **2010**.
[286] C. J. Jing, L. S. Chen, Y. Shi, X. G. Jin, *Chin. Chem. Lett.* **2005**, *16*, 1519-1522.
[287] W. Holzer, A. Penzkofer, S. H. Gong, A. P. Davey, W. J. Blau, *Opt. Quantum Electron.* **1997**, *29*, 713-724.
[288] O. Lavastre, J. Plass, P. Bachmann, S. Guesmi, C. Moinet, P. H. Dixneuf, *Organometallics* **1997**, *16*, 184-189.
[289] J.-L. Fillaut, J. Andriès, L. Toupet, J.-P. Desvergne, *Chem. Comm.* **2005**, 2924-2926.
[290] I. P. Evans, A. Spencer, G. Wilkinson, *J. Chem. Soc., Dalton Trans.* **1973**, 204-209.

[291] M. T. Bautista, E. P. Cappellani, S. D. Drouin, R. H. Morris, C. T. Schweitzer, A. Sella, J. Zubkowski, *J. Am. Chem. Soc.* **1991**, *113*, 4876-4887.
[292] J. Figueira, V. Vertlib, J. Rodrigues, K. Nättinen, K. Rissanen, *Acta Cryst. E* **2008**, *64*, o765-o766.


UNIVERSIDADE da MADEIRA


CQM
CENTRO DE QUÍMICA
DA MADEIRA


FCT Fundação para a Ciência e a Tecnologia
MINISTÉRIO DA EDUCAÇÃO E CIÊNCIA


Molecular Materials®
RESEARCH GROUP
MADEIRA ISLAND - PORTUGAL


NSC
Nanoscience Center


RNE


PTNMR


Portugal
Portuguese Nanotechnology Network


VIDAMAR
RESORTS
MADEIRA

A Nossa Universidade

Colégio dos Jesuítas
Rua dos Ferreiros - 9000-082, Funchal

Tel: +351 291 209400
Fax: +351 291 209410
Email: gabinetedareitoria@uma.pt

CQM
CENTRO DE QUÍMICA DA MADEIRA

FCT
Fundação para a Ciência e a Tecnologia
MINISTÉRIO DA EDUCAÇÃO E CIÊNCIA